MICROWAVE INTEGRATED CIRCUITS

Preparation and Measurement Techniques for Materials and Components.

- by -

Kemâl Mehmet, M. Sc(Eng.)

A thesis submitted for the degree of Doctor of Philosophy at the University of Warwick, England.

October 29, 1970.

Abstract

Microwave measurement of the properties of thin film dielectrics and lumped elements present difficulties because of the small volume of material involved. In this investigation both capacitively loaded coaxial cavities and capacitively loaded microstrip resonators were used.

The dielectric properties of thin films were measured using symmetrical capacitively loaded coaxial cavities. The theoretical approaches are given for the design of the cavity and for the measurement techniques using (a) the VSWR method and (b) the perturbation method.

The practical construction problems were overcome and highly stable (mechanically as well as electrically) cavities were obtained. The measured electrical parameters of the cavities were very close to the theoretical values.

Thin dielectric films were prepared using an electron beam evaporation source and an rf sputtering unit. The properties of these films were measured using the capacitively loaded coaxial cavity. The thin film properties were correlated with the thin film deposition conditions.

The dielectric properties of substrates used in the construction of microstrip transmission lines were measured on a sampling basis using a waveguide cavity technique. It was shown to be a most useful method.

Capacitively loaded microstrip resonators were used to measure lumped elements at microwave frequencies. But first the microstrip properties had to be measured. Very accurate techniques were introduced for measuring the effective dielectric constant and the capacitance of

a gap in the strip of a microstrip, over a range of frequencies. Alumina, sapphire and quartz substrates were used in these measurements.

The construction of these resonators using thin film deposition and photolithographic techniques was presented.

It is considered that the use of these measurement techniques will contribute significantly to further advances in the field of m.i.c's.

Preface

The work reported in this thesis is my own work unless credited, and it is not submitted at another university. Some parts of the thesis have been or will be published in technical journals.

The permittivity measurement technique for the thin dielectric films was the main part of our exhibit at the 1970 Physics Exhibition (London).

I wish to express my gratitude to Professor J.A. Shercliff, Chairman of the School of Engineering Science, U W, for the facilities provided for conducting these investigations and the Science Research Council, UK, for the financial support.

This work was supervised by M.K. McPhun and I wish to thank him for his guidance during the last three years and his assistance during the preparation of the manuscript (although he was on Sabbatical leave at the Twente Technical University, Netherlands).

During this time I have had the opportunity of meeting people who worked in the same field and discussing with them certain technical aspects of the problem. I take this opportunity of acknowledging their assistance:-

Professor A.L. Cullen (University College London) for his critical review of my capacitively loaded coaxial cavity technique; Dr. J. Curron (then of A.E.I. Rugby and now of G.E.C. HRC Wembley) for his suggestions on coupling mechanisms to coaxial cavities; J.F. Wells (then of Mullard Research Laboratories Redhill and now Phillips, London) for the unpublished technical information on SiO_2 films and supply of molybdenum

crucibles; the staff of Cambridge Scientific Instruments (Cambridge) for the microprobe analysis of the thin dielectric film samples; Dr. J.R. Bosnell (R.R.E.), H.J. Harris (Microwave Associates) and G.E.C.(Stanmore) for the alumina substrates; R. Richardson (Langley London Ltd.) for the ruby and amber mica sample; Dr. P.W. McMillan (School of Physics, U W.) for the use of the "Spectromaster" IR Spectroscope.

Also I wish to thank the following in the School of Engineering Science: Dr. H.V. Shurmer, R.S. Butlin, S.B. Hussain, B.G. Marchent, D. Michie, E.P. da Silva and G. Warner for many useful discussions; R.S.B. for the rf sputtered SiO_2 films and his assistance during the preparation of the manuscript; D.M. for the masks used in the photolithographic processing; P.J. Smith for his highly skilled construction of the coaxial cavities; E.G. Coates for the supply of some of the shortcircuited microstrip lines; H.G. Woodgate for the supply of bulk material of SiO and J.J. Darmon for the measurements of the thicknesses of thin films.

Also I would like to thank Mrs. S.M. Turner for the decipherment of the hand written manuscript and typing; and Mrs. C. Allsopp for tracing some of the figures.

During the last three years I have had a family patiently waiting and I dedicate this work to that family at Taşpinar.

CONTENTS

Abstracts	.....	ii
Preface	.....	iv
Chapter 1	INTRODUCTION	1
1.1	General	1
1.2	Material aspect of lumped elements	4
1.3	Microwave measurement of lumped elements	7
1.4	The aim of the investigation	9
Chapter 2	THEORETICAL APPROACH TO PERMITTIVITY MEASUREMENTS	13
2.1	Introduction	13
2.2	List of principal symbols	14
2.3	The capacitively loaded coaxial cavity	15
2.3.1	The capacitive gap and em field distribution of the cavity	15
2.3.2	Q factor of the cavity	20
2.4	The dielectric film loaded cavity	27
2.4.1	Calculations of the real part of the relative permittivity	27
2.4.2	Calculations of the Q factor of the dielectric film ..	31
2.5	Application of the perturbation theory to the ..... measurement of the thin film dielectric properties ..	40
2.6	Measurement of self supporting dielectrics	46
Chapter 3	THEORETICAL APPROACH TO MICROWAVE LUMPED ELEMENT MEASUREMENT	50
3.1	Intoroduction	50
3.2	Properties of microstrip transmission lines	50
3.3	Resonant method of determining the lumped element values	52
3.3.1	Capacitively loaded microstrip resonator	52

Chapter 3

3.3.2 Measurement of a capacitor using the microstrip resonator 56

3.3.3 Comments 60

Chapter 4 MECHANICAL DESIGN AND MATERIAL PROBLEMS OF THE COAXIAL CAVITY 61

4.1 Introduction 61

4.2 Mechanical construction of the cavities 62

4.2.1 Brass cavities 63

4.2.2 Invar cavities 63

4.3 Materials for the cavity 69

4.3.1 Electroplating of the cavities 72

4.3.2 Comments on plating 74

Chapter 5 MICROWAVE MEASUREMENT TECHNIQUES FOR THE CAVITY 76

5.1 Introduction 76

5.2 Precision waveguide reflectometer 78

5.2.1 Frequency stability of the signal source 82

5.2.2 Measurement of the reflectometer errors 83

5.2.3 Calibration of the reflectometer system 90

5.2.4 Swept reflection coefficient measurements 92

5.3 Measurement of the unloaded Q factor of the cavity ... 93

Chapter 6 THE CAPACITIVELY LOADED COAXIAL CAVITIES 98

6.1 Introduction 98

6.2 Coupling mechanisms of the cavities 99

6.2.1 Electric probe: Waveguide system 99

6.2.2 Floating disk - probe: Waveguide system 101

6.2.3 Magnetic loop coupling: coaxial system 101

Chapter 6

6.2.4 Dumbbell slot coupling : Waveguide system 103

6.3 Measured properties of capacitively loaded cavities .. 105

6.3.1 Brass cavities 105

6.3.1.1. Measurement of capacitive network parameters of a gap in the centre conductor of a coaxial line 106

6.3.2 Invar cavities 109

6.3.2.1 Measurement of the series gap capacitance of the cavity 113

6.3.2.2 The stability of invar cavities 114

6.4 Comments 116

Chapter 7 MEASUREMENT OF THE THIN DIELECTRIC FILM PROPERTIES ... 119

7.1 Introduction 119

7.2 Experimental verification of the theory applied to dielectric loaded cavity 120

7.3 Deposited dielectric films 123

7.4 Measurement of self - supported dielectric materials.. 130

7.5 Comments 136

Chapter 8 ERROR ANALYSIS OF THE PERMITTIVITY MEASUREMENT USING THE COAXIAL CAVITY 140

8.1 Introduction 140

8.2 Error analysis of the permittivity measurements 148

8.3 Comments 148

Chapter 9 THIN FILM PROCESSING 151

9.1 Introduction 152

9.2 Preparation of thin films using electron gun evaporator 152

9.2.1 Electron gun evaporating unit 152

Chapter 9

9.2.2 Preparation of metal films 155

9.2.2.1 Deposition of metal films for microwave integrated circuits 158

9.2.2.2 Comments on the processing of thin metal films 160

9.2.3 Deposition dielectric films 165

9.2.3.1 Dielectric films for microwave measurements 168

9.2.3.2 The analysis of thin dielectric films 171

9.2.3.3 Discussion on electron beam evaporated dielectric films

9.3 RF sputtered dielectric films 182

Chapter 10 MICROWAVE MEASUREMENT OF LUMPED ELEMENTS 184

10.1 Introduction 184

10.2.1 Microstrip resonators 185

10.2.1 Measurement of the effective dielectric constant 185

10.2.2 Capacitively loaded microstrip resonators 189

10.2.2.1 Construction of microstrip resonators 189

10.2.2.2 Measurement of resonator properties 191

10.2.2.3 Measurement of the capacitance of a gap in the strip of a microstrip line 191

10.3 Measurement of lumped elements 193

10.3.1 Verification of the theory on the measurement of lumped elements 193

10.3.2 Measurement of lumped elements 196

10.3.2.1 Measurement of lumped capacitors 200

10.3.2.2 Measurement of lumped inductor 202

10.4 Comments 206

Chapter 11 CONCLUSIONS 210

References 214

Appendices 226

Exhibition 246

Conference publications 247

1. INTRODUCTION

1.1 General

The development of microwave integrated circuits, m.i.c!s, has followed two parallel approaches. The real m.i.c!s start with microstrip lines. This is the distributed line approach, which has been used in other types of transmission lines i.e. Waveguide and Coaxial lines. This approach was proposed in the early 1950's[1] but the majority of the progress has been made in the last six or seven years. During this period more accurate theoretical treatment of microstrip line properties,[2-6] together with high dielectric constant materials and improvement in processing techniques became available. Figure 1.1 shows such a transmission line.

The second approach to m.i.c!s which was reported in 1965,[7] is that of the lumped elements, LE's. These elements are inductors, capacitors, transformers and resistors,[7-20] similar to the components used at much lower frequencies. These elements to be really lumped should have no phase change across them and therefore must be physically much smaller than a wavelength. Some of the configurations of these components for use at microwave frequencies are shown in figure 1.2.

Lumped elements reduced the size of m.i.c!s more than high dielectric constant microstrip networks, especially below X-band frequencies. It will be seen from figures 1.3 and 1.4 that a lumped element tuned circuit at X-band is much smaller than the quarter of a wavelength microstrip resonant circuit.

These lumped elements found uses in amplifiers,[13, 17] filters,[17, 19, 23] oscillators,[15] 3 dB-magic Tees[14] and 3 dB-couplers.[14]

It will be seen from figure 1.3 and figure 1.4 that the LE tuned

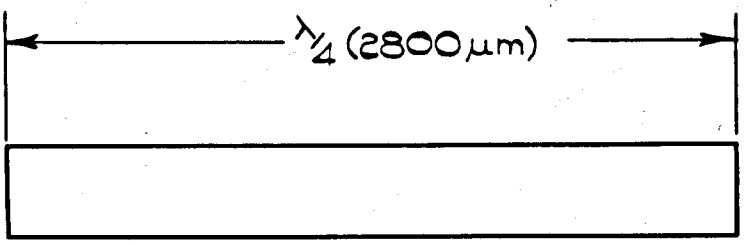

$z_o = 50\Omega$

$f_o = 10\ GHz$

$Q_o = 400$

FIGURE 1.3.

DISTRIBUTED RESONANT CIRCUIT.

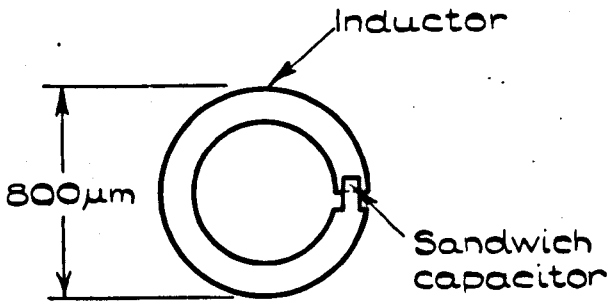

$L = 1{\cdot}1\ mH$

$C = 0{\cdot}25\ P$

$f = 10\ GHz$

$Q_o = 100$

FIGURE 1.4.

LUMPED ELEMENT RESONANT CIRCUIT.

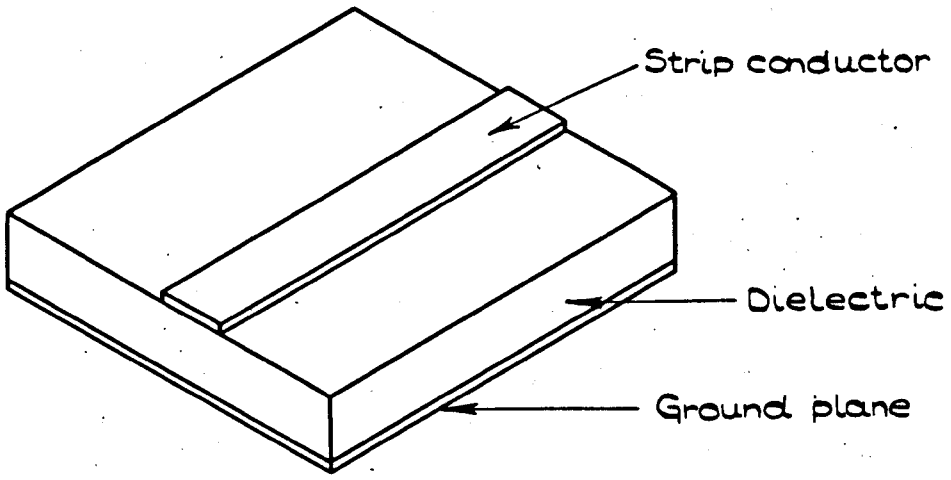

FIGURE 1.1.

MICROSTRIP TRANSMISSION LINE.

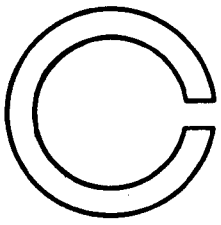

SINGLE TURN INDUCTOR

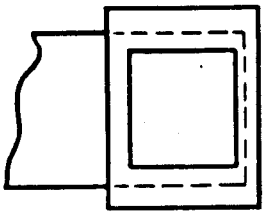

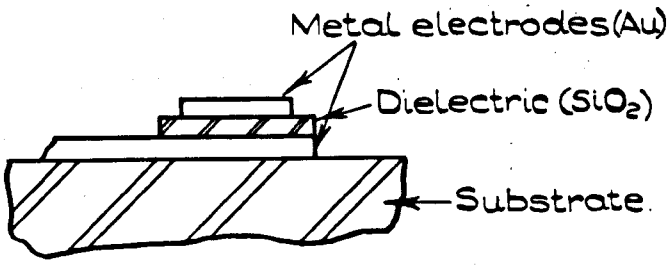

SANDWICH CAPACITOR

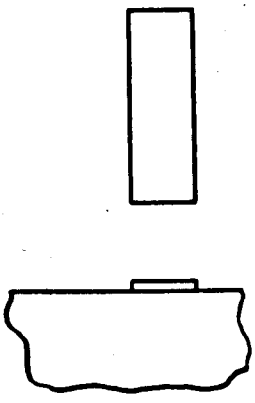

RESISTOR

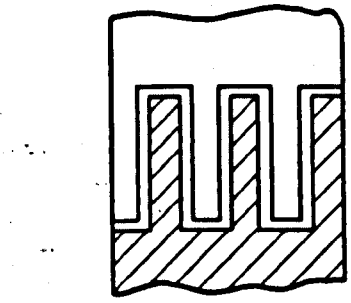

INTERDIGITATED CAPACITOR

FIGURE 1.2.

MICROWAVE LUMPED ELEMENTS.

circuit has one quarter of the Q-factor of the microstrip resonator. These Q-factors were derived from the published practical results. The low Q-factor is due to the small volume of the material used for the energy storage[42] and to the materials used in the construction of the LE tuned circuit. The second point is very important because the component is made from two materials, namely a metal film and a dielectric film. Therefore their separate properties should be known.

1.2 The Material Aspect of Lumped Elements.

These minute lumped elements are prepared in planar form using thin film processing techniques. For example a capacitor, 0.25pf to 10 pf, requires a dielectric film of 1 to 10 μm thick sandwiched between two metal electrodes the thickness of which must be at least 3 times the skin depth at the frequency to be used. Different techniques are used to prepare materials (see section 9.1) for these capacitors but it has been reported that the measured and predicted parameters do not tie up.[17, 18]

At low frequencies the properties of a thin film dielectric is investigated by sandwiching it between two thin film electrodes. Measuring at two different frequencies the electrode as well as the dielectric properties can be determined. A similar approach was used in microwave measurements of Capacitors [8, 10, 16] and there was found to be an order of magnitude difference between predicted and measured values.[17-18] The difference may be caused by electrode losses or changes in the dielectric properties. This suggests that the thin film dielectric should be measured by itself, thus eliminating the losses owing to the electrode material.

The first direct measurement of the properties of a thin dielectric film at microwave frequencies was reported in 1967 by Sobol.[21] He used a re-entrant coaxial cavity resonating in E01 mode, at around 3 GHz (figure 1.5). More recently, Park[22] made measurements using a perturbation technique applied to a split cylindrical cavity resonating in the H01n mode at X-band. He deposited the dielectric film on to a thin dielectric substrate and inserted this substrate at an electric field maxima in the cavity. He used two steps. One of them was to measure the proerties of the dielectric substrate and the second was to measure the properties of the film loaded dielectric substrate. He evaluated the properties from these measurements. In this method the electric field was in the plane of the film (figure 1.6).

These two direct measurement methods may not be used for the thin film dielectric measurements at X-band, on the following reasons:

(a) Sobol's[21] method uses an adjustable centre conductor, the dielectric film is deposited on the plane end. The accuracy of the measurement of the dielectric film properties depends on the adjustment of this centre conductor. Although this adjustment of the centre conductor is quite satisfactory for the measurements below S-band frequencies it becomes very difficult if not impossible, at X-band frequencies. Sobol realized this difficulty even at S-band and he used a 10 μm thick dielectric film.

(b) Park's[22] method uses a dielectric substrate onto which the dielectric film is deposited. Usually dielectric films deposited onto dielectric substrate do not adhere to it and a glueing metallic film is deposited in between the dielectric film and the substrate. Therefore the true dielectric properties of the film may bemasked by the glueing film, if this method is used.

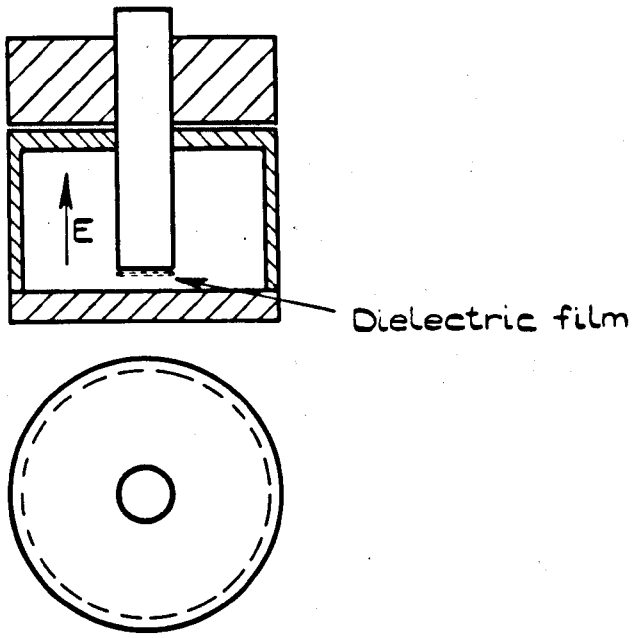

FIGURE 1.5.
RE ENTRANT COAXIAL CAVITY METHOD.

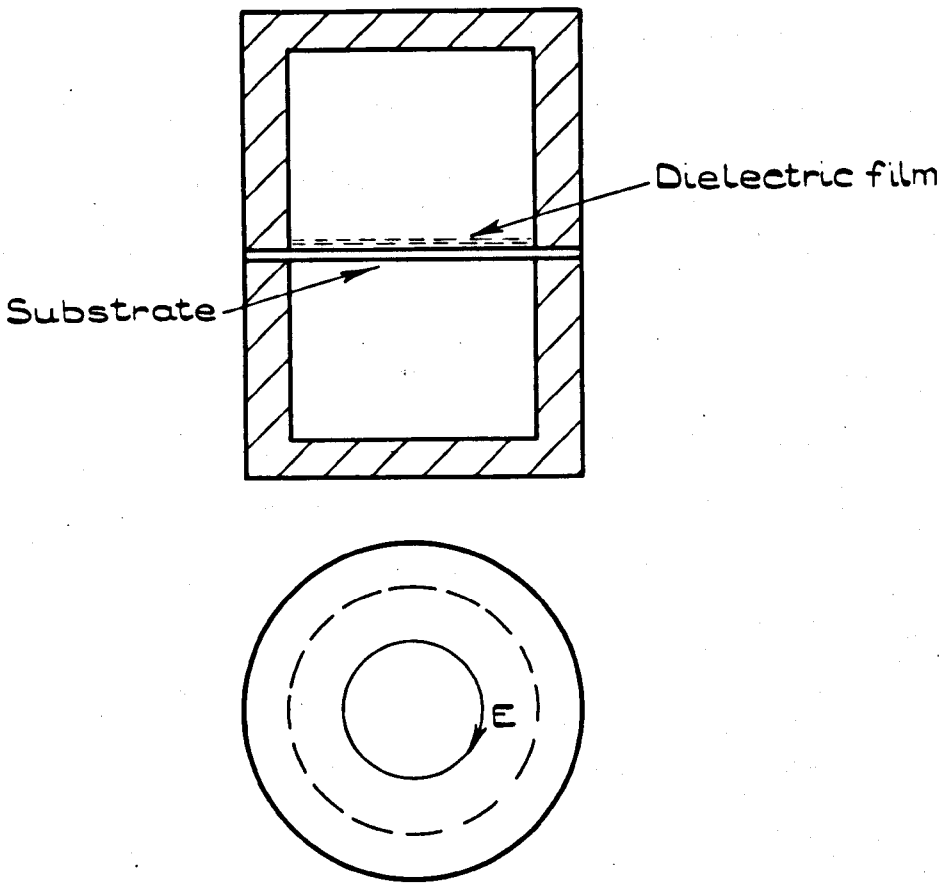

FIGURE 1.6.
SPLIT CAVITY METHOD

Also the electric field in the cavity is in the plane of the dielectric film to be measured. The electric field in m.i.c!s (capacitors and crossovers), is usually applied at right angles to the plane of the dielectric film. Therefore if there is any directional inhomogenuity such as crystallographic orientation, this method may not show the required parameters for that film.

Further comments on these methods are made when the practical work is described.

1.3 Microwave Measurement of Lumped Elements.

These lumped elements are quite small (figure 1.2 and 1.4) and therefore measurement on them is very difficult. Daly[8] and Wells[10] attempted to measure these elements directly, i.e. connecting them across a slotted line and measuring the shift in minima and VSWR with and without the element (figures 1.7a and 1.7b). Although this method seems simple it is inaccurate especially in measurement of component losses.

Recently (1969 and later) this point was realized and lumped elements have been measured in resonant circuits. Capacitors were measured in a transmission type coaxial resonators[24] (figure 1.7c), and inductors were measured in open ended microstrip resonators[23] (figure 1.7d)

The advantage of the resonant circuit approach is that the transition discontinuities from other types of lines connecting the line to the measuring system can be eliminated. Hence elements parameters can be measured quite accurately. The only disadvantage of the resonant circuit method is that it is a fixed frequency measurement whilst the direct measurement is a broad band technique.

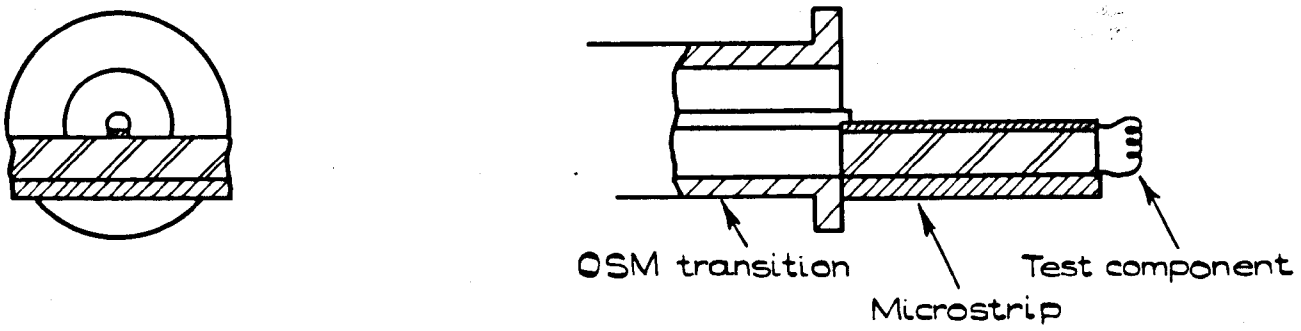

(a)

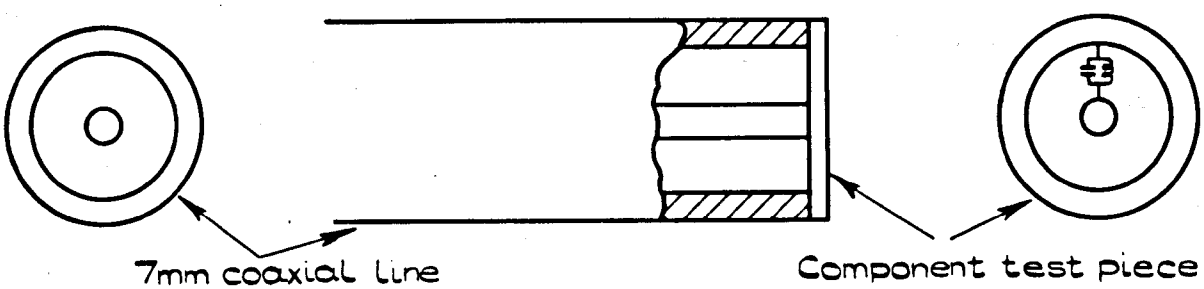

(b) COAXIAL LINE

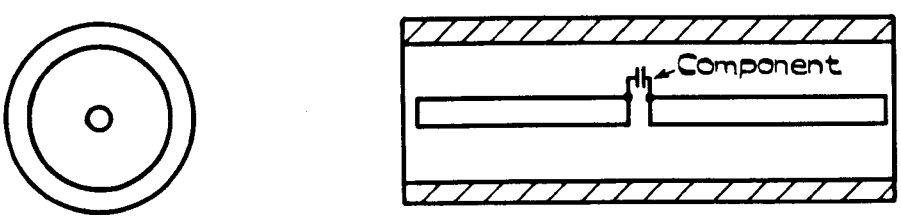

(c) COAXIAL RESONATOR

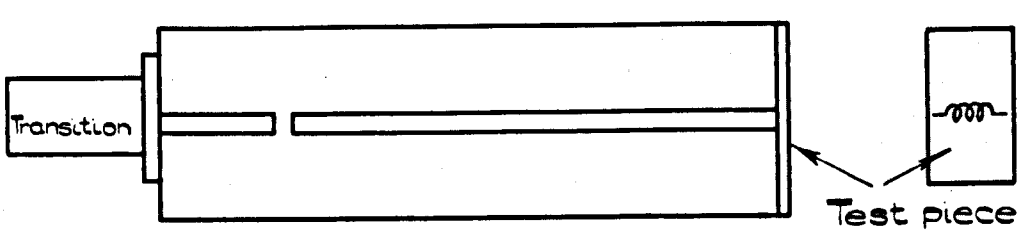

(d) MICROSTRIP OPEN RESONATOR

FIGURE 1.7.

MICROWAVE MEASUREMENT TECHNIQUES FOR LUMPED ELEMENTS.

1.4 The Aim of the Investigation.

Most of the investigations on LE's reported so far have been performed on a "make it and measure it" basis. For this reason the material properties obtained from these experiments have not been in close agreement with the predicted values. One way to eliminate these discrepancies is to separate the dielectric and metal films contributions to LE parameters.

The dielectric films are used for capacitors and crossovers sandwiched between two metal electrodes. The capacitor values for microwave circuits (excluding bypass capacitors) range from 0.1 pF to 10 pF. The relative permittivity used for LE's can be up to 10. This upper limit is due to the requirements that the crossover capacitance to be low and also to the LE circuit fabrication difficulties. Thus the dielectric film thickness that can be used for LE's ranges from 0.5 μm to 10 μm.

The first aim of the investigation was to find a simple and practical method of measuring the permittivity of thin dielectric films, which are used in m.i.c's. The approach taken was to use a symmetrical, capacitively loaded coaxial cavity. In this method (described later) the dielectric film is deposited in the capacitive gap between the centre conductors of the cavity. This method has the following advantages.

(a) The film is deposited onto a metal substrate as in the m.i.c. fabrication.

(b) For non adherent dielectric films a 'glueing' metal film can be deposited between the dielectric film and the cavity conductor without any effect on the dielectric film properties. This technique is normal in integrated circuit fabrication processes.

(c) As in Capacitors and Crossovers the electric field is applied at right angles to the plane of the thin dielectric film. Some films during the preparation stages show directional inhomogenuity i.e. the properties vary from the plane to plane. The required plane parometers are measured using this method.

(d) The method can be used to sample the dielectric film and measure its properties during the circuit fabrication.

The theoretical treatment of this problem is given in section 2. The practical approaches taken and microwave measurements of the thin dielectric films are shown in section 4 to 7.

In addition to the above investigation on thin dielectric films some work was done on self supporting dielectric materials such as microstrip substrates. The theoretical approach is given in section 2.6 and practical results are given in section 7.4.

The preparation of the dielectric and metal films plays an important part in determining the properties of the film.

These practical problems together with the known theoretical treatments are discussed in section 9. Although these films were used in the microwave measurements low frequency values were also measured. These results are also included.

The second aim was to find a method of measurement for the lumped elements. The approach taken was to use a capacitively loaded microstrip resonator. This was to a certain extent, an extension of principles of permittivity measurement using capacitively loaded coaxial cavity. The theoretical treatment is given in section 3. The preparation of these microstrip resonators and their measured properties are given in section 10. The use of these resonators in the LE measurements is given in section 10.3.

The whole investigation was centred around microwave measurements. Nearly all of the measuring systems have errors and it was thought necessary to do a full error analysis on the measuring system adopted. This is described in section 8.

The investigation spread over the measurement, material processing and fabrication aspects of microwave circuits. This covered various techniques for each part of the investigation. Therefore it was found necessary to present each main section as a self contained section A brief introduction is given at the beginning, and comments are included at the end of each main section.

The conclusions and summary of comments are given in Chapter 11. Some suggestions are also made for the future work on LE's at microwave frequencies. These include investigations into material processing and measurement techniques.

Chapter 2.

THEORECTICAL APPROACHES TO PERMITTIVITY MEASUREMENTS.

2.1 Introduction.

The permittivity of bulk materials at microwave frequencies is usually measured using cavity techniques. Although there are other techniques of measurements, when the volume of the material is small the cavity methods give accurate results. In case of thin dielectric films specially constructed cavities are required to measure the properties. A brief description of two known methods is given in section 1.2 and below.

The small volume of a thin film introduces certain limitations on the type of cavity that can be used for these measurements. The dielectric films deposited on substrates usually require an adhering layer. Normally this is a metal such as chromium, nichrome, molybdenum, and this may mask the true properties of the dielectric film.

Sobol[21] reported a measuring technique where the dielectric film was deposited onto a metal substrate. He used a re-entrant coaxial cavity resonating in TE 01 mode at around 3 GHz, and used the adjustable centre conductor of the cavity as the substrate for the film. This technique is not suitable for X-band because during the measurement the gap is changed by adjusting the centre conductor. The adjustment of the centre conductor of the cavity becomes very difficult, if not impossible.

The approach presented here, uses a symmetrical, capacitively loaded coaxial cavity resonating in the principal mode i.e. TEM mode (figure 2.2).

In the following sections the theoretical approaches to the microwave measurement of the permittivity of a dielectric film will be described. The cavity properties will be derived and used in the calculations of the permittivity of a dielectric film depsosited into the capacitive gap of the cavity. Two theoretical approaches are introduced, one using the voltage standing wave ratio, VSWR, the other, the well known perturbation method. The reason for the two approaches is given in section 8.

In the theoretical derivation of the thin film dielectric properties using the VSWR method, it was assumed that the cavity losses were uniformly distributed in the cavity walls. This assumption can only be verified by measuring the dielectric properties of a known material, so another measuring method is introduced. In this the perturbation theory is applied to a rectangular waveguide resonator. This method uses self supporting dielectric materials.

2.2 List of Principal Symbols.

C_o, C_p, C_s = defined as in section 2.3.1.

D_i = diameter of the inner conductor of the cavity.

D_o = diameter of the outer conductor of the cavity.

E_r = radial component of the electric field inside the cavity.

f = frequency in Hz.

f_1 = resonant frequency without the film.

f_2 = resonant frequency with the film.

G_o = the gap between the centre conductors.

H_ϕ = circumferencial magnetic field inside the cavity.

L = length of the centre conductors of the cavity.

Rs = surface resistivity $= \left(\frac{\pi f \mu_0}{\sigma}\right)^{\frac{1}{2}}$

v = velocity of e.m wave in the free space, 3×10^8 m/s

ϵ_0 = permittivity of free space

ϵ = relative complex permittivity of the film

$= \epsilon' - j\epsilon''$

$\text{Tan}\delta = \epsilon''/\epsilon'$

$Q_D = (\text{Tan}\,\delta)^{-1}$

$\eta = (\mu_0/\epsilon_0)^{\frac{1}{2}}$

σ = conductivity of metal surfaces inside the cavity

w = frequency in radians per second $= 2\pi f$

λ = wavelength at resonance $= v/f_1$

2.3 The Capacitively Loaded Coaxial Cavity.

2.3.1 The Capacitive Gap and e m field distribution of the cavity.

A gap in the centre conductor of a coaxial line is represented by a two port π network[25-27] as shown in Figure 2.1. In this representation Co is the capacitance between two inner conductor planes, Cp is the fringing capacitance due to the fringing field between the inner conductor and outer conductor, and Cs (= mCo) is the fringing capacitance due to fringing field around the gap.

It was shown that as the gap approaches zero the fringing capacitance Cp tends to zero. For small gaps the total gap

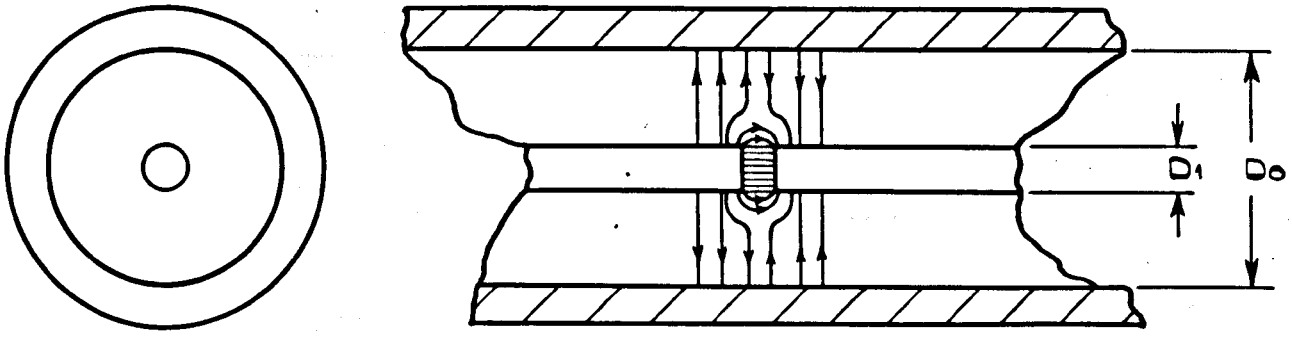

(a)

ELECTRIC FIELD DISTRIBUTION ACROSS THE GAP.

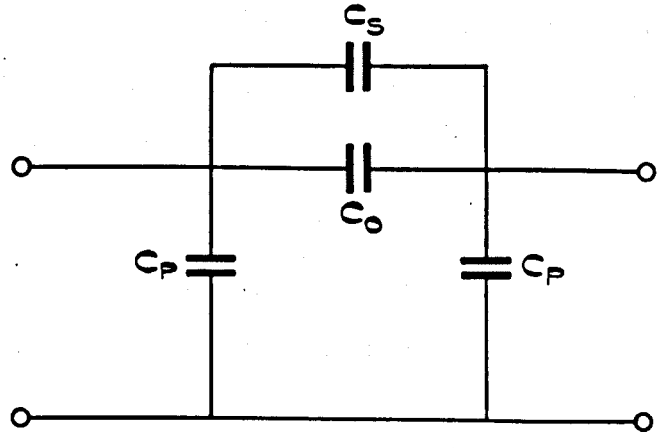

(b)

EQUIVALENT π REPRESENTATION OF THE GAP.

FIGURE 2.1.

CAPACITIVE GAP IN THE CENTRE CONDUCTOR OF A COAXIAL LINE.

capacitance can be represented by the following equations[25,26,28]

$$C_o T_i = \frac{\pi}{4} D_1^2 \frac{\epsilon_o}{G_o} + \epsilon_o D_i \ln \frac{D_o - D_1}{G_o}$$

$$= \frac{\pi}{4} D_i^2 \frac{\epsilon_o}{G_o} \left(1 + \frac{4 G_o}{\pi D_1} \ln \frac{D_o - D_i}{G_o} \right) \quad 2.1$$

Where $C_o = \frac{\pi}{4} D_1^2 \frac{\epsilon_o}{G_o}$ 2.2a

$m = \frac{4 G_o}{\pi D_i} \ln \frac{D_o - D_1}{G_o}$ 2.2b

$C_o T_1$ = Total series gap capacitance 2.2c

Therefore $C_o T_1 = C_o (1 + m)$ 2.3

Figure 2.2 shows a section through a symmetrical, capacitively loaded coaxial cavity. Distances between the gap and shortcircuit planes are equal.

Assuming that the e.m. field propagation in the cavity is TEM, the fields at a distance Z from the short shortcircuit plane and at a radius r from the axis of the cavity will be

$$E_r = \frac{V_o}{r} \sin \frac{wz}{v} \quad 2.4$$

$$H_\phi = j \frac{V_o}{\eta r} \cos \frac{wz}{v} \quad 2.5$$

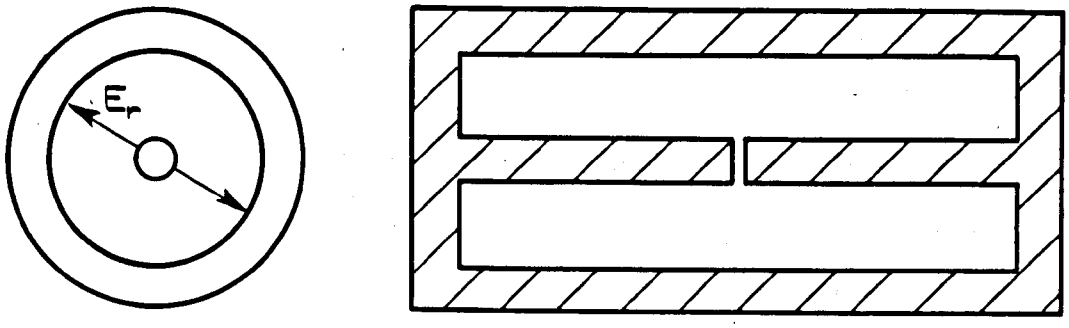

MODES OF RESONANCE.

Approx. fo for L=32mm $\frac{D}{D_0}=5$

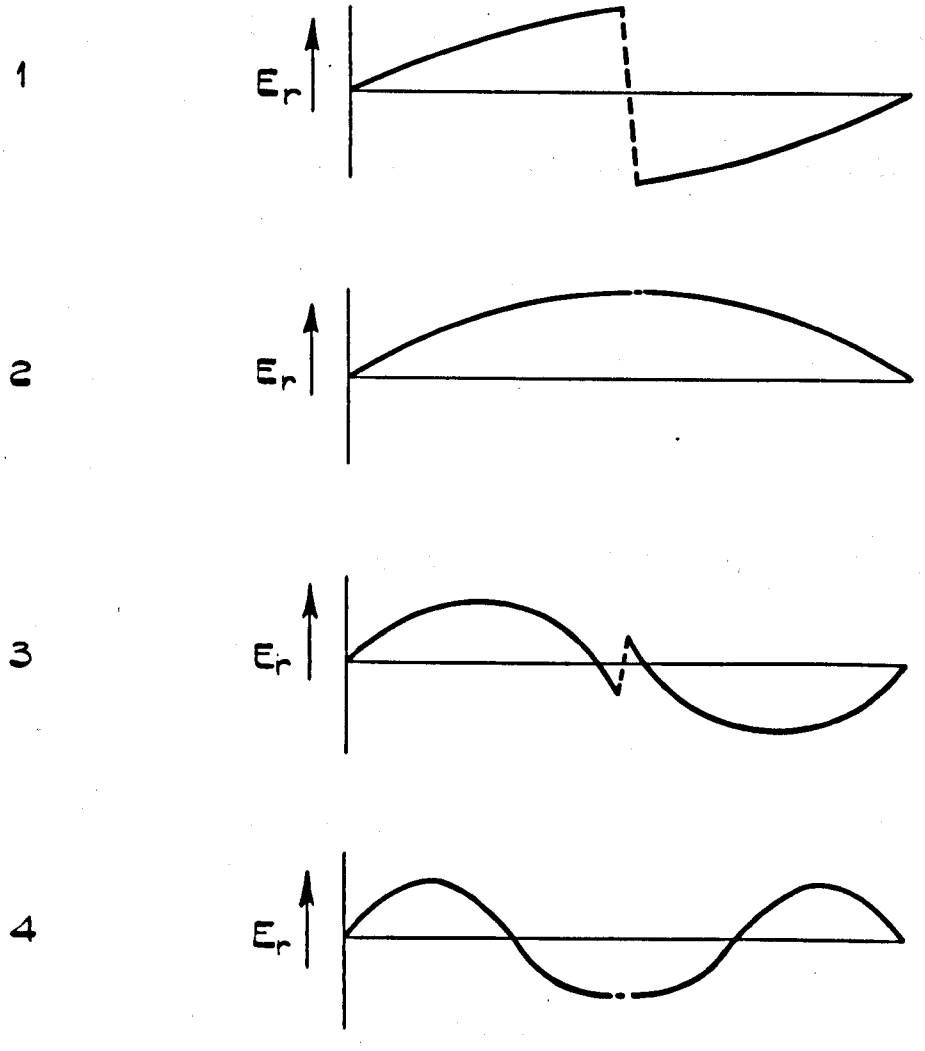

FIGURE 2.2.

ELECTRIC FIELD DISTRIBUTION AT DIFFERENT RESONANT MODES (for principal mode in coaxial line).

Slater[29] treated such a cavity for a klystron and his derivation will be followed, but modified to suit the present problem.

Some possible electric field distributions along the length of the cavity are sketched in figure 2.2. It will be seen from these plots that whenever electric fields on both sides of the gap have the same polarity (figure 2.2 Modes 2 and 4) the series capacitance has no effect on the resonant frequency of the cavity but Cp controls the resonant frequency. On the other hand when the fields, on either sides of the gap have different polarity (figure 2.2 Modes 1 and 3) the series capacitance as well as Cp will control the resonant frequency of the resonator.

In the following solutions, to simplify the mathematics Cp's are neglected.

Consider the cavity shown in figure 2.2, Mode 3. The voltage across the gap

$$V_{ab} = \int_{\frac{Di}{2}}^{\frac{Do}{2}} Er \Big|_{Z=\frac{L}{2}} dr + \int_{\frac{Di}{2}}^{\frac{Do}{2}} Er \Big| dr \quad Z = \frac{L}{2}$$

Substituting the values of Er from the equation 2.4 gives

$$Vab = 2Vo \ln \frac{Do}{Di} \sin \frac{wL}{2v} \qquad 2.6$$

The current flowing in the inner conductor at $\frac{L}{2}$ will be the same as

PAGE NUMBERING AS ORIGINAL

the current through the gap, i.e.

$$I = \int_0^{2\pi} H\phi \Big|_{Z = \frac{L}{2}}^{\left(\frac{D1}{2}\right)} d\phi$$

Substituting $H\phi$ from equation 2.5 gives

$$I = j \frac{2\pi}{n} \quad Vo \quad Cos \quad \frac{wL}{2v} \qquad 2.7$$

But also $I = j\, w\, COT\, Vab$

Therefore $$I = 2\, Vo\, ln \frac{Do}{D1} \quad sin \quad \frac{wL}{2v} \qquad 2.8$$

Equating equations 2.7 and 2.8 gives

$$\frac{I}{w\, C_{oT1}} = \frac{n}{\pi} \ln \frac{Do}{D1} \quad Tan \quad \frac{wL}{2v} \qquad 2.9$$

Substituting the value of C_{oT1} from equations 2.1 and 2.3 we obtain

$$\frac{Go}{\left(\frac{D1}{2}\right)^2} = \frac{(1 + m)}{4} \quad ln \quad \frac{Do}{D1} \quad \frac{w}{v} \quad Tan \quad \frac{wL}{2v} \qquad 2.10$$

As an example this equation is used to calculate the resonant frequency of a cavity having L = 32 m.m, D1 = 3 m.m, Do/ D1 = 5 and varying gap, Go, for the mode shown in figure 2.2 Mode 3. Figure 2.3 shows the variation of the resonant frequency of such a cavity with the gap. An additional plot in this graph

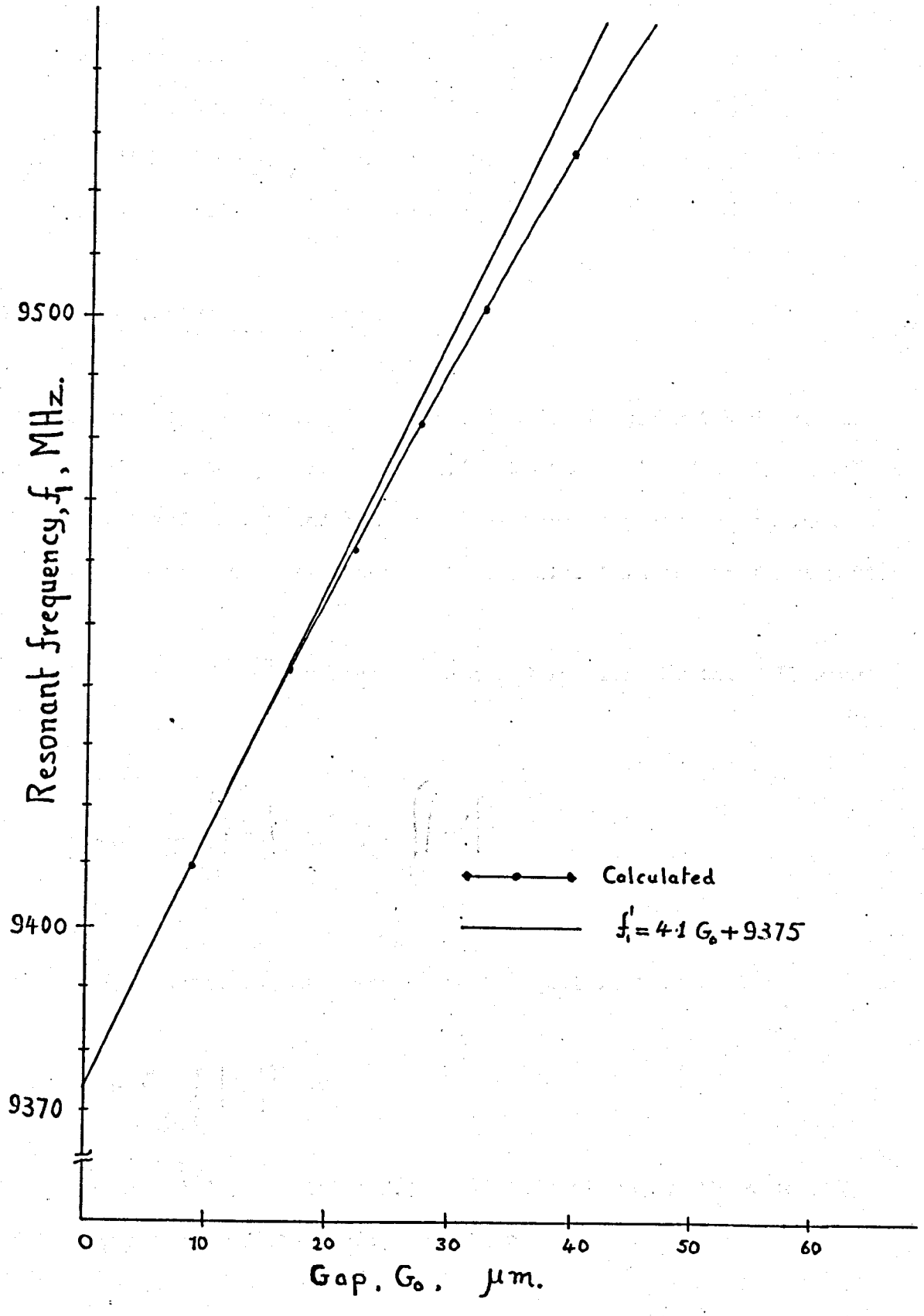

Figure 2.3 Variation of the Resonant frequency, f_1, with the Gap for a Cavity having L=32 mm & $\frac{D_o}{D_i} = 5$.

shows a linear relationship between the resonant frequency and the gap of the cavity. This relationship, $fo^1 = 4.1\ Go + 9375$ (fo^1 in MHz and Go in μm) is within 0.1% of the calculated results using equation 2.10, for gaps below 35 μm

2.3.2 Q - factor of the cavity

The cavity resonating in the third mode, figure 2.2 Mode 3, can be divided into two parts, figure 2.4a, Sections A and C will have the same stored energy and losses. Therefore they can be combined to give a resonant system as shown in figure 2.4b this is the first part.

The energy stored in sections A and C is given by the following relationship:

$$W1 = \frac{\epsilon_o}{4} \iiint_V |Er|^2 \, dV + \frac{\mu o}{4} \iiint_V |H\phi|^2 \, dV$$

since electric and magnetic energies are equal in this system

$$W1 = \frac{\epsilon_o}{2} \int |Er|^2 \, dV$$

Substituting Er from equation 2.4 and integrating over the volume V of the first part of the cavity we obtain

$$W1 = \frac{\pi}{2} \epsilon_o \ln \frac{Do}{D1} \lambda \, Vo^2 \qquad 2.11$$

Power lost in the cavity surfaces (sections A and C)

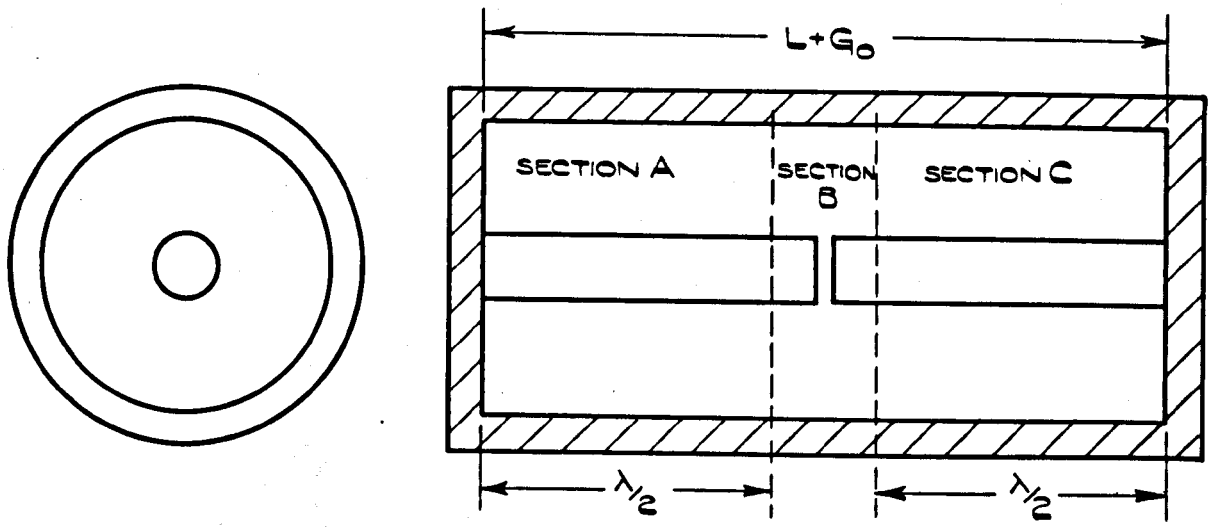

(a) COMPLETE CAVITY

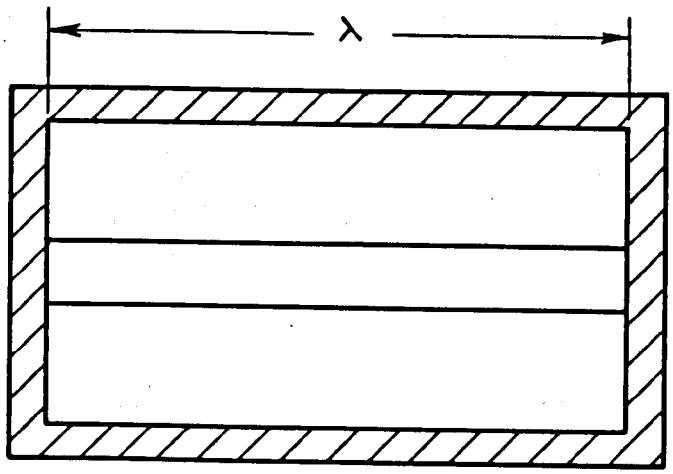

(b) SECTIONS A AND C

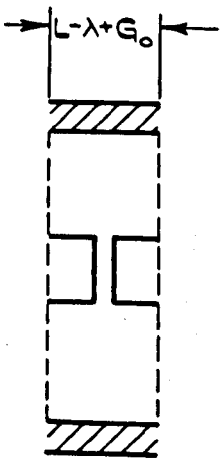

(c) SECTION B

FIGURE 2.4.

SECTIONAL REPRESENTATION OF CAVITY RESONATING IN MODE 3.

$$Pc1 = \frac{Rs}{2}\int_S |H\phi|^2 \, dS$$

substituting $H\phi$ and integrating over the cavity surfaces S (shown fully in Appendix 1) we obtain

$$Pc1 = \frac{Rs\,\Pi}{\eta^2}\left[\left(\frac{1}{D1} + \frac{1}{Do}\right)\lambda + 2 \ln \frac{Do}{D1}\right] Vo^2 \qquad 2.12$$

Now considering the second part, section B shown as a separate section in figure 2.4C.

Energy stored in section B, W_2 = Energy stored in coaxial section, Wb + Energy stored in Capacitor Wca

$$Wb = 2\left[\frac{\epsilon_o}{4}\int_V |Er|^2 \, dV + \frac{\mu o}{4}\int_V |H\phi|^2 \, dV\right]$$

As shown in Appendix 2, substituting the values of Er and $H\phi$ and integrating over the volume V of section B we obtain

$$Wb = Vo^2 \frac{\Pi}{2} \epsilon_o \quad (L - \lambda) \ln \frac{Do}{D_1} \qquad 2.13$$

Energy stored in Capacitor

$$Wca = \tfrac{1}{4} C_{oT1} (Vab)^2$$

As shown in Appendix 3, substituting the values of Vab and C_{oT1} from equations 2.6 and 2.3

$$Wca = \frac{\pi}{2} \frac{\epsilon_o V_o^2}{\frac{w}{v}} \ln \frac{Do}{D1} \sin \frac{wL}{v} \qquad 2.14$$

Energy stored in section B

$$W2 = \frac{\pi}{2} \epsilon_o \left[L - \lambda + \frac{\sin \frac{wL}{v}}{\frac{w}{v}} \right] V_o^2 \ln \frac{D_o}{D_1} \qquad 2.15$$

As shown in Appendix 4, the power lost in section B

$$Pc2 = \pi \frac{Rs}{\eta^2} \left(\frac{1}{D1} + \frac{1}{Do} \right) \left[L - \lambda + \frac{\sin \frac{wL}{v}}{\frac{w}{v}} \right] \qquad 2.16$$

The Q factor of complete cavity,

$$QoT = w \left(\frac{\text{Total Stored Energy}}{\text{Total Power Lost}} \right)$$

$$= w \left(\frac{W1 + W2}{Pc1 + Pc2} \right)$$

Substituting the values of W1, W2, Pc1 and Pc2 from equations 2.11, 2.15, 2.12, 2.16 and taking the surface resistivity Rs as

$$Rs = (\pi \mu o \ f/\sigma)^{\frac{1}{2}}$$

$$QoT = (\pi f \sigma \mu o)^{\frac{1}{2}} \frac{Do \ \ln \frac{Do}{D1}}{\frac{Do}{D1} + 1} \left[1 + \frac{2 \, Do \ln Do}{\left(\frac{Do}{D1} + 1\right) \left(1 + \frac{\sin \frac{wL}{v}}{\frac{wL}{v}} \right)} \right]^{-1} \qquad 2.18$$

The cavity has been divided and treated as two separate parts, namely A + C and B. These parts will have a resonant frequency the same as the resonant frequency of the whole cavity. Therefore the Q factors of these parts can be calculated separately.

$$Qo1 = w \left(\frac{\text{Energy stored in sections A and C}}{\text{Power lost in sections A and C}} \right) \qquad 2.19$$

Substituting for these quantities from equations 2.11 and 2.12, it becomes

$$Qo1 = (\pi f \mu_o \sigma)^{\frac{1}{2}} \frac{Do \ln \frac{Do}{D1}}{\frac{Do}{D1} + 1} \left[1 - \frac{2Do \ln \frac{Do}{D1}}{\left(\frac{Do}{D1} + 1\right) \lambda} \right] \qquad 2.20$$

$$\text{Similarly } Qo2 = w \left(\frac{\text{Energy stored in section B}}{\text{Power lost in section B}} \right) \qquad 2.21$$

$$Qo2 = (\pi f \mu_o \sigma)^{\frac{1}{2}} \left[\frac{Do \ln \frac{Do}{D1}}{\frac{Do}{D1} + 1} \right] \qquad 2.22$$

Equations 2.18, 2.20 and 2.22 give the properties of the cavity and the only measurable one is QoT. Figure 2.5 shows the variation of QoT with frequency for a cavity having $\frac{Do}{D1} = 5$, $L = 32$ m.m and $Do = 15$ m.m. It should be noted that the frequency varies with Go. Figure 2.6 shows the variation of QoT with respect to $\frac{Do}{D1}$. Lower QoT values are obtained for the $\frac{Do}{D1}$ values greater than 4.

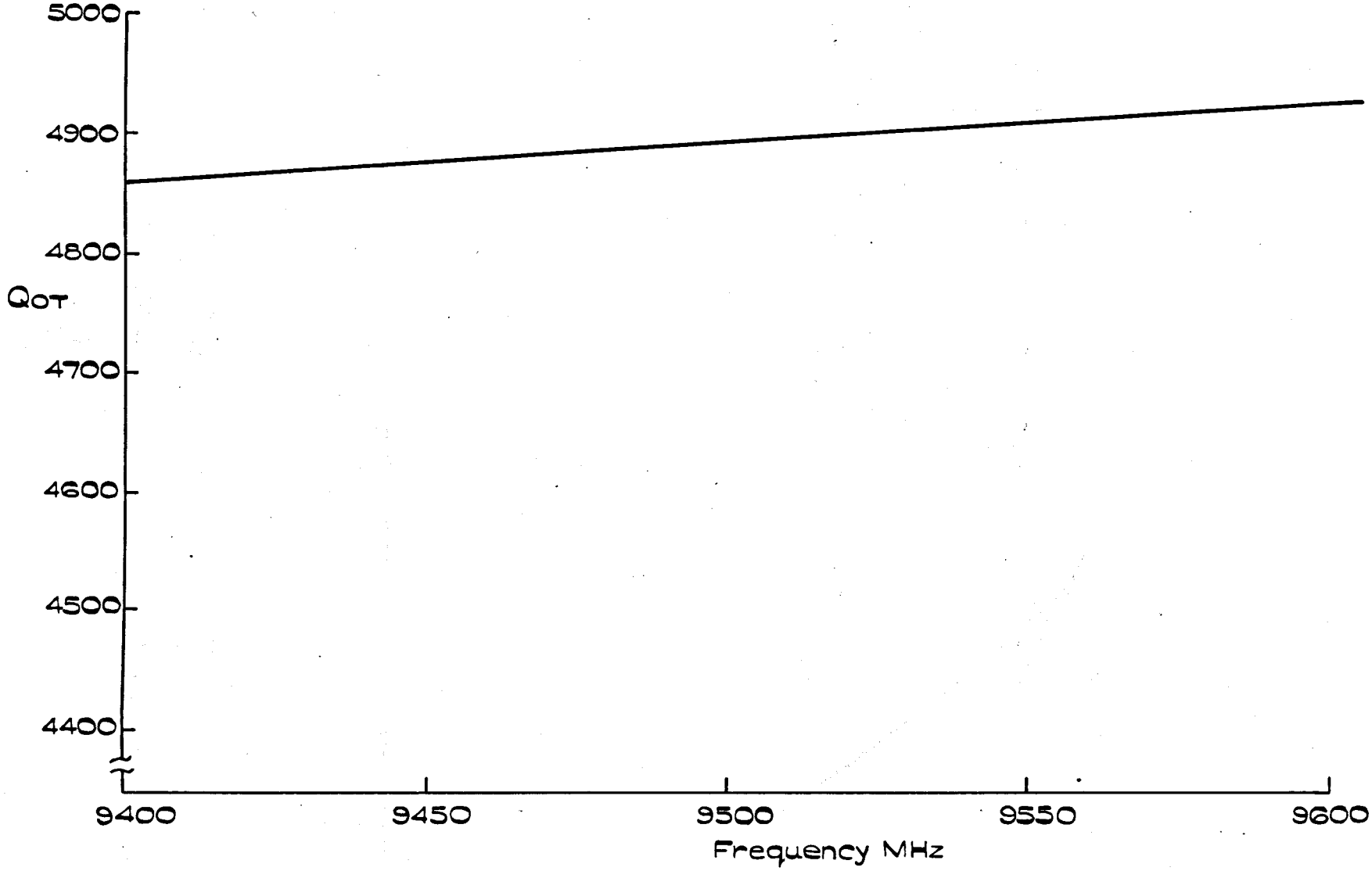

FIGURE 2.5.

FREQUENCY DEPENDENCE OF THE Q FACTOR OF THE CAVITY (Theoretical).

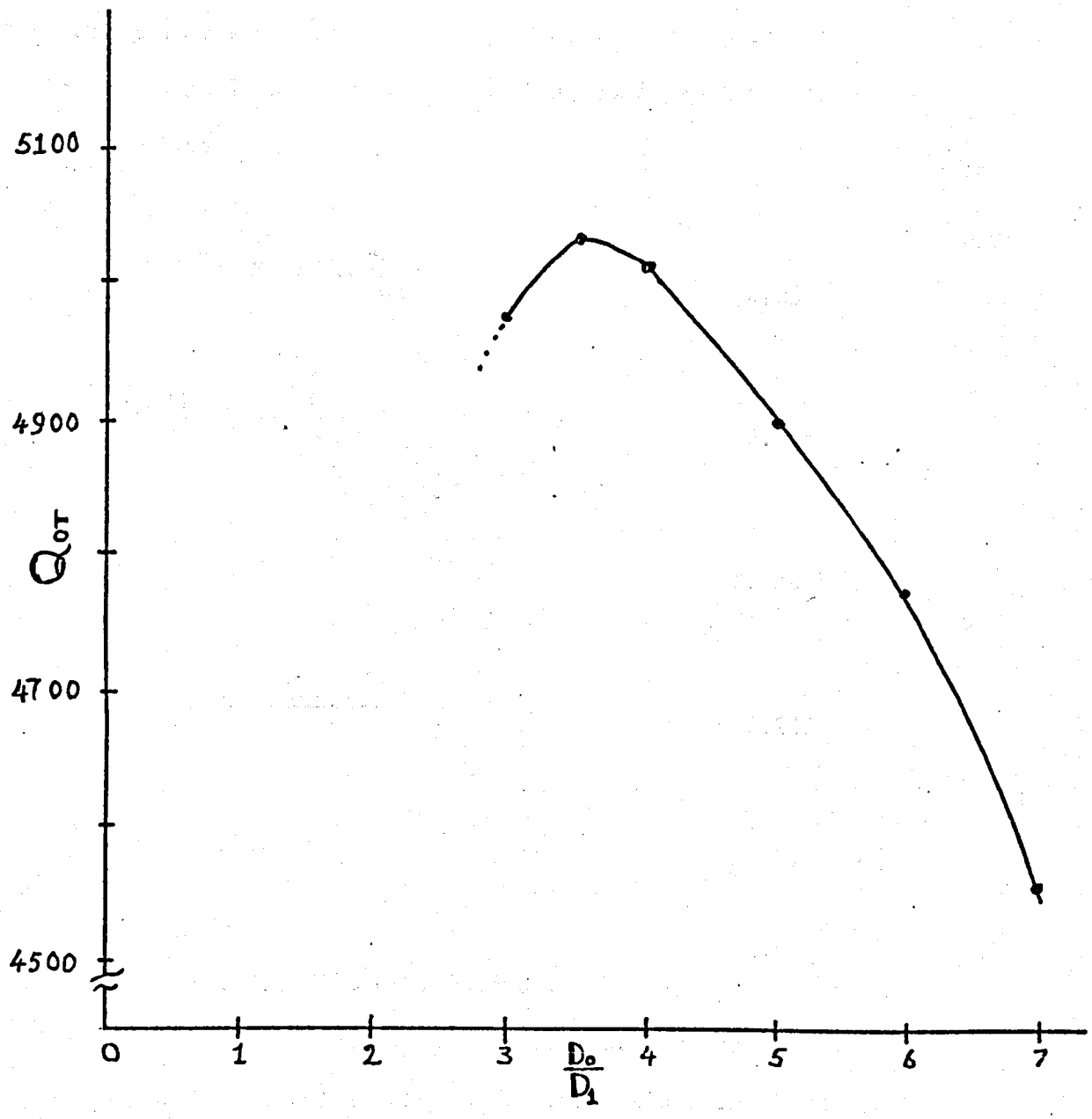

Figure 2.6 Q_{OT} vs $\frac{D_o}{D_i}$

[$D_o = 15$ mm, $G_o = 30\,\mu$m and $L = 32$ mm in all cases.]

2.4 The Dielectric film loaded cavity

2.4. Calculation of real part of relative permittivity.

The cavity is loaded with a thin dielectric film by depositing it in the gap as shown in figure 2.8a the loaded gap capacitance now is represented as in figure 2.8d, the total gap capacitance is now increased to C_{oT2}

where

$$C_{oT2} = m\,Co + \frac{Cox\ Cx}{Cox + Cx} \qquad 2.23$$

$$Cox = \frac{\pi}{4}\,\frac{D1^2\ \epsilon_o}{Go\ (1 - x)} \qquad 2.24a$$

$$Cox = \frac{Co}{1 - x} \qquad 2.24b$$

$$Cx = \frac{\pi}{4}\,\frac{D1^2\ \epsilon_o\ \epsilon^1}{x\ Go} \qquad 2.24c$$

$$= Co\ \frac{\epsilon^1}{x} \qquad 2.24d$$

Cx represents the film capacitance in the gap

Cox the capacitance of air gap portion of the gap

x is the fractional thickness of dielectric film relative to initial gap, Go.

From equations 2.23, 2.24b and 2.24d we get

$$C_{oT2} = \left[m + \frac{\epsilon^1}{x + \epsilon'(1 - x)} \right] Co \qquad 2.25$$

Let f_1 be the resonance frequency and C_{oT1} the capacitance of the gap of cavity without the film and f_2 the resonant frequency of the cavity with the film. Using equation 2.9 and substituting the respective values of f and C_{oT} we obtain

$$\frac{1}{C_{oT1}} = \frac{n}{\pi} \ln \frac{Do}{D1} \, 2\pi f_1 \, \text{Tan} \frac{\pi L}{v} f_1 \qquad 2.26a$$

and

$$\frac{1}{C_{oT2}} = \frac{n}{\pi} \ln \frac{Do}{D1} \, 2\pi f_2 \, \text{Tan} \frac{\pi L}{v} f_2 \qquad 2.26b$$

Dividing equation 2.26a by equation 2.26b

$$\frac{C_{oT2}}{C_{oT1}} = \frac{f_1 \, \text{Tan} \frac{\pi L}{v} f_1}{f_2 \, \text{Tan} \frac{\pi L}{v} f_2} \qquad 2.27a$$

and substituting the values of C_{oT2} and C_{oT1} from equations 2.25 and 2.3 we obtain

$$m + \frac{\epsilon^1}{\frac{x + \epsilon^1 (1 - x)}{m + 1}} = \frac{f_1 \, \text{Tan} \frac{\pi L}{v} f_1}{f_2 \, \text{Tan} \frac{\pi L}{v} f_2} \qquad 2.27b$$

Solving this equation for ϵ^1 gives

$$\epsilon^1 = x \left\{ \left[(m + 1) \frac{f_1 \, \text{Tan} \frac{\pi L}{v} f_1}{f_2 \, \text{Tan} \frac{\pi L}{v} f_2} - m \right]^{-1} + x - 1 \right\}^{-1} \qquad 2.28$$

Comments:

In deriving this expression, it was assumed that the frequency shift is small and the partial filling of the gap with the dielectric film does not change the fringing field capacitance, m Co.

Taking a fixed cavity length L and Go, the unloaded resonant frequency of the cavity can be calculated from equation 2.10., this is plotted in figure 2.3 for a cavity having L = 32 m.m, $\frac{Do}{D1} = 5$ D1 = 3 m.m, over a range of gaps.
Knowing f_1 and m , the cavity is loaded with a dielectric film of relative thickness x, and the new resonant frequency f_2 is measured. ϵ^1 can be calculated from these four quantities.

A graph of ϵ^1 against the frequency shift, $f_1 - f_2$, has been plotted, (figure 2.7), for cavities having different $\frac{Do}{D1}$ ratios and varying gaps, for a 3 μm thick dielectric film.
This graph shows that the rate of change of ϵ^1 with respect to frequency shift, $\frac{\partial \epsilon^1}{\partial (f_1 - f_2)}$, is greater for a cavity having low $\frac{Do}{D1}$ ratio than a cavity having a large $\frac{Do}{D1}$ ratio, especially high dielectric regions of the plots. Therefore for high dielectric constant materials the ratio $\frac{Do}{D1}$ should be large. The disadvantage of the ratios $\frac{Do}{D1}$ greater than 4 is that the unloaded Q factor of the cavity gets smaller than the value obtained for $\frac{Do}{D1}$ between 3 and 4 (this can be seen in figure 2.6). The influence of low QoT on dielectric loss measurement can be seen in section 2.4.2.

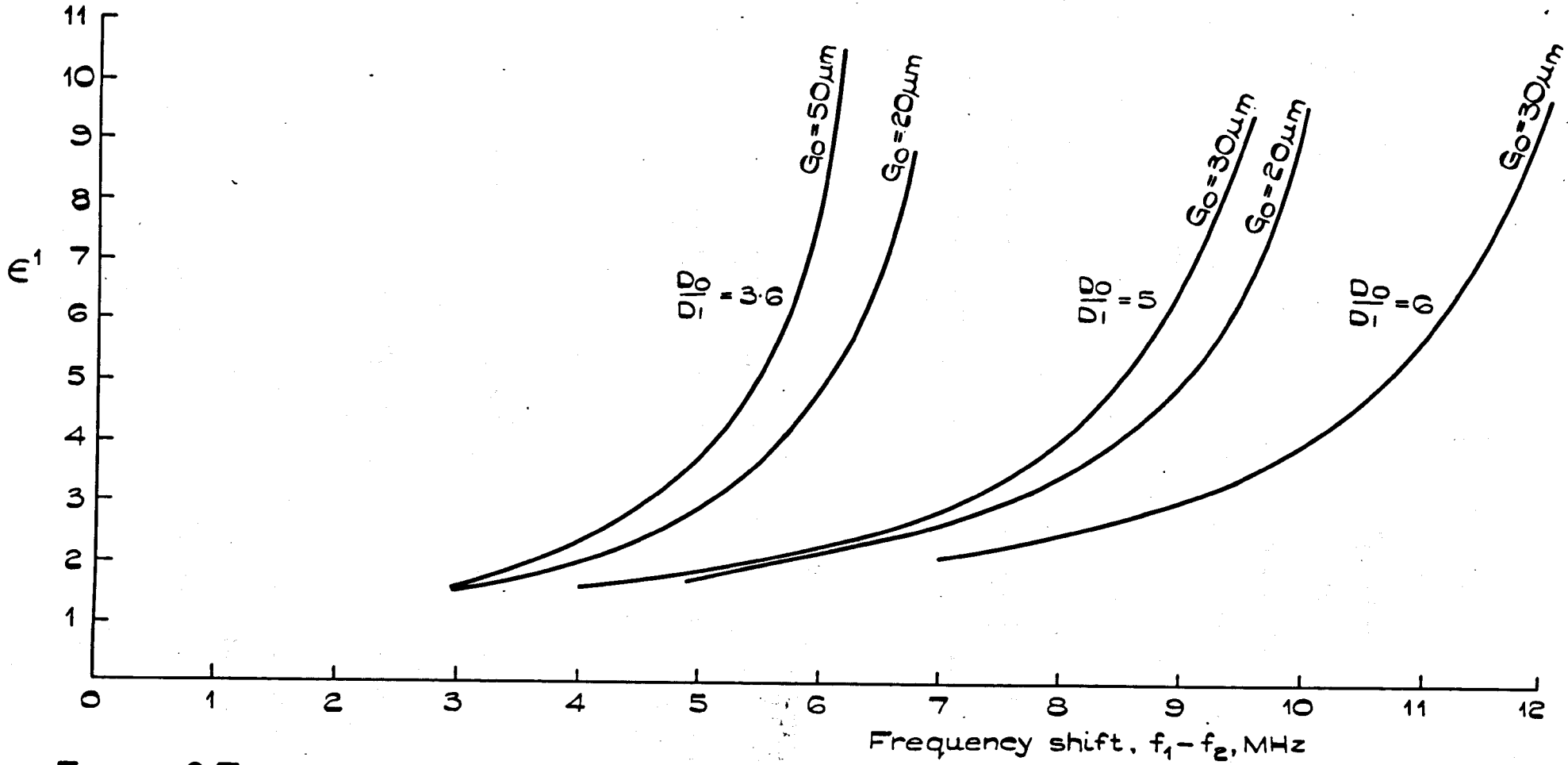

FIGURE 2.7.

ϵ^1 VS SHIFT IN RESONANT FREQUENCY WHEN CAVITY IS LOADED WITH 3μm THICK DIELECTRIC FILM FOR VARIOUS CAVITY PARAMETERS.

2.4.2 Calculation of the Q factor of The Dielectric Film

Here the Q factor of the dielectric film Q_D is calculated using the equivalent circuit approach. The capacitively loaded coaxial cavity is represented as two series tuned circuits. Sections A and C represent one circuit and section B the other. Both of these circuits are resonant at the same frequency. Subscript 1 refers to equivalent circuit components of sections A and C, and subscript 2 refers to the cavity section B. The physical arrangement of the cavity is shown in figure 2.4 and the Q-factor of these tuned circuits have already been derived in section 2.3.2.

Consider the equivalent circuits of the unloaded and loaded cavity as shown in figure 2.8c and d. At resonance, the impedance looking into these tuned circuits will be resistive.

The input impedances are:-

without the film $Z_1 = r_1 + r_2$ 2.29a

and with the film $Z_2 = r_1^1 + r_2^1 + r_x^1$ 2.29b

where r_1^1 and r_2^1 are the resistances of the tuned circuits at the new resonant frequency f_2. The losses in the cavity walls are proportional to the square-root of frequency so that:-

$$r_1^1 = r_1 \left(\frac{f2}{f1} \right)^{\frac{1}{2}} \qquad 2.30a$$

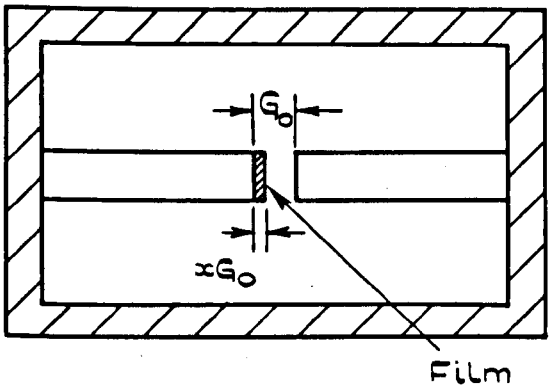

(a) DIELECTRIC LOADED CAVITY

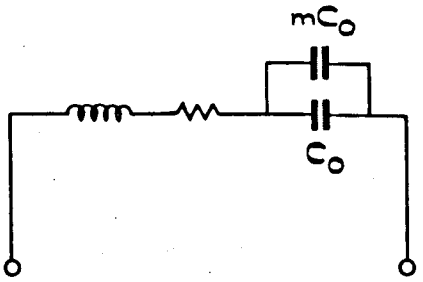

(b) EQUIVALENT CIRCUIT FOR MODE 1.

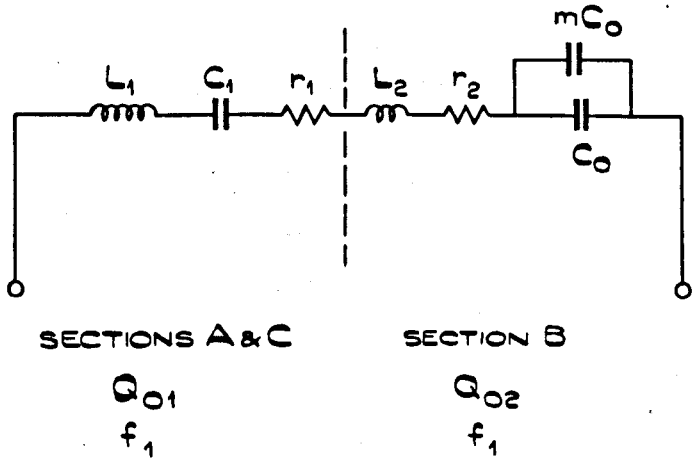

(c) EQUIVALENT CIRCUIT FOR MODE 3.

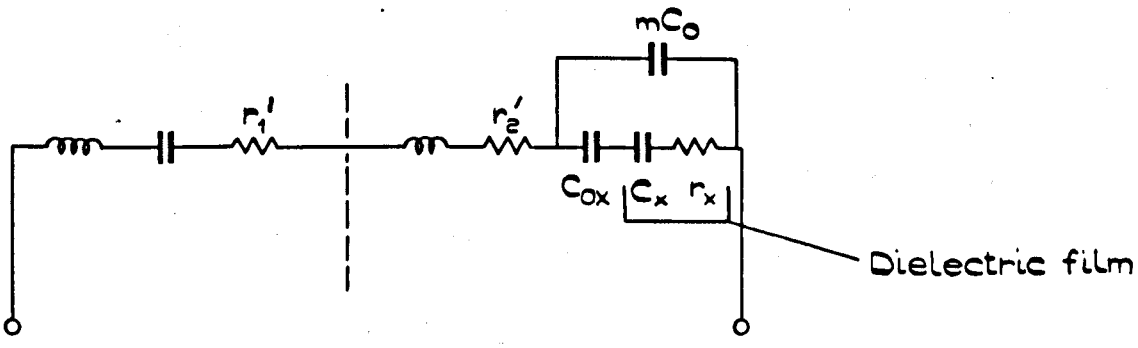

(d) DIELECTRIC LOADED CAVITY (MODE 3)

FIGURE 2.8.

EQUIVALENT CIRCUITS OF THE CAVITY.

$$r_2^1 = r_2 \left(\frac{f2}{f1} \right)^{\frac{1}{2}} \qquad 2.30b$$

r_x^1 is the equivalent loss resistance of the gap impedance.

r_x is the equivalent series loss resistance of the dielectric film. The relationship between r_x and r_x^1 is given in figure 2.9.

The tuned circuits may be considered to be coupled to a measuring system through a mutual inductance M[30] (figure 2.10). The transformed impedance at resonance on the measurement side of the cavity is represented by the following relationships:

$$Zo_1 = \frac{(w_1 M)^2}{r_1 + r_2} \qquad 2.31$$

and with the film

$$Zo_2 = \frac{(w_2 M)^2}{r_1^1 + r_2^1 + r_x^1} \qquad 2.32$$

Dividing equation 2.31 by equation 2.32 and substituting the values of r_1^1 and r_2^1 from equations 2.30a and b we get

$$\frac{Zo_1}{Zo_2} = \left(\frac{f1}{f2} \right)^2 \left[\left(\frac{f2}{f1} \right)^{\frac{1}{2}} + \frac{r_x^1}{r_2 + r_1} \right] \qquad 2.33$$

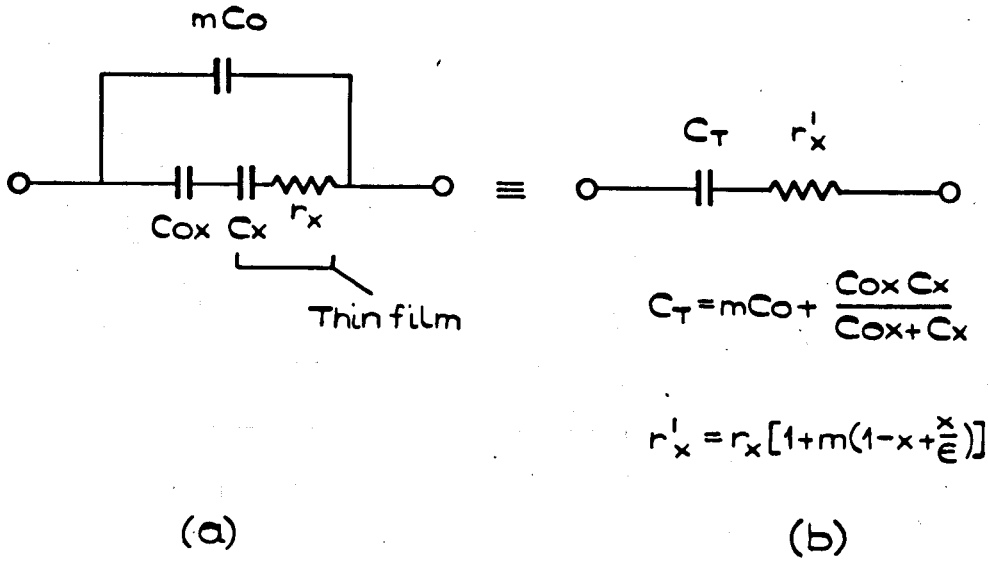

FIGURE 2.9.

(a) EQUIVALENT CIRCUIT OF THE DIELECTRIC LOADED GAP.

(b) SERIES REPRESENTATION OF (a).

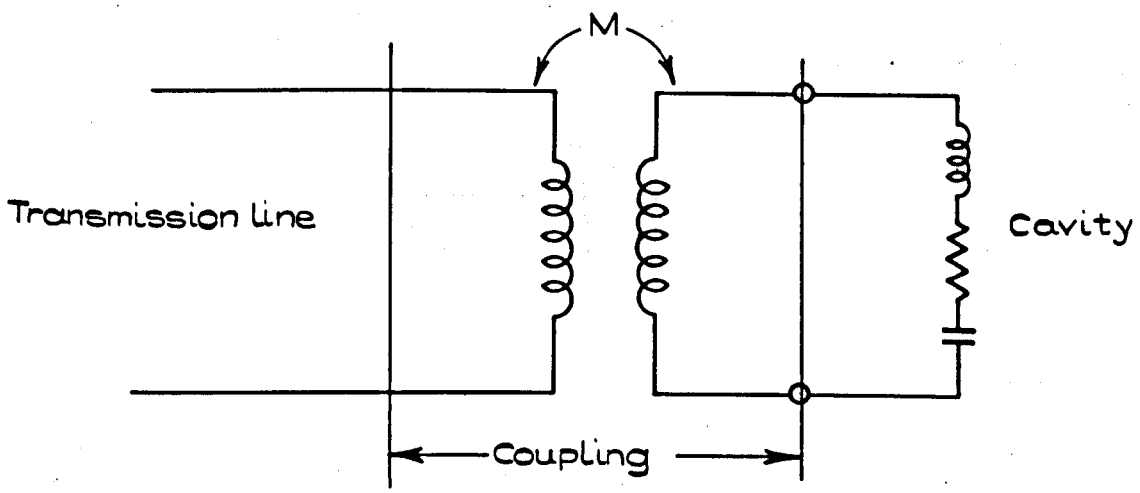

FIGURE 2.10.

EQUIVALENT CIRCUIT OF THE CAVITY AND ITS COUPLING MECHANISM.

Returning to the circuit with no dielectric, figure 2.8c we have from lumped circuit theory

$$QoT = \left[\frac{w_1 L_1 + w_1 L_2}{r_1 + r_2} \right]$$

rearranging QoT

$$= \left[\frac{\frac{w_1 L_1}{r_1} + \frac{r_2}{r_1}\frac{w_1 L_2}{r_2}}{1 + \frac{r_2}{r_1}} \right] \qquad 2.34$$

But

$$Qo1 = \left[\frac{w_1 L_1}{r_1} \right] \qquad 2.35$$

$$Qo2 = \left[\frac{w_2 L_2}{r} \right] \qquad 2.36a$$

also

$$Qo2 = \left[\frac{1}{w_1 Co (1 + m) r_2} \right] \qquad 2.36b$$

Substituting equations 2.36a and 2.35 in equation 2.34 we obtain

$$r_2 + r_1 = r_2 \frac{Qo2}{Qo1} \left[\frac{1 - Qo1/Qo2}{1 - Qo1/QoT} \right] \qquad 2.37a$$

with equation 2.36b this simplifies to

$$r_2 + r_1 = \frac{1}{w_1 C_o (1 + m) Q_{oT}} \left[\frac{1 - Q_{o1}/Q_{o2}}{1 - Q_{o1}/Q_{oT}} \right] \qquad 2.37b$$

Substituting this equation together with the value of r_x^1 (figure 2.9) in equation 2.33, we get

$$\frac{Z_{o1}}{Z_{o2}} = \frac{(f_1)^2}{(f_2)^2} \left[\left(\frac{f_2}{f_1} \right)^2 + \frac{r_x w_1 C_o (1 + m) Q_{oT} \left[1 - Q_{o1}/Q_{oT} \right]}{\left(1 + m \left(1 + \frac{x}{\epsilon} - x \right) \right)^2 \left[1 - Q_{o1}/Q_{o2} \right]} \right] \qquad 2.38$$

The Q factor of the dielectric film

$$Q_D = (w_2 C_x r_x)^{-1} \qquad 2.39a$$

Using $C_x = C_o \frac{\epsilon^1}{x}$ (from equation 2.24)

Therefore

$$r_x = x (w_2 Q_D C_o \epsilon^1)^{-1} \qquad 2.39b$$

Also the normalized input impedances, of an undercoupled cavity, are equal to the inverse of the voltage standing wave ratios at the resonance.

$$\text{i.e.} \quad \frac{Z_{o1}}{Z_o} = S1^{-1} \qquad 2.40$$

$$\frac{Z_{o2}}{Z_o} = S2^{-1} \qquad 2.41$$

Substituting equations 2.40, 2.41 together with equation 2.39a gives

$$\frac{S2}{S1} = \left(\frac{f1}{f2}\right)^2 \left[\left(\frac{f2}{f1}\right)^2 + \frac{\frac{f1}{f2}\,\frac{x}{\epsilon'}(1+m)\,Q_oT}{Q_D\left(1 + m\left(1 + \frac{x}{\epsilon'} - x\right)\right)^2} \right] K$$

and rearranging it

$$Q_D = \left(\frac{S2}{S1} - \left(\frac{f1}{f2}\right)^{3/2} \right)^{-1} \left(\frac{f1}{f2}\right)^3 \frac{x(1+m)\,Q_oT}{\epsilon'} \frac{K}{\left[1 + m\left(1 + \frac{x}{\epsilon'} - x\right)\right]^2} \qquad 2.42$$

where $K = \dfrac{1 - Qo1/QoT}{1 - Qo1/Qo2}$ 2.43

As previously mentioned (section 2.3.2) Qo1 and Qo2 cannot be measured for the practical cavity. Therefore any nonuniformity of the losses in the cavity will destroy the validity of the equation 2.43. This factor K can be measured using a dielectric with a known Q_D.

Assuming a uniform loss distribution inside the cavity, the theoretical values of Qo1, Qo2 and QoT can be used to evaluate K. Using equations 2.20, 2.22 and 2.18 together with equation 2.43 the following simple relationship for K is derived,

$$K = 1 - 2\pi \left[\frac{w1L}{v} + \sin \frac{w1L}{v} \right]^{-1} \qquad 2.44$$

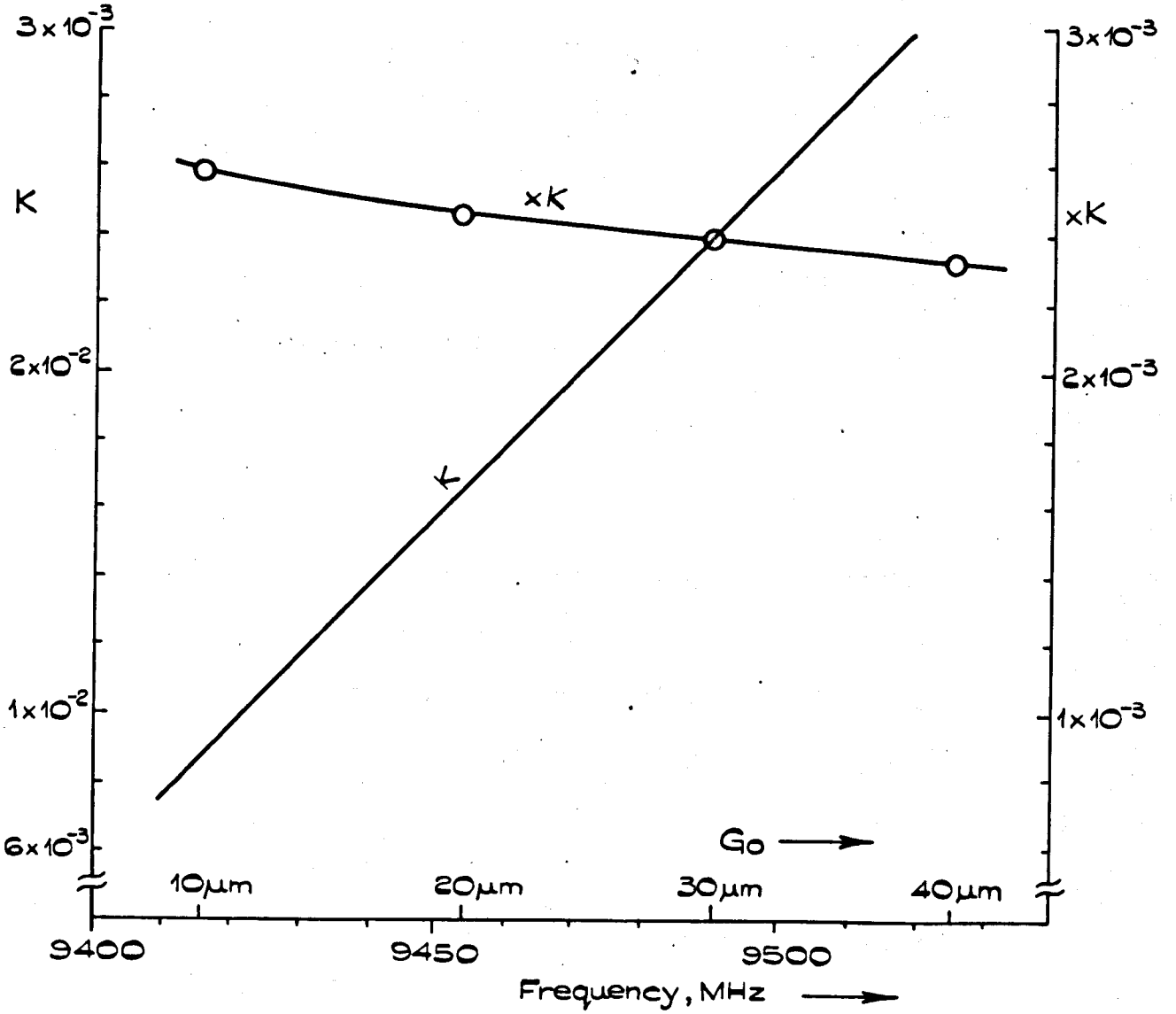

FIGURE 2.11.

FREQUENCY DEPENDENCE OF K.

This expression shows that K is dependent on the L value and the cavity resonant frequency. Therefore this expression can be used for other cavities provided that the cavity has the same L and resonates around the same frequency range. Figure 2.11 shows a plot of K against the resonant frequency for L = 32 m.m.

The above derivation for K applies to the cavity resonance shown in figure 2.2 Mode 3. When the cavity resonates in low frequency mode figure 2.2 Mode 1, the Q_{o1} is zero and Q_{o2} is equal to Q_{oT}, hence the value of K becomes unity.

The equation 2.42 can be used for the Mode 1 as well as Mode 3 provided that the correct value of K is taken.

Comments on Q_D measurement:

The frequency shift of the resonant frequency of the cavity without and with the film is so small that the frequency terms in equation 2.42 can be left out. The terms including the fringing term m has small effect on Q_D measurement.

The important parameters are:

(i) The ratio of VSWR's: Q_D is inversely proportional to $\frac{S2}{S1} - 1$ parameter and should be small for large Q_D values. The minimum value of this parameter that can be used is dependent on the accuracy of the VSWR measurements.

The influence of this parameter on the Q_D error is discussed in section 8.

(ii) The Q factor of the cavity, QoT: Q_D is proportional to QoT and hence large QoT values are required. The variation of QoT with $\frac{Do}{D1}$ ratio is shown in figure 2.6 therefore for a high QcT the $\frac{Do}{D1}$ ratio should be between 3 and 4. This requirement has to be modified because it was shown in section 2.4.1 that the ratio $\frac{Do}{D1}$ should be high especially for the high ϵ^1 materials, therefore a compromised ratio is used.

QoT is approximately proportional to Do. One way to increase QoT is to use a large diameter cavity. The largest diameter that can be used is limited by the propagation of higher order modes[43] in the coaxial cavity.

(iii) The relative dielectric constant ϵ^1: since ϵ^1 is inversely proportional to Q_D, the range of Q_D values that can be measured is limited by the value of ϵ^1. It will be seen from equation 2.4.2 that for high ϵ^1 values, high filling factors, x, should be used.

(iv) The filling factor, x: this is the only factor that can be easily varied. The thickness of the dielectric film can be increased and high x values can be obtained. An additional point is that having a fixed film thickness, x increases with reducing gap Go. This reduces the resonant frequency of the unloaded cavity (figure 2.3) as well as K, which is frequency dependent. But there is still quite an improvement as can be seen from the x K plot shown in figure 2.11.

Above discussions have shown that when a material having a high Q_D is measured, the filling factor should be large.

2.5 Application of the Perturbation Theory to the Measurement of the Thin Film Dielectric Properties.

Perturbation method is a well known tool used in microwave measurement of material properties.[31-35] The limitations of the theory applied to cavities is that the frequency shift, when the sample is introduced into the cavity, should be much less than 1% and the volume of the material introduced should not alter appreciably the field inside the cavity.

Here this method is applied to the capacitively loaded coaxial cavity which was treated in section 2.3. It was shown in section 2.3.1 that the voltage across the gap (equation 2.6) is given by

$$Vab = 2\,Vo \ln \frac{Do}{D1} \sin \frac{(wL)}{2v}$$

With no dielectric film to load the cavity

$$Vab1 = 2\,Vo \ln \frac{Do}{D1} \sin \frac{(w_1 L)}{2v} \qquad 2.45a$$

and with dielectric film loading

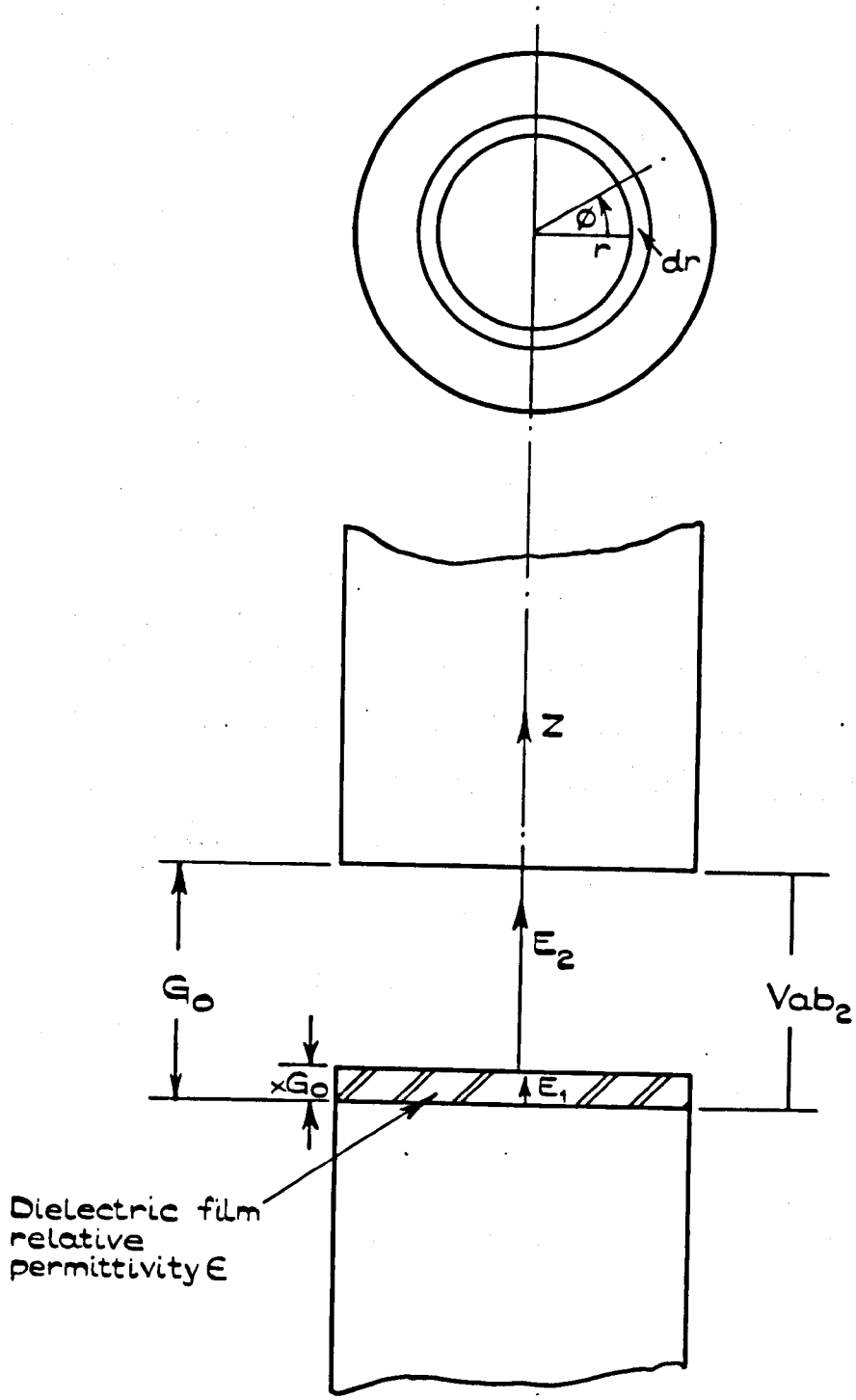

FIGURE 2.12.

ELECTRIC FIELDS IN DIELECTRIC LOADED GAP OF THE CAVITY (only the gap shown).

$$Vab2 = 2\,Vo \ln \frac{Do}{D1} \sin \frac{(w_2 L)}{2v} \qquad 2.45b$$

Let Eo = the electric field in the gap without the film.

Since the electric field does not change with z in the gap (figure 2.12)

$$Eo = \frac{Vab1}{Go}$$

$$= \frac{2\,Vo}{Go} \ln \frac{Do}{D1} \sin \frac{(w_1 L)}{2v} \qquad 2.46$$

When a film partially fills the gap, there will be two electric fields, one in the dielectric material, E1 and the other in the remaining air gap, E2 (figure 2.12). These quantities can be expressed in differential form,

$$E1 = \frac{\partial V}{\partial z} \quad o < z < xGo \qquad 2.47a$$

$$E2 = \frac{\partial V}{\partial z} \quad xGo < z < Go \qquad 2.47b$$

Since E1 and E2 are independent of z within their respective regions

$$V1 = E1\,z + A \qquad 2.48a$$

$$V2 = E2\,z + B \qquad 2.48b$$

The boundary conditions are

$$\begin{aligned} V1 &= o \quad \text{when} \quad z = o \\ V2 &= Vab2 \quad \text{when} \quad z = Go \\ V1 &= V2 \quad \text{when} \quad z = xGo \\ \epsilon E1 &= E2 \end{aligned} \qquad 2.49$$

Substituting the boundary conditions in equations 2.48a and b, we obtain

$$Vab2 = \epsilon E1 \; Go + B$$

$$E1 \times Go = \epsilon E1 \times Go + B$$

which simplify to give

$$E1 = \frac{Vab2}{Go\left[\epsilon(1 - x) + x\right]}$$

and from equation 2.45b

$$E1 = \left[\frac{2Vo}{Go} \; \frac{\ln \frac{Do}{D1} \sin \frac{w_2 L}{2v}}{(\epsilon - \epsilon x + x)}\right] \qquad 2.50$$

The perturbation theory applied to a cavity loaded with a non-magnetic dielectric film, gives the following relationship[31-35]

$$\frac{\delta f}{f} + j\delta\left\{\frac{1}{2Q}\right\} = \frac{-\epsilon_o (\epsilon - 1) \int_v Eo \; E1 \; d v}{4 \; (\text{Energy stored in the Cavity})} \qquad 2.51$$

where $\frac{\delta f}{f}$ = fractional frequency shift of the resonant frequency when the sample is introduced

$$\delta\left(\frac{1}{2Q}\right) = Q_{ox}^{-1} - Q_o^{-1}$$

Q_o = Unloaded Q factor of the cavity without the film

Q_{ox} = Unloaded Q factor of the cavity with the film

E1 = Electric field inside the dielectric film

Eo = Electric field in the same place but without the dielectric film

$\int_v$ = volume integral over the volume of the film.

E1 and Eo are independent of z therefore equation 2.51 can be written for the set up shown in figure 2.11 as follows:

$$\frac{\delta f}{f} + j\,\delta\left(\frac{1}{2Q}\right) = \epsilon_o\,(\epsilon - 1)\,\frac{\int_0^{\frac{D1}{2}} \int_0^{2\pi} \int_0^{x\,Go} Eo\,E1\,r\,d\phi\,dr\,dz}{4 \text{ Energy stored in the cavity}}$$

$$= \epsilon_o\,\frac{(\epsilon - 1)\,Eo\,E1\,\frac{D1^2}{8}\,2\pi\,x\,Go}{4 \text{ Energy stored in the cavity}}$$

substitution of the values of Eo, E, from equations 2.46 and 2.50; energy stored in the cavity from equations 2.11 and 2.15 and $\frac{D1^2}{Go}$ from equation 2.10 (as shown in Appendix.5) gives the following relationship:

$$\frac{\delta f}{f} + j\,\delta\left(\frac{1}{2Q}\right) = \frac{(\epsilon - 1)\,x}{(\epsilon - \epsilon x + x)}\,P \qquad 2.52$$

But $$\epsilon = \epsilon^1 - j\epsilon^{11}$$

$$= \epsilon^1 - j\frac{\epsilon^1}{Q_D}$$

substituting this in equation 2.52 and equating the real and imaginary parts, the following relationships are derived:

$$\epsilon^1 = \frac{1 + P\frac{\delta f}{f1}}{1 - \left(\frac{1-x}{x}\right) P\frac{\delta f}{f}} \qquad 2.53$$

$$Q_D = \left[\epsilon^1 \left(1 - x + \frac{x}{\epsilon}\right)^2 \frac{P}{x}\,\delta\left(\frac{1}{2Q}\right)\right]^{-1} \qquad 2.54$$

where $$P = (m+1)\left[\frac{w_1 L}{v} + \sin\left(\frac{w_1 L}{v}\right)\right]\left[2\sin\left(\frac{w_2 L}{2v}\right)\cos\left(\frac{w_1 L}{2v}\right)\right]^{-1} \qquad 2.55$$

Comments: In this method all the quantities used in Q_D calculations can be measured. This is the advantage of the method over the VSWR method. The accuracy of the Q_D measurement depends, in this case, on the accuracy of measurement of Q values without and with the dielectric film.

The error analysis of the two methods are given in section 8.

2.6 Measurement of Self Supporting Dielectrics

The properties of self supporting thin dielectric specimens such as m.i.c. substrates are easier to measure than thin dielectric films. For these measurements perturbation of field method will be used. The cavity in this case is a rectangular waveguide cavity resonating in H1on mode.

The field distribution in such a cavity for n = 2 is shown in figure 2.13. At resonance the fields in the cavity are represented by the following relationships[36]

$$E_y = Ea \sin \frac{\pi x}{a} \sin \frac{n \pi z}{d} \qquad 2.56a$$

$$Hx = -j \frac{Ea}{\eta} \frac{\lambda}{2d} \sin \frac{\pi x}{a} \cos \frac{n \pi z}{d} \qquad 2.56b$$

$$Hz = j \frac{Ea}{\eta} \frac{\lambda}{2a} \cos \frac{\pi x}{a} \sin \frac{n \pi z}{d} \qquad 2.56c$$

At a position $\frac{\lambda g}{4}$ from the short circuit plane

$$E_y = Ea \sin \frac{\pi x}{a} \qquad 2.57$$
$$Hx = o$$
$$Hz = o$$

Let a thin dielectric sheet be placed across the waveguide at this point as in figure 2.13. For thin dielectrics the electric field inside the specimen Ei and at the same point when the specimen is removed Eo will be equal.

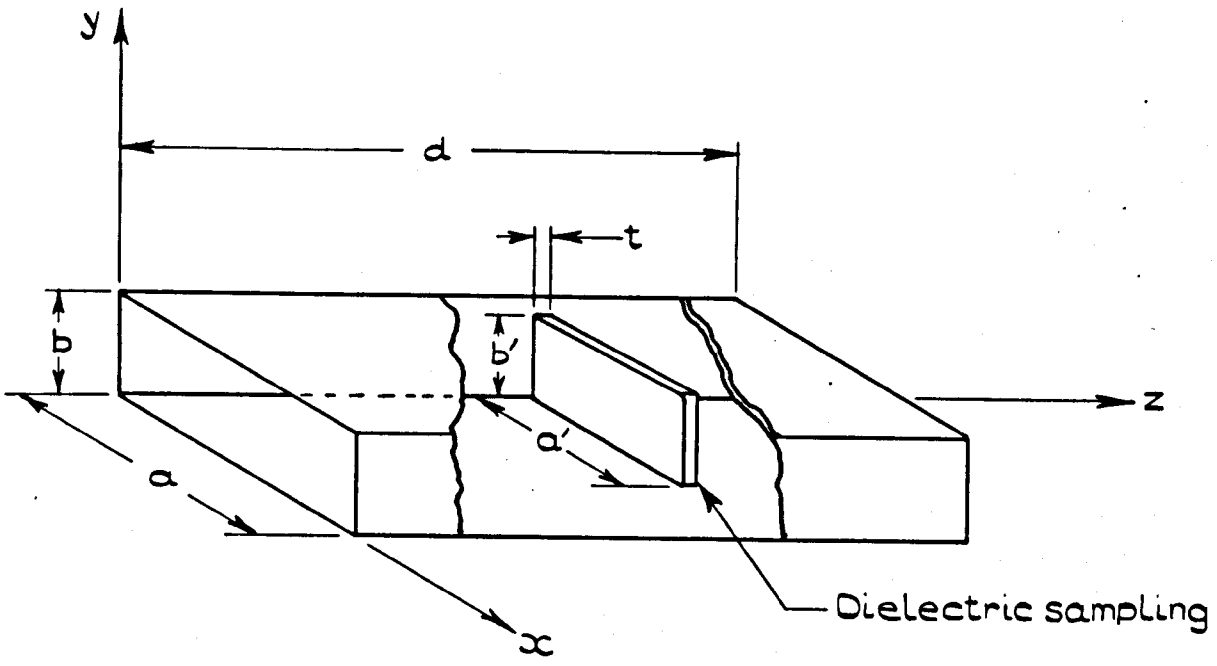

(a) CAVITY LOADED WITH DIELECTRIC SAMPLE.

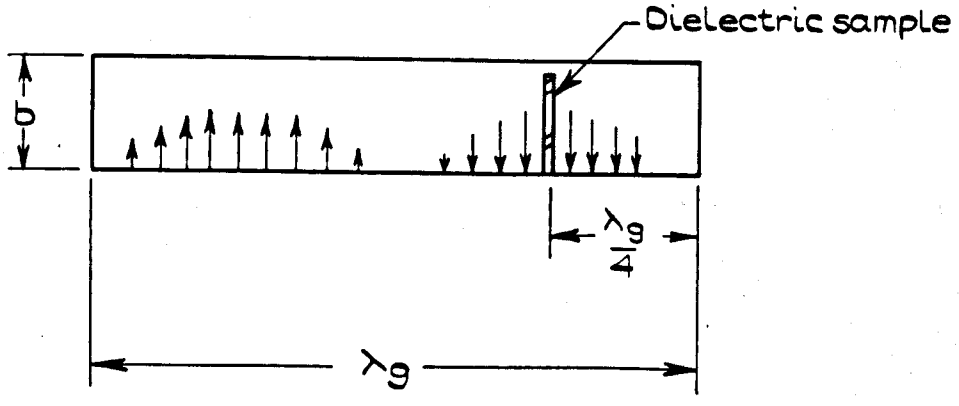

(b) ELECTRIC FIELD DISTRIBUTION IN THE CAVITY

FIGURE 2.13.

RECTANGULAR WAVEGUIDE RESONATOR FOR PERMITTIVITY MEASUREMENT.

Therefore the two electric fields are

$$E_i = E_o = E_y = E_a \sin \frac{\pi x}{a} \qquad 2.58$$

Substituting these values in the cavity perturbation expression (equation 2.51) gives[35]

$$\frac{\delta f}{f} + j\,\delta\left(\frac{1}{2Q}\right) = \frac{-(\epsilon - 1)\epsilon_o \int_0^t \int_0^{a^1} \int_0^{b'} \left(E_a \sin \frac{\pi x}{a}\right)^2 dz\,dx\,dy}{2\epsilon_o \int_0^a \int_0^b \int_0^d \left(E_a \sin \frac{\pi x}{a} \sin \frac{n\pi z}{d}\right)^2 dz\,dy\,dx}$$

$$= (\epsilon - 1)\frac{t}{d}\frac{b'}{b}\frac{a^1}{a}\left[1 - \frac{a}{2\pi a'} \sin \frac{2\pi a^1}{a}\right] \qquad 2.59$$

But $\epsilon = \epsilon^1 - j\frac{\epsilon^1}{Q_D}$

Using this value of ϵ and equating the real and imaginary parts of equation 2.59 gives

$$\epsilon^1 = 1 + N\frac{\delta f}{f} \qquad 2.60$$

$$Q_D^{-1} = \frac{N}{\epsilon'}\,\delta\left(\frac{1}{2Q}\right) \rightarrow Q_{ox}^{-1} - Q_o^{-1} \qquad 2.61$$

$$\text{i.e } \tan\delta = \frac{N}{\epsilon'}\left[\frac{1}{Q_{ox}} - \frac{1}{Q_o}\right] + Q_D = \frac{1}{\tan\delta}$$

$$\text{where } N = \frac{ad}{a^1 t}\frac{b}{b'}\left[1 - \frac{a}{2\pi a'} \sin \frac{(2\pi a^1)}{a}\right]^{-1} \qquad 2.62$$

This is quite an easy and practical technique for the measurement of the self supporting dielectric materials. The same technique may also be used for supported thin dielectric films. The supporting material should be thin and low loss so that the film dielectric properties are not masked.

Park[22] used an approach similar to this for the supported films. He used a cylindrical cavity resonating in Ho1 n mode. Although his cavity had a higher Q factor than a rectangular waveguide cavity it required special type of substrates to suit the electric field distribution and the mathematical treatment was more involved than the present treatment.

Practical difficulties of this system for the self supported dielectric specimens will be discussed in sections 7.4 .. .

Chapter 3

THEORECTICAL APPROACH TO MICROWAVE LUMPED ELEMENT MEASUREMENTS

3.1 Introduction.

The microwave lumped elements, LE's, are quite small i.e. overall dimensions are much less than a wavelength. It is very difficult to measure these minute elements. Early attempts using coaxial or microstrip lines and connecting the LE's across the end of the line did not give accurate results especially for high Q LE's for frequencies above 3GHz. To overcome these difficulties resonant lines were used successfully.[23.24]

In this section the theoretical approach to the LE's measurement will be presented. The method uses a symmetrical, capacitively loaded microstrip resonator similar to the coaxial cavity used for dielectric measurements.

At first a technique will be introduced where the microstrip line properties will be determined. Then lumped element measurement technique will be introduced.

3.2 Properties of Microstrip Transmission Lines.

When a microstrip line is incorporated in a measuring system its properties, such as its characteristic impedance Zo, phase velocity and the attenuation constant, should be known. Since Wheeler's[2] simple expressions based on TEM mode approximation on microstrip, several theoretical works have been reported but none of them agree with the measured properties of the microstrip. The properties of a microstrip

depend upon the strip width, substrate material and the material of the conductors. The characteristic impedance and the phase velocity of the microstrip line are dependent on the width of the strip, the thickness and the permittivity of the substrate material. It was found that the microstrip lines have dispersion i.e. the phase velocity is dependent on frequency. The cause of the dispersion is attributed to the launching of surface waves.[38]

Various techniques have been used to measure the variation of phase velocity with frequency.[34-40] Some of these were direct phase measurement whilst the others were indirect methods. In the indirect method the effective dielectric constant is measured. Most of the reported measurement methods of effective dielectric constants present certain practical difficulties. For example the resonant ring method, although very accurate for narrow strips, loses its accuracy for wide strips.

To simplify the experimental technique for the effective dielectric constant, ϵ_e, measurements a new approach is proposed. This method uses a microstrip shorted at both ends, that is a half wavelength resonant line. This will be resonant whenever the line length becomes a multiple of a half wavelength at that frequency, (figure 3.1 but no gap).

For a dispersionless line the relationship between effective dielectric constant ϵ_e and the relative dielectric constant of substrate ϵ is given by

$$\epsilon_e = 1 + q(\epsilon - 1)$$

where q is the filling factor (the ratio of dielectric area to the total area of the Wheeler's conformal mapping).

Assuming an air line with no dispersion, shorted at both ends, the resonance frequency will be

$$fo = \frac{n\ v\ o}{2\ L}$$

where n = number of half wavelengths

vo= velocity of e m waves in air, 3×10^8 m/s

L = Length of the resonant line

Let f o x = resonant frequency of the same line but with dispersion. v will be reduced to vo $(\epsilon_e)^{-\frac{1}{2}}$

then $f_{ox} = \frac{n}{2L} \frac{vo}{(\epsilon_e)^{\frac{1}{2}}}$

and $\epsilon_e = \left(\frac{n}{2L} \frac{vo}{fox}\right)^2$ 3.1

Knowing the value of n and the resonance frequency of the line, ϵ_e can be calculated from equation 3.1. It will be seen from this equation that the accuracy of measurement of the ϵ_e is dependent on L and fox

The practical side of this measurement technique is discussed in section 10.

3.3 Resonant Method of Determining the Lumped Element Values.

3.3.1 Capacitively Loaded Microstrip Resonator

Take a resonant transmission line similar to the capacitively loaded coaxial resonator (section 2.5) but in microstrip. This microstrip resonator is shown in figure 3.1. The circuit can be represented by two transmission lines having characteristic

impedances Zo. The lines are short circuited on one end and the other ends are connected onto the two ports of the capacitive π network representing the gap capacitances (figure 3.2a).

The input impedance of these short circuited lines at the gap π terminals

$$Z_{in1} = Zin\ 2$$

$$= Z_o \tanh \left(\alpha_1 + j \frac{w_1}{v} \right) \ell \qquad 3.2$$

where α_1 = attenuation of the line in nepers per unit length

$\frac{w_1}{v}$ = phase constant per unit length

Asumming that the line losses are small, equation 3.2 simplifies to

$$Z_{in1} = Z_o \frac{\alpha_1 \ell + j \tan\left(\frac{w1}{v}\ell\right)}{1 + j\alpha_1 \ell \tan\left(\frac{w_1 \ell}{v}\right)} \qquad 3.2$$

The total series impedance of the resonant circuit at the gap, Cp, is

$$Z_T = \frac{1}{jw_1 C} + 2 Z_{in1}$$

$$= \frac{1}{jw_1 C} + 2 Z_o \left[\frac{\alpha_1 \ell + j \tan\left(\frac{w_1 \ell}{v}\right)}{1 + j\alpha_1 \ell \tan\left(\frac{w_1 \ell}{v}\right)} \right] \qquad 3.3$$

The unloaded Q factor, Q_o of a transmission line can be derived from the following relationship[41]

$$Q_o = \frac{w_1 \left.\frac{\partial x}{\partial w}\right|_{w = w_1}}{2 \text{ Re } Z_T \Big|_{w = w_1}} \qquad 3.5$$

where $\left.\frac{\partial x}{\partial w}\right|_{w = w_1}$ = differential of the reactive part of Z_T with respect to w at resonance

$\text{Re } Z_T \Big|_{w = w_1}$ = Real part of Z_T at resonance

Differentiating equation 3.3 with respect to w, substituting in equation 3.5 and neglecting $(\alpha \ell)^2$ term we obtain

$$Q_o = \frac{1}{2} \left[\frac{\frac{1}{wC} + 2Z_o \frac{w_1 \ell}{v} \sec^2\left(\frac{w_1 \ell}{v}\right)}{2Z_o \alpha_1 \ell \left[1 + \tan\left(\frac{w_1 \ell}{v}\right)\right]} \right] \qquad 3.6$$

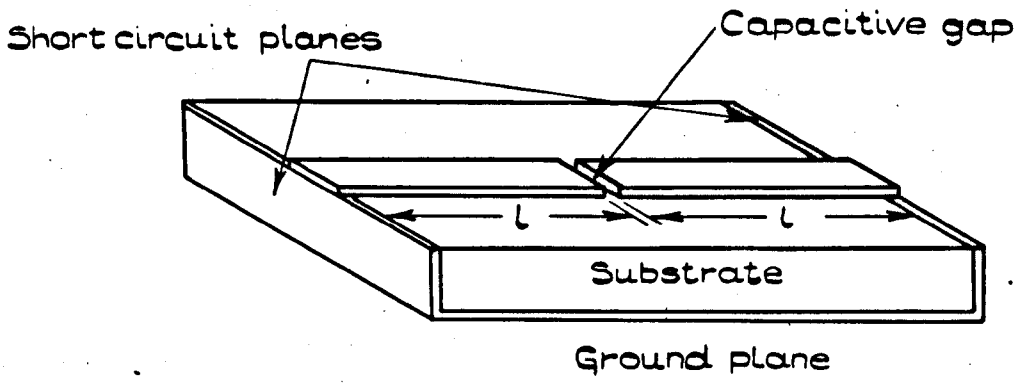

FIGURE 3.1.

CAPACITIVELY LOADED MICROSTRIP RESONATOR.

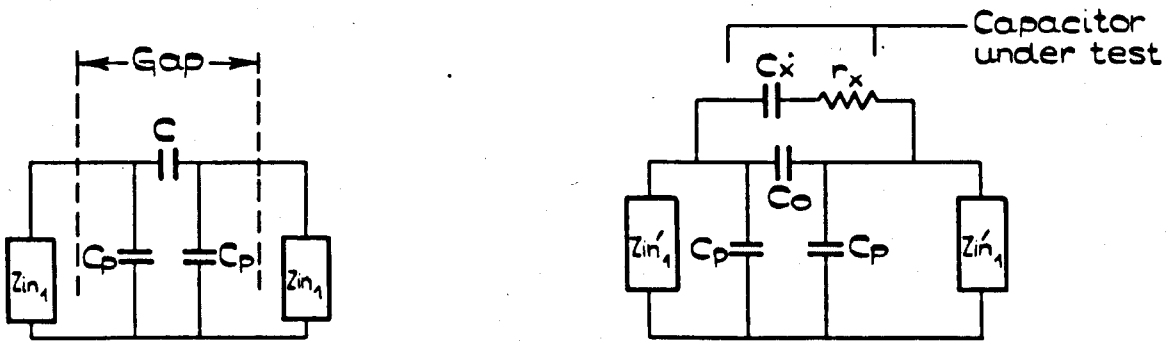

(a) UNLOADED RESONATOR (b) LOADED RESONATOR

FIGURE 3.2.

EQUIVALENT CIRCUITS OF THE RESONATOR.

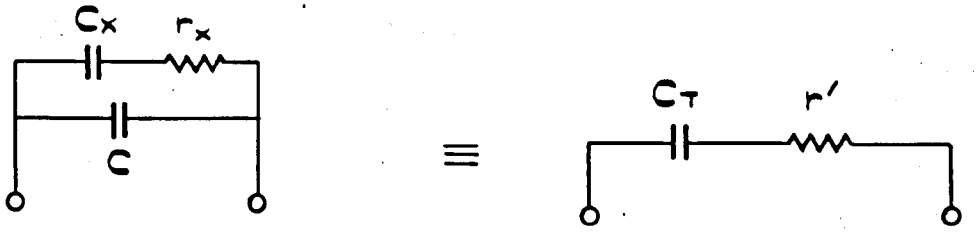

$$C_T = C_x + C \qquad r' = \frac{r_x}{\left(\frac{C}{C_x}+1\right)^2} = \frac{1}{W_2 C_x \left(\frac{C}{C_x}+1\right)^2 Q_x}$$

FIGURE 3.3.

EQUIVALENT CIRCUITS USED IN CALCULATIONS.

But at resonance the imaginary parts of the equation 3.3 tune out, neglecting $(\alpha \ell)^2$ we get

$$\frac{1}{w_1 C} = 2Zo \tan\left(\frac{w_1 \ell}{v}\right) \qquad 3.7$$

Equations 3.6 and 3.7 give:

$$Qo = \frac{1}{4\alpha_1 \ell}\left[\frac{2 w_1 \ell_1}{v} + \sin\left(\frac{2 w_1 \ell_1}{v}\right)\right] \qquad 3.8$$

In the above derivations the capacitance Cp as shown in figure 3.2a has been neglected and also short circuit plane losses are assumed to be included in the line losses.

3.3.2 Measurement of a Capacitor using the Microstrip Resonator.

A lumped element capacitor having a capacitance Cx and equivalent series loss resistance r_x (r_x takes into account the electrode losses plus the dielectric loss) is shunted across C (figure 3.2b). The new circuit will have a capacitance

$$C_T = C + Cx \qquad 3.9a$$

and loss resistance

$$r^1 = r_x \left(\frac{C}{Cx} + 1\right)^{-2}$$

$$= \left[w_2 \, Cx \left(\frac{C}{Cx} + 1\right)^2 \, Q_x\right]^{-1} \qquad 3.9b$$

where Qx = Q factor of the capacitor

$$Q_x = (w_2 \, Cx \, r_x)^{-1}$$

w_2 = the frequency of capacitor loaded resonator

Using equations 3.7 and 3.9(a) we get the new condition for the resonance

$$\frac{1}{w_2 C_T} = 2Zo \tan\left(\frac{w_2 \ell}{v}\right) \qquad 3.10$$

Solving this equation for Cx with the help of equations 3.7 and 3.9a we obtain

$$Cx = \left[\frac{\cot\left(\frac{w_2 \ell}{v}\right) - \left(\frac{w_2}{w_1}\right) \cot\left(\frac{w_1 \ell}{v}\right)}{2 \, Zo \quad w_2}\right] \qquad 3.11$$

Calculation of Q factor of the Capacitor:-

The new reactance (neglecting line losses)

$$X_2 = \frac{1}{wC_T} + 2 \, Zo \tan\left(\frac{w \ell}{v}\right) \qquad 3.12$$

$$\left.\frac{\partial X_2}{\partial w}\right|_{w = w_2} = \frac{1}{w_2 C_T} + 2Zo \sec^2\left(\frac{w_2 \ell}{v}\right) \qquad 3.13$$

$$\text{and } R_e Z_{T2}\Big|_{w = w_2} = r^1 + 2Zo\alpha_2\ell\left[1 + \tan^2\left(\frac{w_2\ell}{v}\right)\right]$$

$$= \frac{1}{Qx}\frac{w_2 Cx}{(w_2 C_T)}^2 + 2Zo\alpha_2\ell\left[1 + \tan^2\left(\frac{w_2\ell}{v}\right)\right]$$

In this derivation $(\alpha_2 \ell)^2$ are neglected because $(\alpha_2\ell)^2 << 1$.

Substituting the values of w_2Cx and w_2C_T from equation 3.11, 3.10

$$R_e Z_{T2}\Big|_{w = w_1} = \frac{1}{Qx} 2Zo \tan^2\left(\frac{w_2\ell}{v}\right)\left[\cot\left(\frac{w_2\ell}{v}\right) - \frac{w_2}{w_1}\cot\left(\frac{w_1\ell}{v}\right)\right]$$

$$+ 2Zo\alpha_2\ell \sec^2\left(\frac{w_2\ell}{v}\right) \qquad 3.14$$

Let Qox = the Q factor of loaded resonator

$$\frac{1}{Qox} = \frac{2 \text{ Re } Z_{T2}}{w_2 \left.\frac{\partial X}{\partial w}\right|_{w = w_2}}$$

Substituting these values from equation 3.13 and 3.14 together with the value of C_T from equation 3.10 we obtain

$$\frac{1}{Q_{ox}} = 4\left\{\frac{\frac{1}{Q_x}\sin^2\left(\frac{w_2\ell}{v}\right)\left[\cot\frac{w_2\ell}{v} - \left(\frac{w_2}{w_1}\right)\cot\left(\frac{w_1\ell}{v}\right)\right] + \alpha_2\ell}{\sin\left(\frac{2w_2\ell}{v}\right) + \left(\frac{2w_2\ell}{v}\right)}\right\} \qquad 3.15$$

Attenuation of the microstrip is proportional to the square root of the frequency i.e.

$$\alpha_2\ell = \alpha_1\ell\left(\frac{f_2}{f_1}\right)^{\frac{1}{2}} \qquad 3.16a$$

Using equation 3.8 and 3.16a we obtain

$$\alpha_2\ell = \left(\frac{f_2}{f_1}\right)^{\frac{1}{2}}\left[\frac{\left(\frac{2w_2\ell}{v}\right) + \sin\left(\frac{2w_2\ell}{v}\right)}{4\,Q_o}\right] \qquad 3.17$$

The Q factor of the Capacitor, Qx, can be evaluated from equations 3.15 and 3.17

$$Q_x = \frac{\frac{\left[\sin\left(\frac{2w_2\ell}{v}\right) + \left(\frac{2w_2\ell}{v}\right)\right]}{Q_{ox}} - \left(\frac{w_1}{w_2}\right)^{\frac{1}{2}}\frac{\left[\sin\left(\frac{2w_1\ell}{v}\right) + \frac{2w_1\ell}{v}\right]}{Q_o}}{4\sin^2\left(\frac{w_2\ell}{v}\right)\left[\cot\left(\frac{w_2\ell}{v}\right) - \frac{w_2}{w_1}\cot\left(\frac{w_1\ell}{v}\right)\right]} \qquad 3.18$$

Equations 3.7, 3.8, 3.11 and 3.17 are used in evaluation of the capacitance Cx and the Q factor of the capacitor. Qx has two components. One of them is the dielectric Q factor Q_D and the other is the conductor loss factor Qc. RCA people[8,17] give the following equation for Qc

$$Qc = \left[\frac{2}{3} \; Rs \; \frac{y}{W} \; w_2 \; Cx\right]^{-1} \qquad 3.19$$

where Rs = surface resistivity of conductor ($\propto f^{\frac{1}{2}}$)

y = length of the capacitor

W = width of the capacitor.

this relationship shows that $Qc \propto f^{-3/2}$

The relationship between these three Q factors is

$$Qx^{-1} = Qc^{-1} + Q_D^{-1} \qquad 3.20$$

Therefore a plot of Qx^{-1} against $f^{3/2}$ should give a straight line and the intersection on Qx^{-1} axis will be equal to Q_D, if Q_D is independent of frequency.

3.3.3 Comments

The above mathematical treatment of the capacitor measurement shows that lumped element parameters can be measured using a capacitively loaded microstrip resonator. Although the above equations were derived for a capacitor, similar equations could be derived for an inductor.

Chapter 4

MECHANICAL DESIGN AND MATERIAL PROBLEMS OF THE COAXIAL CAVITY

4.1 Introduction.

It was shown in section 2.4 that the filling factor, x, i.e. the ratio of the thickness of the dielectric film to the gap width, Go, should be large. The dielectric film thickness used in m.i.c's ranges from 0.5 μm up to 10 μm and therefore Go should be limited to a width less than 50 μm. The advantages of small gap widths on the measurement of thin dielectric films using a Capacitively loaded Coaxial Cavity is shown in figures 2.7 (for ϵ^1) and 2.9(for xK).

Figure 4.1 shows an axial cross section of the cavity. The dielectric film to be measured is deposited onto the plane end of the inner conductor at the gap. Therefore the cavity was designed in two parts named the top and the base, so that there could be an easy access to the gap. The inner conductor of one of the parts extends to the full length of the outer conductor. This was chosen so that the film could be deposited and after the measurement removed quite easily. The other part of the cavity, the base part, had its inner conductor shortened by a length equal to the required gap width Go, but still keeping the length of the inner conductor equal to that of the top part of the cavity. The Coupling of the cavity to the measuring system was also incorporated on the base.

During the thin film measuring process the cavity parts were disassembled and assembled again many times. Any misalignment of

the two parts could have introduced large errors in the measured quantities (section 8). This is a mechanical problem and proper design can eliminate it. This is discussed in detail in section 4.2.2.

Another important point was the material of the cavity. The cavity should be constructed from a material having the following properties:

(i) very low coefficient of expansion so that any small change in temperature does not upset the measurement.

(ii) high conductivity. The Q factor of the cavity is proportional to the square root of the conductivity of the material lining the inside of the cavity.

(iii) material compatibility: The top part of the cavity passes through a series of thin film processing steps and cavity properties should not change during these steps. Most important of these processings, is the high temperature required during deposition of the film.

The manufacturing and the material problems are discussed in the following sections.

4.2 Mechanical Construction of the Cavities

The design chosen for the capacitively loaded Coaxial Cavity has been described above. This design was used on cavities made from brass and invar. The construction of these cavities is described below. Although brass cavities were not used in the thin film dielectric measurements, they were used in determining the properties of the cavity.

4.2.1 Brass Cavities.

The first cavity was made of brass. The inners of the two parts were screwed on to the short circuit plane ends and joints were painted with a silver paint. This gave an easy system assembly but it was lacking mechanical as well as temperature stability. The dimensions of this cavity, CB1, are given in table 4.1

The CB1 was used to check the theory derived in section 2.3. This approach although confirming the theory was abandoned and a new brass cavity CB2, was constructed, bored out of solid brass blocks.

This solid brass cavity was used in investigation of the most suitable coupling system. These coupling systems are described in sections 4.2.2 and 6.2.

The CB2 was more stable than CB1, but the high coefficient of expansion and softness of the brass makes an unsuitable material for this type of measuring system. If a brass cavity is used it requires a temperature stabilizing unit. Another problem is that the zinc component of brass, when heated in vacuum, sublimes and contaminates the vacuum system as well as the deposited film. Although these shortcomings of brass cavities could be overcome, this material was abandoned.

4.2.2. Invar Cavities

Invar[49] is an alloy of iron 64% and nickel 36% and has a very low thermal coefficient of expansion. This property of invar makes an ideal material for the present investigations.

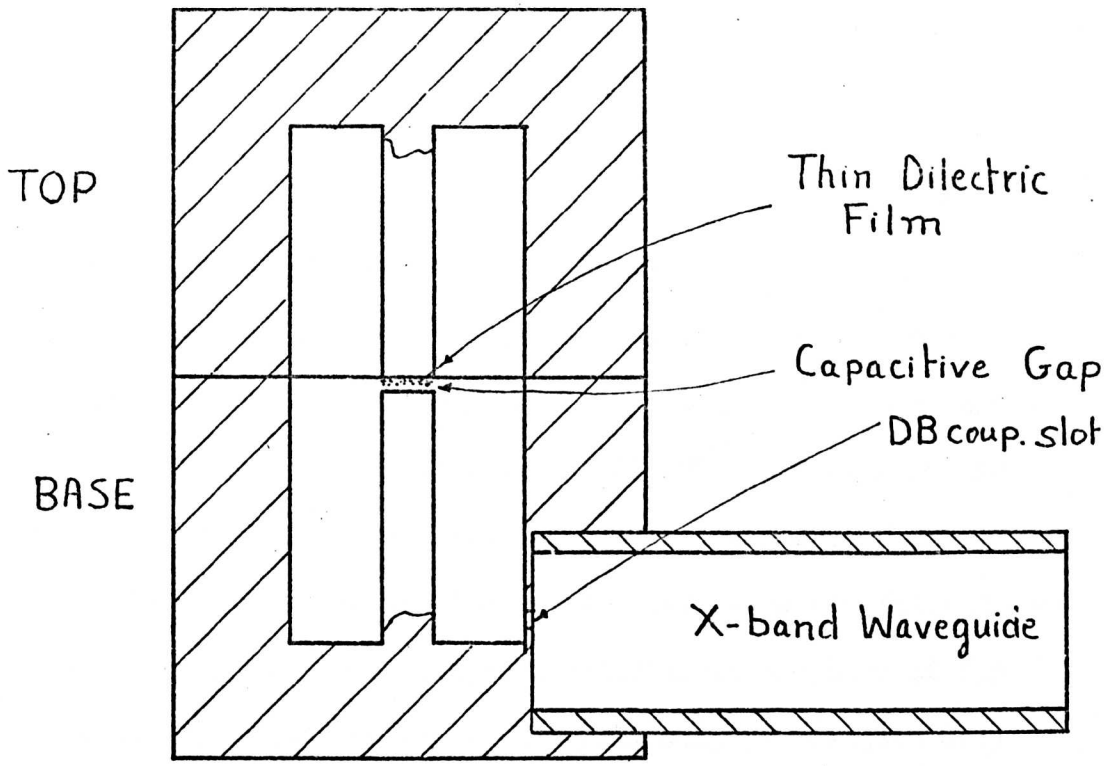

Figure 4.1 Axial Cross section of the Cavity

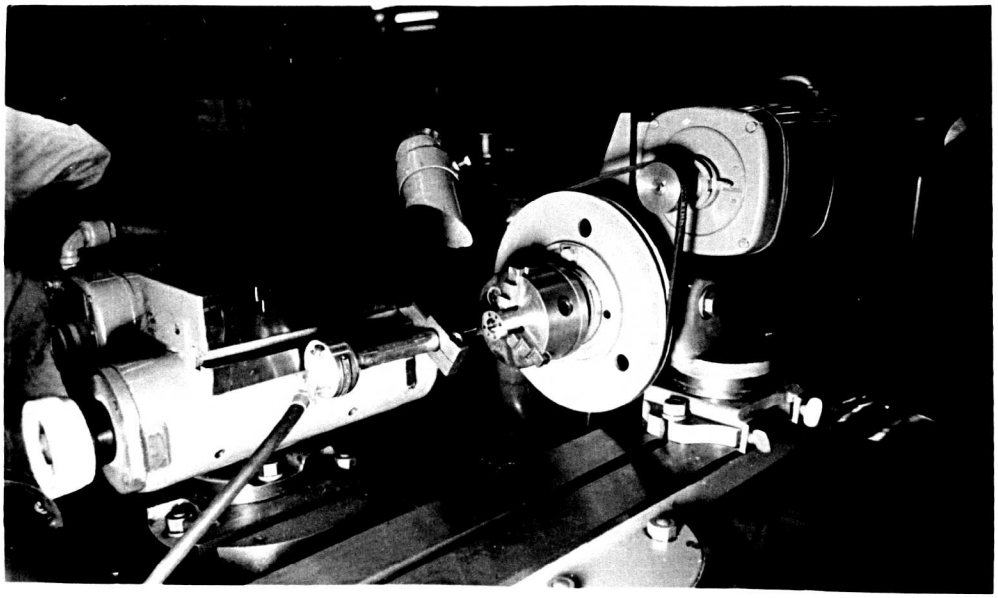

Figure 4.2 Lathe and the high speed burr set up.

These cavities, as before were made up of two parts each as shown in figure 4.1. The parts were prepared from the solid metal. The bore of each part was prepared first by milling it and then ground down to about 10 μm surface finish with the help of a high speed tungsten carbide burr at 28000 RPM and a lathe. The high speed burr and lathe set up is shown in figure 4.2. The bore of each part was then polished with diamond polishing paste ranging from 6 μm to $\frac{1}{4}$ μm grade. The mating faces of the cavity parts were carefully ground so that the plane of the faces was perpendicular to the bore of the cavity. The cavity parts were held in a polishing jig (Figure 4.3) and these faces were lapped down to < 0.25 μm surface finish.

The alignment of the cavity parts is the most important parameter affecting the accuracy of measurements. For precision alignment the cavity parts were held together whilst a jig filling was used to align the bores of the two parts, and dowel holes were drilled. With dowels in place 4 holding screw holes were prepared.

Figure 4.3 shows one of the top parts of the cavity in a polishing jig collar. Two large holes are dowel holes and four small holes are for the screws which hold the two parts of the cavity together. During the electrical testing of the cavity parameter, the screws holding the two parts of the cavity were tightened using a constant torque screw driver.

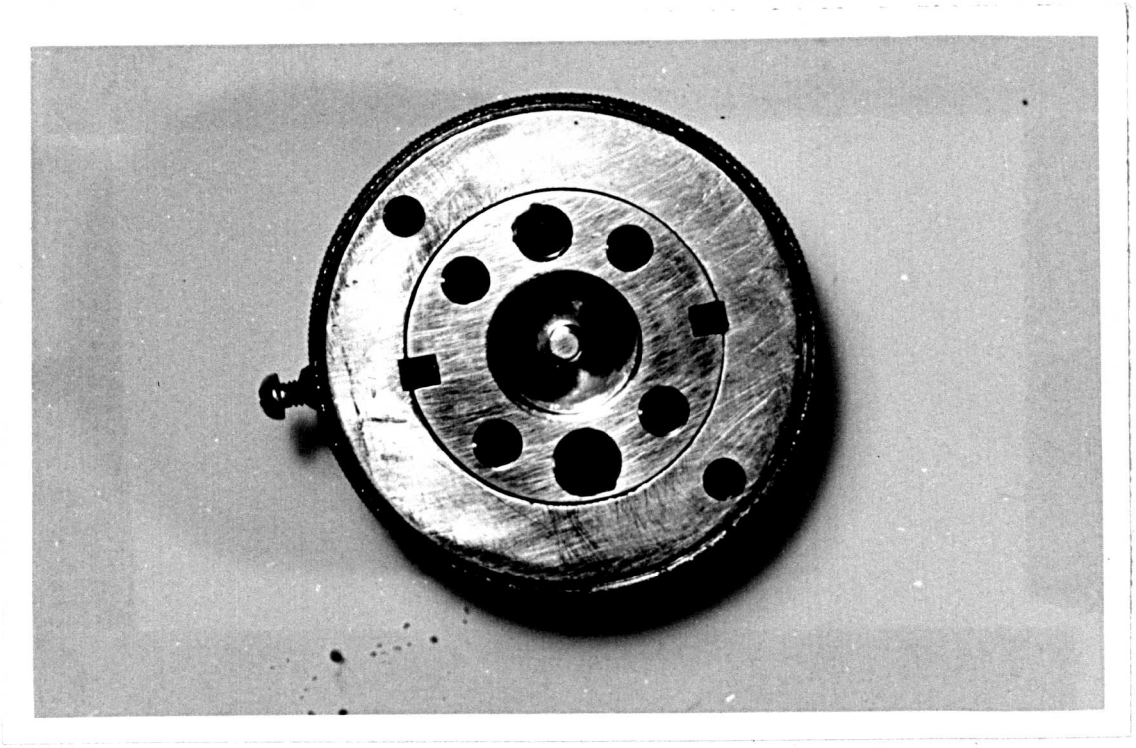

Figure 4.3 A Cavity Top in a Polishing Jig Collar

The above system of aligning the cavity parts gave reasonably repeatable results. The construction of the base part of the cavity which included the coupling system was found by a difficult process. As the dielectric film was deposited on to the top part, it was thought that more than one top should be used with one base part. The above method of dowelling was not suitable for this arrangement. The new cavity CI2 had one base part and 4 top parts, all interchangeable. The dowel holes of this cavity system were jig bored. The location accuracy of these holes was within 2.5 μm relative to the bore of the cavity parts.

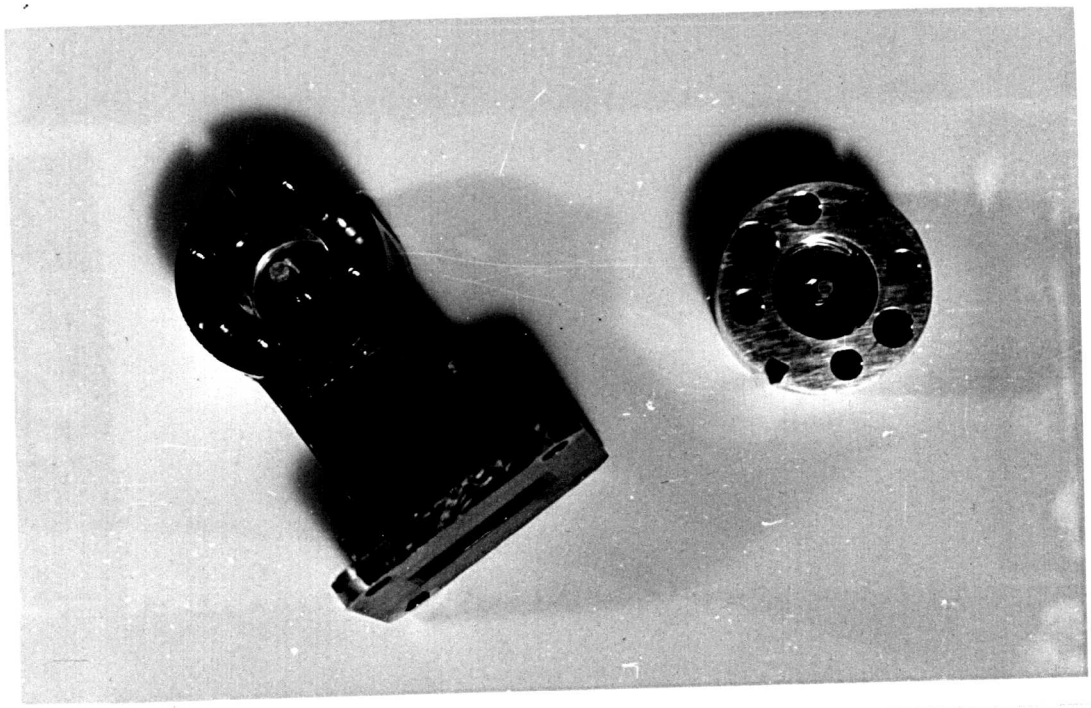

(a) CI_1

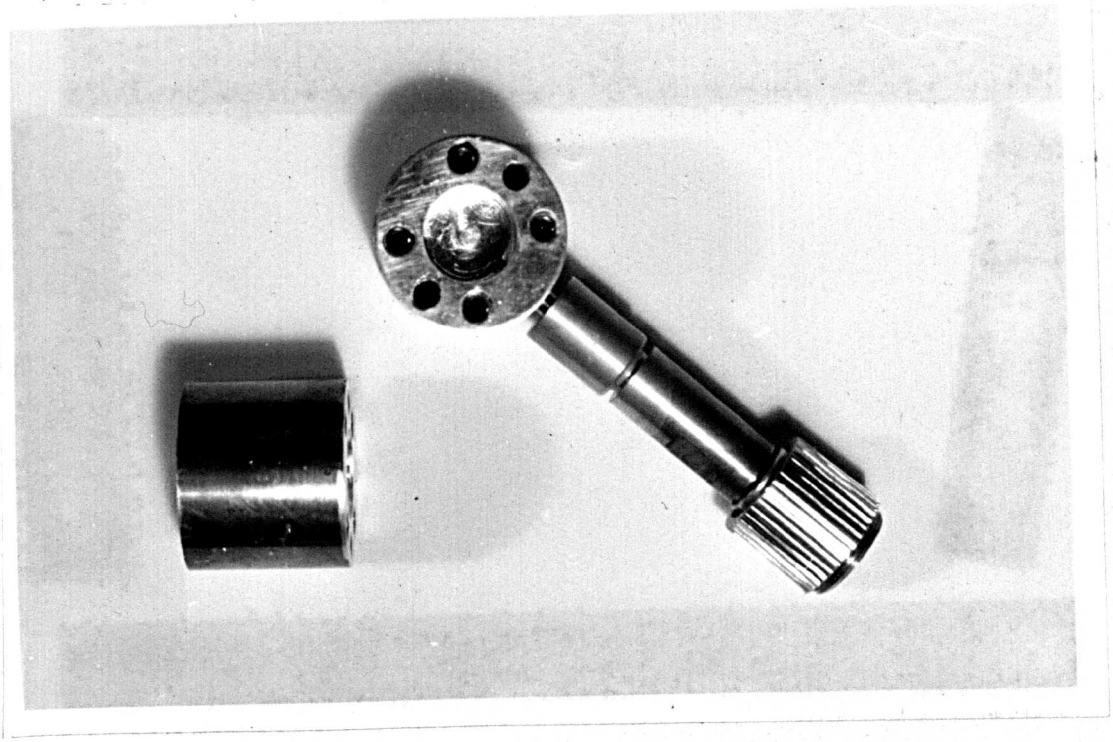

(b) CI_3

Figure 4.4. The Invar Cavities.

The dimensions of these cavities are given in table 4.1 and their photographs are shown in figure 4.4

Table 4.1

Properties of the Cavities.

CAVITY	Dimensions				Remarks
	L, mm	D_o, mm	D_o/D_1	Go, μm	
CB1	37	10.3	3.6	300-500	Various Couplin-gs
CB2	32	15	3.6	50-100	" "
CI1	32	15	5	<40	DB to WG16
CI2	32	15	5	<40	DB to WG16
CI3	32	15	5	<60	ML to Coaxial Line

DB = Dumbbell Coupling, ML = Magnetic Loop Coupling

CB = Brass cavities, CI = Invar cavities

4.2.3 The Coupling of the Cavity to Measuring System

The type of coupling used on a cavity is determined by the available measuring set up. These points are discussed in section 6.2. It is shown that the best coupling arrangement at X band was the dumbbell slot coupling. At lower frequencies a magnetic loop coupling was used.

For dumbell coupling a slot to accomodate a WG 16 waveguide,

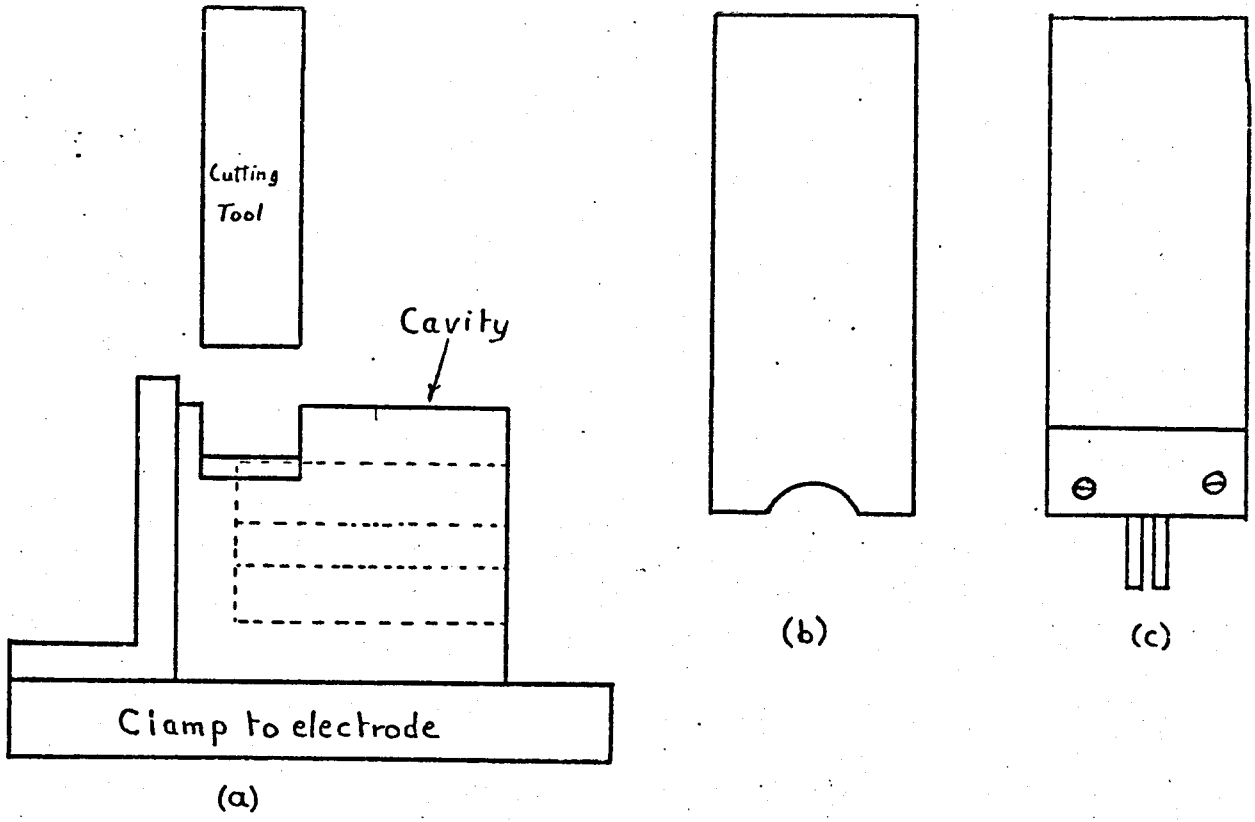

Figure 4·5 Spark Machining of Cavity Slot
(a) Set up
(b) Shaping Tool
(c) Dumbbel Slot drilling toll.

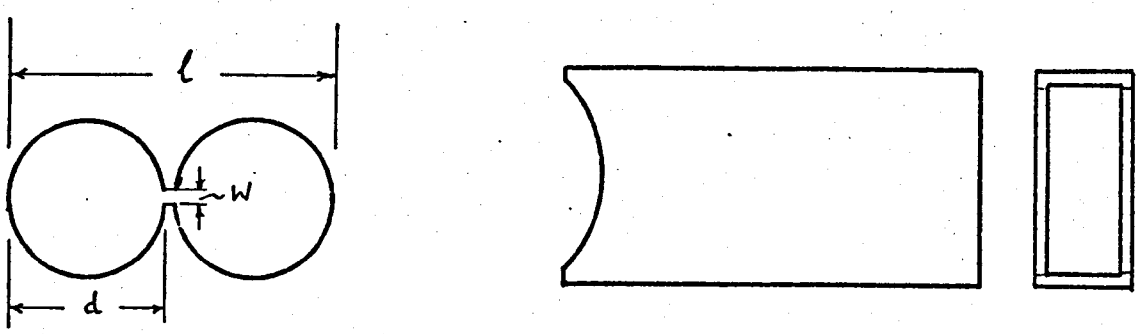

(a) Dumbbell Slot

(b) Waveguide part (WG16)

$l = 5.8$ mm, $d = 2.8$ mm & $W \doteq 0.2$ mm $[CI_1]$

$l = 5.3$ mm, $d = 2.3$ mm & $W \doteq 0.2$ mm $[CI_2]$

Figure 4.6 Cavity Parts.

was machined across the cavity part which had its inner conductor shortened by Go. The metal left between the slot and the bore of the cavity was thinned down to about 200 μm with a hand grinder. As the hand grinding was very time consuming, the author developed a spark machining process to do this. In this process two spark eroding electrodes were used. The first one was to rough out and the second one to get the required fine finish. Also the dumbbell slot was prepared with this machine. Figure 4.5 shows the set up and the tools used in the spark machining process. The latter process was ten times quicker than the former. A dumbbell coupling prepared using the former process is shown in figure 6.3 (section 6).

A Waveguide was shaped to suit the slot of the base part and was soldered on. The dimensions of the coupling slot and the connecting waveguide are shown in figure 4.6.

4.3 Materials for the Cavity.

The Q factor of a dielectric material when measured in a cavity, is compared with the Q factor of that cavity (together with other parameters). This was shown in the theoretical evaluation of the Q_D of thin film dielectrics in sections 2.4 and 2.5 (equations 2.42 and 2.61). The Q factor of a cavity is proportional to the square root of the conductivity of the current carrying surfaces of the cavity (equation 2.18) and hence high conductivity materials such as silver, copper, aluminium or gold should be used. But high conductivity

materials usually have high thermal coefficient of expansion.

For our purposes we can assume that the current penetrates into metals down to a few skin depths. In high conductivity metals mentioned above, the skin depth at X band is approximately 1 μm. Therefore the cavity can be constructed from a metal having low thermal coefficient of expansion and plated with one of these high conductivity metals up to 5 skin depths at that frequency.

In the present investigation the cavity material was Invar, which is a poor conductor (σ = 1.24 x 10^8 mho per metre, only 1/47 th that of copper)[49] This disadvantage was overcome by plating the cavity with silver.

The silver was chosen on the following grounds:

(a) It has the highest conductivity (excluding superconductors) hence best cavity Q factor could be obtained.

(b) The low resistivity materials such as silver, copper and aluminium tarnish when left in the atmosphere and hence they require an antitarnishing process. The organic antitarnishing processes could not be practical because of the high processing temperatures used. The best solution is to use a thin layer of electroplated gold. The diffusion coefficients[4-6] of gold into silver and gold into copper are 4 x 10^{-19} $m.m^2$ per day and 4 x 10^{-13} $m.m^2$ per day respectively both at 21°C. Therefore gold on silver will have a longer operating life than the gold on copper system.

4.3.1 Electroplating of Cavities.

The plating process adopted was as follows:

(i) The cavity part was degreased

(ii) It was dipped in 10% $H_2 SO_4$ solution for one minute to remove any oxide film from the surface to be plated

(iii) Copper strike, using copper strike solution given in Appendix 6

(iv) Silver Strike, using Silver strike solution given in Appendix 6

(v) Silver plating, using the Elfit Silver plating solution[47]

(vi) Gold plating, using PMD Transtherm gold solution[48]

If direct silver plating was used the plated material would have not adhered to the cavity surfaces and steps (i) to (iv) were followed for this purpose.

The cavity parts had an awkward shape and plating of such a shape with a plane anode would have not given a uniform plating around the cavity. To eliminate this a special cylindrical anode was prepared as shown in figure 4.7. This anode extended inside the cavity and was held by the plane anode. The anode assembly was fixed on to a P.t.f.e. base plate. This baseplate was used in aligning the cavity and the cylindrical part of the anode which it was extending along the bore of the cavity. The electrolyte of the silver plating system was circulated around the bore of the cavity with the help of a "flow inducer" pump (figure 4.7). The cavity parts which were silver plated

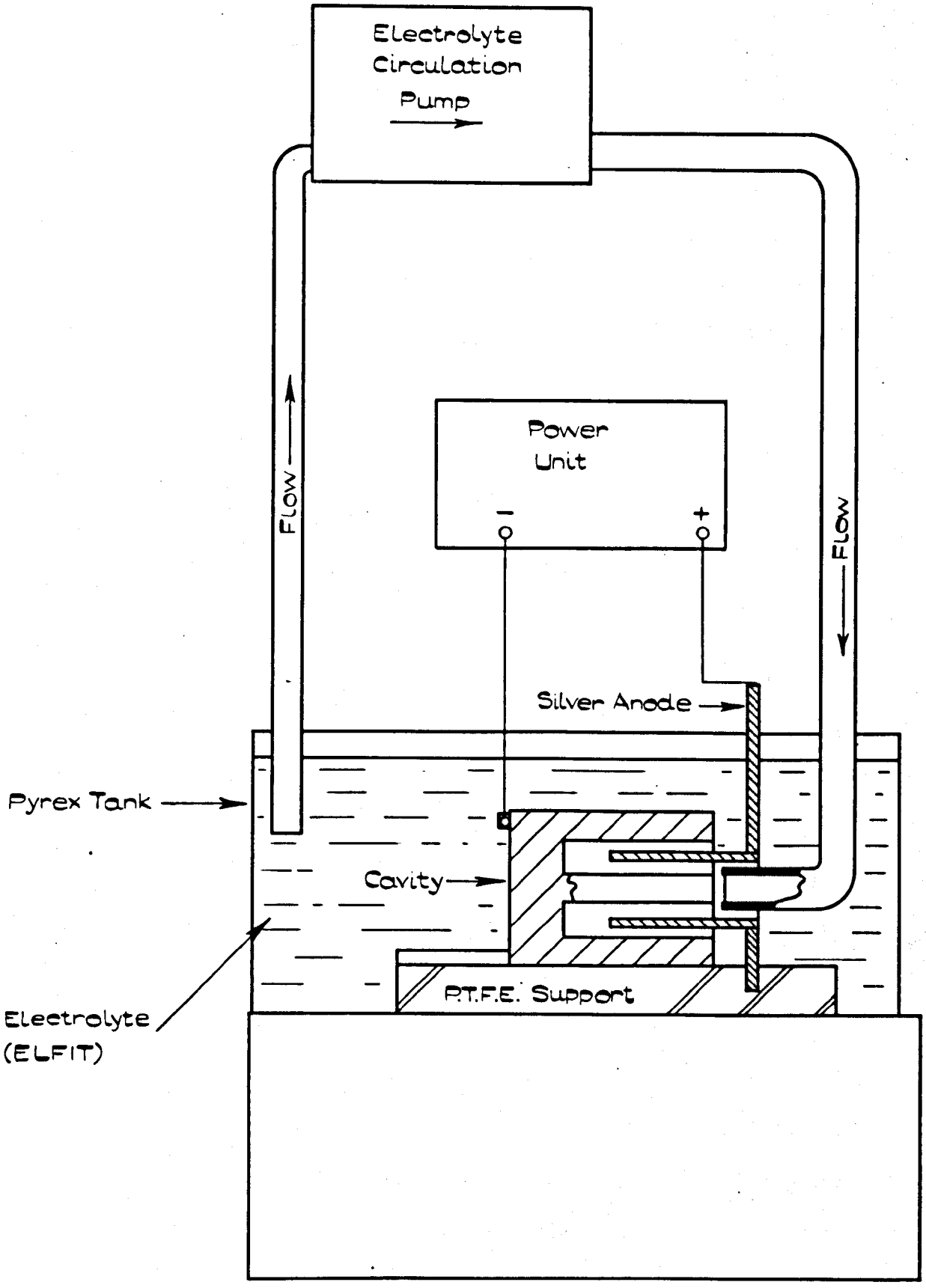

FIGURE 4.7.

CAVITY PLATING SYSTEM.

using this system, gave quite good and reproducable electrical characteristics (see section 6.3.2)

The average thickness of the electroplated silver film on the cavity surfaces was about 20 μm. This was greater than the theoretically required thickness which is about 4 μm. The reason for having a thick film was that the silver plated films up to a thickness of 5 μm have pinholes.[44]

The electroplated top parts of the cavity were heat treated at around 300°C under vacuum. This treatment had two aims:-

(1) The electroplated film behaves like a cold worked metal, thus having stresses. This gives rise to a higher resistivity for electroplated films than the bulk material.[45] Heat treatment at temperatures around 300°C should relieve the film from this stress and lower the resistivity.

(2) The deposition of the thin dielectric film was carried out at around 200°C and therefore the cavity properties must not change after repeated heating to this temperature.

4.3.2 Comments on Electroplating.

An electroplating system has two properties affecting plating of difficult internal corners. One of these is the macrothrowing power where low anode current is used and sharp corners could be filled up

by electroplating. The second property is the microthrowing power where high anode current is used in a well stirred system. The latter method gives smooth surfaces, but sharp corners cannot be plated well.[50] When complicated shapes like cavity parts are plated an optimum electroplating condition should be found. In the present case it was found that the best current density for the Elfit silver plating solution was between 4 and 5 mA / cm^2 and the solution should be well circulated.

The heat treatment was discussed above and the electrical properties of the treated cavities are in section 6.3.2. An additional advantage of the heat treatment is that if the electroplated film did not adhere to the cavity surface it will blister during the heat treatment. This is a destructive test but there is no other practical non-destructive testing method. This test eliminates faulty parts and helps to save valuable time.

The antitarnishing process used i.e. a flash of gold (6-10 nm) on silver plated surfaces, was found to be effective. The Q factor of one of the invar cavities CI1 dropped by $< 2\%$, 12 months after plating.

Chapter 5

MICROWAVE MEASUREMENT TECHNIQUES FOR THE CAVITY.

5.1 Introduction.

The theoretical approaches to measurement of the dielectric properties of thin films using a cavity were described in section 2. Here, the microwave measuring systems used to measure the cavity properties, will be discussed.

The choice of measuring system depends upon the type of coupling mechanism used on the cavity. These were discussed in section 6. It was found that the dumbbell coupling to the waveguide-type measuring system was the best method. Therefore the waveguide system was adopted.

The waveguide system has the following advantages over the coaxial system:

(i) The mismatch errors in waveguide components are much smaller than the coaxial componets, hence directivity of waveguide directional couplers is much better than the coaxial couplers. Directional couplers were used in the reflectometer set up.

(ii) Any coupling susceptance of the cavity can be tuned out easily in a waveguide system.

The advantage of the coaxial system is that it can be used practically over the whole frequency range from 1 to 12.4 GHz.

This property of the coaxial system was used when the full range of cavity resonances were measured.

The measurement techniques used for the cavity are as follows:

(a) Transmission method: the cavity was coupled to the waveguide through a probe (section 6.2) which extended into the cavity at one end and the waveguide at the other end. The schematic diagram of the measuring system is shown in figure 5.1. In this diagram the cavity is represented as a series tuned circuit shunted across the line. The cavity properties were determined from the plot of received power against frequency near resonance.

This technique has the following advantages over the other transmission type measurement where two couplings are employed:
(i) only one coupling parameter measurement is required and
(ii) the error introduced by the coupling susceptance[51] can be eliminated with one tuner.

This method was used in the preliminary measurements. It was found that the mechanical and electrical stability of the coupling mechanism was poor and the system was abandoned.

(b) Reflection method: in this method the cavity was connected to a reflectometer and its reflection coefficient near resonance was plotted as a function of frequency. The Q factor and the resonant frequency of the cavity were determined from this graph.

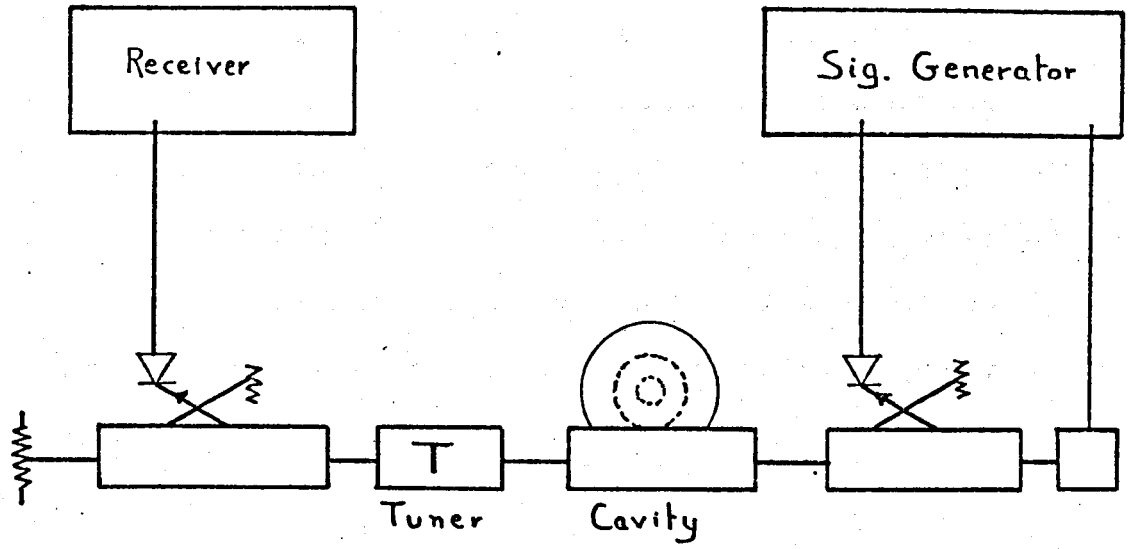

(a)

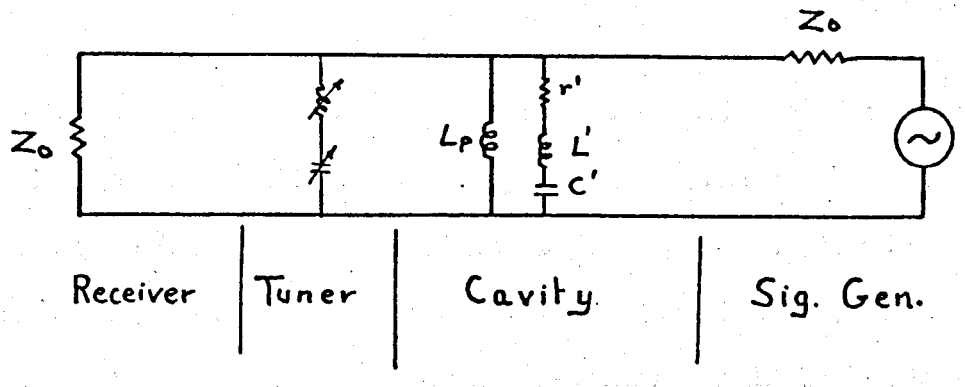

(b)

Figure 5.1 Measurement of the Properties of a Cavity using Transmission Method.
(a) Setup and (b) Equivalent Circuit.

This method was used in the coaxial and waveguide systems. Two types of coaxial reflectometers were used. One of these was using a coaxial directional coupler. The other reflectometer was the H.P. Network Analyser together with the Reflection Unit (Type 8742A) Both of these coaxial reflectometers were not accurate enough at X band frequencies and they were used only for the low frequency resonances.

In the following sections the properties of the waveguide reflectometer system, its calibration and the calculation of the unloaded Q factor of the cavity using the plot of the reflection coefficient against frequency will be described. Also the system errors will be analysed.

5.2 The Precision Waveguide Reflectometer.

The reflectometer system consisted of two X-band high directivity waveguide directional couplers as shown in figure 5.2a and b. The signal source (H.P. sweep oscillator type 8690A with plug in H01-8694B) having an automatic power levelling loop (made up of a 10dB directional coupler and a waveguide detector) could be swept from 8 to 12.4 GHz. The receiver system consisted of the "H.P. harmonic frequency converter" (type 8411A) and the network analyser type 8410A with the "gain / phase" plug-in type 8413A. This system could be used to measure the phase as well as the magnitude of the reflection coefficient.[52]

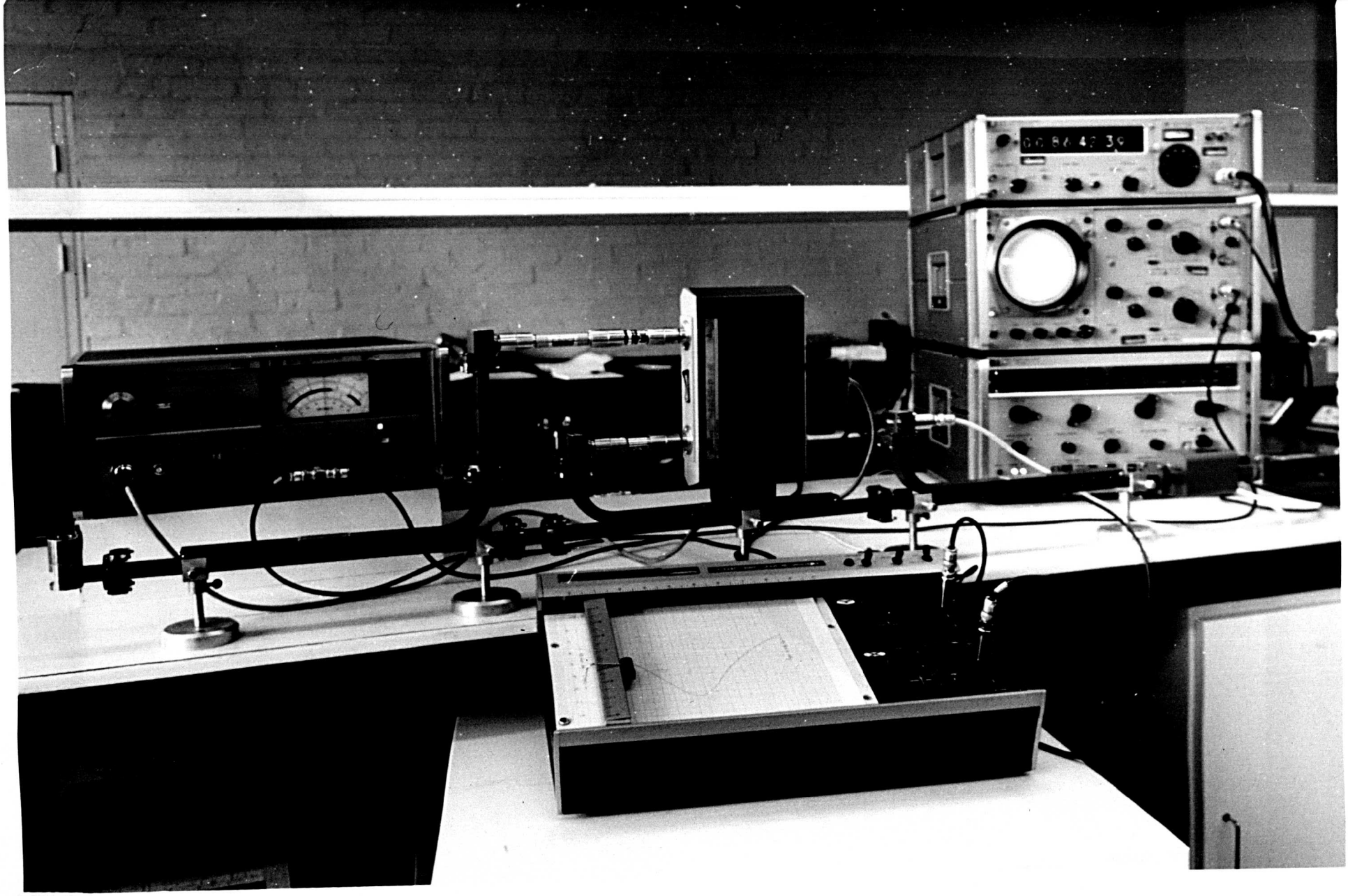

Figure 5.2a Reflectometer Unit

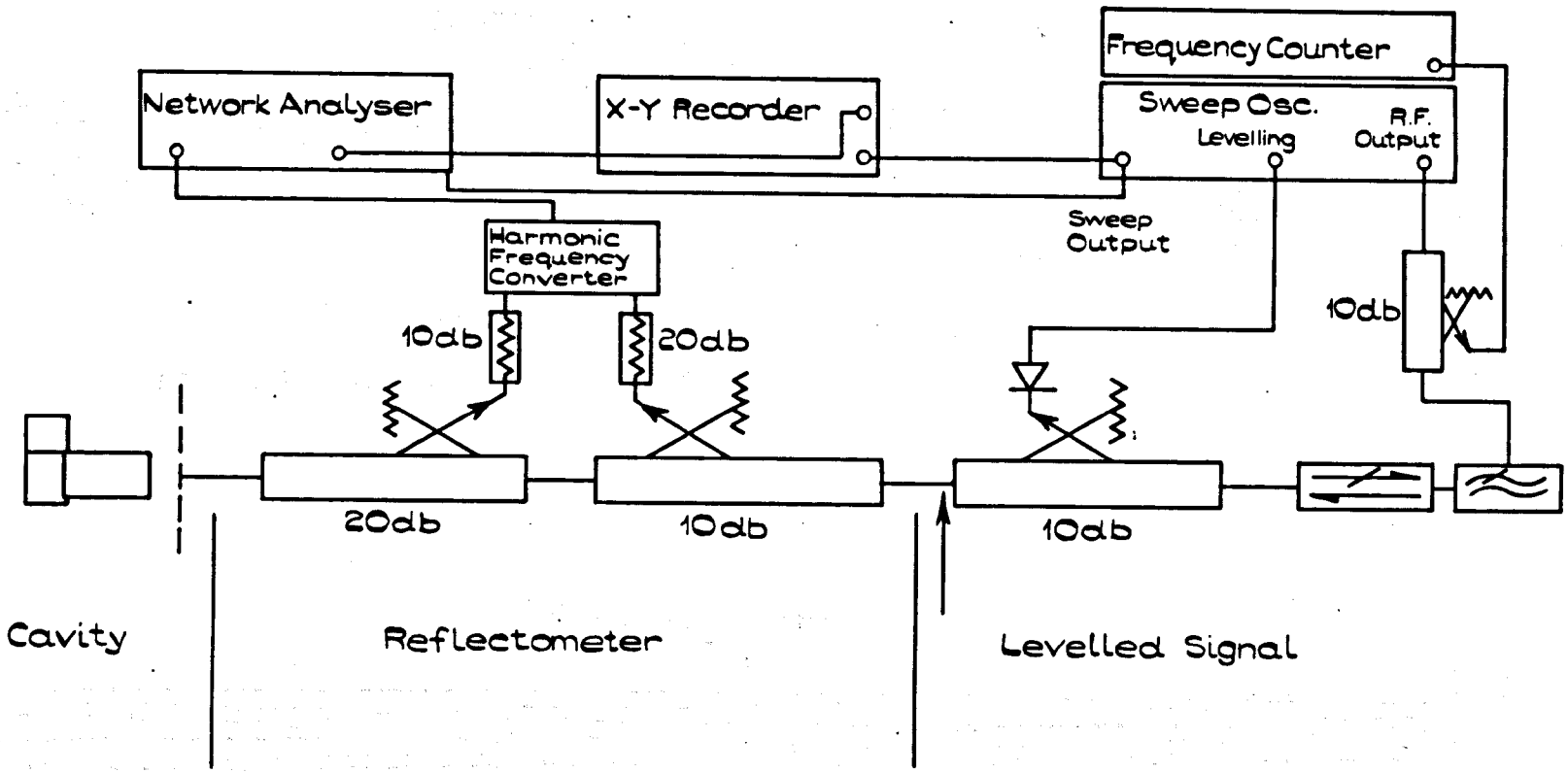

FIGURE 5.2b.

PRECISION WAVEGUIDE REFLECTOMETER SYSTEM.

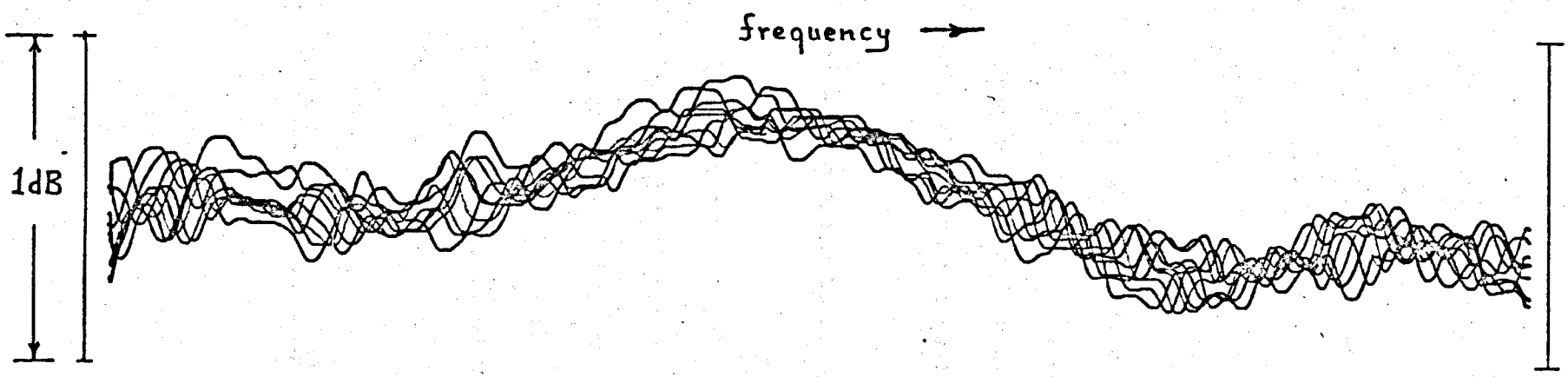

(a) Frequency sweep: 8–12 GHz.

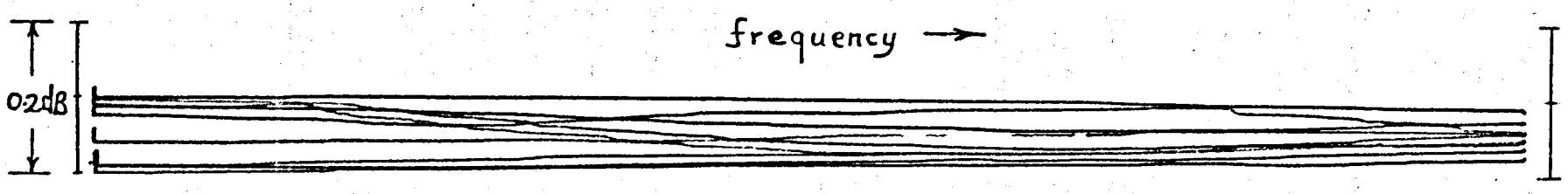

(b) Frequency sweep: 9480–9520 MHz

Figure 5·3 Reflection coefficient vs Frequency for various sliding shortcircuit positions.

The additional components of the system were:-

(i) Low pass filter (HP type X 362 A) with 12.5 GHz cut off frequency, to eliminate the harmonics (20 dB below the fundamental frequency) of the signal source when the VSWR was measured.

(ii) An isolator having very low VSWR at the output port(VSWR $\leq$ 1.04) to reduce the mismatches between the signal generator and the reflectometer.

(iii) Coaxial directional coupler 10 dB, (Narda 3045C-10) was used in conjunction with the HP frequency counter (type 5246L) with the frequency converter plug in type 5255A to monitor the frequency of the signal source as it was swept.

(iv) X - Y recorder to record the measured reflection coefficient.

The system was a self contained precision reflectometer with with recording facilities and which could be swept over the entire frequency range of the waveguide WG 16, i.e. 8 - 12 GHz. The flatness of the response with a shortcircuit terminating the measurement port was better than 0.7 dB over the whole bandwidth. Figure 5.3a shows the reflectometer response as the shortcircuit position was changed.

5.2.1 The Frequency Stability of the Signal Source.

Errors in the measured dielectric properties are shown to depend on the errors of the resonant frequency and the Q factor of the cavity (section 8). The accuracy of the measurement of these parameters depends on the frequency stability of the signal source which is used in the system. The signal source used in the present investigation was an HP Sweep Oscillator type 8690A with the plug-in type HoI- 8694B. The frequency stability of the signal generator was fully investigated.

The effect of the mains voltage on the frequency stability of the oscillator was investigated. The measured frequency change per volt of mains change was 31 kHz over ± 10% mains voltage variation. This was improved by incorporating a solid state voltage stabilizer (Claude Lyons) between the mains and the signal source. The new variation was 4.6 kHz/V over the same range.

The signal source was switched on and the frequency set to a fixed value. The equipment was run for two hours before the test and it was found that with precautions the laboratory temperature stayed within ± 0.2°C after that time. This room temperature stabilization also stabilized the frequency of the oscillator. Under these conditions the frequency variation of the set frequency was less than 40 kHz over a period of 100 seconds. This 100 seconds was the sweep time used during the measurement of the cavity response.

5.2.2 Measurement of the Reflectometer Errors.

The system errors can be estimated if the directivity of the directional coupler and mismatches at different points along the reflectometer connections are known.

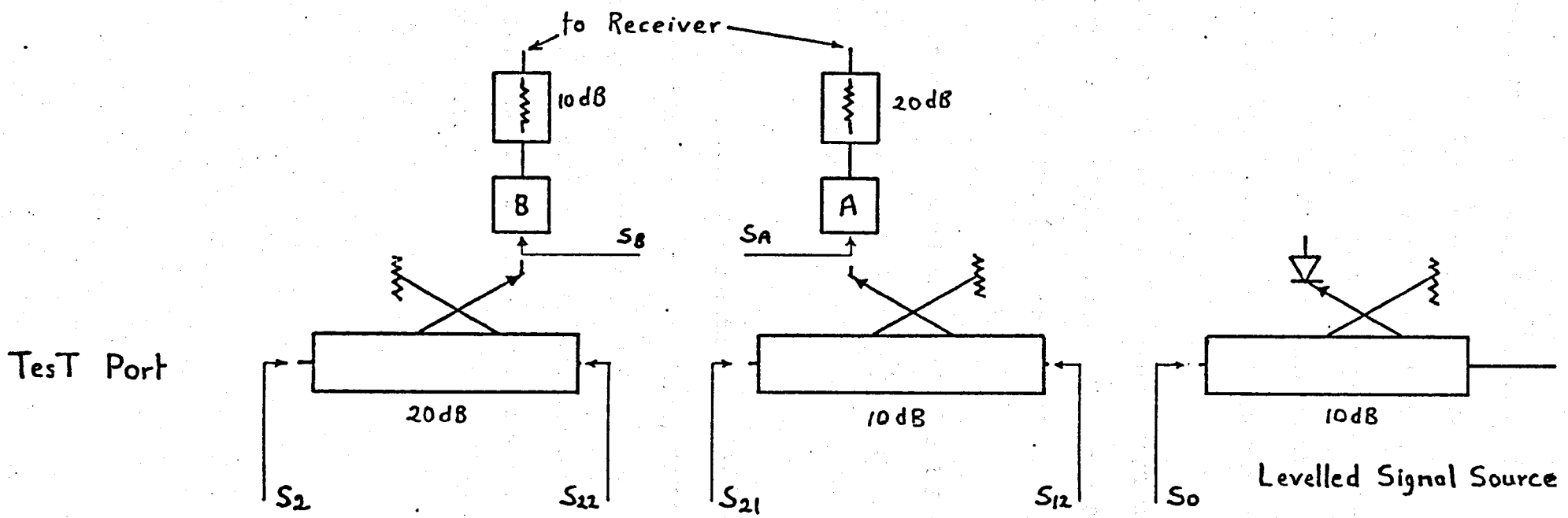

Figure 5·4 Break Points of the Reflectometer for VSWR Measurements.

The directivity of thewaveguide directional coupler was determined. The coupler was used in the reflectometer set up and a movable matched load was connected across the measurement port. The load was moved to and fro along the line whilst the frequency was swept. The reflection coefficient was recorded. From this measurement and the graph supplied by the HP,[53] the directivity of the coupler was measured.

The directivity of the 20 dB directional waveguide coupler which was used in the precision reflectometer set up was found to be better than 45 dB at 9500 ±100 MHz, (better than 48 dB at 9500 ± 20 MHz).

The same measurement technique was also used for a precision coaxial directional coupler (Narda type) ard the measured directivity was 35 dB at 9600 ± 200 MHz.

The mismatches at different joints of the reflectometer system were measured as voltage standing wave ratios, VSWR's. The measurement was carried out by disconnecting the set up at the required joint and in case of directional coupler the far end was terminated in a matched load. Figure 5.4 shows the break points of the set up. These results are given in table 5.1.

Table 5.1

Frequency GHz	VSWR at the measurement ports						
	20 dB Coupler		10 dB Coupler		Source	Transitions	
	S_2	S_{22}	S_{12}	S_{21}	S_0	S_A	S_B
9.4	$\leq$ 1.03	$\leq$ 1.04	$\leq$ 1.04	$\leq$ 1.04	$\leq$ 1.05	$\leq$ 1.16	$\leq$ 1.16
9.5	$\leq$ 1.02	$\leq$ 1.02	$\leq$ 1.02	$\leq$ 1.02	$\leq$ 1.05	$\leq$ 1.16	$\leq$ 1.12
9.6	$\leq$ 1.02	$\leq$ 1.02	$\leq$ 1.02	$\leq$ 1.02	$\leq$ 1.05	$\leq$ 1.15	$\leq$ 1.14

This reflectometer was used to measure the cavity parameters with and without the dielectric film (section 7). Hence there was a shift in the resonant frequency of the cavity when it was loaded with a dielectric film. This frequency shift could not have exceeded 20 MHz for those films used during the investigation. Therefore the reflectometer mismatch errors were measured at 9500 $\pm$ 20 MHz and it was found to be constant. This is shown in figure 5.3b.

Using the signal flowgraph approach Ely[54] analysed a reflectometer similar to the present one and showed that the measured reflection coefficient

$$\Gamma = K(w)\left[\frac{D_2}{T_2} + \Gamma_x \Gamma_L^2 + \Gamma_L\right] \qquad 5.1$$

where Γ_L = The reflection coefficient of the measured load

D_2 = The directivity of the directional coupler 2

T_2 = The transmission loss of the directional coupler 2

$K(w)$ = Coupler / Detector tracking factor

= constant for narrow frequency sweeps

Γ_x = The effective reflection coefficient of the system

$$= \Gamma_{12} - T_2^2\left(\Gamma_{21} - T_1 D_1\right) - C_2^2 \Gamma_{d_2}$$

Γ_{12} = The mismatch reflection coefficient of DC_2 at the measurement port

Γ_{21} = The reflection coefficient of DC1 at the output port

T_1 = The transmission loss of DC1

D_1 = The Directivity of DC1

C_2 = The Coupling Coefficient of DC2

Γ_{d2} = The reflection coefficient looking into the receiver - test port

Equation 5.1 will have a maximum value when $\Gamma_L = 1$

$$|\Gamma|_{max} = K(w)\left[1 + \left(\frac{D_2}{T_2}\right) + \Gamma_x\right] \qquad 5.3a$$

and a minimum value when $\Gamma_L = -1$

$$|\Gamma|_{min} = K(w)\left[-1 + \frac{D_2}{T_2} + \Gamma_x\right] \qquad 5.3b$$

Dividing equation 5.3a by equation 5.3b we obtain

$$\frac{|\Gamma|_{max}}{|\Gamma|_{min}} = -\left[\frac{1 + D_2 / T_2 + \Gamma_x}{1 - \left(D_2 / T_2 + \Gamma_x\right)}\right] \qquad 5.4a$$

$$= -\left[1 + 2\left(D_2 / T_2 + \Gamma_x\right)\right] \qquad 5.4b$$

The directivity D_2 , the transmission loss, T_2 (= 0.995 for the 20 dBCoupler, DC2) and Γ_x were calculated using the measured values. When these value are substituted in equation 5.4b we obtain

$$\frac{|\Gamma|_{max}}{|\Gamma|_{min}} = 0.126 \text{ dB}$$

The measured maximum variation of the reflected signal with a sliding shortcircuit was 0.08 dB.

The difference between the calculated value and the measured one, may arise from the following causes:

(i) D_2 , Γ_x and T_2 are all vector quantities and in practice they will add vectorially. Only the moduli were measured.

(ii) In the above calculation the worst case values were used.

(iii) Some of the discontinuities might have cancelled out each other, when connected together.

It should be noted that over the narrow frequency range used for our measurements, the measured value of 0.08 dB is the relevant one.

5.2.3 Calibration of the Reflectometer System.

The swept reflection coefficient as measured was displayed on an oscilloscope or recorded using an X- Y recorder. There were two outputs of the "gain / phase plug in" of the Network Analyser, one of these was the magnitude and the other was the phase of the reflection coefficient. Either or both of these outputs could be displayed simultaniously on a double beam oscilloscope. It was found that the X Y plot was more accurate than the oscilloscope display because there was no observer error and the recorded information could be analyzed later on.

Figure 5.5 shows the calibration set up used for the reflectometer system, the frequency was swept $\pm$ 20 MHz on either side of the centre frequency. At each sweep the rotary vane attenuator was set to a specific value and constant attenuation grids were recorded. 1 dB - attenuation setting on the rotary vane attenuator gives 2 dB on the recorder. Then the amplitude gain of the Network Analyser was increased in steps of 1 dB and compared with the constant attenuation grids recorded previously. It was found that variable amplitude gain of the Network Analyser gave same results as the rotary vane attenuator. The accuracy of the rotary vane attenuator was within 0.1 dB.

It was shown in Appendix 7 (and also in section 8.2) that the calibration errors do not introduce appreciable error to the measured thin dielectric film properties if the VSWR method is used.

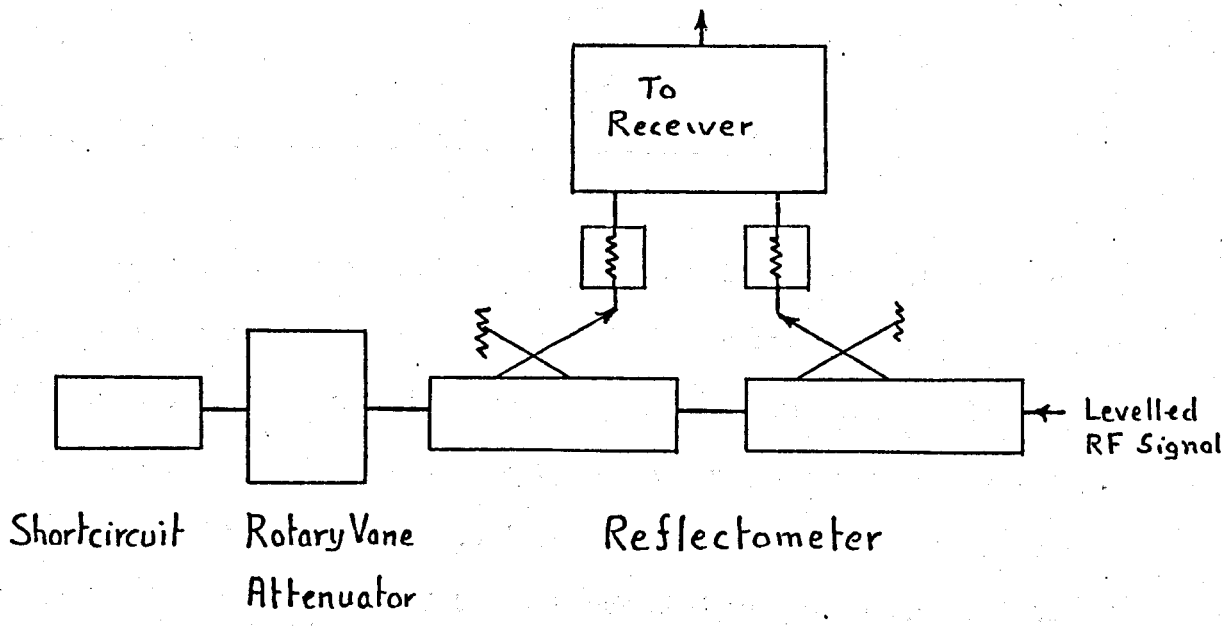

Figure 5·5 Calibration setup for the Reflectometer

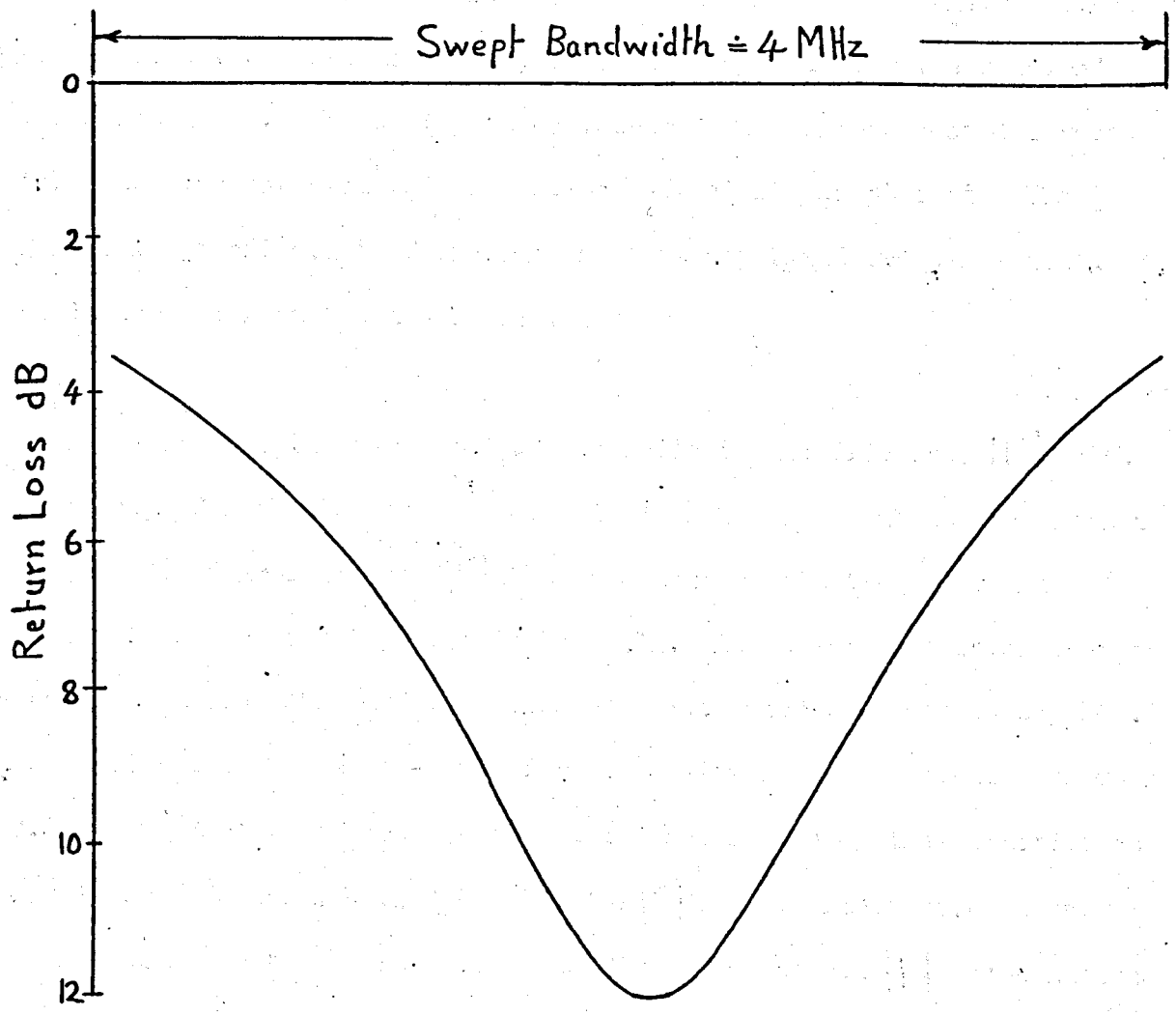

Figure 5·6 Resonance curve of a cavity (CI2)

5.2.4 Swept Reflection Coefficient Measurements.

The signal source had a sweep output voltage proportional to the frequency sweep. The linearity of this voltage against frequency was checked by observing the frequency against the sweep voltage. It was found to be linear over ± 20 MHz around the centre frequency. This sweep voltage was used to drive the X - axis of the recorder whilst the output signal of the Network Analyser was connected to the Y - axis.

After calibrating the X - and Y - axes as described in section 5.2.3 the reflectometer system was used as follows: the measuring port was terminated in a shortcircuit or open circuit and the unity reflection coefficient (0 dB return loss) line was recorded over the required frequency sweep. The cavity to be measured was then connected across the measuring port and the reflection coefficient was plotted. The reflection coefficient of the component at any fixed frequency could be determined from the X - Y plot.

The plot of the magnitude of the reflection coefficient, $|\Gamma|$ with frequency of a high Q resonant circuit is symmetrical about the resonant frequency. Near resonance $|\Gamma|$ changes sharply with frequency and therefore sweep bandwidth should be small. In the present investigation the Qo was about 4500 and the sweep bandwidth used was less than 5 MHz. The calibration of the X - axis for the cavity measurement was less than 0.250 MHz /cm . Under these conditions any frequency instabilities as low as 20 kHz could have distorted the $|\Gamma|$ plot. Figure 5.6 shows such a plot for the cavity CI. This figure shows that $|\Gamma|$ was symmetrical

around the resonant frequency of the cavity. This was the expected result as shown in section 5.3 equation 5.8. This plot also shows that the sweep voltage applied to the X - axis of the recorder, varied linearly with the frequency, otherwise the Γ plot would have been distorted.

5.3 Measurement of the Unloaded Q - factor of the Cavity.

The equivalent circuit of the cavity was represented as a series tuned circuit (section 2). The impedance near the resonant frequency being

$$Z = r + j w_1 L \, 2\delta$$

$$= r \left[1 + j \frac{w_1 L}{r} \, 2\delta \right]$$

$$= r \left[1 + j 2 Q_o \delta \right] \qquad 5.5$$

where r = total series loss resistance

L = total series inductance

δ = cavity tuning parameter

$$= \frac{1}{2} \left[1 - \left(\frac{w_o}{w} \right)^2 \right]$$

The impedance Z transformed to the measurement side through a mutual inductance M will be

$$Z1 = \left(\frac{w M}{Z} \right)^2$$

$$Z_1 = \frac{(w M)^2}{r(1 + j 2 Q_o \delta)} \qquad 5.6$$

The reflection coefficient Γ at any frequency w near resonance will be

$$\Gamma = \left[\frac{Z1 - Z_o}{Z1 + Z_o}\right]$$

substituting the value of Z1 we obtain

$$\Gamma = \frac{\left[\frac{(w M)^2}{r(1 + j 2 Q_o \delta)} - Z_o\right]}{\left[\frac{(w M)^2}{r(1 + j 2 Q_o \delta)} + Z_o\right]} \qquad 5.7a$$

which simplifies to

$$\Gamma = -\frac{[(1 - \beta) + j 2 Q_o \delta]}{[(1 + \beta) + j 2 Q_o \delta]} \qquad 5.7b$$

and $$|\Gamma|^2 = \frac{(1 - \beta)^2 + (2 Q_o \delta)^2}{(1 + \beta)^2 + (2 Q_o \delta)} \qquad 5.8$$

where Z_o = characteristic impedance of the measurement system

$$\beta = \frac{(w M)^2}{r Z_o}, \quad (= \text{coupling coefficient})$$

At resonance $\delta = 0$ and the reflection coefficient will be

$$|\Gamma_0|^2 = \frac{(1-\beta)^2}{(1+\beta)^2} \qquad 5.9$$

At far off from resonance $2 Q_0 \delta << (1+\beta)$ and reflection coefficient $|\Gamma_\infty| = 1$

Let $|\Gamma_L|$ = the magnitude of the reflection coefficient when $2 Q_0 \delta = 1$ equation 5.8 becomes

$$|\Gamma_L|^2 = \frac{(1-\beta)^2 + 1}{(1+\beta)^2 + 1} \qquad 5.10$$

The value of β can be found from equation 5.9 and therefore $|\Gamma_L|^2$ can be calculated.

$|\Gamma_L|^2$ against frequency response of the cavity is shown in the inset of figure 5.7. In this plot the other reflection coefficients $|\Gamma_\infty|^2$, $|\Gamma_L|^2$ and $|\Gamma_0|^2$ are all marked. The main graph designated as the bandwidth graph shows the variation of $|\Gamma_L|^2$ against $|\Gamma_0|^2$. The graph is used as follows:

The reflection coefficient of the cavity near resonance is plotted and the $|\Gamma_0|^2$ is determined from the plot. This value of $|\Gamma_0|^2$ is used to determine $|\Gamma_L|^2$ from figure 5.7 then going back $|\Gamma_L|^2$ is marked on the $|\Gamma|^2$-frequency plot and the two frequencies on either side of the resonant frequency are read off the graph.

$$2\delta = 2\left[\frac{(f_0 - f_1)}{f_2 + f_1}\right]$$

But $2 Q_o \delta = 1$ at $|\Gamma|^2 = |\Gamma_L|^2$

$$Q_o = \left(\frac{1}{2\delta}\right)$$

$$= \left[\frac{f_o}{f_2 - f_1}\right] \qquad 5.11$$

where $f_o = \left[\frac{f_1 + f_2}{2}\right]$

This procedure was followed throughout the measurements on the cavity. The swept reflection coefficient was recorded in dB's and the frequency at the beginning and the end of the plot was recorded using the frequency counter. The latter procedure was used in calibration of the frequency axis of the plot. The reference reflection coefficient was obtained with the cavity off tuned.

When a cavity is coupled to a measuring system the coupling mechanism gives rise to a coupling susceptance. This susceptance should be included in the reflection coefficient calculations. This has not done in the above derivations because the coupling mechanism used on the cavity had negligible susceptance. The effect of the coupling susceptance on $|\Gamma_o|$ of the cavity can be measured using the phase information of the reflection coefficient. The procedure is as follows: The cavity is off tuned and the phase information of the off-tuned cavity is recorded as a function of frequency. Then the cavity is tuned and the phase as well as the magnitude of the reflection coefficient is recorded as a function of frequency. If the difference of the two phase informations

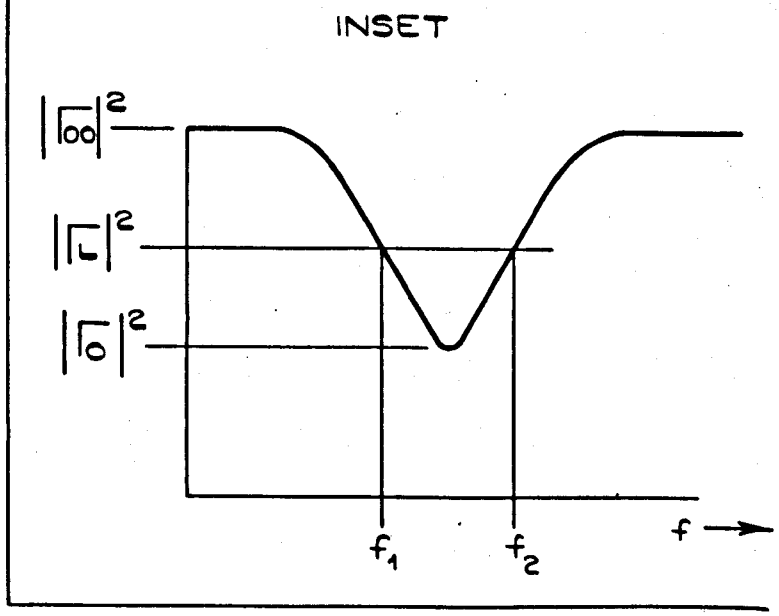

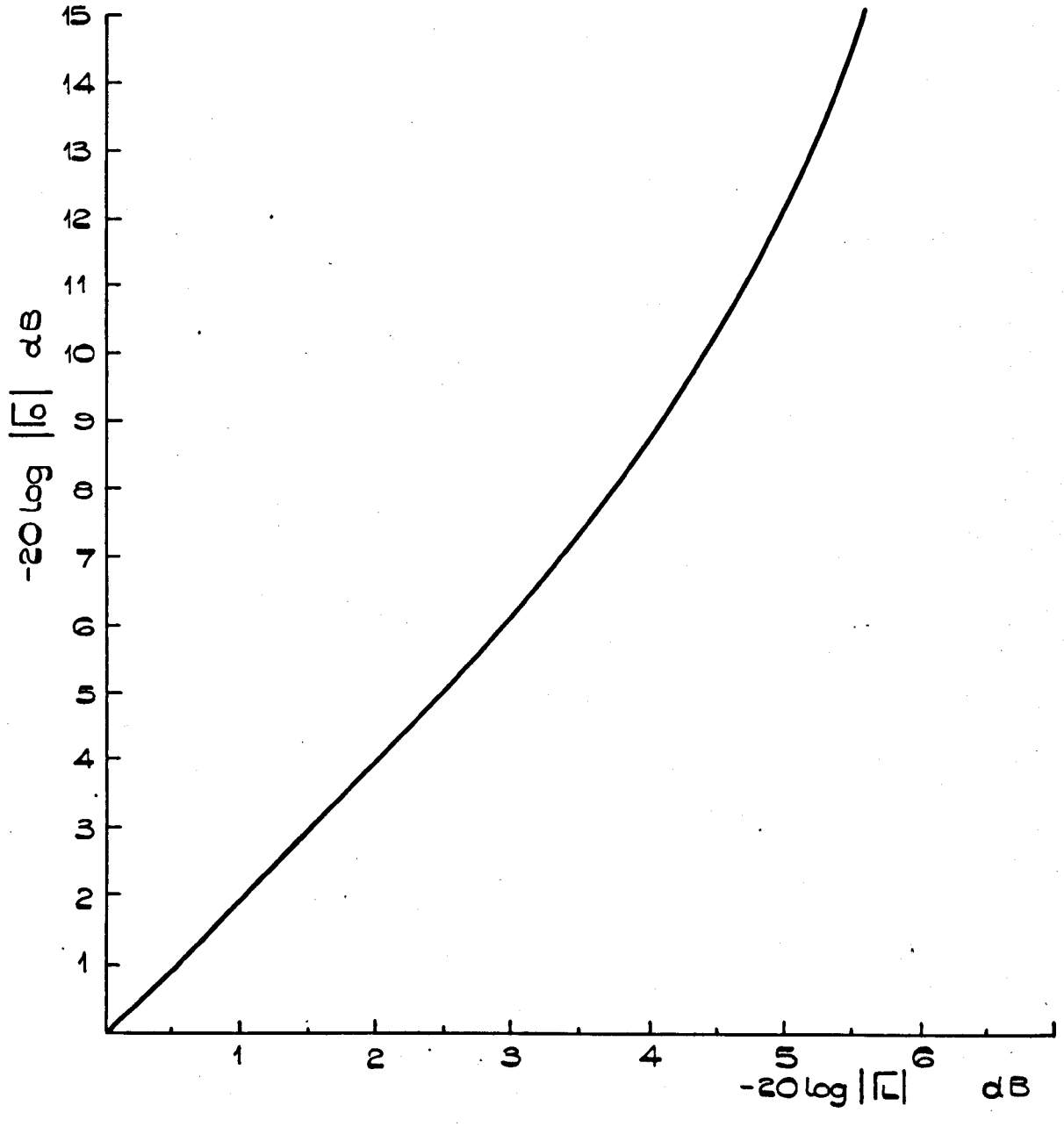

FIGURE 5.

THE BANDWIDTH GRAPH.

at resonance is zero (undercoupled case) then the effect of the coupling susceptance is negligible. The advantage of the precision reflectometer described above is that it measures the phase as well as the amplitude of the reflection coefficient of a cavity. Thus the effect of the coupling susceptance on $|\Gamma|$ can be determined quite easily.

Chapter 6.

CAPACITIVELY LOADED COAXIAL CAVITIES

- COUPLING MECHANISMS AND MEASUREMENT OF CAVITY PERFORMANCE

6.1 Introduction

It is shown in section 2 that the dielectric properties of thin dielectric films can be measured using a capacitively loaded coaxial cavity. The mechanical problems in the construction of such a cavity are discussed in section 4. In this section the electrical properties of capacitively loaded coaxial cavities will be discussed.

Initial tests were carried out to verify the theoretical approach taken during the design of the capacitively loaded coaxial cavities. The cavities used in this part were made from brass. The measurement techniques that were used were dependent on the coupling mechanism of the cavity to the measuring system. Numerous coupling mechanisms were tried and the final choices were:
(a) the dumbbell coupling to the waveguide (WG 16) and (b) the coaxial loop coupling to the coaxial line, measuring systems. The latter was used for lower frequencies than X - band whilst the dumbbell slot was used for X - band work.

The cavities used for the measurement of the thin film properties, were made from invar and plated with silver as described in section 4.3.1. These cavities had properties different from the brass cavities.

The cavity parts were taken apart and reassembled during the measurement of the thin film dielectric properties. Ideally the resonant frequency and the Q factor of the cavity should not vary upon repeated disassemblying and reassemblying the cavity parts, but in practice they

do vary. The enormous effect of these variations in fo and Qo on errors of the measured dielectric properties is shown in section 8.2. Therefore these variations should be reduced to the lowest practical values. In the present investigation it was aimed to get variations of $< \pm 1\%$ in Qo and $< \pm 0.2$ MHz. in fo.

In the following sections the properties of these cavities together with experimental verification of the theoretical approach and different coupling mechanisms that were tried, will be discussed. The cavity properties were measured on the systems described in section 5.

6.2 Coupling Mechanisms of the Cavities.

6.2.1 Electric Probe: Waveguide System.

The attempt was to take the advantages of a single coupling transmission method, together with the low errors of the waveguide measuring system. The coupling consisted of an electric probe, supported by a p.t.f.e. insulating support, extending on one end into the waveguide and the other end entering into the cavity at the electric field maximum point. Figure 6.1 shows the cross section and the photograph of the assembled unit.

It was found that it was difficult to separate the cavity parts without disturbing the coupling probe. Another disadvantage of the electric probe coupling was that the electric field inside the cavity was disturbed by the probe. Further details on the probe can be found in Appendix 7.1.

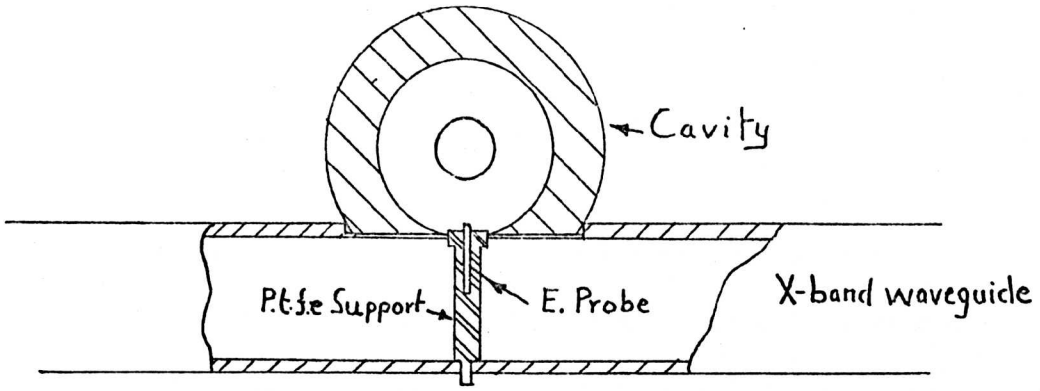

(a) E. Probe coupling to the cavity

(b) Floating Disc-Probe

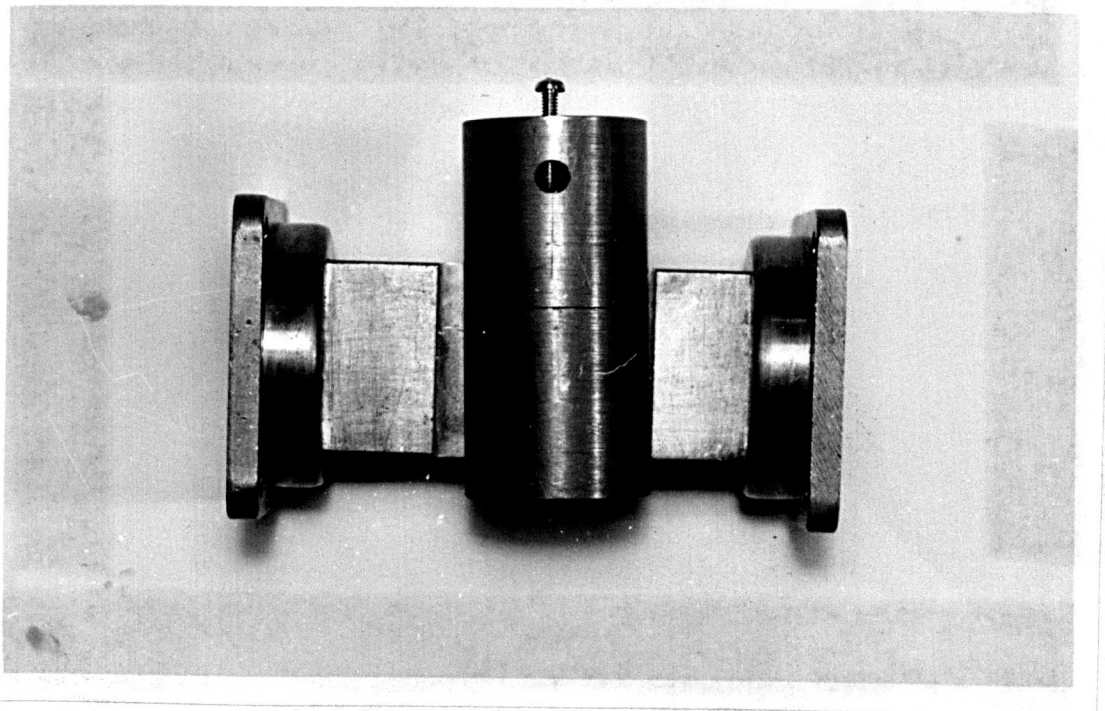

(c) Assembled Cavity - Waveguide System

Figure 6·1 Probe Coupling mechanisms.

6.2.2 The Floating Disc - Probe: Waveguide System.

It was found that a simple electric field probe disturbs the electric field inside the cavity and hence reduction in the resonant frequency of the cavity. To eliminate this a floating disc - probe coupling system was tried (further details can be found in Appendix 7.2), (Fig. 6.1b). Although this technique had improved the performance of the cavity coupling over the electric probe, the system was mechanically unstable. Also the power coupling into the cavity was so small that after a few tests it was abandoned.

6.2.3 Magnetic Loop Coupling: Coaxial System.

The probe was designed using a 50 ohms, 7 m.m coaxial line having an APC - 7 connector on one end. Using the compensated step transformation approach[55] the line dimensions at the other end were reduced while keeping Zo at 50 ohms. The diameter of the inner conductor was reduced from 3.03 m.m to 1.3 m.m. At the end of the coaxial line the extension of the inner conductor was reduced further in diameter to 0.5 m.m and made into loop by soldering the free end onto the outer conductor (Figure 6.2b).

The step transformation on the coaxial line preceding the loop was tested on the Time Domain Reflectometer[56] (HP 1415A) and no discontinuity at the step could be observed, (Figure 6.2a).

The magnetic loop was situated near the maximum current point i.e. close to the short circuit plane of the base part of the cavity and the penetration into the cavity could be adjusted.

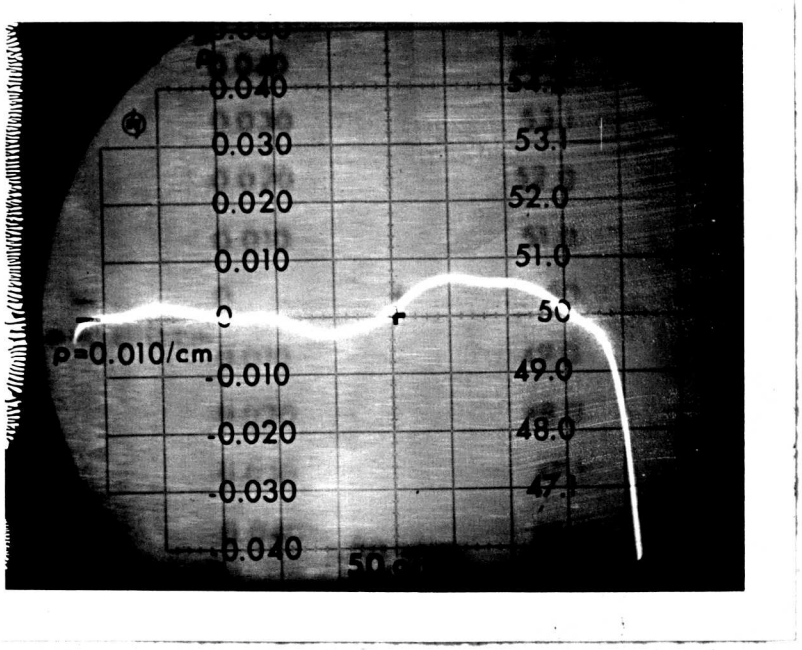

(a)

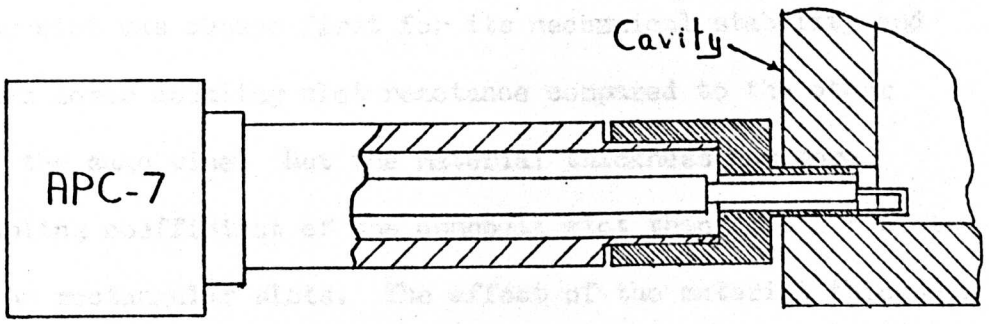

(b)

Figure 6.2 Magnetic Loop Coupling to Cavity.
(a) TDR display of the coaxial line section of MLC
(b) Cross sectional view of coupling mechanism.

The coupling system was used with cavities to observe the full range of resonances from 1 GHz up to 12.4 GHz. Because of the higher errors in the coaxial measuring system compared to the waveguide system, this method of coupling was not used for X - band measurements on dielectrics.

Recently Shurmer[57] developed a system where the errors of the network analyser measurements could be corrected by a computer, whilst the measurement was carried out. This system can be used for the coaxial coupling system provided that the frequency of the signal generator can be swept by the computer in small steps. No attempt was made to use the system because the frequency could not be swept as required, at the time of the investigations.

6.2.4 Dumbbell Slot Coupling: Waveguide System.

This coupling slot was chosen first for its mechanical stability and then because it has lower coupling slot reactance compared to the other coupling slots of the same size. But the material thickness has more effect on the coupling coefficient of the dumbbell slot than on other slots such as circular or rectangular slots. The effect of the material thickness on the slot parameters was determined experimentally. Three identical dumbbel coupling slots were prepared from a thin copper foil. These coupling slots were used one at a time first to couple a halfwavelength waveguide resonator to the reflectometer as described in section 5. The return loss of the cavity at resonance was measured. The cavity was then coupled through a slot made up of the three slots stuck together and its return loss at resonance was measured as before. Results are given in Table 6.1

Table 6.1

The effect of the material thickness on the coupling coefficient of the dumbbell slot

Slot No.	Thickness of Slot	Return loss at Resonance
11	0.130 mm	13.6 dB
12	0.130 mm	14.6 dB
13	0.130 mm	15.0 dB
11 + 12 + 13	0.390 mm	7.4 dB

Another effect that influences the coupling into the cavity is the diameter, d, of the coupling slot holes , this was tested on the coaxial cavity CB 1. The measured return loss at resonance for different d's are given in table 6.2.

Table 6.2

Diameter of slot holes d, mm	Return loss at resonance dB
1.8	0.5
2.0	1.0
2.5	1.25
3.0	2.3

These results show the importance of the thickness as well as the diameter of the slot on the coupling power to the cavity. It is better

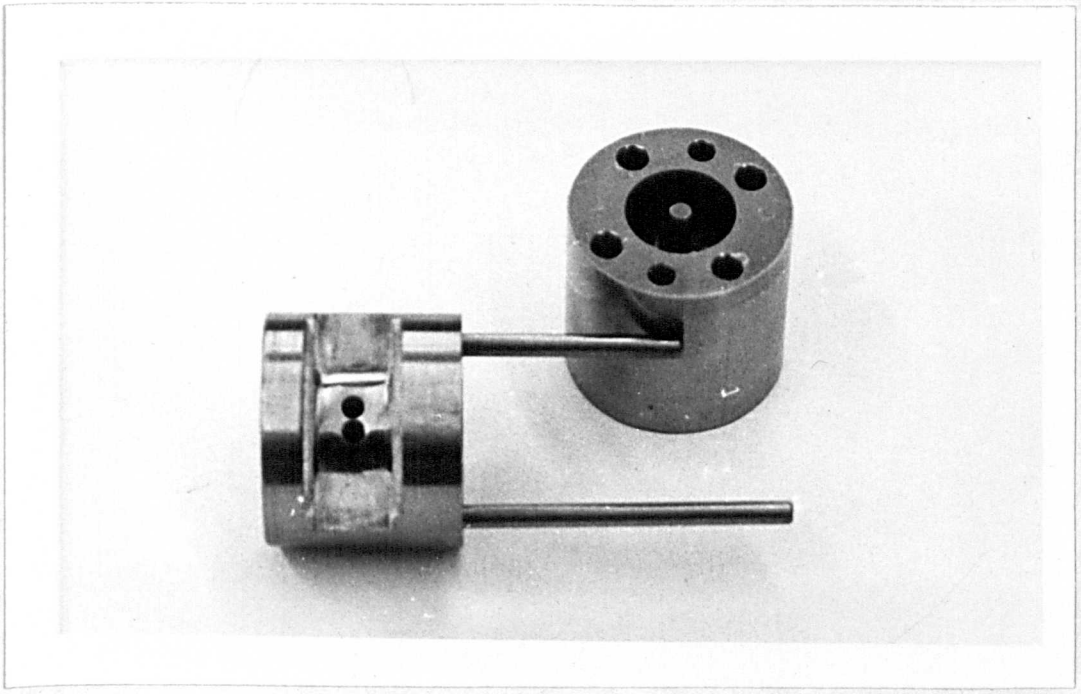

Figure 6.3. Dumb-bell Coupling and Cavity parts before fixing the waveguide.

to have small hole diameter and thin slots because large holes give larger coupling reactance than the small slots.

The dumbbell slot coupling was used on invar cavities for the X - band measurements. CI 1 had d = 2.8 m.m and CI 2 had d = 2.3 m.m. The separation between the centres of the holes was 3. m.m. and the slot between the holes was 0.2 m.m wide. The thickness of these slots was about 200 μm. Figure 6.3 shows the coupling slot , a photograph of the slot prepared on CI 1, before fixing the waveguide end and plating the cavity.

6.3 Measured Properties of the Capacitively Loaded Cavities.

As mentioned earlier initial work was carried out on brass cavities, and then for the main work, plated invar cavities were used. The softness of the brass compared to the invar gave the flexibility of doing many modifications to the brass cavities. The cavity properties were first measured on brass cavities. These properties were the coupling mechanisms and the capacitive network representation of the gap. The latter was the most important point as there was practically no experimental data on these quantities.

In the following sections the properties of brass and invar cavities will be discussed.

6.3.1 Brass Cavities.

It was reported that a coaxial cavity has a maximum Q factor when the ratio of the outer conductor diameter to the inner conductor

diameter of the cavity Do/D1 lies between 3 and 4. Figure 2.6 shows the variation of Qo with Do/D1 of the present capacitively loaded coaxial cavity. So initial cavities were designed to have Do/D1 ratios around 3.6.

The first cavity, as all the other cavities was designed such that it had two parts. The base part had the coupling to the transmission line and the gap, whilst the top part had the centre conductor the same length as the outer conductor. This was described in detail in section 4.

Table 6.4 shows the characteristics of these cavities, such as the resonant frequency, f_1 , unloaded Q factor Qo, outer diameter, Do, the ratio of Do/D1, the length of the cavity excluding the gap and the capacitive gap Go. It will be seen from the table that CB1 had a lower Qo than CB2. The reason for this was that CB2 had a larger Do than CB1. Also CB2 was made from a solid material and its surfaces were highly polished whilst the inner conductors of CB1 were screwed on and its surfaces were not polished.

6.3.1.1. Measurement of Capacitive Network Parameters of a Gap in the Centre Conductor of a Coaxial Line.

The gap in the centre conductor of a coaxial line can be represented as shown in the theory of the capacitively loaded coaxial cavity (section 2) by a two-part π network (figure 2.1). This apprach was adopted from Green's work[25] where the gap parameters were derived from the numerical solution of the field in the gap. Young[26]

claims that for small gaps the fringing field capacitance between the centre and outer conductors at the gap, Cp, can be neglected. The only practical work[27] found in the literature described, the gap represented by a π network. Its parameters were measured by measuring the input impedance of the network whilst the output was terminated in a matched load. It was claimed that Cp was constant with varying gap, thus contradicting Green's results.

The capacitive gap parameters can be measured using the symmetrical capacitively loaded coaxial cavity. The electric field distribution of the cavity is shown in figure 2.2 section, 2. It will be seen from this figure that whenever the fields on both sides of the gap have the same polarity, figure 2.2 modes 2 and 4, then the resonant frequency is only dependent on Cp, but the series capacitance Co (1 + m) has no influence. On the other hand when the fields on both sides of the gap have different polarities all the capacitances control to the resonant frequency of the cavity.

Using mode 2 and mode 4 resonances, we have the following resonant state

$$(2\pi f\, Cp)^{-1} = Zo \tan\left(\frac{2\pi f L}{v\ 2}\right) \qquad 6.1$$

which simpflies to $Cp = \left(2\pi f\, Zo \tan\left(\frac{2\pi f\ L}{v\quad 2}\right)\right)^{-1}$ 6.2

Cp can be calculated from this equation if the resonant frequency f, the characteristic impedance of the cavity, Zc and the length of the inner conductors L are known.

Measured values of Cp using the above equation together with the values interpolated from Green's results are shown in table 6.3. These results show that Cp decreases with decreasing gap Co. This proves that Cp approaches zero as Go tends to zero and hence contradicts the reported[27] experimental results. It was claimed in his report[27] that his experiment was carried out for large gaps and it is possible that for large gaps Cp approaches to a constant value.

Table 6.3

Gap	Cp pf	
	Measured	Green's value
500 μm	0.0139	0.0142
300 μm	0.0075	0.0084

Cavity CB1 was used at X - band

It will be seen from these results that for gaps < 60 μm Cp will be negligible compared to $(n + 1)Co$. Therefore the assumption in the theory that Cp is negligible was justified.

This approach of the measurement of the discontinuity parameters

can be applied to other types of transmission lines such as strip and microstrip lines. Some results obtained from the microstrip capacitive gap are given in section 10.

6.3.2 Invar Cavities.

The theoretical treatment of the capacitively loaded cavity was given in section 2, and some data was presented in graphical form on certain types of cavities having a length of 32 m.m + Go. This length was chosen because the resonant frequency of the cavity of around 9.5 GHz could beachieved for gaps below 60 μm and Do/D1 = 5. The ratio of Do/D1 = 5 was chosen on the following grounds:

(i) The resonant frequency of the cavity is higher than Do/D1 < 5 for the same Do.

(ii) The frequency shift of the resonant frequency of the cavity when loaded with the dielectric film is higher than Do/D1 < 5 for the same Do. It will be seen from figure 2.7 that Do/D1 > 5 will give still higher frequency than Do/D1 = 5.

(iii) Although cavities having Do/D1 > 5 give higher frequency shift than the cavity with Do/D1 ≤ 5, they have a lower Qo than the cavity with Do/D1 ≤ 5. The Q factor the dielectric film Q_D is proportional to Qo, therefore high Qo should be used. In the present case the compromise to the Do/D1 ratio was taken as 5.

(iv) Cp is lower for high Do/D1 ratio than Do/D1 = 3.6.

Having these points in mind the following cavity dimensions were chosen: Do = 15 m.m, Do/D1 = 5, L = 32 m.m.

and Go < 60 µm. All of the invar cavities were constructed using these dimensions.

The Q factor of the cavity is proportional to Do (section 2.3.2 equation 2.18) but there is a limit to the largest value of Do that can be used. This limit arises from the propagation of higher order modes in the coaxial line. The E11 mode has the lowest cut off frequency and the cut off wavelength $\lambda c \simeq \pi (Do + D1)/2$. Substituting the invar cavity dimensions gives a cut off frequency of 10.6 GHz. The invar cavity resonated in this mode at about 11.75 GHz with a Q factor 7300. This justifies the Do chosen for the invar cavities.

There were three invar cavities, CI1 and CI2 having dumbbell coupling to waveguide (WG 16) system figure 4.4a and CI3 had the magnetic coupling to coaxial system figure 4.4b. The last cavity was used only for low frequency work.

CI1 had only one top part whilst CI2 had 4 top parts (T_1, T_2, T_3, and T_4). These invar cavities had a very low Q factor at X - band ($\simeq 700$) and had to be plated. The cavities were silver plated as described in section 4.3.1. and the cavity properties were measured using the measuring system described in section 5. The best measured Qo value was 95% of the calculated value. Qo values better than 92% of the calculated value could be obtained with ease.

The characteristics of these cavities together with the brass cavities are given in table 6.4.

Table 6.4.

Properties of Cavities.

Parameter	BRASS CAVITIES		INVAR CAVITIES		
	CB1	CB2	CI1	CI2	CI3
L, mm	37	32	32	32	32
Go, μm	300-500	50-100	30	32.5	58
Do mm	10.3	15	15	15	15
Do/D1	3.4	3.6	5	5	5
f1 MHz	9430	9590	9490.7	9498.3	1347
Qom	1250	2350	4514	4490	1780
QoTH	-	2500	4890	4890	2051

Qom = measured value, QoTH calculated from the theory

The differences between the measured and theoretical values of Qo were due to the following factors:

(a) The conductivity of the silver plating was not as good as the highest purity silver (σ = $(1.59 \times 10^{-8}$ m.$)^{-1}$ at 20°C) which was assumed in the theoretical calculations. This was expected since the bright electroplating solutions contain many organic compounds and other materials. The electroplated material will contain some of these materials and its conductivity will be lower than the high purity metal.

Also gold flash, 6 - 10 μm thick, used as an antitarnish layer will increase the surface losses.

(b) The surface texture due to electroplating affects the surface losses. This can be remedied by the chemical or electropolishing of the surface. To test the effect of the surface finish on the Qo value of the cavity, one of the top parts of the cavity was electroplated in the Elfit electroplating solution without the brightener additive. The measured Qo was 80% of the theoretical value. This test showed the advantage of using a bright electroplating solution which gives smoother surface than an ordinary plating solution. Because of the complicated shape of the cavity, no attempts were made to polish it after plating.

(c) As explained in section 4.3.1, the electroplated metal surfaces are under stress like cold worked metals and therefore would have lower conductivity than the stress released plating.

The top part of the cavity was heated up to 200°C during the deposition of the dielectric film and this could relieve the stressed plating and improve the Qo value. To eliminate any effect during the film deposition, the top part of the cavity was heat treated in the vacuum system. The heat treatment was carried out between 250 and 300°C. The following results were observed during one of these processings (Table 6.5).

The base and the top parts of the cavity after plating were cleaned in running water and isopropyl-alcohol and measured at 22.5°C room temperature.

Table 6.5.

Time after plating	QoT	% of QoTheoretical	Improvement %
2 hours	4000	81.9	-
26. hours	4250	87.0	5.1
1 week later top part heat treated at 250°C for 2 hours	4460	91.3	9.4

These results show quite an improvement of the measured Qo.

Further investigation on the 5 to 8% drop of the measured Qo from its theoretical value brought out the following information : even with the highest purity metal deposition and freshly polished surface the best measured Qo could not be better than 98% of the theoretical value.[60,61] In our system there was an additional layer of gold as an antitarnish coating and therefore it would have reduced the measured value. Taking into consideration the above points it is reasonable to assume that for cavities having measured Qo values greater than 90% of the theoretical value, the loss distribution could be assumed to be uniform, unless there is a definite observable fault on the plated surface.

6.3.2.1 Measurement of the Series Gap Capacitance of the Cavity.

The shunt capacitance, Cp, of the gap was measured using the brass cavity CB1. The series capacitance of the gap, (n + 1) Co, could not be determined accurately, because it was found that the resonant frequency of the cavity was dependent on the torque put on the screws clamping the two parts of the cavity. This was due to the compression of the soft material (brass) of the cavity and hence reduction in Go.

The resonant frequency of an invar cavity CI 1 was measured before the plating with silver. The conditions were, Go = 42 um, L = 32 mm, Do = 15 m m, D1 = 3 m.m. The measured resonant frequency fi was 9534 MHz whilst the calculated resonant frequency was 9532 MHz. These results showed that the theoretical treatment of the gap capacitance was the right approach.

After this verification of the theory, the plated cavities were used as follows: the dimensions, except Go, and the resonant frequency of the cavity were measured. Using these quantities in equation 2.10, the gap Go was calculated. Thus the effect of the material compression was eliminated. Although no material compression was observed with the plane invar cavities, when plated with silver the silver plating between the mating surfaces of the cavity parts could be compressed. This effect was observed when the torque applied on the clamping screws was greater than 4 lb - inch.

6.3.2.2 The Stability of the Invar Cavity.

The cavity parts were disassembled and assembled again during the measurement of the film properties. To have reliable and reproducable measured results, there should be precision alignment of the outers as

well as the inners of the cavity parts. The first mechanical approach taken was to use a tight aligning jig filling the inner of the assembled cavity. After clamping two dowelling holes at 180° apart were drilled. The cavity parts were held together with four steel screws which were tightened by a constant torque screw driver.

Any misalignment of the cavity parts would introduce a spread in the measured resonant frequency, so cavity parts were disassembled and assembled many times and at each process the Qo and fo were recorded. The statistical analysis gave the following results. (table 6.6)

Table 6.6

	Qo	f1
Average value	4505	9490.66 MHz
Standard Deviation	42.6	0.435 MHz
Number of Data	15	14
Temperature	21°C	21°C

These measured results for cavity CI1 showed that Qo could be measured within ± 1% but the frequency scatter was too high.

The scatter in frequency was reduced to less than ± 0.1 MHz., this was achieved by jig boring the dowelling holes to within 2.5 μm relative to the bore of the cavity and also reducing the constant

torque applied on the screws from 7 lb inch to 3 lb inch. The latter results were obtained for the cavity CI2.

6.4. Comments.

The theoretical treatment of the capacitively loaded coaxial cavity was verified experimentally. In this experimental methods were introduced successfully, for the measurement of the capacitive gap parameters.

The importance of the mechanical as well as the electrical stability of the cavity depends upon the coupling mechanism used to couple the cavity to the measuring system. It was shown experimentally that the most suitable way for X - band uses was the dumbbell slot coupling.

The required stability of the resonant frequency of the cavity, f, was achieved by proper alignment of the cavity parts and using constant torques on the screws holding these parts together. This is an important parameter, because the cavity parts were disassembled and assembled again during the measurement of the dielectric film properties.

The Q factor of the cavity depends on the plating of its surfaces. It was shown that as high as 95% of the theoretical value of Qo could be obtained by proper treatment of the plated surfaces. The stability of Qo was found to be quite good even without proper temperature stabilization. The quality of Qo showed that there was no loss at the joint between the two parts of the cavity.

The conductivity of the electroplated metal is temperature dependent according to the following relationship:

$$\sigma = \sigma_o \ (1 - \alpha \ t \ )$$

where σ = conductivity at temperature t

σ_o = conductivity at t = 0^oC

α = coefficient of resistivity of material with temperature

= 4.1×10^{-3} per ^oC for silver

t = temperature of plating in ^oC

Taking two temperatures t_1 and t_2 where $t_2 > t_1$, the following relationships are obtained

$$\sigma_1 = \sigma_o \ (1 - \alpha t_1) \qquad (a)$$

$$\sigma_2 = \sigma_o \ (1 - \alpha t_2) \qquad (b)$$

Dividing equation (b) by equation (a) gives

$$\sigma_2 / \sigma_1 = (1 - \alpha t_1)^{-1} (1 - \alpha t_2)$$

and for small values of αt_1 and $\alpha t_2 << 1$

$$\sigma_2 / \sigma_1 = 1 - \alpha (t_2 - t_1)$$

This relationship shows the variation of the conductivity with temperature. The Q factor of the cavity is proportional to the square root of the conductivty.

In the theoretical calculations the conductivity of the silver was taken at 20°C. Therefore Qo values measured at other temperatures should be converted to 20°C value before comparing them with the theoretical value.

The heat treatment introduced during the cavity processing showed the advantage of the process. Heat treatment when applied to other plated circuits such as m.i.c.'s should give improvement over the untreated circuits.

CHAPTER 7

MEASUREMENT OF THE THIN DIELECTRIC FILM PROPERTIES

7.1 Introduction

Theoretical approaches to the measurement of the properties of the thin dielectric films were introduced in section 2. In that section the capacitively loaded coaxial cavity was used as the measuring unit. The construction of the cavity, the measuring system and the practical properties of this cavity were discussed in the previous sections. It was shown in those sections that the measured and the calculated properties of the cavity were in agreement. In this section these cavities together with the measuring system described in section 5 will be used for measurement of the thin dielectric film properties.

Cavities used in these measurements were CI1,CI2 and CI3, i.e. Invar cavities. These cavities were plated and after the heat treatment in the vacuum system, their properties, i.e. Q_{oT}, f_1 and the reflection coefficient at resonance, were measured. The description of the experimental procedure for the measurement of the thin film dielectric properties and the results will be presented in the following sections.

During the theoretical calculations of the Q-factor of the dielectric film the cavity wall losses were assumed to be uniformly distributed. It was found during the measurement of the Q-factor of the cavity, Q_{oT}, that the measured Q_{oT} value was 5 to 8% lower than the theoretical value. Although firm conclusions were made in section 6 that the loss distribution could be assumed to be uniform, it was

decided to check this experimentally. This point is discussed in the following section. To verify the theory we had to measure a material which had predetermined dielectric properties. The dielectric properties of the materials used in the above test were measured using the perturbation method in a rectangular waveguide cavity. This will be discussed in section 7.4.

7.2.

Experimental Verification of the Theory Applied to Dielectric Loaded Cavity.

The VSWR approach to the measurement of the Q-factor of the dielectric film Q_D, introduced in section 2., assumes that the losses in the cavity walls were uniformly distributed. This assumption was tested by measuring the permittivity of materials which had been measured previously (described in section 7.4.) Cavities were prepared with Q_{oT} values varying between 83 and 93% of the theoretical value. This was achieved by plating the top part of CI1 under different plating conditions, thus giving different surface smoothness and conductivities. The dielectric samples used were: (a) Thinned down soda lime glass (microscope cover slides made by Chance Bros.) and (b) Amber mica samples split down to the required thickness (samples were supplied by the Langley London Ltd.).

The permittivity of soda lime glass was measured as described in section 7.4. The glass slides were then thinned down to a thickness <15 um in a solution made up of 2% HF, 2% HCl and 96% deionised water. This solution could etch at the rate of 1 μm per minute. Then disks of 3 mm diameter were cut (disk diameters were the same as

the diameter of the inner conductor of the cavity) and placed in the gap of the cavity. The properties of [illegible] the dielectric loaded cavity, f_2, Q_{ox} and the reflection coefficient were measured. This data together with the data of the cavity without the sample were used in equations 2.28, 2.53, and 2.54 (sections 2.4 and 2.5) and the dielectric properties were determined. Measured results are shown in table 7.1. There three sets of results are given:

(1) The dielectric properties calculated using the VSWR approach applied to the capacitively loaded coaxial cavity (section 2.4)

(2) As (1) but the perturbation method was used (section 2.5)

(3) The dielectric properties of the samples measured in a waveguide cavity as described in section 7.4.

Table 7.1

Measured Dielectric properties of Soda Lime Glass using cavities with different Q factors.

CAVITY	Measured Q_{oT} % Q_{oTH}	Capacitively Loaded Cavity				Waveguide cavity	
		VSWR method		Perturbation m			
		ϵ^1	Q_D	ϵ^1	Q_D	ϵ^1	Q_D
CI2+T_1	83	6.1	53	-	-	6.1	62
CI2+T_2	85	5.7	52	-	-		
CI+T_3	87	6.4	69	6.35	68		
CI 1	93	5.7	64	5.7	62		

T_1, T_2, T_3 = Top parts of cavity CI2

Q_{oTH} was the theoretical value.

T_1, T_2 and T_3 were the top parts of the cavity CI2

Q_{oTH} was the theoretical value.

Also amber mica disks were cut from the laminar materials and split down to 12.6 μm. The properties of these disks were measured using the capacitively loaded cavity. Using the cavity CI2 with Q_{oT} >90% Q_{oTH}, measured results for amber mica were:

(i) $\epsilon' = 6.12$ and $Q_D = 450$ (using VSWR Method)

(ii) $\epsilon' = 6.16$ and $Q_D = 390$ (using Perturbation Method)

(iii) $\epsilon' = 5.7$ and $Q_D = 440$ (Waveguide Cavity Method)

It will be seen from these results that the most important parameter Q_D measured using the VSWR method in which uniform loss distribution was assumed and the perturbation method agree if Q_{oT} >87% Q_{oTH}, with the Q_D values measured using a completely different method, i.e. the rectangular waveguide cavity.

The above test has verified the VSWR method in which the cavity was treated as a lumped element circuit and equally well the perturbation method applied to the capacitively loaded coaxial cavity. The VSWR method suffers in accuracy if the measured Q factor of the cavity is less than 87% of its theoretical Q factor.

The test has also shown the usefulness of the coaxial cavity for the measurement of the self supporting dielectric material properties, on a sampling basis. 3 mm diameter disks can be cut from the material and their properties are measured one at a time and if

there is any inhomogeneity in the material it can be detected. The trouble with the self supporting disk is that it may slide to the side of the gap and this gives an erroneous result. This difficulty was overcome by repeating the experiment and observing the frequency shift of the cavity without and with the sample. With a properly aligned disk the frequency shift is a maximum.

7.3 Deposited Dielectric Films.

The measurement procedure for the deposited dielectric films was the same as the technique used on self supporting disks discussed in the previous section. The difference was the processing used in the preparation of the dielectric films and the films were supported by the plane end of the centre conductor. The films used in these measurements were obtained using different thin film processing techniques as discussed in section 9. The film thicknesses used varied between 1 μm and 6 μm. The film to be measured is deposited on to the plane end of the centre conductor of the top part of the cavity. Figure 7.1 shows the arrangement used for this.

In the set up: A is the cross section of the top part of the cavity

B is the ptfe mask. This material was used because it would not damage the cavity surfaces.

C is the copper coated glass mask. It was also used in the measurement of the thickness of deposited dielectric film.

D is the substrate holder. Its plan view is shown in Figure 7.1b. It could accomodate up to 5 cavity

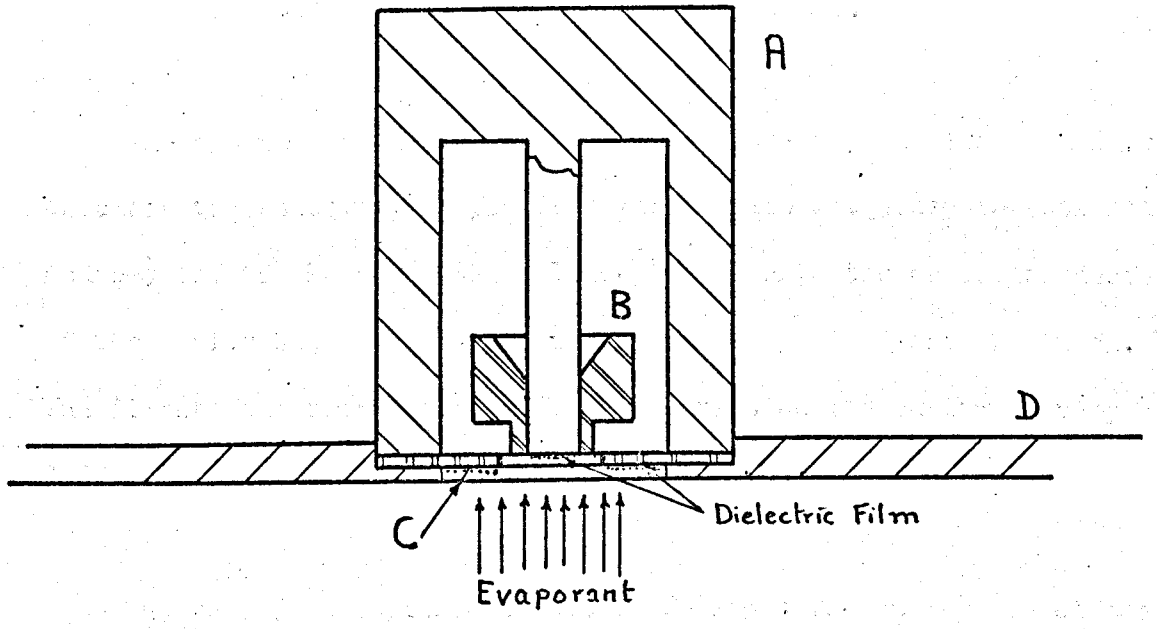

(a) Cross section showing the Masking arrangement

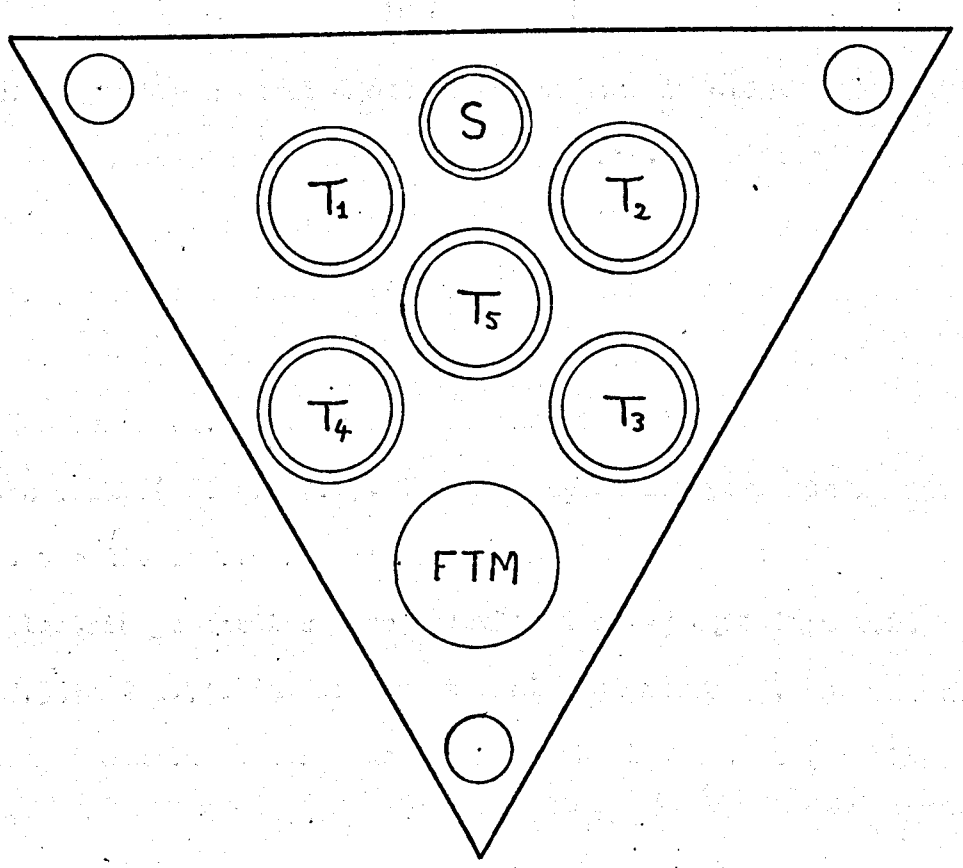

(b) Plan view of the Substrate Holder

Figure 7.1 Deposition of Dielectric Film.

tops (T_1 , T_2 etc.), a sampler, S and a quartz crystal for the film thickness monitor(F T M).

The system has the following advantages:- a-) sampling the film as close to the cavity as possible for the low frequency investigations and b-) the thickness of the film deposited onto the centre conductor of the cavity was determined from the film deposited onto the mask. The direct measurement of the film thickness on the cavity is very difficult.

The measurement procedure was as follows: The cavity was cleaned as required for the film processing. The cavity parts were dried and assembled in the clean room. The assembled cavity was taken into the measurement laboratory and after an hour its parameters were measured. The measured parameters were f_1 , Q_{or} and the return loss at resonance, (return loss in dB $-20 \log|\Gamma_0|$ where Γ_0 is the reflection coefficient). The measurement was carried out after an hour in order to raise the cavity temperature up to the room temperature. Even after two hours non of the parameters were different from the first measurement, The cavity was taken back into the clean room and the dielectric film was deposited as discussed in section 9. The new cavity parameters were then measured.The thickness of the dielectric was measured on from the mask (Figure 7.1). Knowing the cavity parameters with and without the dielectric film loading, and the thickness of the film, the dielectric properties were calculated using equations 2,28 2.42, 2.53 and 2.54. In this two techniques were used, one was the VSWR method and the other was the perturbation method (Sections 2.4 and 2.5)

A typical measurement gave the following cavity parameters:

Table 7.2

MICROWAVE PROPERTIES OF THIN DIELECTRIC FILMS.

Material	Measured at X band			Results Reported by others		
	ϵ^1	Q_D	Remarks	ϵ^1	Q_D	Remarks.
SiO	4.9-5.9	120 - 136	EB, D = 20 - 50 nm/s	6-8	30	T, ref. 12
				4-4.8	110 - 250	T, D = 5nm/s, F = X-band ref. 22
SiO_2	3.9-4.4	10 - 100	EB.	4	70	EB, MIM, F = 7 GHz, ref. 62
SiO_2	4	150-150	R.F. Sp.	4	500-600	RFSp, MIM, F = X-band ref. 18
Al_2O_3	8 - 10	34 - 40	EB	7-10	-	A., Ev . ref. 12

A = Anodizing, EB = Electron Beam Evaporation, Ev. Evaporation, RF Sp = R.F. Sputtering, Tr = Thermal Evap.

D = Rate of Deposition, F = frequency, MIM = Tested as sandwich capacitor

NOTE; More detailed results (i.e. evaporation condition, frequency) are given in Tables 7.3, 9.2 and 9.5.

Cavity without the film	Cavity with the film
Q_{oT} = 4348	Q_{ox} = 4238
f_1 = 9501.249 MHz	f_2 = 9494.000 MHz
S_1 = 1.586	S_2 = 1.631

Gap, G_o = 32.7 μm

Film thickness xG_o = 2.70 μm

Calculated results are:

ϵ' = 4.2 $\quad Q_D$ = 77 using the VSWR method.

ϵ' = 4.19 $\quad Q_D$ = 86 using the perturbation method.

The dielectric measurement procedure can be summarized in a process flow chart as shown in figure 7.3. which explains the steps taken during each of the measurements of the films. It will be seen from the chart that two loops were used. One of these loops was used for repeated measurement by removing the film and depositing a film again. This loop was also used to check the system after removal of the film to ensure that the cavity properties had not changed during the film deposition process. The second loop was used for the calibration of the measuring system.

The silicon monoxide SiO, silicon dioxide, SiO_2 and Alumina Al_2O_3 films prepared using an electron beam evaporation source were investigated. The spread in the parameters values i.e., ϵ' and Q_D were due to various preparation techniques used in the film processing. Also SiO_2 films prepared using the diode r.f. sputtering technique were evaluated. These results are shown in the table. 7.2.

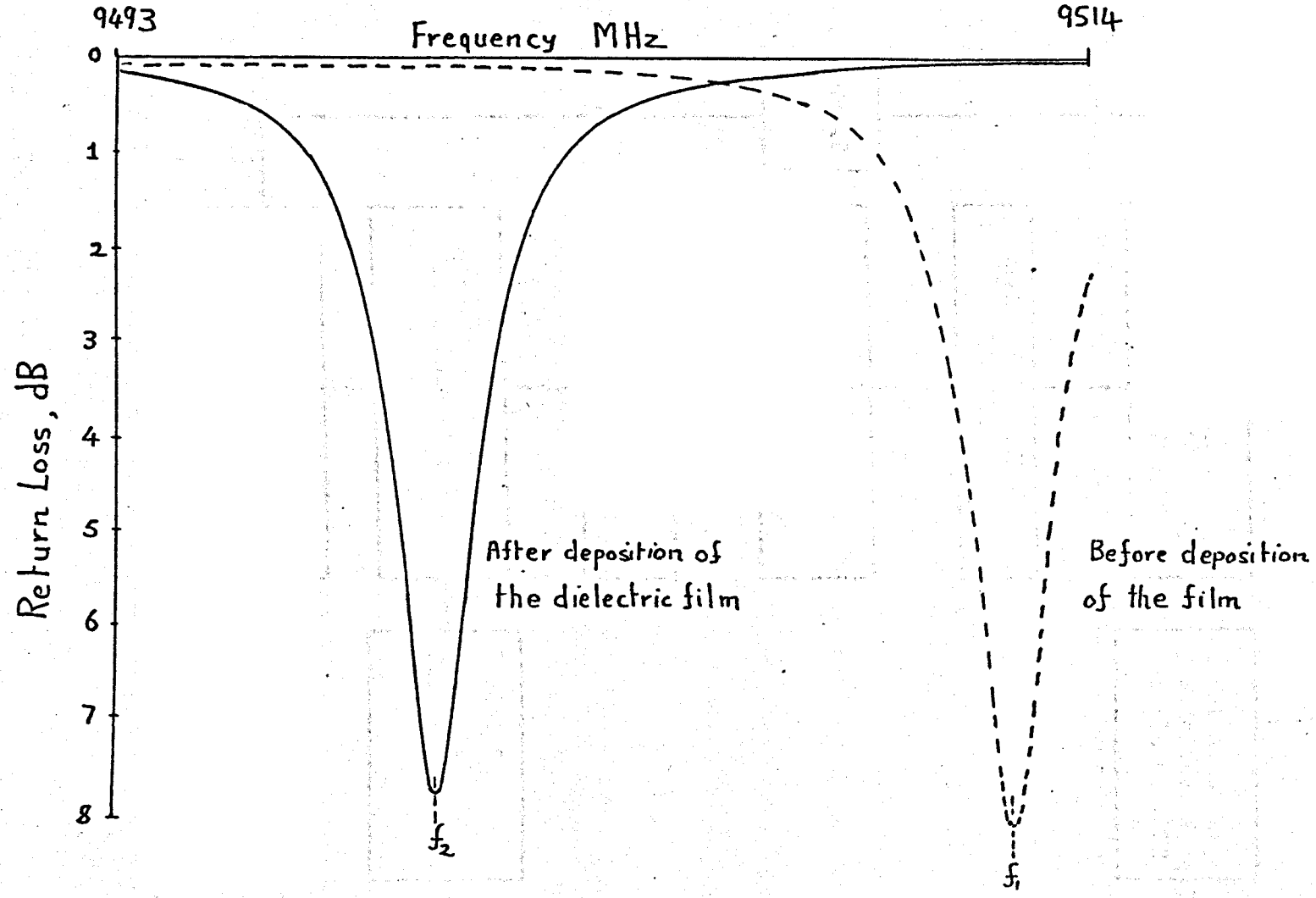

Figure 7·2 Resonance Curves of the cavity with and without the Dielectric Film.

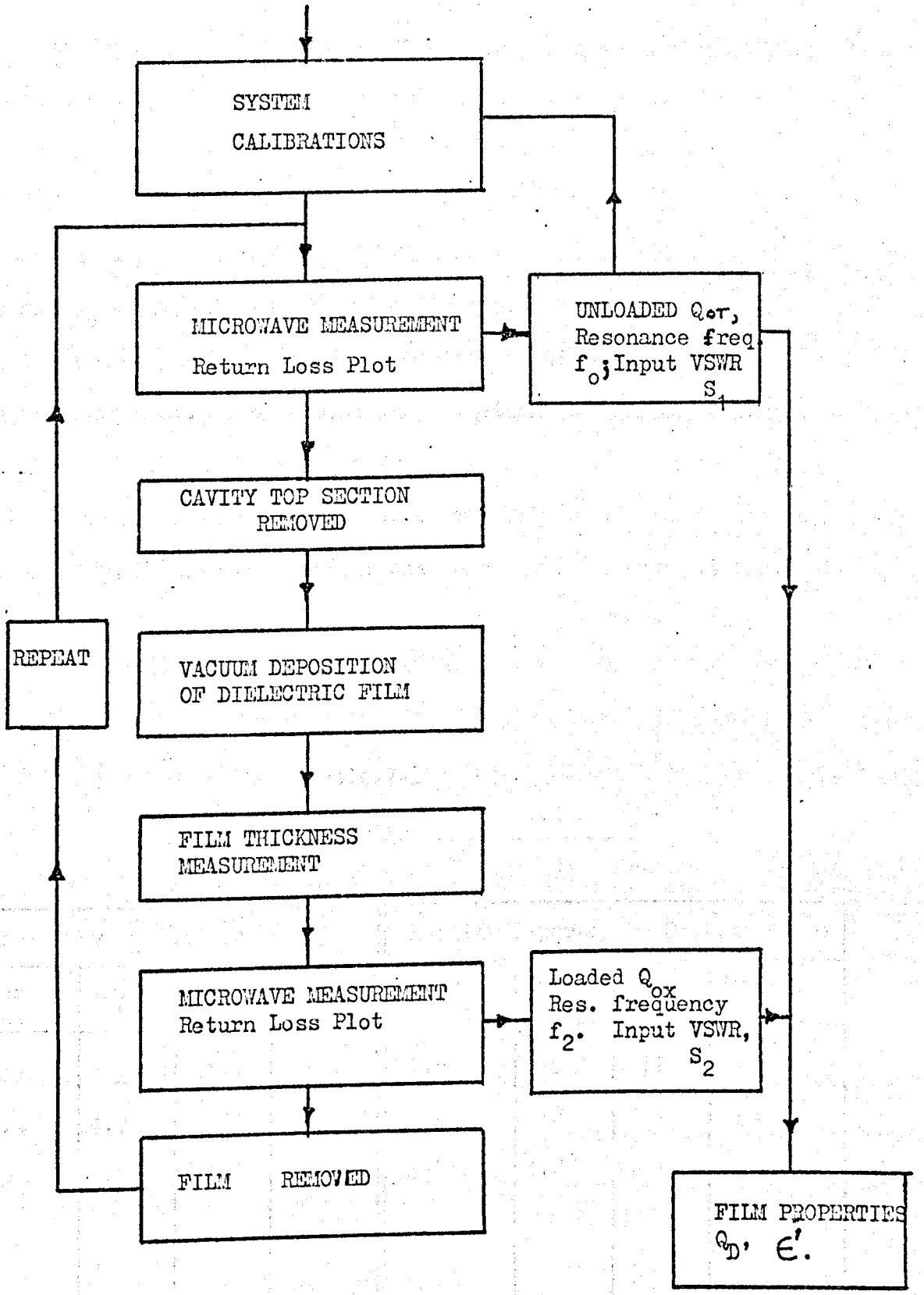

Figure 7.3 Process FLOW CHART

The Resonance Curves of the Cavity with and without the Dilectric film is shown in Figure 7.2

Results obtained by others are also included int the table. These people used various film preparation and measurement tehcniques.

My measured results for the SiO film and result quoted by Sobol[21] $\epsilon' = 4\text{-}5$ and $Q_D = 34.3$ at ≈ 3 GHz did not agree. The differences between the two methods were the preparation techniques and the measurement frequency. The present investigation was centred around X-band frequencies. On observing this point one of the cavities, CI3, was designed to resonate around 1.3 GHz. The film which was deposited in the same film deposition process, was measured at around 9.5 GHz, as well as around 1.3 GHz. These results together with results quoted by others are shown in Table 7.3.

Table 7.3

Dielectric Properties of Thin SiO Films

Measured by the Author				Results Reported by Others			
Frequency GHz	ϵ'	Q_D	Remarks	Frequency GHz	ϵ'	Q_D	Remarks
1.35	8 $\pm$0.8	100	a	2.9	4-5	34	c
9.5	4.9	120	a	-	6-8	30	d
9.5	5.9	136	b	x-band	4.2	110-250	e

a: rate of deposition = 22 nm/s

b: rate of dep. = 43 nm/s

c: rate of dep. = 4 nm/s ref.21

d: rate of dep. not given ref.12

e: rate of dep. = 5 nm/s ref. 22

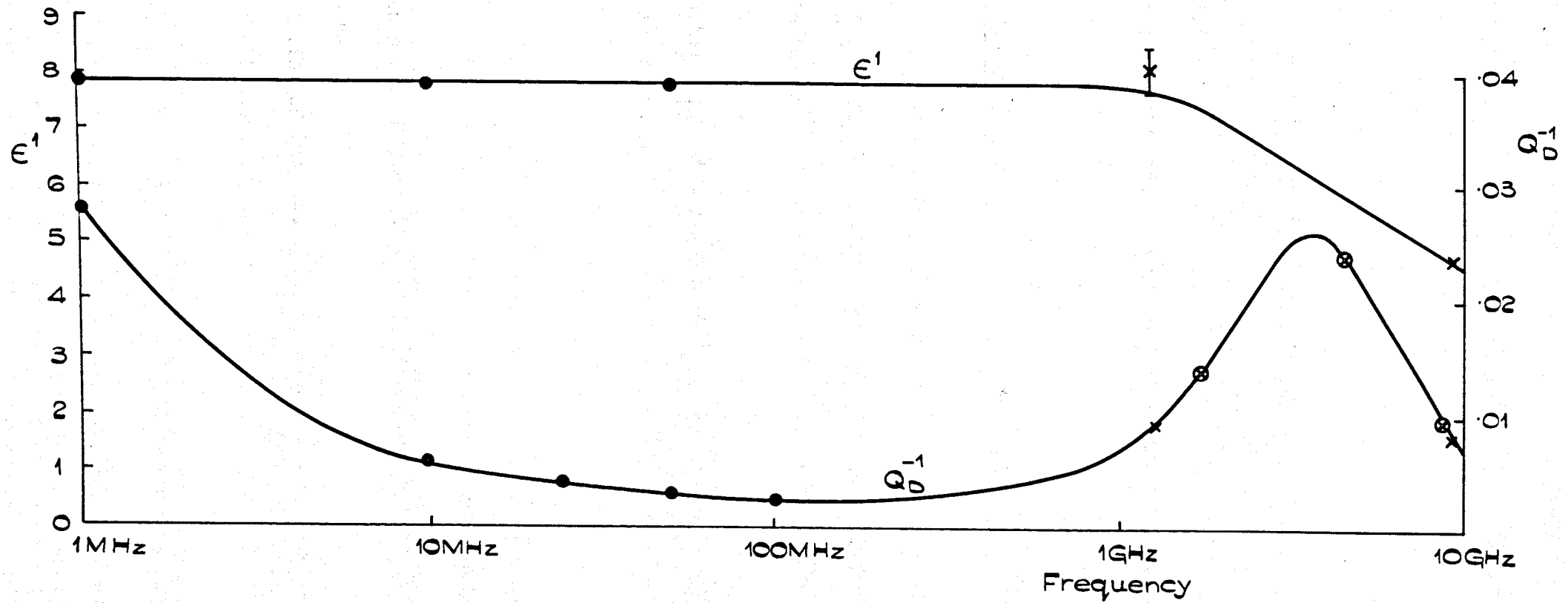

FIGURE 7.4.

DIELECTRIC PROPERTIES OF SiO FILM.

Measurement Methods : ● Lf , × Coaxial Cavity and ⊗ Microstrip Resonator (section 10)
(I represents measurement error)

It will be seen from these results that the dielectric properties of the silicon monoxide film vary with frequency. This variation is due to a material relaxation process called torsional relaxation. Thin film capacitors were also made from the silicon monoxide film sampled during the deposition of the SiO film, the dielectric properties of which were measured at 1.7, 5.3 and 9.1 GHz. The results are shown in figure 7.4. This plot shows clearly this relaxation phenomena. Further discussion on SiO will be found in section 7.5.

7.4 Measurements on Self Supported Dielectric Materials.

The permittivity of a thin sheet of dielectric material can be measured using the perturbation method[35]. The present investigation is concerned with the measurement of such materials using a Waveguide cavity. Two cavities were made of rectangular waveguide, WG 16, and one was resonating in the H_{012} and the other in H_{014} mode. The dimensions of the cavities are given in figure 7.5a. Each cavity was divided into two parts.

The split between the sections was at a quarter of a guide wavelength $\lambda_g/4$, from the short circuit plane and the material to be measured was placed at this point (Figure 7.5a). This was the electric field maxima and no effect was observed on the cavity Q_o and f_1 for repeated disassembling and assembling of the cavity parts. The cavities were excited through a dumbbell coupling slot.

The cavity resonating in H_{012} mode was made of copper and when polished the measured Q_o was about 7000, but tarnishing reduced this to around 6000. (The H_{014} mode one was made of brass and it was

silver plated. Qo $\simeq$ 7400 were measured. Due to tarnishing this value would drop to about 6800 . Most of the measurements were carried out around the latter values of Qo.

The measurement procedure was as follows: The Q factor and the resonant frequency of the cavity without the dielectric was measured. Then the dielectric material was introduced into the cavity at the split with its plane parallel to the electric field at that point. The cavity parameters i.e. Q_2 and f_2 were measured. These measured parameters together with the cavity and material dimensions, figure 7.5d, were substituted in equations 2.60 and 2.61 (section 2.6) and the dielectric properties of the material were calculated. In one of the measurements on the amber mica the following results were obtained:

Cavity without the dielectric.	Cavity with the dielectric.
Q_o = 6308	Q_{ox} = 5620
f_1 = 9522.08 MHz	f_2 = 9492.75 MHz

Length of the cavity = 41.66 mm

Dimensions of the dielectric material:

a' = a dimension of the cavity

b' = b dimension of the cavity

The thickness, $t = 30\ \mu m$

From equation 2.62 section 2.6 $N = d/t$

$$N = 1.39 \times 10^3$$

Substituting the above values in equations 2.60 and 2.61 we obtain the dielectric properties of Amber mica. These are $\epsilon' = 5.3$ and $Q_D = 396.$ 196?

Self supporting dielectric materials were cut in different sizes such that the frequency shift of the cavity with the dielectric loading was less than 30 MHz. This requirement put certain limitationns on the size of the material, e.g. a thick material should have either $a' < a$ or $b' < b$. The same condition applies to the high permittivity materials.

Initially materials to be measured were held in position in the cavity by an expanded polystyrene (Figure 7.5a). But itwas founddifficult to cut the hard material to have a close fit into the cavity and hence errors were introduced in the measured parameters due to air gap between the material and the cavity walls. This difficulty was overcome with a recessed cut around the waveguide at the split. Figures 7.5a to c show the samples in position.

Measurements on alumina substrates showed that the real part of the relative permittivity depends on the way the material was fixed into the cavity. This can be summarised as follows :

(i) $b' < b$ Figure 7.5 C sample C .

It was found that the measured ϵ' is lower than the value quoted by the manufacturers of the substrates. Measured results together with the manufacturers data are given in Table 7.4. It will be seen from this that the measured values are approximately 0.5 below the quoted values. This discrepancy cannot be from the variation of the material properties, anyway not in four different substrates. The cause of this may be due to the electric field discontinuity at the boundary between the sample and the air gap [64].

Table 7.4

Alumina Substrates

Material	Measured		Manufacturers Data*		Difference
	ϵ'	freq. GHz	ϵ'	freq. GHz	$\Delta\epsilon'$
Deranox 975	8.92	9.5	9.49	9.3	- 0.57
Deranox 995	9.17	"	9.6	9.3	- 0.43
AL 300	8.47	"	9.06	10	- 0.59
ALSIMAG 770	9.28	"	9.8	10	- 0.52

*Manufacturers Data obtained from ref. 70.

Sample and Cavity Dimensions: $a' = 8$ mm $a = 22.86$ mm

$b' = 5$mm $b = 10.16$ mm

$t = 0.6 - 0.67$ mm $d = 87.6$ mm

Table 7.5

Properties of Self supporting Dielectric Materials

MATERIAL	Measured Parameters at 9.5 GHz		Reported by others			
	ϵ^1	Q_D	ϵ^1	Q_D	freq.	Ref.No.
Corning 7059	4.4	230	5	250	10 GHz	9
Exp. polystyrene	1.06	3000				
Microscope Slides	6 ± .25*	62 ± 6*				
Ruby Mica						
Sample 71 μm thick	5.9	2200	6.5-8.7	2500-10000	Lf	67
" 75 μm thick	5.7	5000				
Amber Mica						
Sample 1, 50 μm thick	5.3	460	5-6	18 - 250	Lf	66
" 2, 60 μm "	6.0	440				
" 3, 70 μm "	5.4					
" 4						
ALUMINA SUBSTR.						
Coors 99.5	10	8000	9.8	10000	10 GHz	68
Sample 11**	9.95	900				
13	9.9	1050				
14	9.9	1100				
51	9.3	560				
52	9.0	570				
91	9.54	1250				
93	9.4	1180				
131	9.64	550				
134	9.58	760				

* The figure after ± sign is the measurement error

** These are condensed data. Full data can be found in ref. 70b

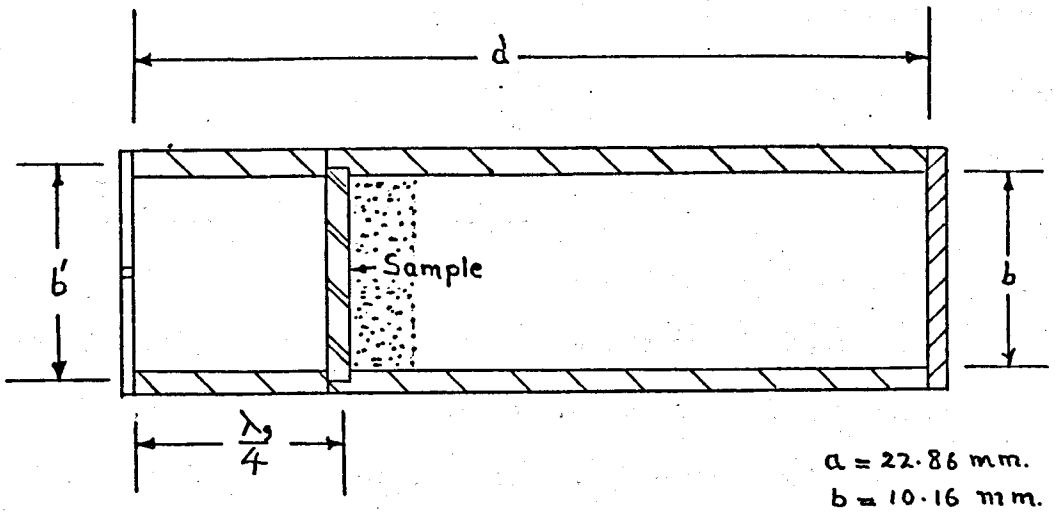

a = 22.86 mm.
b = 10.16 mm.
d = 41.66 mm (for H012)
d = 87.6 mm (for H014)

(a)

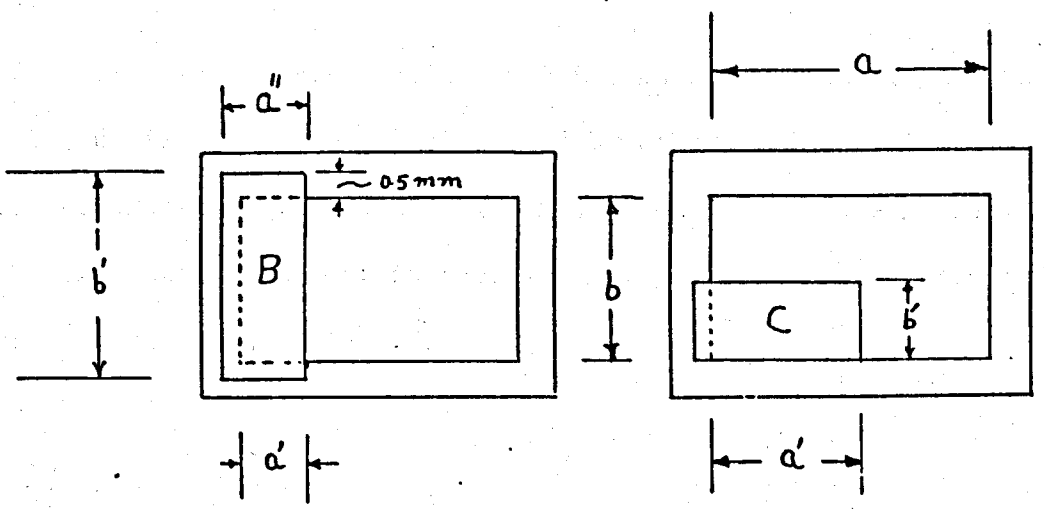

(b) (c)

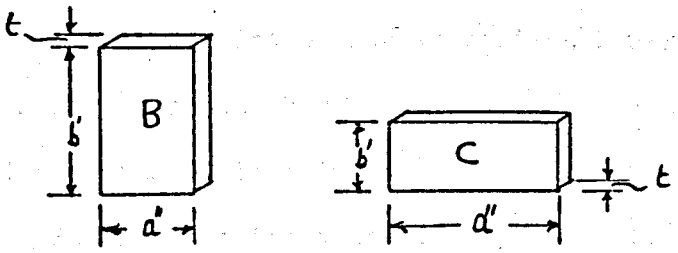

(d)

Figure 7·5 (a) Cross Section of Cavity with Sample in recessed slot.
(b) and (c) Samples B and C in position.
(d) Shapes of Samples Used.

(ii) $b^1 > b$ figure 7.5b sample B.

In this type of sample, fixing the measured value of b^1 should be used in the calculations of N in equation 2.62 section 2.6, because the recessed volume forms part of the cavity. The measured results using this approach gave ϵ^1 values within 1% of those obtained from the measurement where $b^1 = b$.

Materials measured using this technique are given in table 7.5.

It will be seen from these results that the measured mica parameters i.e. ϵ^1 and Q_D, differ from the values quoted by others. Amber mica and to a much lesser extent ruby mica have impurities enclosed between their layers.[69] Therefore their dielectric parameters may differ from sample to sample, these are shown in table 7.5.

7.5 Comments

In this section the symmetrical capacitively loaded coaxial cavity was used successfully for the measurement of the dielectric properties of thin films. Methods introduced in section 2 were experimentally tested and the assumptions which were made during the derivations of the properties of the dielectric loaded cavity were found to be valid. It was shown in this section that either of the two methods could be used for the measurement of the dielectric properties. The choice of the method depends on the measurement accuracy of the most critical parameters of

these methods. The important parameter of the VSWR method is the ratio of the voltage standing wave ratios with and without the film and the Q-factors of the cavity, with and without the film in the perturbation method. The error analysis of these methods are given in section 8, where it is shown that the VSWR method is the more accurate.

It was shown in the theory (section 2) that this type of cavity could be used to measure the dielectric properties at two different frequencies. This approach was not used widely in the present investigations , because the available coaxial measuring system could not provide the accuracy required for this type of measurement. However the feasability of the approach was demonstrated when the dielectric properties of SiO_2 (Table 9.3., section 9.2) and SiO (Table 7.3) were measured at 1.3 GHz and 9.5 GHz.

The most interesting result was the variation of the dielectric properties of the SiO films, with the frequency. It was found that SiO films have a relaxation phenomenon around 3 GHz. Hirose[63], working on the SiO films up to 100 MHz suggested that a dielectric relaxation process called torsional relaxation should take place above 100 MHz, without realising this phenomenon, Sobol[21] measured the permittivity of SiO at 2.9 GHz and obtained a rather low Q_D value (≈ 30). He also quotes a Q_D value for the same film at 1 MHz, which was not much different from the microwave value.

The capacitively loaded coaxial cavity can measure the dielectric properties of thin films deposited onto the centre conductor as well as the self supported materials. The advantages of the method are:

(a) The dielectric film in this method is deposited onto a metal substrate. This is the usual method of m.i.c fabrication. Therefore the film can be measured in a situation similar to that in actual circuits.

(b) The electric field is perpendicular to the film. When the film is used in circuits the electric field will be applied in a similar way.

(c) During the deposition of the dielectric film it is normal practice to improve adhesion by the prior deposition of a thin layer (5 to 20 nm) of chromium or nichrome. This procedure was also used during the deposition of the dielectric film onto the centre conductor of the cavity. At the end of the measurement, the dielectric film was removed and the chromium film was left on the cavity. Measurement on this cavity showed that this metal film did not effect the measured dielectric properties of the thin film.

Although the coaxial cavity method can be used to measure the self supporting materials it requires specially shaped materials i.e. disks. A completely different approach using a waveguide cavity was tested. The cavity perturbation technique was again used. The construction of the cavity was much simpler than the coaxial cavity and laminar sheet materials cut in rectangular shapes were tested. It was found that the technique could be used to measure the dielectric properties of substrate materials used in the construction of microstrip circuits. The advantage of the system was its simplicity, and accurate results could be obtained provided that (a) the perturbation conditions

are not violated and (b) the dimensions of the cavity and the material are measured accurately.

CHAPTER 8

ERROR ANALYSIS OF THE PERMITTIVITY MEASUREMENTS USING THE COAXIAL CAVITY

8.1 Introduction

Errors in a measuring system arises from systematic and random errors.[71] Systematic errors are those which effect each measurement the same amount, such as the calibration errors of a measuring system. Proper design and calibration of the measuring system can reduce these to a negligible value. On the other hand random errors, as can be understood from the name, are due to random fluctuation of the measured quantities. Random errors can be estimated by statistical analysis of results obtained from large numbers of measurements. These are oversimplified statements because in certain circumstances the systematic errors cannot be distinguished from the random errors. This was apparent in contributions presented at a recent collaquium on analysis of errors in measurement systems.[72] Assuming that the error in the measured quantity x_i ($i = 1, 2 \ldots n$), are due to random errors, then the error calculation using the statistical approach can be summarized as follows:

$$\text{Mean value, } \bar{x} = \frac{\sum_{i=1}^{n} x_i}{n} \qquad 8.1$$

$$\text{Variance, } \sigma^2 = V(x) = \frac{\sum_{i=1}^{n} (x_i - \bar{x})^2}{n - 1} \qquad 8.2$$

Then any measured x can be represented as

$$x = \bar{x} \pm \frac{U\sigma}{\sqrt{n}} = \bar{x}\left[1 \pm \frac{U\sigma}{\sqrt{n}\,\bar{x}}\right] \qquad 8.3$$

where U = certainty factor

n = number of observations

Let E(x) = fractional error in x

$$E(x) = \frac{U\sigma}{\sqrt{n}\,\bar{x}} \qquad 8.4$$

Using equations 8.3 and 8.4 we obtain

$$x = \bar{x}\,(1 \pm E(x)) \qquad 8.5$$

It will be seen from equation 8.4 that the fractional error in x will be reduced if n is increased (. σ can be calculated using equation 8.2). The certainty factor U depends on the type of distribution of random errors in the measured values of x. In case of normal distribution U = 3 for 99.7% certainty i.e. the measured value of x will be within the range determined from the equation 8.3 with 99.7% certainty.

The above derivation holds for a single variable, but can be modified to hold for a number of variables. This can be achieved by determining the variance of the function having more than one variable.

This approach will be introduced in the following steps:

Let x = measured quantity and is a function of $y_1 , y_2 \ldots . y_q$

Then $x = \theta (y_1 , y_2 \ldots . y_q)$ 8.6

where θ is a function of $y_1 , y_2 \ldots . y_q$

The variance of this equation is given by[73,74]

$$V^2(x) = \left(\frac{\partial x}{\partial y_1}\right)^2 V^2(y_1) + \left(\frac{\partial x}{\partial y_1}\right)^2 V^2(y_2) + \frac{\partial x}{\partial y_1}\frac{\partial x}{\partial y_2} V(y_1)\, V(y_2) + \quad 8.7$$

where $\frac{\partial x}{\partial y}$, ... are the partial differentials of x with respect to y_1, y_2 .... etc at $y = \bar{y}$

The third term is the covariance of y_1 y_2, etc., and is zero for the independent variables.

This value of the variance can be substituted in equation 8.4 and the fractional error due to random errors can be calculated.

In a measurement it is usual to quote the spread of the measured quantities. In the present case this spread is assumed to be the maximum spread value and since this spread is due to random fluctuations it is a random error having a maximum value.

In the following investigation of the errors of the permittivity

measurement the spread values of the variables will be used. This will give a maximum error due to random errors of the variables. In this case U, n and σ are dropped and the maximum error values are used

i. e. $y = \bar{y}(1 \pm e_{max})$

where e_{max} is the maximum fractional error in y. It can be shown that for a normal distribution[75] $\sigma = \frac{e_{max}}{3}$. Substituting this value of σ in eqn. 8.4 and taking U for 99.7 % certainty, the fractional error becomes

$$\frac{U\, e_{max}}{3} = e_{max}$$

8.2 Error Analysis of the Permittivity Measurements.

We can calculate the probable errors in the permittivity calculations using the above principles. These are applied to the VSWR method and the perturbation method.

Using the VSWR method the real part of the permittivity is given by

$$\epsilon' = \frac{t}{G_0}\left\{\left[(m+1)\frac{f_1 \tan\frac{\pi L f_1}{v}}{f_2 \tan\frac{\pi L f_2}{v}} - m\right] + \frac{t}{G_0} - 1\right\}^{-1}$$

and

$$Q_D = \frac{t}{G_0}\left[\frac{S_2}{S_1} - \left(\frac{f_1}{f_2}\right)^{3/2}\right]^{-1} \frac{(1+m)\left(\frac{f_1}{f_2}\right)^3}{\left[1+m\left(1+\frac{x}{\epsilon'}-x\right)\right]^2} \cdot \frac{Q_{0T}}{\epsilon'}\left[1 - \frac{2\pi}{\frac{2\pi L}{v} + \sin\frac{2\pi L}{v}}\right]$$

Where $t = x G_o$

= the thickness of the dielectric film.

In one of the measurements on the electron beam source evaporated SiO_2 film, the results are collected and shown in Table 8.1

Table 8.1

Measured Parameters

Variables y_n		Errors* dy_n
Q_{oT}	4348	±0.5 %
Q_{ox}	4238	±0.5 %
f_1	9501.25 MHz	±0.1 MHz
f_2	9494.00 "	±0.1 "
G_o	32.7 μm	±0.2 μm
t	2.7 μm	±0.02 μm
L	32.00 mm	±4.00 μm
	4.2	
S_2 / S_1	1.0282	±0.16 %

* Errors are the maximum values of the spreads.

Leaving out the rather complicated mathematics the error in E (ϵ') for the above case is given by

$$E(\epsilon') = \left[1.57\times10^{7}\left(\frac{df_1}{f_1}\right)^2 + 1.5\times10^{7}\left(\frac{df_2}{f_2}\right)^2 + 5.4\times10^{4}\left(\frac{dL}{L}\right)^2 + 10\left(\frac{dt}{t}\right)^2 + 10\left(\frac{dG_0}{G_0}\right)^2 \right]^{\frac{1}{2}}$$

where $\frac{df_1}{f_1}$..... etc. are the maximum fractional errors in each variables. Substituting the values of the errors terms we obtain

$$E(\epsilon') = \pm 7.3\ \%$$

The fractional error in Q_D is

$$E(Q_D) = \left\{ \frac{S_2}{S_1}\left[\frac{S_2}{S_1} - \left(\frac{f_1}{f_2}\right)^{3/2}\right]^{-1}\left(\frac{d\frac{S_2}{S_1}}{\frac{S_2}{S_1}}\right)^2 + \frac{3}{2}\left[\frac{S_2}{S_1} - \left(\frac{f_1}{f_2}\right)^{3/2}\right]\left[\left(\frac{df_1}{f_1}\right)^2 + \left(\frac{df_2}{f_2}\right)^2\right] + \left(\frac{dt}{t}\right)^2 + \left(\frac{dQ_{OT}}{Q_{OT}}\right)^2 + \left(\frac{dG_0}{G_0}\right)^2 + \left(\frac{d\epsilon'}{\epsilon'}\right)^2 + \frac{d\epsilon}{\epsilon}\left(\frac{dt}{t} + \frac{dG_0}{G_0}\right) \right\}^{\frac{1}{2}}$$

Substituting the values we obtain

$$E(Q_D) = \left\{ 1.44 \times 10^3 \left[d\frac{\frac{S_2}{S_1}}{\frac{S_2}{S_1}} \right]^2 + \left(\frac{dt}{t}\right)^2 + \left(\frac{dG_0}{G_0}\right)^2 + \left(\frac{d\epsilon'}{\epsilon'}\right)^2 + d\epsilon\left(\frac{dt}{t} + \frac{dG_0}{G_0}\right) \right\}^{\frac{1}{2}}$$

and $E(Q_D) = \pm 10\%$

Errors in the Perturbation Method.

The equations used for the permittivity calculations are given by equations 2.53 and 2.54 section 2.5. Substituting the partial differentials with respect to each variables of these equations, in equation 8.7 we obtain

$$E(\epsilon') = \frac{\left\{ \left[\left(\frac{G_0}{t} - 1\right) P \frac{f_2}{f_1} \right]^2 \left[\left(\frac{df_1}{f_1}\right)^2 + \left(\frac{df_2}{f_2}\right)^2 \right] + \left(\frac{G_0}{t} P \frac{\delta f}{f_1}\right)^2 \left[\left(\frac{dG_0}{G_0}\right)^2 + \left(\frac{dt}{t}\right)^2 \right] + \left[\frac{\delta f}{f_1}\left(\frac{G_0}{t} - 1\right)(m+1)\left(\frac{\omega_1 L}{v}\right)^2 \cot\left(\frac{\omega_1 L}{v}\right) \operatorname{cosec}^2 \frac{\omega_1 L}{v} \right]^2 \frac{dL}{L} \right\}^{\frac{1}{2}}}{1 - \left(\frac{G}{t} - 1\right) P \frac{\delta f}{f_1}}$$

Substituting the values given in Table 8.1 we obtain

$$E(\epsilon') = \left\{ 1.48 \times 10^7 \left[\left(\frac{df_1}{f_1}\right)^2 + \left(\frac{df_2}{f_2}\right)^2 \right] + 10.2 \left[\left(\frac{dG_0}{G_0}\right)^2 + \left(\frac{dt}{t}\right)^2 \right] + 3 \times 10^4 \left(\frac{dL}{L}\right)^2 \right\}^{\frac{1}{2}}$$

$$= \pm 6.9\,\%$$

And the error in Q_D is

$$E(Q_D) = \left[\left(\frac{dt}{t}\right)^2 + \left(\frac{dG_0}{G_0}\right)^2 + \left(\frac{d\epsilon'}{\epsilon'}\right)^2 + \frac{d\epsilon'}{\epsilon'}\left(\frac{dt}{t}\right) + \frac{d\epsilon'}{\epsilon}\left(\frac{dG_0}{G_0}\right) + \left(1 - \frac{Q_{0x}}{Q_{0T}}\right)^{-2} \left(\frac{dQ_{0x}}{Q_{0x}}\right)^2 + \left(\frac{Q_{0T}}{Q_{0x}} - 1\right)^{-1} \left(\frac{dQ_{0T}}{Q_{0T}}\right)^2 \right]^{\frac{1}{2}}$$

$$E(Q_D) = \left\{ \left(\frac{dt}{t}\right)^2 + \left(\frac{d\epsilon'}{\epsilon'}\right)^2 + \left(\frac{dG_o}{G_o}\right)^2 + \frac{d\epsilon}{\epsilon}\left(\frac{dt}{t} + \frac{dG_o}{G_o}\right) + 1.5 \times 10^3 \left[\left(\frac{dQ_{oT}}{Q_{oT}}\right)^2 + \left(\frac{dQ_{ox}}{Q_{ox}}\right)^2\right] \right\}^{\frac{1}{2}}$$

and $E(Q_D) = \pm 28.5\ \%$

Table8.2

The error in the measured values of ϵ' and Q_D due to random errors in each of the variable parameters as shown in Table 8.1 .

Variables	V S W R method		Perturbation Method	
	$E^2(\epsilon')$	$E^2(Q_D)$	$E^2(\epsilon')$	$E^2(Q_D)$
f_1	16.8	. .	16.4	. .
f_2	16.8	. .	16.4	. .
L	8.4	. .	4.7	...
t	10.	1.0	10.2	1.0
G_o	1.	. .	1.	. .
	-	53.0	-	47.7
S_2/S_1		37.8		. .
Q_{oT}				373.0
Q_{ox}				389.0
Covariance		7.3		
TOTALS	53	99.1	47.7	810.7

. . values less than 1 %

$E(\epsilon')$ and $E(Q_D)$ are the percentage errors.

8.3 Comments

The probable error in the measured values of Q_D and ϵ' due to the individual random errors of the variable quantities are given in table 8.2. It will be seen from this table that the most critical parameters of ϵ' measurements were the frequency terms followed by t and L. This was true in both of the methods of ϵ' measurements and hence both methods give very nearly equal probable errors.

However probable error in Q_D measurement is dependent on the method of its measurement. The VSWR method in the present investigation had the lower probable error in Q_D (= ± 10%) then the perturbation method (± 29%). The reasons for this difference are :

(a) The measurement accuracy of the critical parameters of the VSWR method depends on the ratio of the two VSWR's. This ratio can be measured to a high accuracy because any systematic error introduced into the measured VSWR's cancels out leaving only the random error contribution (Appendix 7)

(b) The critical parameters of the perturbation method are Q_{oT} and Q_{ox}. The measurement accuracy of these quantities depends on the frequency stability of the signal generator used during the test. In the present set up the accuracy of Q's was ± 0.5% which gives quite high probable error in Q_D.

The VSWR method accuracy does not depend on the frequency stability of the signal generator.

The probable error in Q_D using the perturbation method can be improved by stabilizing the frequency of the signal generator beyond the present set up (described in section 6). This was not attempted because the frequency locking unit, which would need to be incorporated into the sweep generator system was not available. If such a unit is incorporated the expected accuracy of the Q_{oT} and Q_{ox} will be within $\pm$ 0.2%, thus giving a probable error in Q_D of $\pm$ 13%. This value will then be comparable to the present probable error in the Q_D using the VSWR method.

Improvement in the frequency stability of the signal generator will also improve the random errors in f_1 and f_2. Thus higher accuracy in ϵ' values than the present case can be achieved, and this in turn would give a further increase in accuracy of Q_D measurement.

It was shown above that the most important parameter contributing to the error in measured quantity can be determined. This is shown for a particular system in table 8.2. This error analysis method should be incorporated in any measurement approach so that the critical parameters of the system are measured more accurately than the others. During the system testing this point was kept in sight. After much painstaking work the frequency scatter of the resonant frequency of the cavity upon disassemblying and assemblying the cavity parts was reduced from $\pm$ 0.5 MHz to $\pm$ 0.1 MHz by improving the alignment of the cavity parts.

CHAPTER 9

THIN FILM PROCESSING

9.1 Introduction

Thin metal and dielectric films are used in the construction of m.i.c's. The properties of these films have more influence on the performance of microwave circuits than the low frequency circuits. At microwave frequencies the surface of the metal film should be smooth i.e. roughness $\ll$ the skin depth at the frequency because the current flows on the surface of the metal film. The dielectric films may have dielectric losses and relaxation peaks near the required frequencies.

The properties of these films are dependent on the processing techniques used. There are various thin film deposition techniques.[76-97] Some of these techniques may be summarized as:

(i) Filament evaporation.[76-79]

(ii) Electron gun evaporation.[76-85]

(iii) D.C. and rf. sputtering.[86-93]

(iv) Chemical vapour deposition.[18,94]

(v) Laser evaporation[95]

The filament evaporation is one of the most widely used thin metal film deposition process. The disadvantage is that the deposited film is contaminated from the evaporation of the filament material and or the boat which supports the evaporant.

The other four methods can be used for the deposition of dielectric as well as metal films.

In the present investigation only two of these methods, namely the electron gun evaporation and the rf. sputtering, were used. The advantage of the electron gun evaporation, EGE, is that a high evaporation rate of metals as well as dielectric materials is possible. The disadvantages of this system will be discussed as the practical work is discussed.

The properties of the deposited thin films are dependent on the preparation conditions. These are:

(a) Substrate material.

(b) Substrate temperature.

(c) Evaporation rate;

(d) Residual gas pressure inside the vacuum system.

These conditions should be controlled as much as possible if repeatable results are required. The first three conditions can be controlled but the residual gasses in the system can not be easily controlled.

Both metal and dielectric films were prepared using the electron gun evaporating unit. These films were used in the construction of microwave integrated circuits such as lumped elements and microstrip resonators. The properties of these dielectric films were investigated using the capacitively loaded coaxial cavity (described in section 7). Also the dielectric properties of rf. sputtered thin films were measured.

The preparation techniques and the properties of these films will be discussed in the following sections. First of all a short description

of the ECE unit will be given. Then the preparation of metal films and the deposition of metal films for the microstrip circuits will be given. The difficulties of the EGE unit for the preparation of thin metal film and how it was overcome and other problems will be discussed at the end of that section.

A lot of time was spent on the preparation of the thin dielectric films. The low frequency properties of these films will be compared with the microwave properties and the variation of the properties from those of their bulk materials will be described.

9.2 Preparation of thin films using Electron Gun Evaporator.

9.2.1 Electron Gun Evaporating Unit.

The vacuum system used in the present investigation was a BirVac TG 2 Unit. The system consisted of a rotary pump (Edwards High Vacuum, Model ES 150, capacity 150 litres/minute) backing an oil vapour diffusion pump (Edwards High Vacuum, Series EO 4 B903, peak air speed (unbaffled) 600 litres/second). There was a nitrogen cold trap between the diffusion pump and the vauum chamber. The lowest pressure obtained in the vacuum chamber with liquid nitrogen in the cold trap was 5×10^{-7} torr.

The evaporating part consited of a work-accelerated electron ring gun using a molybdenum filament. The power to the gun was supplied from the Bir-Vac Torr Plan Power Pack type RC. The power pack provides an a.c. output of 10 volts at 30 amps and an unsmooth d.c. supply of 4.5 kV at

300 milliamps as well as various safety devices to protect the operator and the equipment. The electron gun requires an a.c. supply to the filament and the H.T. connected between earth and the electron source, the source being at a negative potential to earth, (more details in reference 96).

The material to be evaporated was held in crucible compatible to that material, held on a turntable with a molybdenum clip. The turntable which could be rotated from the outside of the vacuum chamber could accomodate up to 6 crucibles and thus 6 different materials could be evaporated one after the other without breaking the vacuum. On the other hand thick films could be obtained by filling more than one crucible and evaporating one after the other.[97]

The evaporation process was as follows; the material held in a crucible was brought under the Ring Gun and aligned such that the electron beam was focussed on the material and not on the crucible material. By adjusting the filament current, the h.t. voltage, and the vertical position of the turntable, various rates of evaporation could be achieved.

The maximum heating temperature that can be obtained from the gun was claimed[96] to be around 4000°C with the electron beam focussed to its minimum diameter ($\simeq$1 mm). This means that almost all the known materials. can be evaporated using this system.

The evaporation from the system is upwards and a substrate held on top of the gun collects some of the evaporated material and hence the film is deposited. The substrate used for the deposition of the thin films were

held on a substrate holder which was supported by three adjustable pillars above the electron gun. Figure 9.1 shows the system set up.

The additional equipment used with the above set up were:

(i) Substrate heater. Two types of substrate heaters were used. One of them was a radiant heater and the other was in-contact heater.

(ii) Thermocouple. The temperature of the substrate was was measured using a Cromel-Alumel Thermocouple. Its output was fed into the temperature controller.

(iii) Temperature Controller. The substrate temperature could be controlled with this unit, to within 1% of the set value. The unit was used in conjunction with items (i) and (ii).

(iv) A quartz oscillator film thickness monitor, FTM, (Edward High Vacuum, FTM Model 1). This unit could also measure the rate of deposition. During the evaporation the floating charges picked up by the leads connecting the crystal to the FTM oscillator could damage the oscillator. This was eliminated by shielding these leads with an earthed metal shield.

Dielectric as well as metal films were prepared using this evaporation unit.

9.2.2. Preparation of Metal Films.

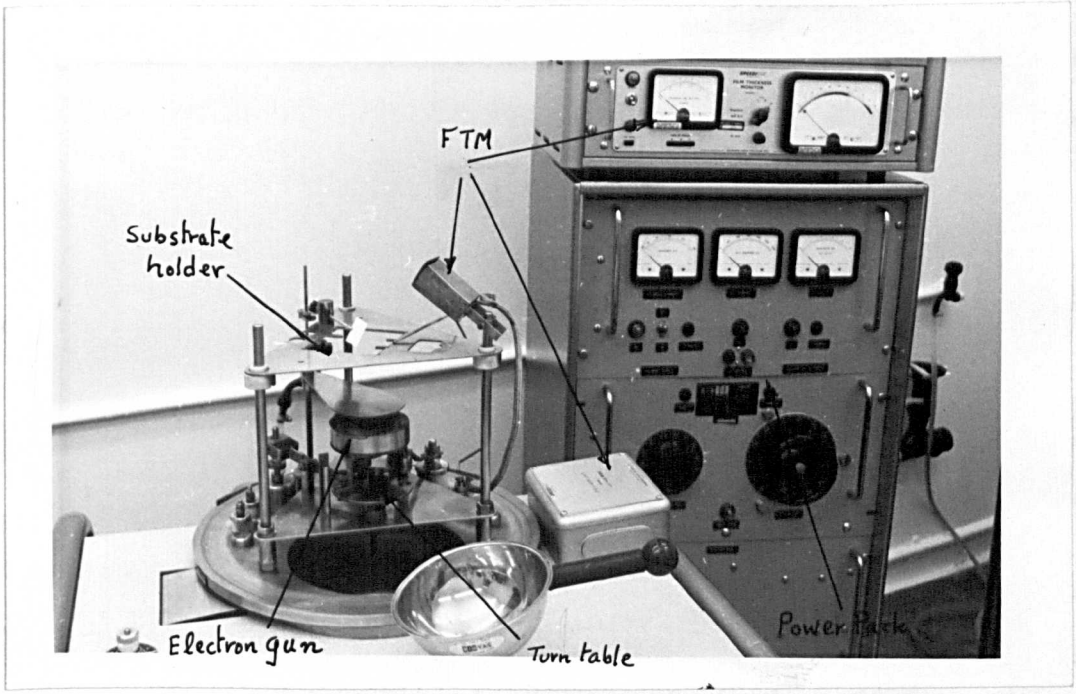

Figure 9.1 Electron Beam Evaporation Unit

Thin metal films were prepared for the low frequency investigation of the thin film dielectric properties as well as for the microwave integrated circuits. The principles used in both cases are similar except the m.i.c! s require much smoother films than the low frequency components, because the current at microwave frequencies flows in the skin at the surface of the metal film. It was shown[109] that the surface resistance of a metal film can increase as much as 29% of its value calculated from d.c. conductivity measurement of the surface roughness was equal to the skin depth of that metal.

The film properties are dependent on the substrate, substrate temperature, contamination, evaporation rate and film thickness[76]. Contamination plays an important part and also cannot be eliminated completely. Contamination arises from the purity of the evaporated material, cleaning process of the substrates and the residual gases in the vacuum system.

In the present investigation the highest available purity metals (Johnson Matthey's spectrographically standardized metals, see Appendix 9 for more details,), were used and hence one source of the contamination was eliminated.

Cleaning of the substrate is another important problem. Many laboratories use different cleaning processes. The cleaning processes we adopted are as follows:

The substrate was:

(i) Scrubbed with a piece of cotton wool soaked in Teepol washing liquid.

(ii) Cleaned in running tap water and then cleaned in ultrasonic dionised water bath for 5 minutes.

(iii) Sprayed with tricoethylene.

(iv) Sprayed with isopropylalcohol.

(v) Dried in isopropyl bath for 10 minutes

It was found during deposition of the thin films that the last step is not essential.

Silver, copper god, aluminium, chromium and nichrome thin films were deposited successfully on soda lime glass (microscope slides supplied by Chance Bros.), corning 7059 glass substrates, silica, saphire and alumina substrates. These metals have different evaporating temperatures and reactions with other metals. Therefore suitable crucibles should be used. The following crucibles were used:

(a) Cermet crucibles for nichrome, chromium and aluminium.

(b) Carbon crucibles for gold, silver and copper.

(c) Molybdenum crucibles for gold.

Initially a carbon crucible was used for the deposition of gold film but it was learned[110] that the crucible evaporates too and hence the film is contaminated by carbon. The same source quoted that the contamination of the deposited film from a molybdenum crucible was only 10 parts per million so from then onwards molybdenum crucibles were used for gold. The difficulty of deposition of the gold film from the molybdenum crucible is that whilst heating the charge it diffuses into

the molybdenum and each crucible can only be used for three or four times.

Good adhesion of metal films to the substrates and other films is very important. The adherence of Ag, Cu and Au on glass substrates is poor, but that of Cr, Al and Mo is very high[98]. Therefore a thin layer (10-20nm) of one of the latter metals deposited onto glass substrates before the deposition of the former group of metals provide the required adhesion. This adherence film does not change the electrical characteristics of the main film. Using this technique good adherent films of copper and gold on substrates and on previously deposited dielectric films, were obtained. Films prepared by this method used either nichrome or chromium adherence layers of 10-20nm thick.

9.2.2.1 Deposition of Metal Films for Microwave Integrated Circuits

Microstrip transmission lines[1-6] requires deposition of metal films on two sides of the substrates; for the ground plane and the strip. Here microstrip resonators are used to measure the characteristics of microstrip lines, and these circuits require the depostion of thin metal films also on the edges of the substrates. To deposit the film on one side, then break the vacuum to turn the substrate and restart the process is a waste of time. Author developed a simple techniquo whereby the substrate was rotated whilst the film was deposited. The system was built around the rotary shaft holding the shutter. Figure 9.2 shows the system. An additional pair of bevel gears was used in the vacuum system to turn the horizontal rod holding the substrate. The shutter could be held stationary on the side of the bell jar

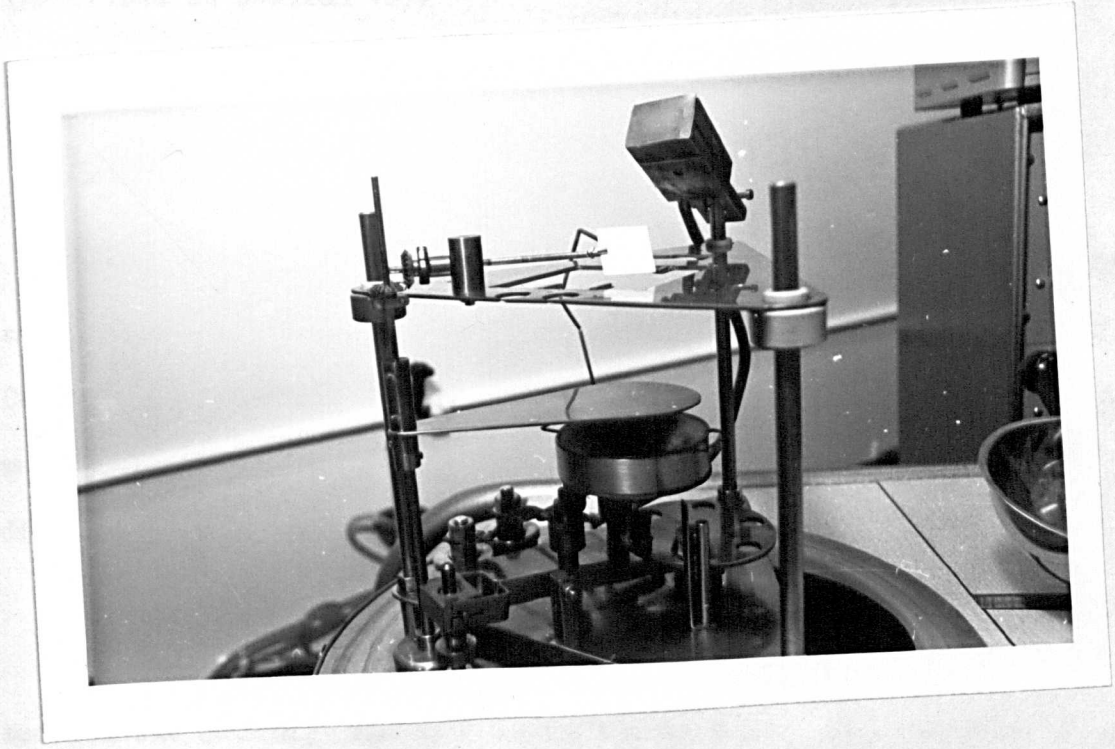

Figure 9.2 E.B. Evaporator and the set up used to deposit metal films for the Microstrip lines.

whilst the substrate holder was rotated. This is a simple technique for the deposition of thin film on four or two sides of a substrate. Further improvement on the system would be to use a motor to spin the substrate.

This system was used in the preparation of microstrip resonators and microstrip lines on silica, sapphire and alumina substrates (described in section 10).

9.2.2.2. Comments on the Processing of Thin Metal Films.

The conditions and preparation techniques used in the deposition of the thin metal films were quite different [illegible]. Silver Copper and Aluminium could be evaporated quite easily, whilst the gold was difficult. Now these problems and their elimination will be discussed.

The adhesion of Cu, Au and Al were discussed in the preceding section but nothing was said about the Ag film. The adhesion of Ag to Cr film was found to be inconsistent. In one deposition it might adhere well and in another process might not. The reason for this was the residual gases in the vacuum system. The most troublesome of these gases is the water vapour. At a vacuum pressure of 10^{-5} torr most of the residual gas is water vapour. If the deposition is conducted at this residual pressure level the Cr adhesion layer oxidizes and the Ag film deposited on to the oxide of Cr will not adhere to it. On the other hand if the vacuum chamber pressure is better than 10^{-6} torr and the system is outgassed for a long time, the film deposited on top of

Cr adhering layer will give the required adherence for the Ag film.

This problem was not observed with the Au and Cu film depositions, even when they were deposited at 2-3 x 10^{-5} torr residual pressures. It should be anticipated that the same oxidization of Cr film would have taken place. The adherence of films on glass substrates is believed[111-112] to be due to some sort of chemical reaction between the layers. The highly adherent films are usually the most chemically active metals.

The band strengths[113] of diatomic molecules of oxygen - Cr and Cu - O are 102 and 96 kcal/mole whereas Ag - O is 47. It is possible that the adherence of Cu to Cr film is due to chemical reaction and hence chemical bonding due to the oxidization of both of the materials because they have nearly the same bond strength. In case of silver this could not happen because Ag will loose its oxygen to Cr and hence have no adherence.

The best way to eliminate this inconsistency is to evaporate Cr and silver in a well outgassed vacuum chamber at pressures lower than 10^{-6} torr.

The surface smoothness of the metal films depends on the evaporation conditions and the surfaces of the substrates. It was found that surface finish better than 20 nm can be obtained from Cu, Al and Ag films. The most widely used metal was Cu and it was found that if the following evaporation steps were taken repeatable smooth Cu films could be obtained. The charge held in a carbon crucible was heated by focussing the beam on to the charge. Even when the metal was molten a crust (copper oxide) covering the surface of the molten metal could be seen.

Further heating of the charge breaks up this crust which moves towards the perimeter of the crucible. A clear molten surface shows the perfect evaporation of Cu.

The above metioned materials have low resistivities and are suitable for the construction of low loss circuits. These films oxidize quite easily and hence they require protective layers. On the other hand gold has the advantage of having a low resistivity and also a non oxidizing property. It was found that it is difficult to have smooth gold film surfaces. The reason for this is that it has high atomic number. High atomic number materials present certain difficulties in the deposition of thin metal films using electron gun evaporation. This can be explained as follows:

When the accelerated electron beam is bombarding the material some of these electrons are reflected from the surface. It was found[83] that the energy S carried away by these scattered electrons is

$$S = \eta \bar{K}$$

Where η = coefficient of backscattering

$\bar{K}$ = average fractional energy

For electron beam energies from 0.2 to 32 keV

$$\bar{K} = 0.45 + 2 \times 10^{-3} Z$$

Where Z = Atomic number of material

The atomic number of Ag = 47, Al = 13, Cr = 24, Cu = 29 and Au = 79. It will be seen that the Au evaporant will have higher energy backscattered electrons than the other materials quoted above.

This means that the substrate will be overheated by these high energy backscattered electrons. Figure 9.3a shows the electroscan photograph of such a film. It was also found that the chromium adherence layer diffused into the gold film. Diffusion of Cr into Au requires temperatures greater than 800°C and therefore during the deposition, the film temperature must have been greater than this value.

Smooth gold films were obtained by reducing the accelerating voltage and also defocussing the electron beam. η is low for a low accelerating voltage and the defocussing eliminates overheating the inner part of the evaporating charge. This gave a lower rate of evaporation than the previous case but the film was smooth, (Figure 9.3.b)

Typical evaporation conditions for metals used during the investigations are given in Table 9.1.

Table 9.1

Typical Evaporation Conditions for Metals

Material	Filament current A	HT Setting		*Rate of deposition nm/s
		Voltage KV	Current mA	
Aluminium	23 - 24	2.6 - 3.5	45 - 60	2 - 5
Copper	23 - 24	3 - 3.5	40 - 70	2 - 17
Chromium	24 - 25	2 - 2.5	15 - 25	-
Gold	23	2.6**	50 - 60	0.5 - 0.8
Nichrome	25	3.5	40	-
Silver	23	2.8	50 - 55	6 -

* and ** see next page

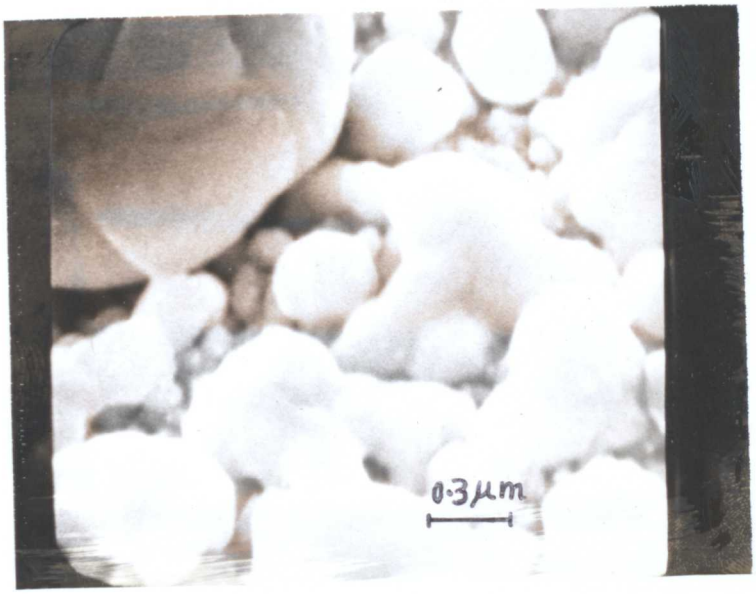

(a) Electron beam energy of E.B.Evaporator = 3.5 keV.

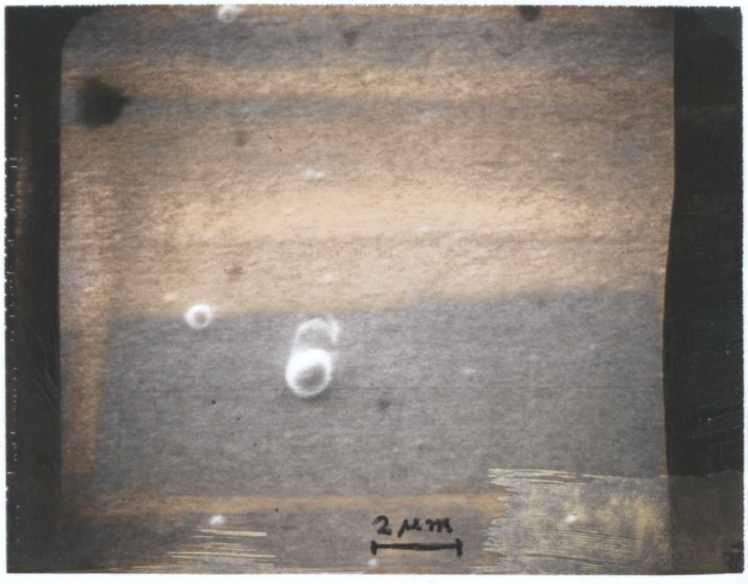

(b) Electron beam energy of E.B.Evaporator = 2.6 keV.

Figure 9.3 Electroscan micrographs of electron beam evaporated Gold Films.

* Rate of deposition depends on the source to substrate distance, L, The quoted values are for various L values.

** Should be less than 3 kV for good surface finish.

9.2.3 Deposition of Dielectric Films.

Thin dielectric films are used in microwave lumped elements and crossovers. Therefore their dielectric constants should be less than 10. Silicon Dioxide, silicon monoxide, alumina and silicon nitride have dielectric constants in this range. The first three of these materials were investigated. In these experiments the thin dielectric films were deposited using the electron beam evaporation source. The dielectric properties of these films were measured at microwave frequencies (section 7) as well as low frequencies.

Silicon dioxide, SiO_2 , is one of the most widely investigated thin film material. Various thin film deposition techniques[18,80,82,88-95] are used. In the present investigation the author used the electron beam evaporation source and rf sputtering (section 9.3) techniques. In the electron beam evaporation SiO_2 various conditions of evaporation were tried. These were (i) evaporation from cermet, carbon and molybdenum crucibles, (ii) different rates of evaporation and (iii) various residual pressures. All of the thin SiO_2 films were deposited onto heated substrates which were held at 200°C with the help of a temperature controller.

The electron beam evaporated SiO_2 films do not adhere to substrates and since they are under stress they flake off. This non-adherence of the SiO_2 film was overcome by depositing a thin layer of chromium (10-20 nm thick) between the SiO_2 film and the substrate. Table 9.2 shows the films and various conditions used during the investigation.

Also in table 9.2 the characteristics of thin films of SiO and Al_2O_3 are included. The silicon monoxide films were deposited on to a cold substrate and the adherence layer between the film and the substrate was nichrome as this does not require heated substrate.

Alumina films were deposited without an adhering film and the substrate temperature (with no external heating) was about 190°C self heated by the electron gun. The distance between the gun and the substrate was 10 cm.

The above films were deposited on copper or aluminium coated soda lime glass (microscope slides), Corning 7059 glass, copper blocks and silver plated invar substrates. The metal substrates were used for the measurement of the low frequency dielectric properties of these films. The metal substrate formed one of the metal electrodes whilst the top electrodes were deposited through a mechanical mask Figure 9.4. shows three of these test pieces for the low frequency measurements.

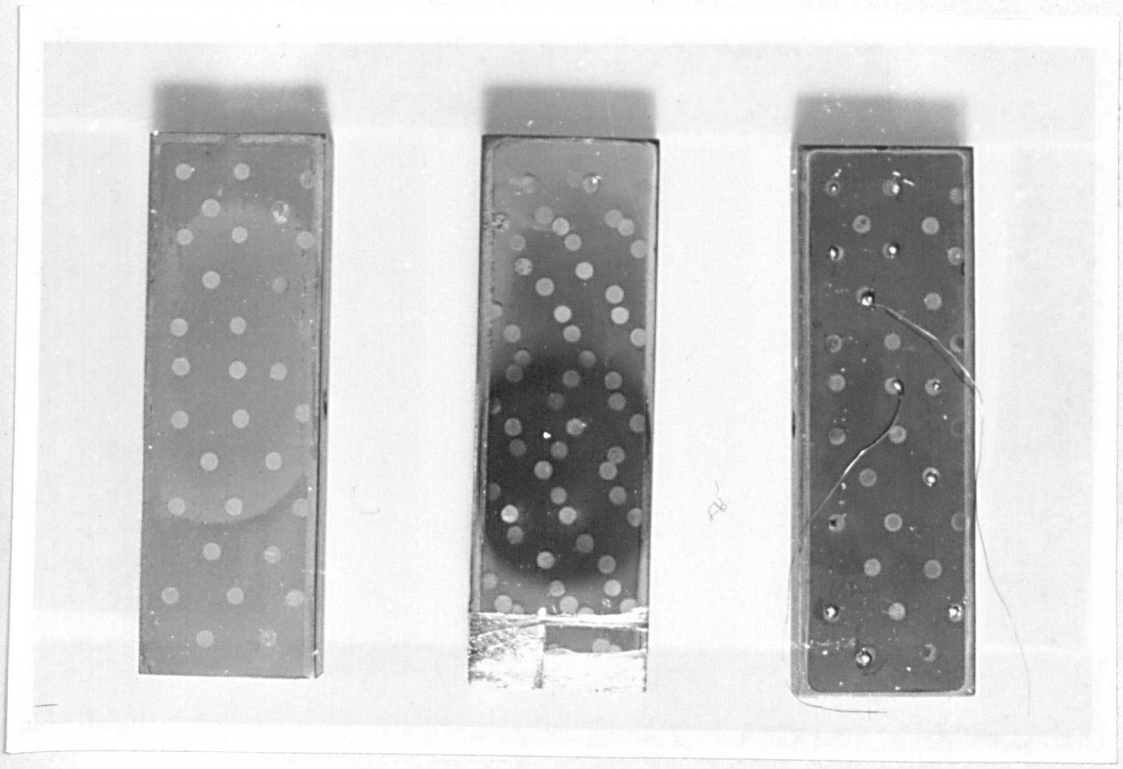

Figure 9.4 Capacitors for Low Frequency Measurements
(a) Copper - Al_2O_3 - Copper
(b) (i) Copper - SiO_2 - Copper
(ii) Copper - SiO_2 - Aluminium
(c) Copper SiO_2 - Copper.

The properties of these capacitors are given in Table 9.4. It will be seen from these results (the first sample) that Q_D depends on the electrode material. Copper electrode gives higher Q_D than the aluminium electrode. The cause, possibly, is due to the diffusion[106] of Al into SiO_2 film whilst the top electrode was deposited.

9.2.3.1 Dielectric Films for Microwave Measurements.

In this part a substrate holder was designed to hold as many as

5 cavity tops which could be loaded with thin dielectric films in the same deposition process. Also a sampler was accomadated. Figure 9.5. shows the substrates in position.

It was shown in section 8.2 that the errors in the measurement of the film thickness deposited on to the cavity, determine the accuracy of the measured microwave parameters of the dielectric film. Although a film thickness monitor was incorporated in the evaporation system its accuracy is not as we wanted it. This is due to variation of the deposited film thickness over the area of the substrate holder [81] and therefore the film thickness should be calibrated for each sampling point. Another drawback is that it depends on the mass deposited on the quartz crystal and if the density of the material varies from deposition to deposition then it will not give an accurate thickness. This difficulty was eliminated by measuring the film thickness deposited on a mask as close to the centre conductor of the cavity as physically possible. The arrangement is shown in Figure 7.1. section 7. Here the dielectric film was deposited on to a glass mask which was used not only as a mask but also as the film thickness monitor. This mask had on one side deposited copper film about $\frac{1}{2}$ um. This precaution was taken because it was found that the films deposited on to a glass and a metal substrate were different in thicknesses. (In case of SiO the film deposited on glass was 5% thinner than the film deposited on silver plated invar sampler.) The film thicknesses were measured using a Taylor Hobson Tallystep MKI, which can be used to measure film thicknesses from 10 μm down to 2 nm.

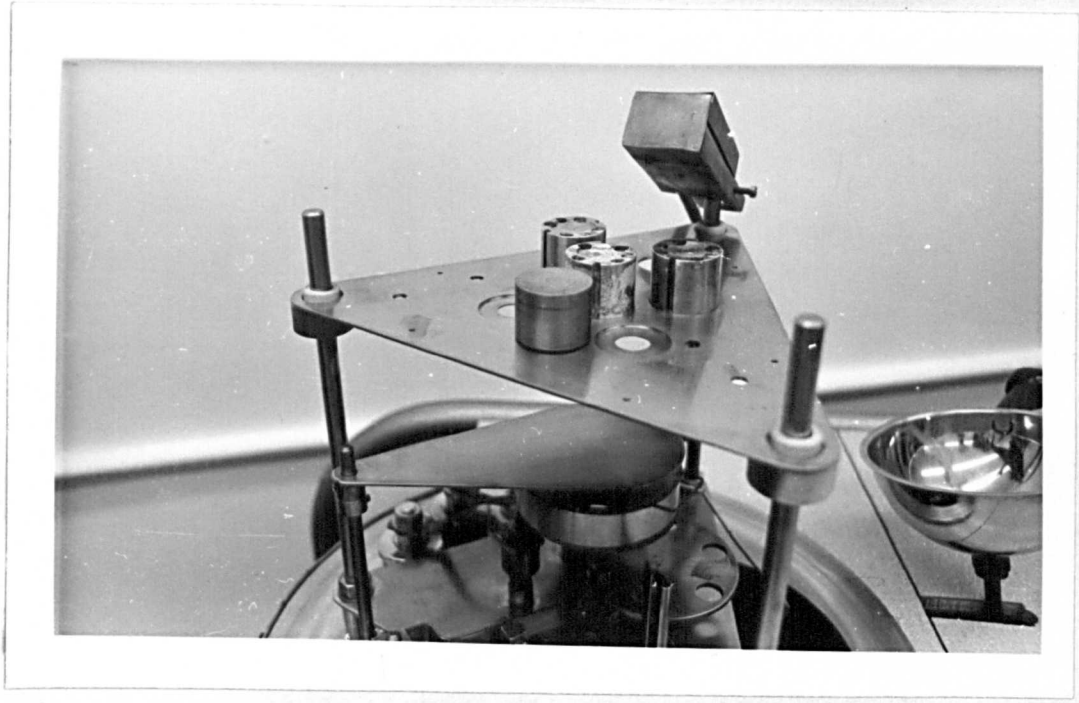

Figure 9.5 Three cavity tops and a sampler in position

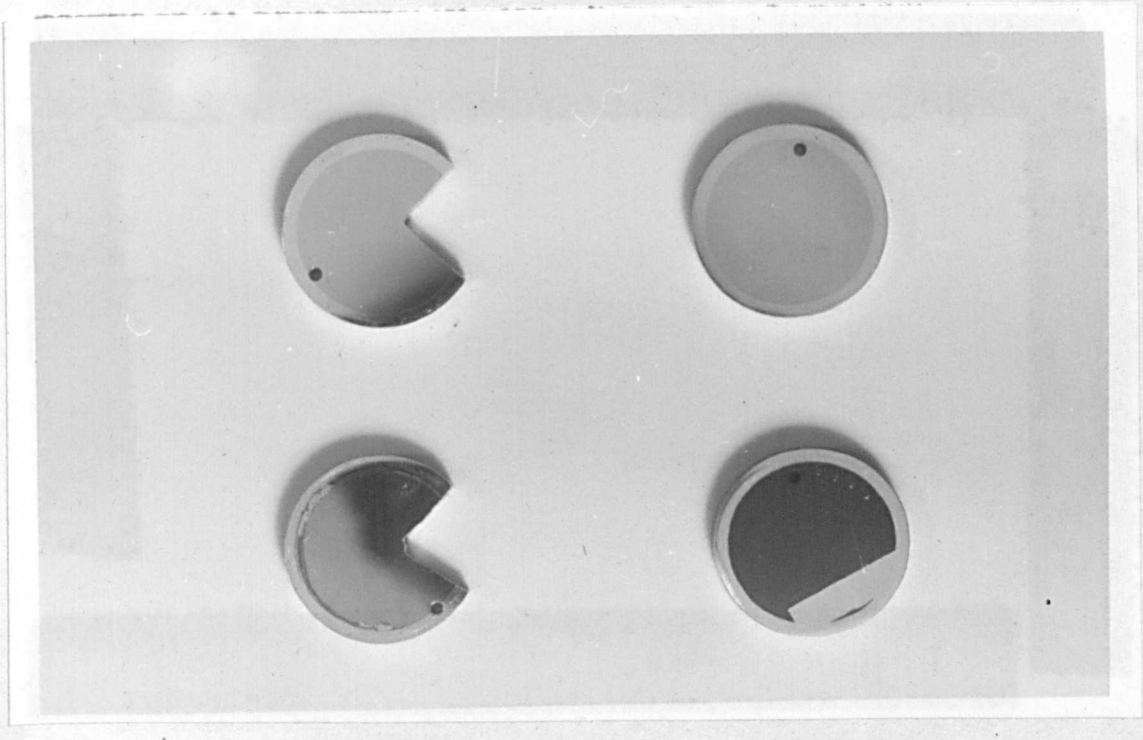

Figure 9.6 The dielectric film samplers (Ag plated Invar)

A second mask made of p.t.f.e. was fixed on the centre conductor of the cavity. This material is very soft. It does not damage the conductor surface, and also it has negligible outgassing in a vacuum system even at as high a temperature as 300°C.

The deposition of the dielectric film was the same as previously discussed. In this the cavity top was heated at 200°C for one hour before the deposition of the dielectric film. Whilst depositing on to the plane end of the cavity, it was also deposited onto a sampler under the same conditions.

The sampler was made of invar, one of its plane surfaces was polished down to $\frac{1}{4}$ µm and then electroplated as in the cavity plating (section 4). Before the deposition of the film it was polished again on a $\frac{1}{4}$ µm polisher.

This sampler served two purposes; it is used to determine the IR spectra of the film and also for making capacitors for the evaluation of the low frequency dielectric properties of the film. Four of these samplers are shown in Figure 9.6.

The deposition of SiO_2 , SiO and Al_2O_3 films for microwave measurements were carried out as described in the previous section. Results are shown in Tables 9.2 and 7.2 (section 7)

9.2.3.2. The Analysis of Thin Dielectric Films.

Table 9.2

EB DEPOSITION CONDITIONS AND PARAMETERS OF THE THIN DIELECTRIC FILMS

Dep. No.	Material	Crucible	Vac. pressure x10^{-5} torr		Beam Power W	Rate of Dep. nm/s	Thickness μm	Relative permittivity		Remarks
			Before Dep.	During Dep.				ϵ^1	Q_D	
1	SiO_2	C	0.32	1.5	150	0.7 - 1	2.0	3.9	10	Subst. temp. 200°C, Cr.layer
2		C	0.4	1-4	150	2.5-3	2.0	4.2	20	" " " "
3 3		Mo	0.34	1-2	168	2.9	3.9	4.3	8	" " " "
4		Mo	0.07	2.5-3.5	140	2.5-3.5	2.7	4.1	86	" " " "
5		Mo	0.8	4	130	6	3.3 ,	4.2	29	" " " "
6		Mo	0.75	3	150	6	3.8	5.0	24	As above but subst. biased to + 25 V
7	SiO	C	-	-	150	43	4.2	5.9	132	Subst. not heated, NiCr. layer
8		C	-	-	150	22	5.5	4.9	116	" " " "
9	$A/_2O_3$	C	0.3	5	280	0.6	0.9	8.8	34	Self heating up to 160°C, none
10		Mo	0.45	4	210	0.6	1.9	9.5	39	" " " "

Dep. No. 1-2 source to substrate distance = 14.5 cm C = carbon, Mo = Molybdenum.

Dep. No. 3-10 source to substrate distance = 10.0 cm.

Note 1: All the electrical parameters quoted were measured at X band.

Note 2: SiO_2 charge was preheated at 10-20 W beam power for 10 minutes before the deposition of the SiO_2 film

A literature survey on the film dielectrics shows that the quoted dielectric properties of a given film material vary widely, however the researchers call it the same compound. The best way to eliminate the ambiguity in the dielectric properties of a thin film is to analyse its chemical composition, and its stoichiometry. There are two non-destructive methods available. These are:

(i) Microprobe Analyser where the film is analysed for its composition[99-100],

and (ii) Infrared spectroscopy[101-104], where known relaxation parameters of the material are used. In the case of the oxides of silicon the Si-O bond vibration frequencies fall in the IR range and many people used this phenomena to analyse material compositions[102-103]

Using the first technique we analysed some of the deposited SiO_2 and SiO films. Results are shown in table 9.3.

Table 9.3.

Composition of the Dielectric Films

Material No	Material	percent Atomic Silicon Composition		Q_D at X band
		Theoretical	Measured	
4	SiO_2	33	31	86
1	SiO_2	33	37	10
*	SiO	50	52	-

Material No. refers to materials in table 9.2; * Rate of Deposition = 3.6nm/s

These results were obtained using a pure silicon piece as the standard and the silicon content of the film was compared with this standard.

It will be seen from these results that No. 4 is slightly deficient in silicon. This is due to the porous nature of electron beam deposited thin films[81,102]. The microprobe analysis compares the silicon contents in an equal volume, of the standard with that of the thin film. Therefore a porous volume will have less silicon than a dense one.

The other film No. 1 can be described as SiO_2 and other oxides of silicon. If we compare the evaporation conditions (Table 9.2) we can see that the film was deposited at a slower rate than No. 4 and also under different conditions.

The slow rate of evaporation gives films of low density[81] and also different chemical composition than the evaporating material. This is shown by the deficiency of oxygen (excess of Si) in the film. Another point is that electron beam evaporated films are stressed[102] and since they are porous react with H_2O in the atmosphere to form SiOH.

The above films were analysed whilst the manufacturers of the microprobe analyser (Cambridge Scientific Ins.) were demonstrating the equipment. That is why no other result is being presented.

At the time of anlysis of these films it was impossible to determine the other elements i.e. oxygen, of the compound. If accurate results are required then all the elements of the compound element film should be determined.

Pliskin[101,102] used IR spectroscopy to analyse glass films and he claims that using this method together with etch rate and refractive index of the film, the material stoichiometry, structure and chemical stability can be determined. Most of their investigations were carried out using the transmission type of IR spectroscopy. Although this method has many advantages over a reflection type IR spectroscope[103] it can not be used to investigate glass films deposited on material which is opaque to radiation.

In the present investigations the films to be investigated were deposited on metal or metallized glass substrates and hence the reflection method was used. The spectroscope used was The Spectromaster (Grubb Parsons) of Newcastle) with the reflection attachment.

The plots of reflection against the i.r. wavelengths are shown in Figures 9.7, 9.8 and 9.9. Comparing plots A and B (Fire 9.7) it will be seen that the films obtained from SiO_2 evaporation have reflection peaks at 9.2 μ and bulk sample at 8.9 μ. 8.9 μ is the Si-O band vibration wavelength of SiO_2. Therefore these results show that the films contain SiO_2.

Figure 9.8 shows the reflection plot of films evaporated using SiO. This material has a weak resonance peak at around 10 μ.

The plots shown in Figures 9.7, 9.8 and 9.9 show that there is a definite reflection minimum (absorption maximum) for each plot at a specific wavelength. These reflection minima are $\simeq$10 μ for SiO_2 and $\simeq$10.8 μ for SiO films.

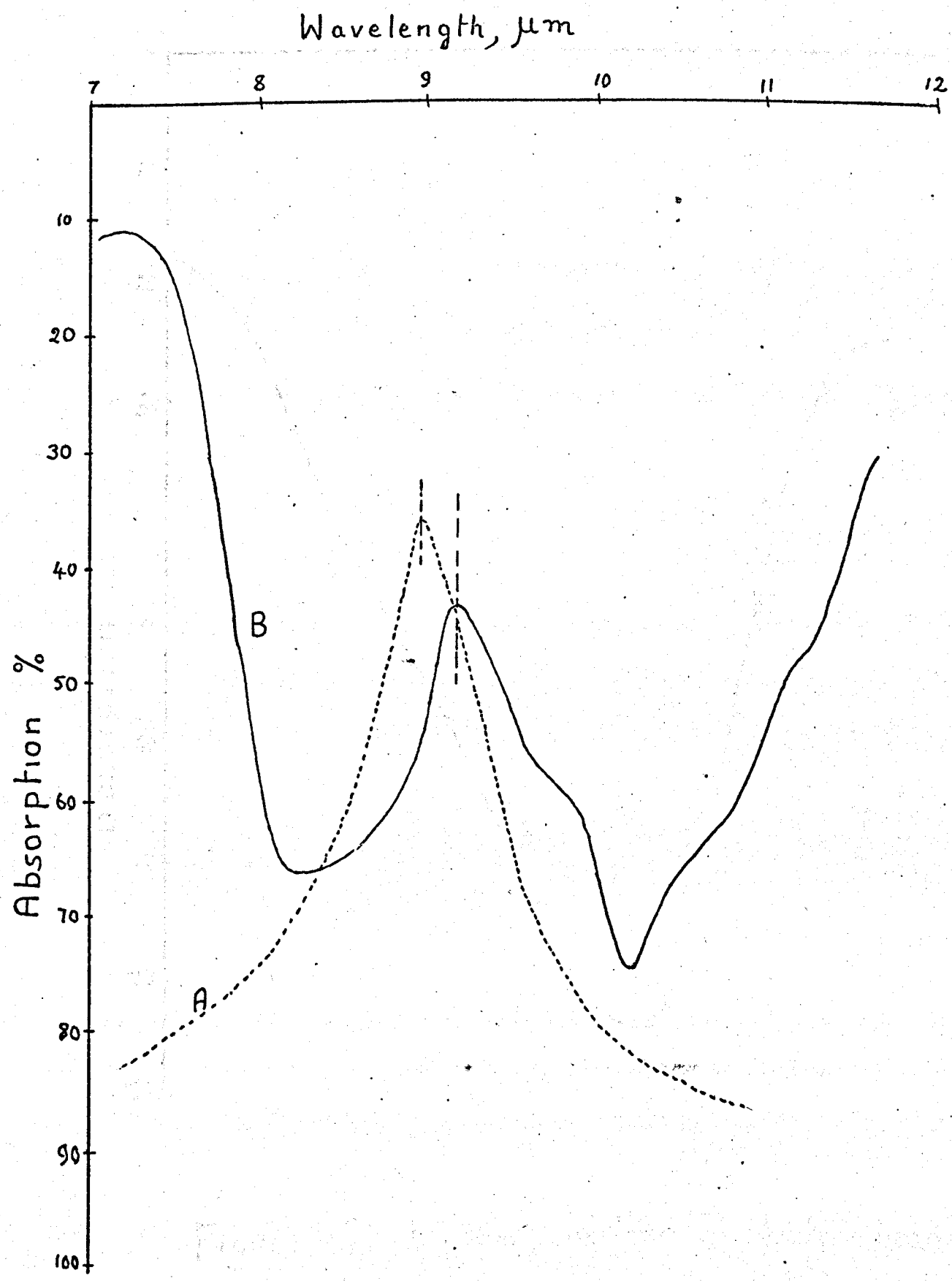

Figure 9·7 Infrared spectra for: A – Spectrosil glass (≈3 mm thick); B – Electron beam evaporated SiO_2 on copper substrate (film thickness ≈ 3·3 μm, dep. rate = 4 nm/s)

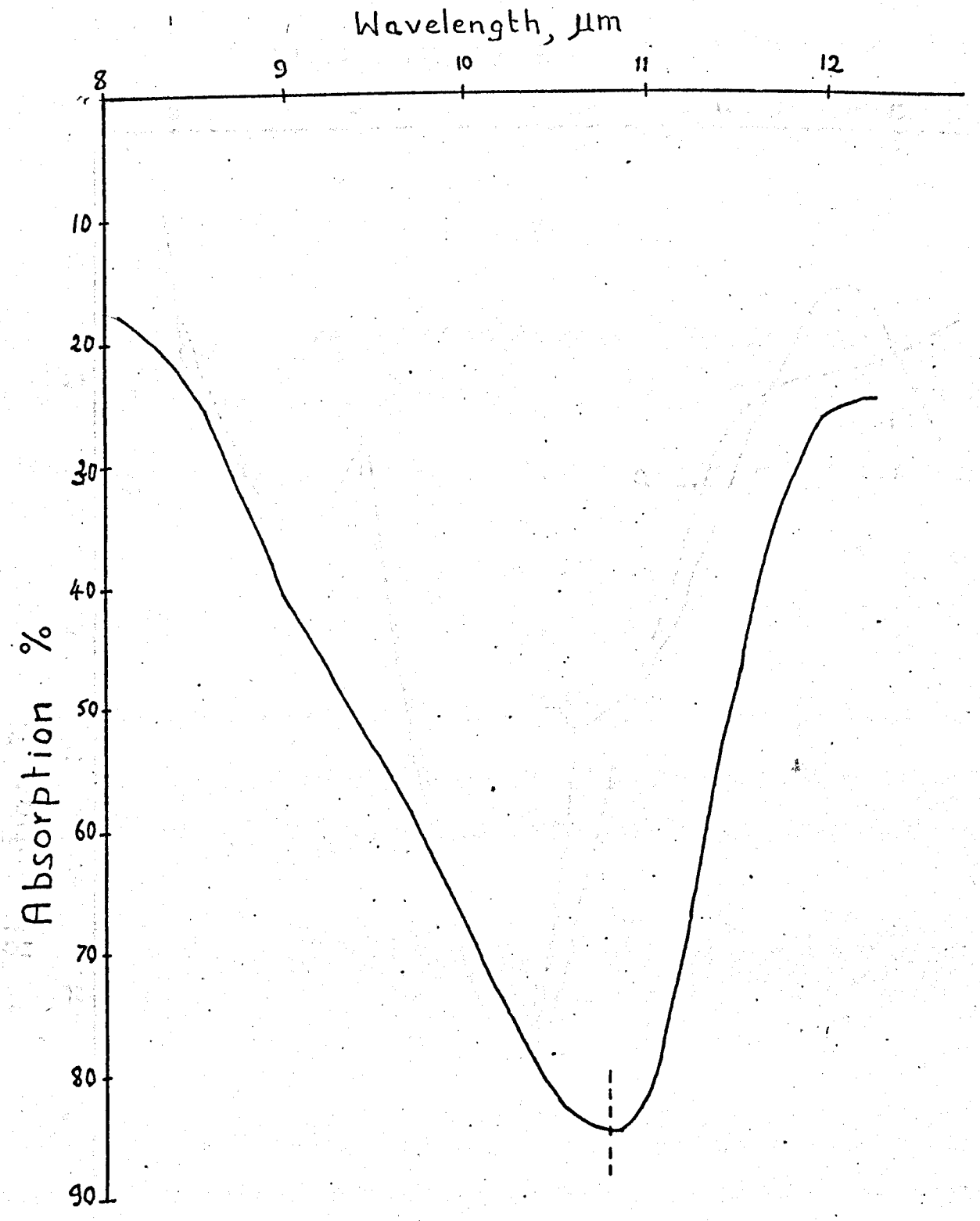

Figure 9·8 Infrared spectrum of electron beam evaporated SiO film on copper coated glass subst. (film thickness = 0·85 μm. rate of dep. = 4 nm/s).

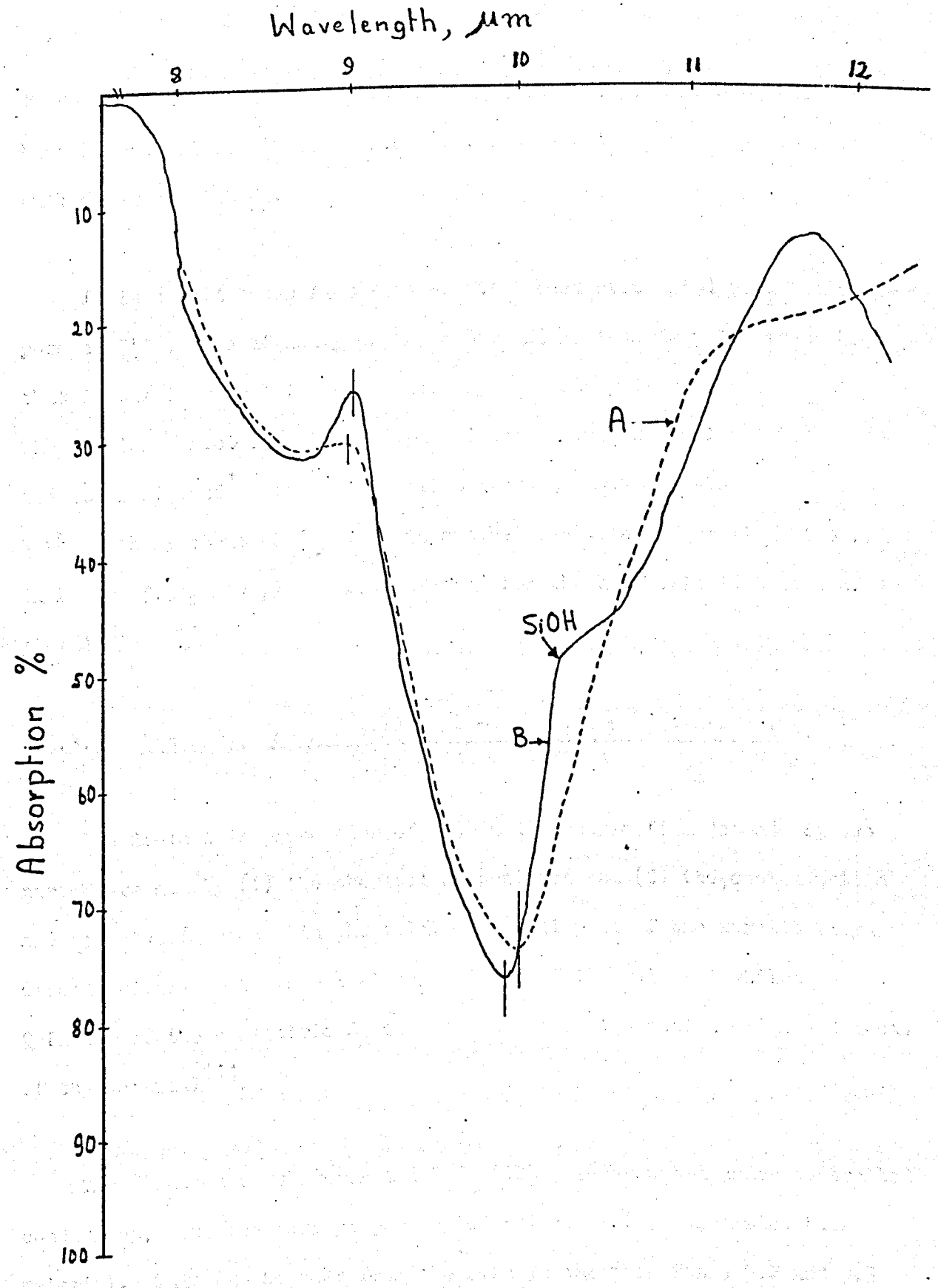

Figure 9.9 Infrared spectra of e.b. evaporated SiO_2 film (0.8 μm thick, dep. rate = 0.5 nm/s on copper subst.); A - 2 days after and B - 12 months after the deposiron.

These observations show that the electron beam evaporated SiO_2 films have IR properties different from SiO films and they are very close to bulk material of SiO_2.

It is a well known fact that electron beam evaporated SiO_2 films are porous[102,81]. The affinity of these SiO_2 films towards water is so high that if the film is left in an ordinary laboratory it will absorb water. The chemical reaction between SiO_2 and water gives Silanol (Si-OH) groups and it is claimed[101] that these silanol groups have a Si-OH resonance wavelength at about 10.6 μm. This can be seen as a deformation at 10.5 μm in Figure 9.9 where plot B was obtained for the same film 12 months after plot A.

9.2.3.3 Discussion on Electron Beam Evaporated Dielectric Films.

The dielectric properties of a thin dielectric film depend on two parameters namely (1) the chemical composition and (2) the contamination and structural defects in the film. The real part of the permittivity ϵ' depends mainly on the chemical composition of the material whilst the Q factor of the dielectric Q_D depends on the contamination and the defects of the material[114].

The electron beam evaporated SiO_2 films if deposited under controlled conditions, have chemical properties identical to the evaporated bulk material. This can be seen from the results shown in Table 9.2 and 9.3 sample 4. Pliskin using IR transmission spectroscopy came to the conclusion that the electron beam evaporated "SiO_2" films are essentially SiO_2 with some oxygen defficiency. The present investigations also have shown that in certain conditions the deposited film can be nonstoichiometric

(Table 9.2 and 9.3 sample 1). Since the SiO_2 films deposited under controlled evaporation are stoichiometric then their dielectric properties should be the same as the bulk material. The measured ϵ^1 is not far out from its bulk value of 3.8, but Q_D is about one hundredth of the bulk value. The cause of this can be summarized as follows:

(i) Contamination of the film by a foreign material this could be from the crucible or from the bulk material. The latter is not possible because the material used in the evaporation was Spectrosil(highest purity fused quartz, Appendix 9.)

If the crucible material evaporated together with the evaporant bulk material there can be either ions in the film which does not effect the dielectric losses at X band or introduce defects into the film which will effect the losses at X band.

Another contaminant is the residual gases in the vacuum system during the deposition. This is usually water vapour. It will be seen from the values shown in table 9.2 that a lower residual pressure gives better Q_D than a high one. (compare deposition No. 2,4 and 5). The discrepancy between No. 2 and No. 5 is due to the difference in source to substrate distances. In the deposition No. 2 the source to substrate distance was longer than the deposition No. 5 and the probability of the evaporated material hitting a residual gas molecule was higher for No. 2 than No. 4 because it had to travel further. In both cases the rate of evaporation was

the same but the rate of depositions were different. This arose because of the different source to substrate distances. The rate of deposition is proportional to WoL^{-2} where Wo is the rate of evaporation and L is the source to the substrate distance[81].

It will also be seen from the table 9.2 that in those two cases discussed above the evaporants were held in two different crucibles namely Carbon and Molybdenum. Measurement at low frequencies showed that losses in the thin dielectric film are not influenced by the crucibles. In table 9.4 the first two results show this. Therefore the increase of dielectric loss in the film, is not due to the evaporant of the crucible material.

(ii) The effect of Water vapour:

It is known that the most important of the residual gases in the vacuum system at residual pressures of the order of 10^{-5} torr is water vapour. Therefore water vapour may strongly influence the losses in the dielectric film. This is shown in table 9.2. It will be seen that the higher the residual pressure the lower is the Q_D value of that deposited film.

Another point is that low deposition rates give porous films. The electron beam evaporated films are also highly stressed and placed in the atmosphere the water vapour in the

atmosphere will readily react with the SiO_2 film to give a silanol(SiOH) group. This reaction will increase the dielectric losses of the film.

Table 9.4

Low Frequency Parameters of Dielectric Films

Material	Thickness μm		Q_D	frequency	electrodes
*SiO_2	1.2	4.2	40 - 60	up to 100 MHz	Cu + SiO_2 + Al
-	"	"	60 - 125	"	Cu + SiO_2 + Cu
**SiO_2	1.3	4	60 - 100	up to 10MHz	Cu + SiO_2 + Cu
SiO	5.5	7.8	8 - 270	up to 50MHz	Ag + SiO + Cu
Al_2O_3	0.84	9.1	50	10kHz	Cu + Al_2O_3 + Cu

* from carbon crucible ** from cermet crucible

Table 9.5

The effect of Water Vapour on Dilectric Properties of SiO_2

CONDITIONS	ϵ'	Q_D	frequency GHz
10 hrs. after deposition, but kept in vacuum	4.2	36	1.33
	4.2	29	9.5
After 3 days in Lab. 70% RH	4.2	18.3	9.5
Heat treated for 1 hr. at 270°C in a 5 x 10^{-4} torr Argon	4.2	21.	9.5
12 hrs. after heat treatment		18.3	9.5

Relative Humidity : 65 - 80%

Material Dep No 5 Table 9.2

Since the film is porous there will be absorption of water vapour as well and there will be additional losses due to this (Water has a dielectric loss peak around 10 GHz). This point was investigated. The results are shown in table 9.5. The heat treatment was carried out in an argon gas atmosphere at a partial pressure of 5×10^{-4} torr and at 270°C for one hour. The measured results showed that there was absorbed water vapour in the film because the dielectric loss has gone back to its pre heat treated value when left in the laboratory for 12 hours.

The difference between the first measured at Q_D and heat treated Q_D most likely is due to the formation of silanol groups in the thin dielectric film. The silanol groups can be eliminated by chemical treatments or by strong heating at 900°C[105] or slow heating in dry ambient to 600°C[101].

These two effects are due to the porous nature of the electron beam evaporated SiO_2 films. This effect is more apparent in slowly deposited films because they are more porous than higher rate deposited films. SiO_2 films prepared by other methods have porousness and they will suffer from the same trouble. One way to eliminate this is to heat the deposited film in an oxidising atmosphere at possibly 900°C and hence densify the film. Caulton[18] did this for the SiO_2 films obtained from chemical vapour deposition.[94] He quotes Q_D values of 50 for undensified films, 600 for moderately densified and 5000 for highly densified films. These high densification

temperatures can not be used in the preparation of integrated circuits because there will be diffusion or alloying between two metals in contact such as Cr - Au or Al - Au. Also Al reacts with SiO_2 at temperatures greater than 700°C[106].

(iii) Structural Defects:

The dielectric films deposited using one of the deposition techniques have structural defects such as bond angles. They also have weak spots like channels[107]. Also films are stressed.[85] These film defects introduce electron trapping. When an r f field is applied these trapped electrons jump from one trap to the next one and the phenomena is named as electron hopping mechanism[108]. Since the mobility of electrons are high this phenomena will be a factor in the increased dielectric losses at microwave frequencies. These stuctural defects can be eliminated by heating the substrate in an inert gas or oxidizing atmosphere at a temperature greater than 450°C.

These above properties show the difficulties of depositing thin dielectric films for m.i.c's. The heat treatment can produce highly densified hence dielectric films having high Q_D values. But none of the high conductivity metals can stand such high temperatures.

9.3 R F Sputtered Dielectric Films

It was shown in the previous sections that the electron beam source deposited dielectric films have about 100 times more losses than the

bulk material which was evaporated. It was explained that these problems can also be eliminated provided that the metal film in contact with the dielectric film can stand the treatment temperature of 900°C.

R F sputtering[86,88-93] is a cold process and may eliminate certain factors which contribute to the dielectric losses. Also there is almost no decomposition of a compound during the sputtering. In this process a high energy ion beam strikes on to the target (the material to be sputtered) and the momentum of the ions are transferred to the materials and small particles are ejected from the surface. These ejected particles travel towards the substrate and hence deposit there.

In the present investigation the dielectric films were sputter deposited using a diode r f sputtering unit. The r.f. sputtering unit was built in the University Laboratory to a design which was reported by Probyn[90].

The SiO_2 films deposited using this technique were found to be much better than the electron beam evaporated SiO_2 films, the Q_D values of three measurements at X band varied between 150 and 400. The reported Q_D values by others[18] were 500 - 600 though no measurement frequency was quoted. The authors[18] who quoted this value were measuring Q_D indirectly, i.e. measuring the parameters of a sandwich capacitor.

The investigation on r.f. sputtering is a separate project, the measured films being prepared at the beginning of the research work[115]. It is therefore not possible to report further on this work here.

CHAPTER 10

MICROWAVE MEASUREMENT OF LUMPED ELEMENTS

10.1 Introduction

The measurement of lumped elements at microwave frequencies is difficult because of their small dimensions. The measurement techniques adopted by other workers were briefly discussed in section 1.3. and in that discussion it was claimed that the resonant method of measurement of a L E by connecting at the end of the transmission line. . . . . ?

In the present investigation the author uses microstrip resonator techniques to measure lumped element values. The theoretical approach to the technique is presented in section 3. In this section the practical side of the approach will be discussed.

The microstrip proerties cannot be calculated as is done for the coaxial line because no exact theoretical solution exists. Most of the reported solutions introduce certain modifying factors to their solution of microstrip properties[3-6]. The best way to overcome this difficulty is to first determine the microstrip line properties and then use it to measure the lumped elements.

The topics covered are:

(a) measurement of the properties of microstrip line

(b) preparation of microstrip resonators and lumped elements using the thin film processing and photolithographic techniques

(c) measurement of the properties of capacitively loaded microstrip resonators and the lumped elements.

10.2 Microstrip Line Resonators

10.2.1 Measurement of the effective Dielectric Constant

When Wheeler[2] derived the properties of microstrip, the dispersion properties of the line were not taken into account. Later works[37-39,116] have shown that the line is not dispersionless. It is claimed[38] that the dispersion in microstrip lines can be considered to be due to surface modes. The dispersion of the line can be determined by measuring the effective dielectric constant ϵ_e, of the microstrip. Many successful methods of measurement of the effective dielectric constant of the microstrip are reported[23,37-39] however they have certain limitations (such as end effects or inaccurate for wide strips).

In the present approach a half-wavelength resonator was used to measure ϵ_e. The resonator consisted of the normal microstrip configuration and the line was terminated by deposited short circuits. These short circuits extended at both ends for the whole width of the ground plane (Figure 10.1).

These microstrip resonators were first prepared to our specification by an industrial firm (G.E.C/ A.E.I - Leicester) but later on they were prepared by the author. The thin film deposition of metal films is given in section 9.2.2.1 and the use of the photolithographic technique in the construction of these resonators is given in section 10.2.2.1.

Table 10.1 shows the lines used in the measurement of ϵ_e over the 1 to 12 GHz frequency range.

Table 10.1

Microstrip Resonators.

Line	L mm	W mm	h mm	NOMINAL IMPEDANCE Z_o ohms
A, Alumina	50.6	1.02	1.02	50
B, Alumina	25.3	3.18	1.02	26
C, Alumina	25.3	3.18	1.02	20
D, Sapphire*	25.4	2.13	0.514	20.5
E. Quartz*	25.4	2.13	0.514	31.6

* results are shown in Figure 10.4

The resonant line was excited through a single probe. The probe consisted of an OSM to microstrip adaptor with its tab filed down to 0.3 mm by 0.2 mm and screwed to the base plate. The resonator was placed on the base plate with the probe in contact with the short circuit, so as to feed a current through it (Figure 10.1b). This gave a sensibly constant coupling over the entire frequency range plotted. Careful checks were made to ensure that coupling did not affect the resonant frequency. The measurements were made using an ordinary swept frequency reflectometer connected to the probe.

It was found that there is some "field spillover" at the far end

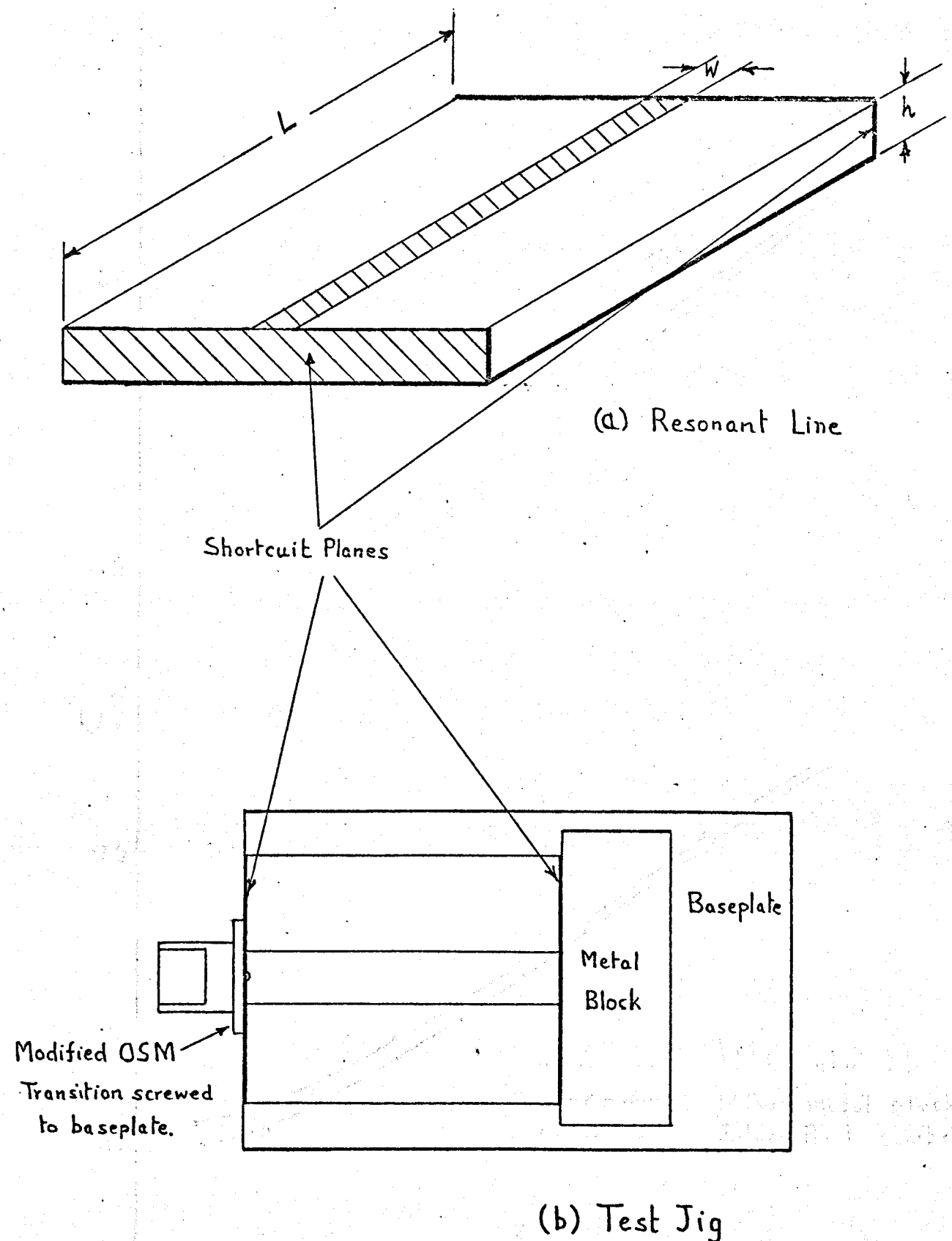

Figure 10.1 Microstrip Resonator.

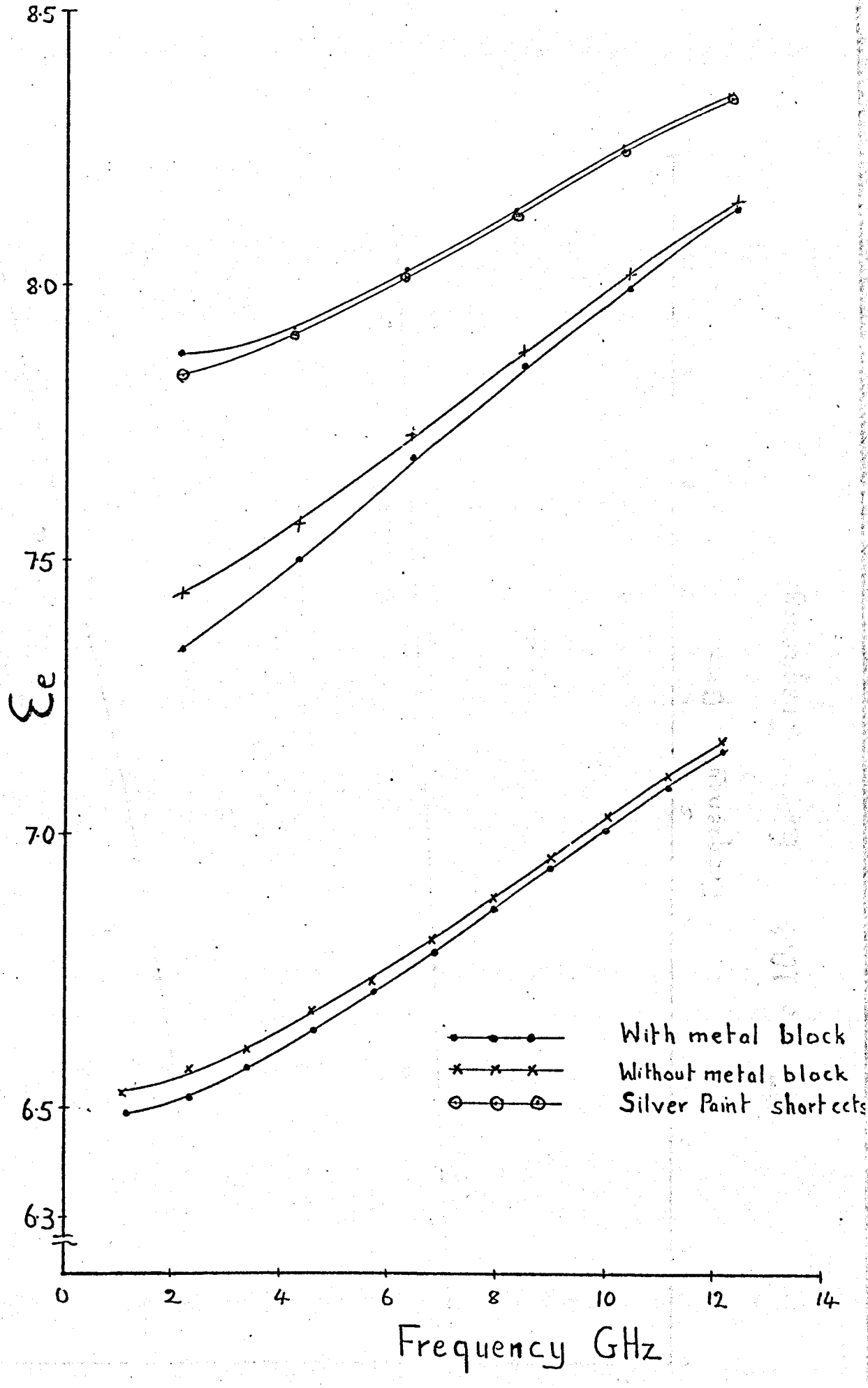

Figure 10.3. Effective Dielectric Constant vs Frequency

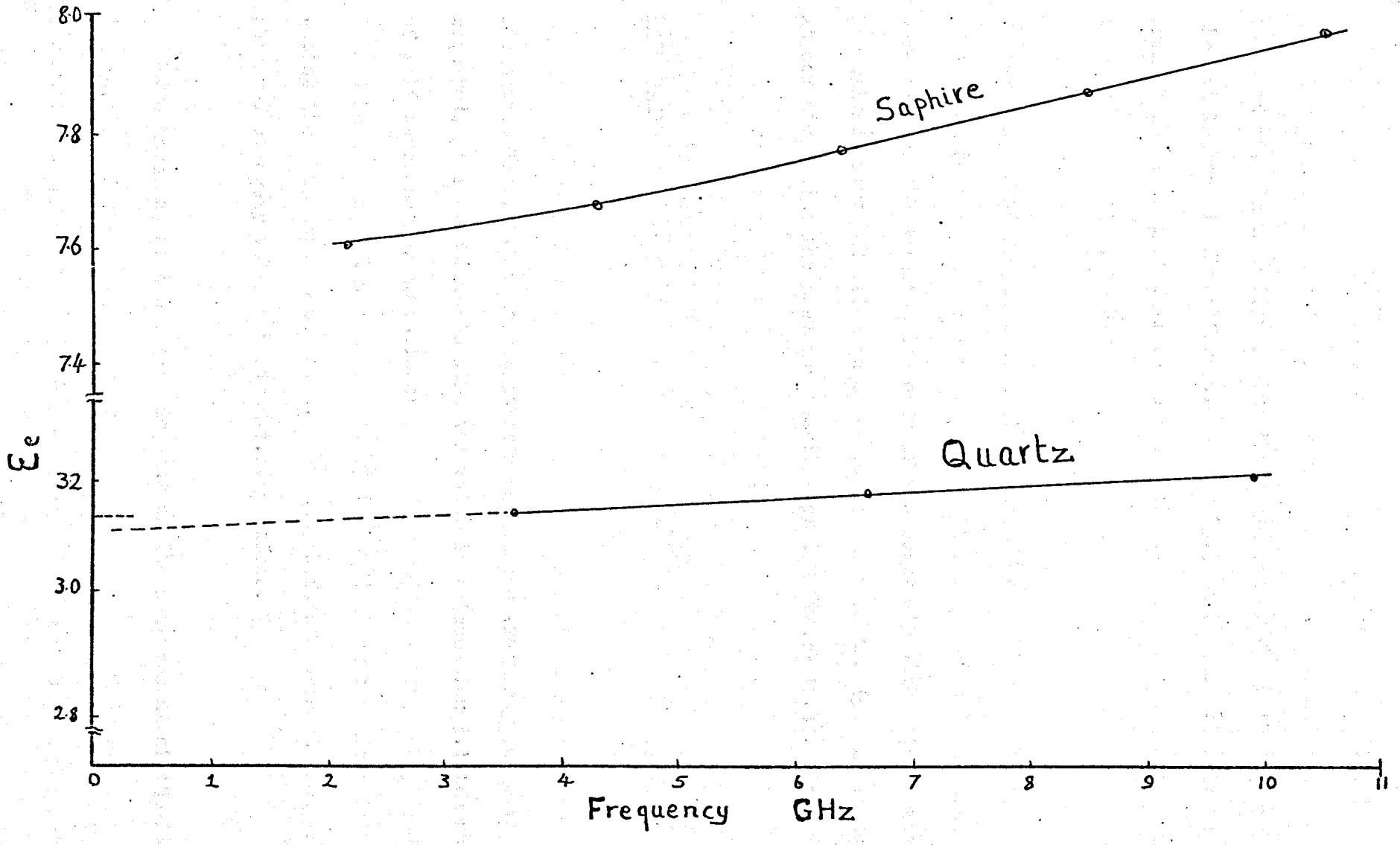

Figure 10.4. ε_e vs Frequency

short circuit plane. This can be overcome by a metal block placed as in Figure 10.1 b to extend the short circuit plane to the fringing fields. At the input end the flange of the OSM adaptor acts as the additional shorting plane. Figure 10.3. shows some of the results obtained with this method. In this figure also the variation of ϵe with and without the metal block is shown for 50.6 mm and 25.3 mm lines. It will be seen from these plots that failure to short circuit the fringing fields can lead to error of up to 0.6%.

To prove the feasability of the system for rapid general use an additional test was carried out. In this the short circuiting planes were prepared by painting the ends of the substrate with silver paint. The silver paint was dried on a hot plate and when the ϵe was measured it coincided with the previous results (plot C Figure 10.3). This method showed that the system gives quite good results.

Comments:

Results have shown that the method can be used on any straight microstrip line. If measurement of a restricted frequency range is required, it is possible to find the value if n (equation 3.1)the number of half wavelengths, as follows:
A hand held probe (e.g. a screwdriver) is moved along the microstrip whilst the resonance is observed. Maximum shift of resonant frequency is observed at every voltage maximum i.e. n times.

The accuracy of the system depends on the measurement of the line length, L, and the resonant frequency, f_{ox}. L can be measured quite accurately using a travelling microscope. Using a frequency counter the

accuracy of f_{ox} depends mainly on the Q factor of the resonator, typically 350. It was found during the test that f_{ox} could be measured to an accuracy better than $\pm$ 0.1%. Thus with care a total accuracy of ϵ_e of $\pm$ 0.2% can be achieved.

The advantage of the system over the others[23,37,39,41,116] are: (i) its accuracy does not change with varying strip width, (ii) the fringing field spillover is so small that even if not terminated in an extra shorting metal block the error introduced is less than 1%, (iii) it can be used on any straight microstrip line provided that its lenght is at least half a wavelength at the measurement frequency, (iv) the accuracy of 0.2% achieved is better than for other methods.

van Heuven[40] claimed that ϵ_e of a microstrip line on fused quartz (thickness of substrate $\approx$0.5 mm) is independent of frequency. Using the present set up I found that this is not so. Table 10.2 shows the results obtained for a resonator with L = 25.4 mm, h = 0.514 mm and W = 2.13 mm.

Table 10.2

Effective Dielectric Constant of Microstrip On Quartz

frequency, MHz	ϵ_e	
	Measured	Calculated
D.C	-	3.14*, 3.12**
3325.3	3.15	
6620.6	3.18	
9892	3.21	

* ref. 4 ** ref. 117

It will be seen from these results that the variation of ϵ_e with frequency is quite small, $< 2\%$ and to detect such a small variation only the present system can measure it. van Heuven[40] admits that the accuracy of his measurement was within 3% and therefore he would not have noticed the variation of ϵ_e with frequency.

10.2.2. Capacitively Loaded Microstrip Resonators.

10.2.2.1. Construction of Microstrip Resonators.

Microstrip resonators were prepared by the author using sapphire and quartz substrates. These substrates were used because they had one of their surfaces highly polished (surface texture < 20 nm).

Initially thin copper films were deposited on four sides of the substrate, as discussed in section 9.2.2.1 . This gave deposited films of copper on two plane surfaces plus two edges. Thus the short circuit planes to terminate the microstrip resonator were already there.

Photolithographic techniques were used for the preparation of the microstrip resonator. The procedure used is shown in Figure 10.5.

The materials such as photo resist, etchants and others are all given in Appendix 11.

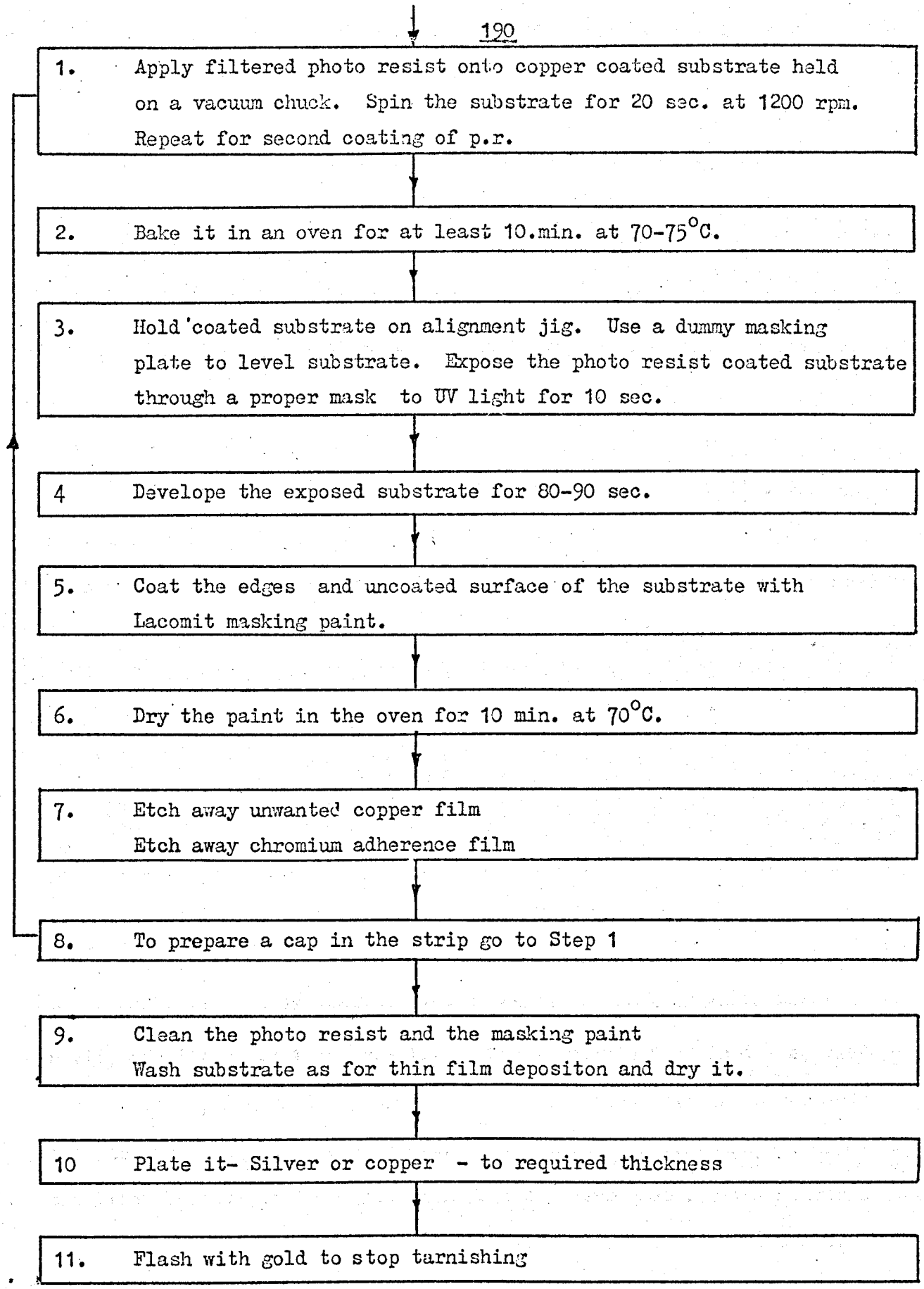

Figure 10.5 Process Flow Chart For the Preparation of a Microstrip Resonator.

10.2.2.2. Measurement of Resonator Properties.

The resonators prepared using the above process were tested on the H P Network Analyser with its Reflection Unit (8741A and 8742A). Since this unit is similar in principle to the reflectometer discussed in Section 5.2 further description of the equipment will not be given. The advantage of this equipment is that it is a coaxial line system and covers the whole band of frequencies from 0.11 to 12.4 GHz.

The capacitively loaded microstrip resonators were excited through an OSM to microstrip adaptor modified as described in section 10.2. This gave sensibly constant coupling over the entire frequency band used in the investigation.

10.2.2.3. Measurement of the Capacitance of a Gap in the Strip of a Microstrip Line.

It is shown in section 10.2.1 that the effective dielectric constant of a microstrip can be determined using a half wavelength resonant line. A gap was cut at the mid point between the short circuit planes. This gives a capacitance π network (Figure 10.6) the same as the coaxial cavity (Sections 2.3.1 and 6.3.1.1). The principle used in the coaxial cavity was applied to the capacitively loaded microstrip resonator and the gap capacitances were measured. Table 10.3 shows the properties of the lines investigated. Resonators 3. and 5 were used for the measurement of lumped elements and more detailed investigations were carried out. Gaps in these resonators were so small that Cp was negligible. Figure 10.7 shows the capacitance of the gaps calculated from the measurements at

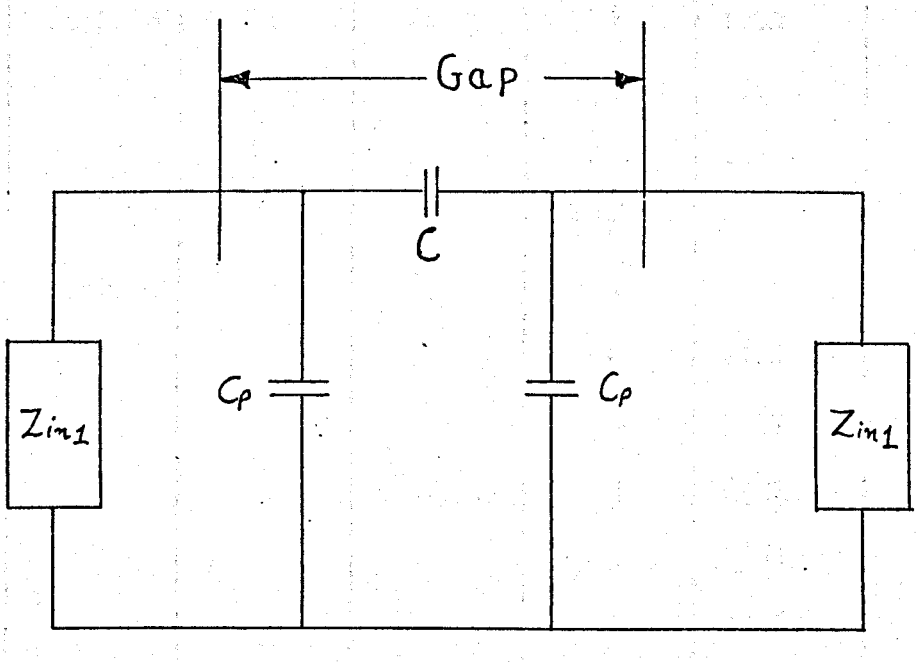

Figure 10·6 Equivalent Circuit of Capacitively Loaded Microstrip Resonator

Table 10.3

MICROSTRIP RESONATOR PROPERTIES.

Resonator No	Substrate Material	Plating	Gap um	Mode No. 1	Resonance frequency MHz	Measured Q
1	sapphire	Cu	26	1	1980	192
				4	9785	552
2	sapphire	Ag	none	$\lambda/2$	2178	327
				$5\lambda/2$	10619	559
3	sapphire	Ag	19	1	1947	154
				2	2164	242
				3	5837	246
				4	6422	355
				5	9691	440
				6	10569	450
4	Quartz	Ag	none	$\lambda/2$	3333	294
				$3\lambda/2$	9909	527
5	Quartz	Ag	19.5	1	2932	197
				2	3330	290
				3	8837	275
				4	9905	483

Substrate Dimensions were 25.4 $\pm$ 0.1 mm x 25.4 $\pm$ 0.1 mm
Resonator Dimensions 2ℓ = 25.4 $\pm$ 0.1 mm (due to different substrates)
h = 0.514 mm W = 2.13 mm
Thickness of metal t = 6-10 μm. after plating; t^1 = 0.5 μm before plating (including 10 nm Cr).

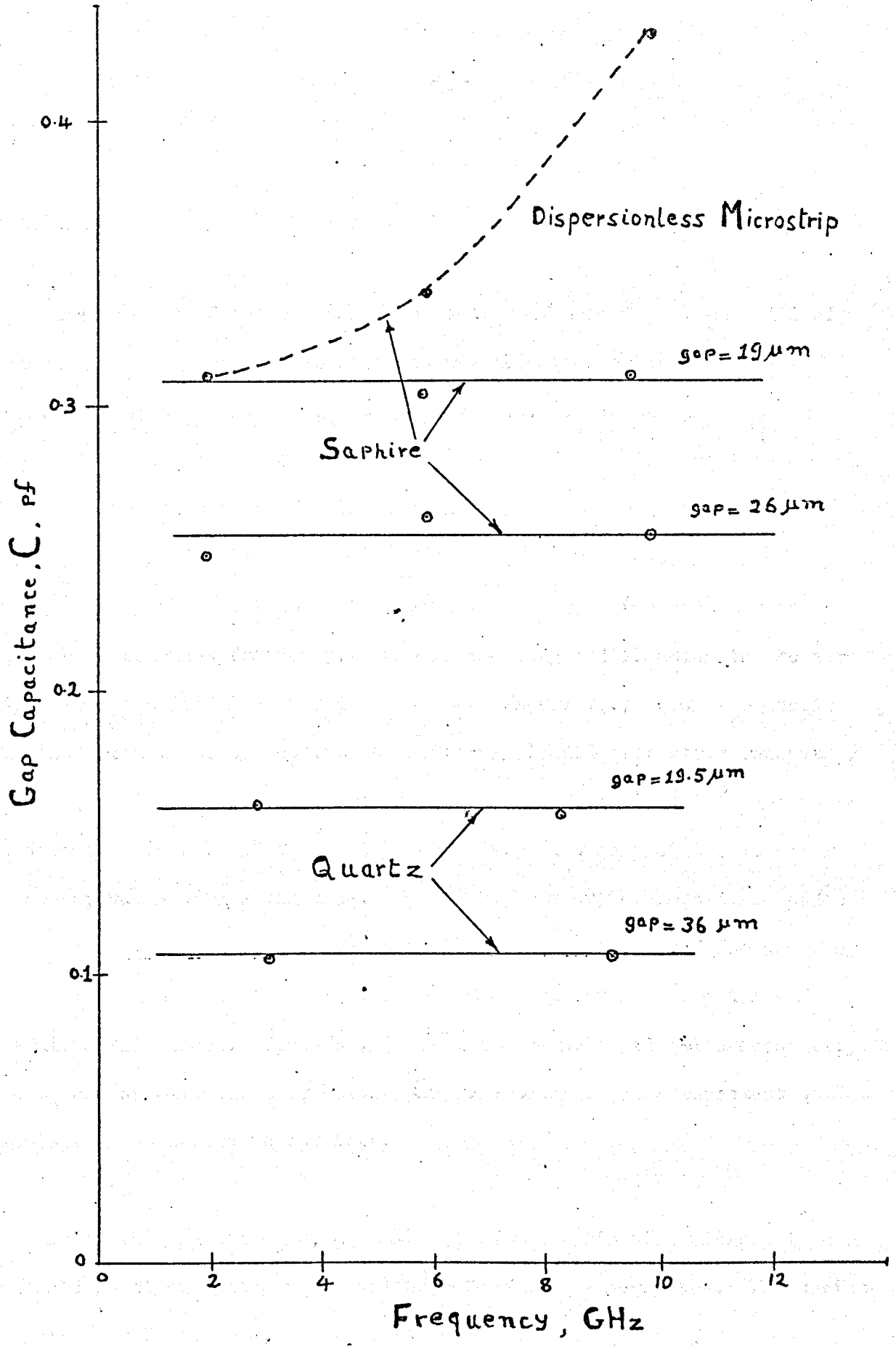

Figure 10·7 Gap Capacitance vs Frequency

various frequencies.

Comments:

Measurement of the resonant frequencies of symmetrical capacitively loaded microstrip resonators makes it possible to measure the gap equivalent π network capacitances (Figure 10.6). In the present case the series capacitances of the gap were measured at different frequencies from 1 to 12 GHz range. The shunt capacitances Cp's were negligible.

In these calculations of C previously measured ϵ_e values were used at each measurement frequency. This is the only modification to the air dielectric coaxial line type measurement. Figure 10.7 shows the results obtained from these symmetrical capacitively loaded microstrip resonators having sapphire and quartz substrates. An additional plot is given where "a dispersionless line" assumption was made. In this plot the low frequency value of ϵ_e was used. These graphs show the importance of ϵ_e on the measurement accuracy of the series gap capacitances. The accuracy of C measurement depends on ϵ_e, f_o, ℓ and characteristic impedance Z_o of the microstrip lines. Since ϵ_e, f_o and ℓ can be measured quite accurately and Z_o can be calculated by knowing ϵ_e, the accuracy of measurement of C within $\pm$ 2% at X-band is possible.

As in the coaxial case, a small gap in the strip of a microstrip has neglible shunt capacitance Cp, and therefore can be neglected. The series capacitances C measured, showed that they are independent of frequency and this also supports the assumption of neglible Cp values.

In Section 3.3. only the symmetrical case was treated, but an

asymmetrical resonator can also be used to measure the gap capacitance. In the latter case it is very difficult to measure Cp, but if Cp is negligible then it is as easy as the symmetrical, capacitively loaded resonator.

10.3 Measurement of Lumped Elements.

In the previous sections the parameters of the capacitively loaded microstrip resonators were measured. In this section lumped elements will be introduced and the measurement techniques will be described.

10.3.1. Verification of the Theory on the Measurement of Lumped Elements

The theoretical approach to the L E measurement using a capacitively loaded microstrip resonator was given in Section 3.3. The approach was tested using a low frequency model resonator. The arrangement used in the model testing consisted of two coaxial lines (characteristic impedance $Z_o = 50 \pm 1\Omega$). Figure 10.8a shows the set up. The far end of one of the lines was short circuited and the middle ends had their inner conductors connected through a capacitor C_s whilst the outers were soldered together. The resonant frequency of the system could be changed by varying the value of C_s.

The resonant line was excited through a coaxial T junction, where the centre conductor of the coaxial line resonator was connected to the centre and outer conductor to the outer conductor of the T junction.

The set up used to measure the model resonator parameters is shown

in Figure 10.8 b and c., The signal source was the H P sweep oscillator used in section 5.2 with "plug ins" type 8698B, 8699B (frequency range 0-110, 100 - 4000 MHz). The receiver was a H P Vector Voltmeter type 8405A. The Vector Voltmeter had two probes which were used to measure the phase just before and just after the $\top$ junction. The result of phase against frequency near resonance was plotted using an X - Y plotter. The experimental set up is shown in Figure 10.8 C.

It is shown in Appendix 10., that the unloaded Q factor of the resonant line (as discussed above)is

$$Q_o = \frac{f_o}{2} \left| \frac{\partial \theta}{\partial f} \right|_{f = f_o}$$

where f_o = the resonant frequency

$\left| \frac{\partial \theta}{\partial f} \right|_{f = f_o}$ = slope of the phase in radians with respect to frequency at resonance, of the resonant line.

Measurements were carried out using resistors and capacitors across C_s. The variation of the resonant parameters, Q_{ox} and f_{ox} of the line were determined as above. Using the equations 3.11 and 3.18, the properties of these resistors and capacitors were calculated. These measured values were compared with the direct measurement of these parameters at 10 KHz.

The system was resonant at a number of frequencies and this allowed the measurement of the parameters of these lumped elements at a number of frequencies. These results are shown in Table 10. 4. It will be seen

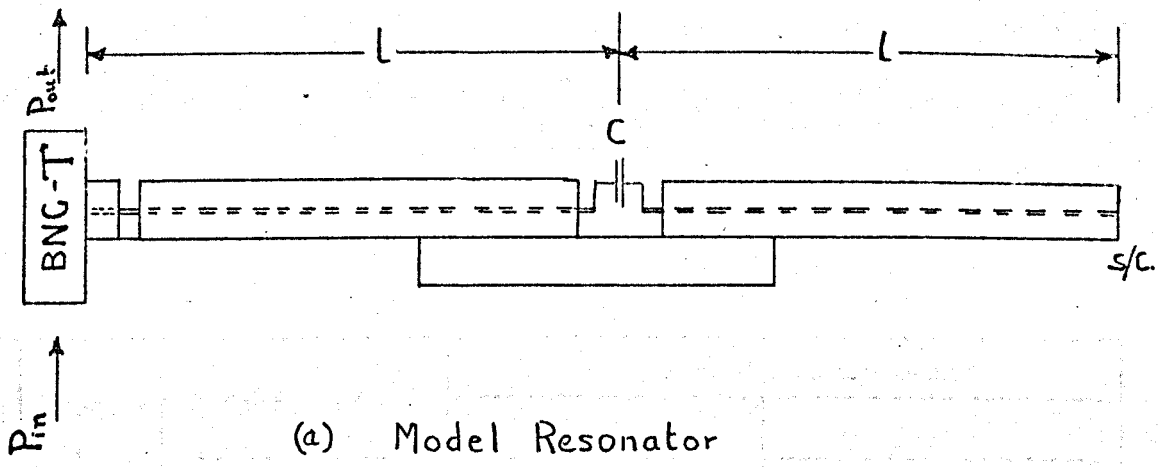

(a) Model Resonator

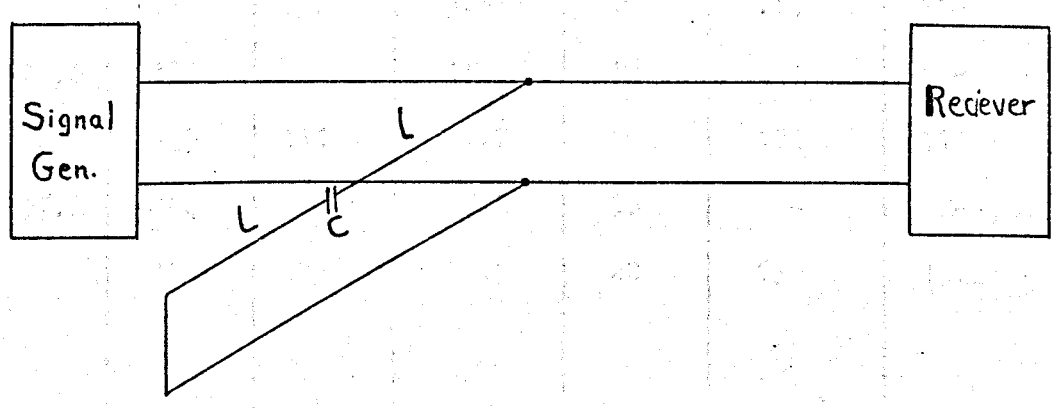

(b) Equivalent Circuit of the Resonator Setup

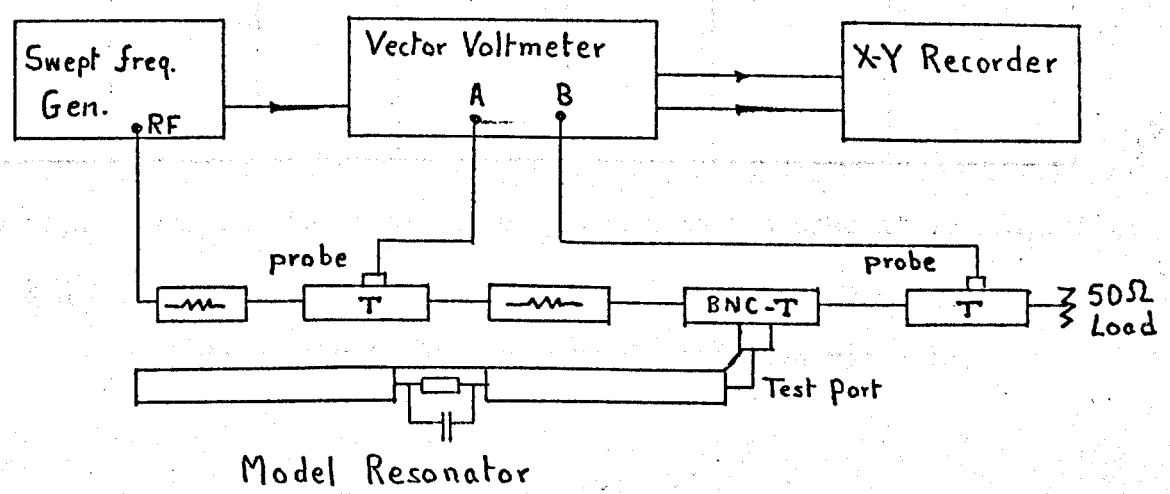

(c) Measurement Setup

Figure 10.8 Model Resonator

Table 10.4

Measured Parameters Using The Model Resonator

Mode	Frequency f, MHz	Q factor of Resonator		Lumped Element Parameters			
				Capacitance, pf		Q factor	
		Q_o	Q_{ox}	Measured	*f value	Measured	Calculated**
1	58.2	146		9.6	10	-	-
		146	95.7	9.6	10	113	110
2	179.8	139		11.2	10	-	-
		139	111	11.2	10	123	114
3	307.2	184		22.5	20	-	-
		184	171	22.5	20	239	19.6

* the capacitance and the resistance values were measured at 10 kHz bridge

** $Q = 2\pi f CR$ where C and R were in parallel with each other and connected between the two inner conductors of the resonator.

from the results that the measured and calculated parameters agree. The discrepancies between the values could be due to variation of parameters with frequency because the ℓf values were obtained from 10 KHz bridge measurements. Although special precautions (such as using the smallest component available and short leads) were taken some of the errors especially at the higher frequency end were due to discontinuities between the connections of the resonator parts, and the measuring parts.

The above experiment has verified the theoretical approach.

10.3.2 Measurement of Lumped Elements

Lumped elements at microwave frequencies are quite small, discrete components. Parameters of these components can be measured using a capacitively loaded microstrip resonator. The theoretical treatement of the approach is given in section 3.3. and this theory was verified using a model resonator as described in section 10.3.1.

The connection of these elements to a measuring system is a problem itself. I concluded that the best method is to bond it to the microstrip using an ultrasonic bonder, the same as bonding active devices to microcircuits. At the time of the investigation no such an equipment was available. To overcome this the author adopted a method in which the component was put across the gap with its face in contact with the strip. The arrangement is shown in Figure 10.11 a.

Before the measurement techniques are discussed some properties of the capacitively loaded microstrip resonators will be presented.

It was found during the investigations that the radiation from the capacitive gap was dependent on the modes of resonance of the resonator. These modes of resonance are shown in figure 10.10. The modes 1,3, and 5 give rise to a voltage across the gap as shown in Figure 10.10b. Therefore radiation will depend on this gap voltage which is itself dependent on the gap impedance. Radiation can be reduced if the gap capacitance is large, hence giving small gap voltage, V_G.

The problem of having large capacitance is dependent on the construction technique of the resonator. If the resonator is going to be used over a wide frequency range (as in the present case) then the thickness of metal strip should be at least 3 times the skin depth at the lowest frequency. Therefore a resonator to work from 1 to 10 GHz should have a metal thickness of at least 8 μm. It is usual to deposit a thin metal film, and prepare the resonator with the gap and then plate it up to the required thickness. The author found that whilst plating, the gap could disappear even though the starting gap was about 20 μm. So the starting gap was made 25 μm and close checks were made on the gap whilst plating. The gaps obtained were about 19 μm over 2.1 mm gap length (i.e. the width of the strip).

In the present investigations low impedance microstrip resonators were used. The advantages of the low impedance resonators are:

(i) The gap capacitance C is larger than the high impedance line using the same gap and the same substrate material. The gap capacitance of a 50Ω line was reported[118] to be about 0.04 pf for a 20 μm gap

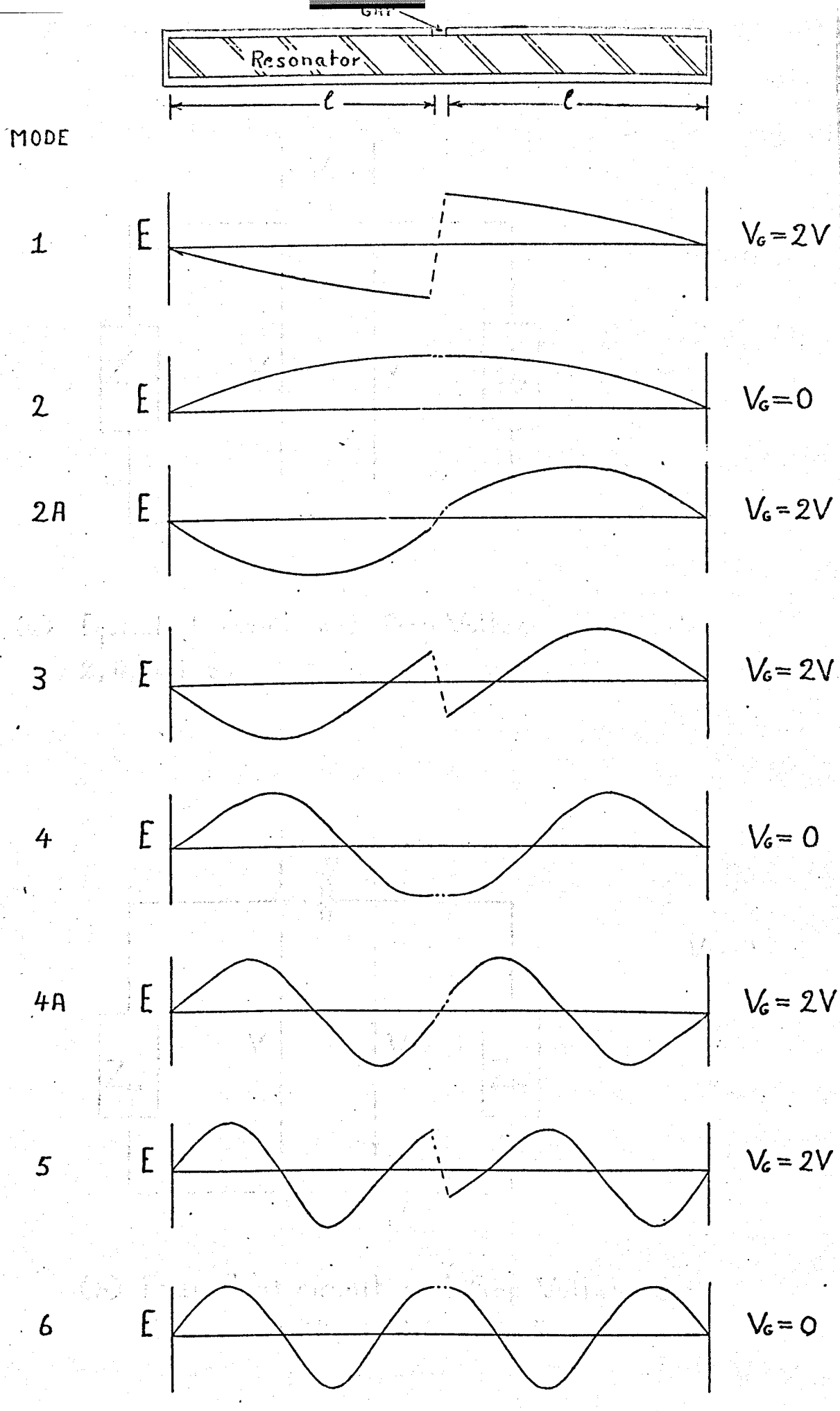

Figure 10.9 Mode Chart for the capacitively loaded Microstrip Resonator.

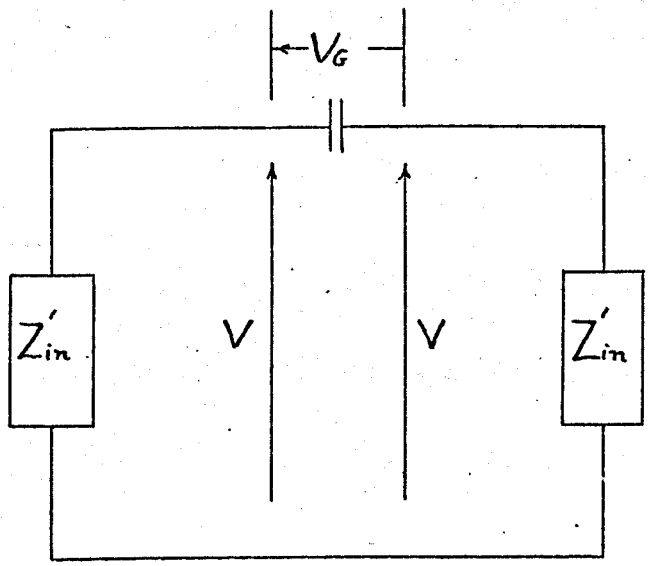

$V_G = 0$

(a) Equivalent circuit and Gap Voltage for Modes 2, 4 and 6.

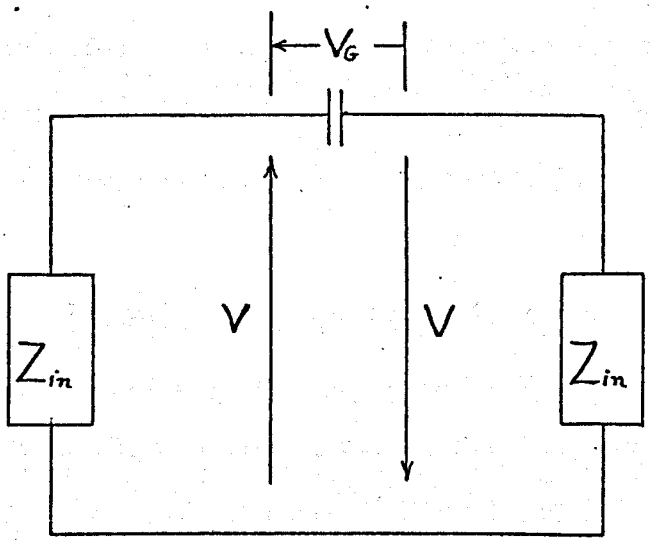

$V_G = 0$

(b) Equivalent circuit and Gap Voltage for Modes 1, 2A, 3, 4A and 5.

Figure 10.10. Equivalent circuits and Gap voltages of the Capacitively loaded Microstrip Resonator.

(on a 0.5 mm alumina substrate). The measured C for a 20 Ω line on a sapphire substrate and a similar gap was≈ 0.3 p f. It will be seen that the gap capacitance on 20Ω line is about 7 times higher than the 50 Ω line.

(ii) The low impedance lines have low losses[3], and hence high Q resonators should be obtained[119].

It was found, during the investigations that higher gap capacitances can be obtained from resonators with high permittivity substrates.

It was observed that the radiation from a capacitively loaded resonator constructed on a quartz substrate was excessive, especially at low resonant frequencies. This was due to the low gap capacitance.

Radiation effect was also observed on the resonator with a sapphire substrate. But it was much less than the quartz one. The results for the sapphire one is given separately in Table 10. 5.

The measured Q values for the modes 1, 3 and 5 had radiation loss because the voltage across the gap V_G was not zero (Fig. 10.10 a). On the other hand the measured Q values for the modes 2,4 and 6 had no radiation loss because V_G was zero (Fig. 10.10 b) therefore the latter measured Q factors were used to calculate the attenuation of the line and hence the " resonator Q " for the modes 1,3, and 5. The"resonator Q" is the Q factor of the capacitively loaded resonator without any radiation. It will be seen that the measured Q and resonator Q factors

Table 10.5

Properties of Capacitively Loaded Resonator on Sapphire Substrate

Mode No	f_o MHz	Q factor			
		Measured Q	Resonator Q	(1) Theoretical	(2) Theoretical
1	1949.6	154	254	238	351
2	2164.3	242		227	334
3	5837	246	367	404	601
4	6422	355		380	582
5	9691	440	460	510	771
6	10 569	450		500	787

(1) Uniform current distribution assumed (ref. 5)

(2) Non uniform current distribution assumed (ref. 3)

for the mode 5 are very close whilst the lower modes i.e. 1 and 3, the Q factor differs more. This was expected because the gap impedance is lower for higher frequencies and hence there are less radiation losses.

The properties of the resonator on sapphire (Table 10.5) were also predicted using two approaches. One of these is the uniform current[5] and the other is the non uniform[3] current approaches. The measured results are closer to the uniform current derivation. It was reported[6], that the second method gives optimistic values.

When the measured results are compared with the predicted Q values it is seen that the drop in Q values is uniform. This shows that the

short circuit planes did not appreciably contribute to the resonator losses.

It will be seen also that the resonator Q values for the modes 1,3 and 5 are higher than the near $\lambda/4$ mode ones even though they have lower resonant frequencies. The reason for this is that of the extra energy stored in the gap capacitance. (Theoretical derivation is given in section 3.3.2 equation 3.6).

10.3.2.1 Measurement of Lumped Capacitors

Because of the bonding difficulties the lumped elements were prepared using a single metal electrode. The dielectric film was deposited on to a silver coated glass substrate and small rectangular areas, chips, were cut from this substrate. These chips were tested by turning over such that the film was in contact with the two sides of the gap. In this arrangement two capacitors, in series , were connected across the gap. These capacitors will have only one electrode each and hence lower conductor losses, because the other electrodes are a part of the resonator and do not contribute to capacitor conductor losses. Their construction and location on the microstrip resonator is shown in Figure 10.11.

In this investigation capacitors were made of silicon monoxide and its dielectric properties were measured using resonators 3 (sapphire) and 5 (quartz). The resonator 3 had low radiation losses compared with R5 and hence the dielectric loss factor was only measured on R3. On the other hand R5 was also used in the investigation of the variation of gap capacitance when a glass slide was put over the gap of the resonator.

Table IO.6

Measured Lumped Elements Parameters.

Resonator	Test frequency MHz	Material Parameters			
		Material +	C pf	Q_X	Q_D
3	I69I	a	0.5I3	83	83
	5278		0.528	44	44
	9088		0.573	I23	I30
5	6864	b	3.03	-	
	7375	c	0.74	-	
	7669	d	0.45	-	
	2809	e	0.06	79	
	2740	f ++	0.II4	74	
	2777	g	0.093	38	

\+ Data given table IO.7

++ Increased pressure on the chip

Table IO.7

Data on samples

Sample	SUPPORT SUBSTRATE			Metal film		Dielectric Film
	Material	Area mm^2	thickness mm	Material	Thickness	
a	Soda Lime	0.9 x 0.6	0.180	Cu+Ag	2 um	5 µm thick SiO
b	"	1.6 x 1.5	0.180	"	"	" " "
c	"	1 x 1	0.180	"	"	" " "
d	"	1.64 x 1.2	0.180	"	"	" " "
e	"	1.5 x 2.0	0.180	-	-	- - -
f	"	1.5 x 2.0	0.180	-	-	- - -
g	Corning 7059	1 x 2	0.200	-	-	- - -

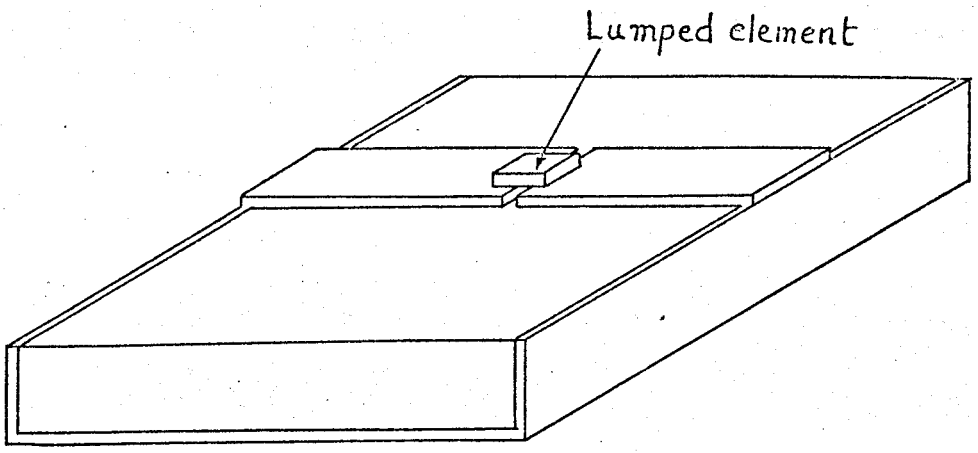

(a) The Resonator with the Lumped Element in position.

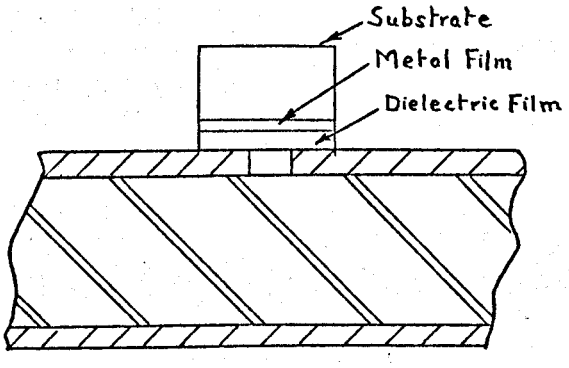

(b) Cross sectional view of the gap with a capacitive L.E.

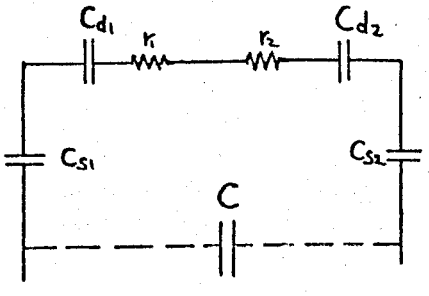

C_{d_1} and C_{d_2} are the capacitances due to the thin dielectric film.

r_1 and r_2 are the loss resistances of C_{d_1} and C_{d_2}.

C_{s_1} and C_{s_2} are due air gap between between the film and strip.

(c) Equivalent circuit representation of (b).

Figure 10.11 Measurement of the Properties of Lumped Elements using a capacitively loaded Microstrip Resonator.

The results are shown in Table 10.6. and the " chip " sample parameters are given in Table 10.7.

It was reported[8,17] that the Q factor of a capacitor Q_x is given by

$$Q_x^{-1} = Q_D^{-1} + Q_c^{-1}$$

where $Q_c = 3\ (wCR_s)^{-1}\ \frac{W}{y}$ (equation 3.19)

where W = width of capacitor (rectangular)

y = length of capacitor (rectangular)

R = surface resistivity

$= 2.5 \times 10^{-7} \sqrt{f}$ ohm per square for silver.

In the present case $Q_c \approx 2000$ at 9.088 GHz therefore the effect on the film Q factor Q_D will be very small.

The measured dielectric properties of SiO show a variation of Q_D with frequency. These were also observed when a dielectric film from the same deposition was measured using the capacitively loaded coaxial cavity (section 7). In the cavity case measurements were made at two frequencies namely 1.3 and 9.5 GHz. Although those results together with low frequency values, showed a loss peak around 3 GHz no actual test could be made at that frequency. This lumped element technique gave a value closer to this resonance loss peak (figure 7.5).

The capacitance value also increases with frequency. This means that the dielectric constant increases with frequency. This is not possible, the cause of this is the variation of contact capacitances C_s (C_s's are due to contact spacing between the film and the strip of microstrip resonator at the gap).

This is shown in Figure 10.11 C where C_{s1} and C_{s2} are the contact capacitances which ideally will be infinite. C_{d1} and C_{d2} are the capacitances due to the dielectric film.

After these observations the author concluded that when lumped elements are measured they should be bonded on the strip of the resonator.

The effect on the resonator of a dielectric material put across the gap was investigated. It was found that it increases the gap capacitance and also reduces the Q factor of the resonator. Using lossy dielectric materials such as soda lime glass (Q_D = 62 at X band), these parameters were measured. Results are given in Table 10.6, R5 material (e and f). The calculated Q_x values are very close to the Q_D of the samples. This is expected, but there are other more complicated effects (such as the thickness, width and the location of the sample relative to the gap) and therefore it is necessary to investigate fully these effects. Using a piece of chemically thinned Corning 7059 glass, the measured Q_x was far below the Q_D value measured at X band ($Q_D \approx 250$).

10.3.2.2 Measurement of Lumped Inductor

A simple inductor is a strip of metal. Therefore if a strip of metal put across the gap of the resonator it will be a lumped inductor. Its length is equal to the width of the gap.

Inductance of such a strip is given by [120,121]

$$L \approx 20\,\ell \left[\ln\left(\frac{2\ell}{W}\right) + 0.5 + 0.2235\,\frac{W}{\ell} \right] \text{ pH}$$

where ℓ = length in mm

W = width in mm

Measurement of inductors using a capacitively loaded resonator may become difficult unless certain precautions are taken. There are two methods of measurements:

(i) The inductor is connected across the gap and it tunes out part of the gap capacitance. In this method the resonant frequency increases and therefore for accurate measurements the inductor should not completely tune out the gap capacitance. Measurement is quite simple. The capacitance before and after is measured and the difference gives the inductance contribution.

(ii) In this the combined reactance at the gap is positive and hence the resonant frequency of the resonator is controlled by the inductance.

Let us consider the capacitively loaded microstrip resonator (Section 3.3.2 and equation 3.7)

Let $X = (j\omega C)^{-1}$

Then equation 3.7 becomes

$$X + j2Z_o \tan \frac{\omega l}{v} = 0$$

At various resonances between $\frac{\omega l}{v} = 0$ and $\frac{\omega l}{v} = 2\pi$

we have the following four conditions

A: $X + j2Z_0 \tan \frac{\omega l}{v} = 0 \quad 0 < \frac{\omega l}{v} < \frac{\pi}{2}$

B: $X - j2Z_0 \tan \frac{\omega l}{v} = 0 \quad \frac{\pi}{2} < \frac{\omega l}{v} < \pi$

C: $X + j2Z_o \tan \frac{\omega l}{v} = 0 \quad \pi < \frac{\omega l}{v} < \frac{3}{2}\pi$

D: $X - j2Z_o \tan \frac{\omega l}{v} = 0 \quad \frac{3}{2}\pi \quad \frac{\omega l}{v} < 2\pi$

It will be seen from these equations that the resonator will resonate only if X is capacitive for cases A and C. The resonator also resonates in cases B and D but the gap loading has to be inductive. The latter cases are shown as modes 2A and 4B in Figure 10.9.

The equations derived for the capacitance case in Section 3.3 apply also to the inductance case.

This method was used to measure the inductance of a ribbon having W = 1.7 mm and l = 19 μm, the thickness of the ribbon $\simeq$ 1 μm, deposited on

quartz substrate of 0.5 mm thick. No. 5 resonator was used.

Table 10.8

Inductor Parameters

Frequency, MHz	Inductance p H	
	Measured	Calculated
4276	31.2	73
8454	26.4	

The deviation of L values from the calculated value are due to (a) the equation is an approximation and nothing is known about high W/ℓ ratios. Others[8] used this inductance equation for $W/\ell < 1$.
(b) This equation was used for self supported ribbon inductor. In the present case, in the measurement set up, there is a ground conducting plane which will reduce its inductance value[12].

10.4 Comments:

The problem of measurement of the lumped elements at microwave frequencies is quite involved and it requires knowledge about the element themselves as well as the measuring system. In the present investigation the problem was tackled in two steps. The step I was to find a suitable measuring system and determine the properties of the system. In choosing the system of measurement the knowledge of the measurement of the thin film properties using a capacitively loaded coaxial cavity was used

extensively. The capacitively loaded microstrip resonator is a continuation of this problem.

The properties of coaxial line, to a certain extent, are well known whilst the microstrip properties are not. Therefore to use such a system i.e. microstrip resonators, their properties were first investigated. In this methods of measurement of

(a) the effective dielectric constant

(b) the gap capacitance of a gap in the strip

(c) the Q factor (in case of resonators)

of a microstrip line were introduced and successfully carried out.

The measured results showed that the gap capacitance is independent of frequency and it value is dependent on the dielectric constant of the substrate. Using a sapphire substrate it was found that capacitance values of the order 0.3 p f are obtained. Using a quartz substrate of similar thickness as sapphire but $Z_o = 31.6\Omega$ the capacitance was about 0.16 p f. High gap capacitances should be used because it was found to have much lower radiation loss than the low C case.

Since these are independent of frequency they are lumped capacitive elements. Gaps are used as lumped elements and hence this moves us into Step 2.

The theoretical approach to the lumped element measurement introduced in section 3.3. was verified using a model resonant line. Measurement of lumped elements using this model line up to 300 MHz was achieved. There is no reason why this technique should not be extended

to higher frequencies.

Measurement of lumped elements at microwave frequencies were made using symmetrical capacitively loaded microstrip resonators. Capacitors and an inductor were prepared and measured successfully. These elements were made in simple forms and hence the problems of connecting leads were eliminated.

The measured dielectric properties (i.e. Q_D) of the silicon monoxide capacitors tie up with the coaxial cavity measurements.

It is shown in this investigation that lumped elements can be measured using capacitively loaded microstrip resonators. No detailed investigation was conducted on inductors as this is a separate investigation[122]. However the measurement technique is now awaiting further exploration by others. The advantage of this measurement technique is that we can measure the parameters of a lumped element at a number of frequencies without disconnecting it. In the present investigation the total resonator length was 25.4 mm and for sapphire substrate, this gave only three usable resonant frequencies. If longer resonators than this are used (say 50 mm) more usable res. frequencies will be obtained and these frequencies will be closer to each other. Hence measurement can be spread over a larger frequency range and narrower frequency spacings than the present one can be achieved.

One should not expect the system to work for a very large number of usable frequencies for the LE loss measurement. Because most of the energy will be stored in the half wavelength resonances and a very small amount will be stored in the section which controls the resonant frequency of the resonator.

In the case of reactance measurement this does not arise.

This method has the following advantages over the other resonant methods of L E measurements:[23,24]

(i) This system uses short circuited terminations. The radiation from a short circuited termination is much smaller than the open circuited ones[123]. The radiation loss calculated for the microstrip configuration used by the author gives about 18 times higher radiation loss for the open circuited termination than the short circuited termination. The calculated radiation loss for the short circuit case was less than 0.1% at 10 GHz.

(ii) Easy to connect components across the resonator

(iii) It can be used for inductive as well as capacitive elements.

CHAPTER II

CONCLUSIONS

It is shown that the dielectric properties of thin dielectric films can be measured using a symmetrical capacitively loaded coaxial cavity. The theoretical approaches to the measurement of the dielectric properties of thin films i.e. the VSWR and the perturbation methods were verified by experiments. Thin dielectric films and thin sheets of bulk materials were successfully measured using these techniques. It was found that the VSWR method gives more accurate Q_D values than the perturbation method, the latter being strongly dependant on the measurement accuracy of the Q factor of the cavity with and without the dielectric film. These Q factors depend on the frequency stability of oscillator. If a frequency locking unit is incorporated into the sweep signal source this discrepancy can be eliminated with the result that an all around improvement in the accuracy of ϵ' and Q_D values will be obtained.

The VSWR method error obtained from the present set up was $< \pm$ 8% in ϵ' and $< \pm$ 12% in Q_D with a dielectric film 2 μm thick.

Thin films of SiO_2, SiO and Al_2O_3 obtained using an electron beam evaporator, and SiO_2 films obtained by rf sputtering were measured. It was found that the electron beam evaporated films of SiO_2 and Al_2O_3 had much higher losses than their respective bulk materials and even a stoichiometric SiO_2 film had losses at least 100 times greater than its bulk material. Tests have shown that the increases are partly due to the absorption of water vapour from the humid air and partly due to structural defects. The rf sputtered dielectric films of

SiO_2 show a promise of reduced losses but it is expected to have intermediate losses ($Q_D \approx 500-1000$) due to structural defects.

The capacitively loaded coaxial cavity could be used at two widely different frequencies. This is a big advantage because more information can be obtained from the measurements at two frequencies than one. Using the cavity at two frequencies it was found that the electron beam evaporated SiO_2 film has increasing losses with increasing frequency. This is partly due to the absorbed water and partly due to structural defects. Also using the same technique this is the first time (to the author's knowledge) that the existance of the torsional relaxation of SiO film was confirmed and its frequency measured. This relaxation frequency is around 3 GHz. This material may be useful above X-band frequencies.

The thin film processing has shown that the SiO_2 film properties obtained using an electron beam evaporator depend on the predeposition residual gas pressure in the vacuum chamber. If the predeposition residual pressure is less than 10^{-6} torr and the dielectric film is deposited at the rate of 3 nm/s good stoichiometric films should be obtained. Deposition rates higher or lower than this value give non stoichiometric films having higher losses.

The knowledge of optimum conditions for the deposition of thin metal films helped in the preparation of microstrip transmission lines. These lines were prepared on quartz, sapphire and various alumina substrates. The relative permittivity of alumina substrates was measured using a perturbation method applied to a waveguide cavity,

using a sampling technique, it was shown that accuracies within ± 1% could be obtained.

As an extension of the capacitively loaded coaxial cavity, the concept of a capacitively loaded microstrip resonator having short circuits at both ends was successfully used to measure lumped capacitors and an inductor. It was shown that a single resonator can measure the parameters of a lumped element at a number of frequencies. Using a 25.4 x 25.4 mm^2 sapphire substrate the properties of SiO capacitors were measured at three different frequencies from 1.9 GHz to 10 GHz.

In this investigation it was found that the microstrip dispersion should be taken into account otherwise erroneous results are obtained. The dispersion of the microstrip lines was measured using a short circuited half wavelenth resonant line. The accuracy of these ϵ_e measurement techniques is within ± 0.2%.

Proposed Future Investigations: When thin dielectric films are used in sandwiched capacitors, the capacitor properties depend on the compatibility of the dielectric film with the metal electrodes. These effects can be separated with the help of the two resonators. The coaxial cavity can be used to measure the thin dielectric film on its own and the capacitively loaded microstrip resonator to measure the capacitor parameters. Then the material interaction and any other effects can be separated.

If the material defects and the impurities in thin dielectric films are determined, then we have a complete picture of the film. This can

eliminate all the spread of the material parameters quoted in technical publications. A suggestion for this approach is

(i) determine the chemical composition of the film

(ii) measure its dielectric properties over a wide frequency range

(iii) vary the temperature and repeat (ii)

Although (i) will show the composition of the film it will not show the defect induced loss mechanisms whilst (ii) and (iii) combined should show us the mechanisms involved in the increased losses.

It is considered that the use of these measurement techniques will contribute significantly to further advances in the filed of m.i.c's.

REFERENCES

1-Assadurian,F.,and Remai,E.,Simplified Theory of Microstrip Transmission System,Proc.I.R.E.,40,1952, 1651-1657

2- Wheeler,H.A., Transnmission Line Properties of Parallel Strips Separated by a Dielectric Sheet, IEEE Trans. MTT-13, 1965, 172-185

3- Pucel,R.A.,et.al.,Losses in Microstrip, IEEE Trans. MTT-16, 1968, 342-350 and 1064.

4- Schneider, M.,V., Microstrip Lines for Microwave Integrated Circuits, Bell System Technical Journal, 1969, 1421-1444.

5- Caulton, M.,et.al., Measurements on the Properties of Microstrip Transmission Lines for Microwave Integrated Circuits, RCA Review, 27, 1966, 377-391.

6- A.Gopinath,A.,et. al., Microstrip Loss Calculations, Electronics Letters 2, 1970, 40-41.

7- Mason,A.E.,and Forber,L.I., Study of Solid State Integrated Micriwave Circuits, Scientific Report No1, U4-811500-4, Texas Instrument[USA], 31/12/1965.

8- Daly,D.A.,et.al., Lumped Elements in Microwave Circuits, IEEE Trans MTT-15, 1967, 713-721.

9- Sobol,H., Exending IC Technology to Microwave Equipment, Electronics, March 20,1967, 112-124.

10- Wells,J.F.,and McPhun, M.K., Lumped Components for Microwave Integrated Circuits, Coll. on "Microwave Integrated Circuits and Microwave Solid State Sources", IEE, London, January 22,1968.

11- Sobol, H. and Carley,D.R., Microwave Integrated Circuits, M O G A, 1968, 385-387.

12- Sobol,H., Technology and Design of Hybrid Microwave Integrated Circuits, Solid State Technology, February 1970, 49-57.

13- Caulton,M.,and Poole, W.E., Designing Lumped Elements into Microwave Amplifiers, Electronics, April 14,1969, 100-110.

14- Bertiger, B.R. , et.al., Microwave Lumped Element Networks, Proc. 1969 Microelectronic Symposium Digest, Part:Microwave Microelectronics, IEEE Cat.:69C49-MICRO, A5-1 -6.

15- Aitchion , Microwave Integrated Circuits, Eoropean Microwave Conf., London, Sept. 8-12, 1969

16- DeBrecht,R. and Caulton,M., Lumped Elements in Microwave Integrated Circuits in the 1-12 GHz range, GMTT- Intnl. Microwave Symposium California, May 1970.

17- Caulton, M., Lumped Element Approach to Microwave Integrated Circuits, Microwave Journal , 13, 1970, 51-58.

18- Caulton, M., RCA, [USA], Private Communication, 1970.

19- Alley, G.D.,et.al., Thin Film Lumped Constant Microwave Integrated Filter Structures, GMTT-Intnl. Microwave Symposium, California, 1970.

20- Alley,G. D., Interdigital Capacitor for use in Lumped Element Microwave Integrated Circuits, ibid.,

21- Sobol, H. and Hughes, J.J., Measurement of the Permittivity of Insulating Films at Microwave Frequencies, IEEE Trans. MTT- 15, 1967, 377-378.

22- Park, K.T., Investigation of Thin Films at Microwave Frequencies employing a Split Cavity Technique, Ph.D. Theses, University of Southampton, 1970.

23- Caulton ,M., Measurement on the Properties of Microwave Integrated Circuits, GMTT- Intnl. Microwave Symposium, [Dallas, Texas], 1969, 38-44 [Digest Pages].

24- Hughes, J.J., et. al., Novel Technique for Measuring the Q-factor of Thin Film Lumped Elements at Microwave Frequencies, Electronics Letters, 5, 1969, 535.

25- Green, H.E., Numerical Solution of Some Important Transmission Line Problems, IEEE Trans. MTT- 13, 1965, 676-692.

26- Young, L., The Practical Realisation of Series Gap Coupling for Microwave Filters , Microwave Journal, 5, 1962, 79-81.

27- Dawris, H.N., On Equivalent Circuit of a Series Gap in the Centre Conductor of a Coaxial Transmission Line, IEEE Trans. MTT- 17, 127.

28- Markuvitz, N., Waveguide Handbook, MIT Rad. Lab. Series 10, McGraw Hill, 1951, 178.

29- Slater, J.C., Microwave Electronics, D. van Nostrant, 1950, 232-237.

30- Ginzton,E.L., Microwave Measurements, McGraw Hill, 1954, 393-394.

31- Spencer, E.G., et.al., Note on Cavity Perturbation Theory, Journal of Applied Physics, 28, 1957, 130-132.

32- Waldron, R.A., Perturbation Theory of Resonant Cavities, Proc. IEE, 107C, 1960, 272-274.

33- Birnbaum, G., and Franeau, J., Measurement of ' and " of Solids and

Liquids by Cavity Perurbation Method, Jour. of Applied Physics, 20, 1949, 817- 818.

34- Labuda, E. F., and LeCraw, R.C., A New Technique for Measurement of Microwave Dielectric Constants, Rev. of Sci. Instrum., 32, 391-392.

35- Gos'kov, P.I., Measurement of ϵ and Tan δ by the Perturbation Methodd in a Rectangular Cavity , Soviet Phys. Journal, 1965,1-4.

36- Ramo, S., et. al., Fields and Waves in Communication Electronics, Wiley, 1965, 542.

37- Troughton, P. ,The Evaluation of Alumina Substrates for use in Microstrip Microwave Integrated Circuits, Proc. European Microwave Conf., [London Sept. 1969], I E E, 49-52.

38-Hartwig, ,et.al., Frequency Dependent Behavior of Microstrip, GMTT- Microwave Symposium, 1968, 110-116 [Digest pages].

39- Arnold, S., Dispercive Effects in Microstrip on Alumina Substrates, Electronics Letters,5, 1969, 673- 674.

40- van Heuven,J.M.C., and van Nie, A.G., Properties of Microstrip on Fuzed Quartz, IEEE Trans. MTT-18, 1970, 113-114.

41- Montgomery, C.J.,et.al., Principles of Microwave Circuits, McGraw Hill, 1948, 231-234.

42-Rand, A., Inductor Size vs Q: Dimensional Analysis, IEEE Trans. CP-10, 1963, 31-35.

43- Moreno, T., Microwave Transmission Design Data, Dover, 1958, 69 -72.

44- Lamb, V.A., Plating and Coatings, Techniques of Metal Research, [Tech. of Material Preparation and Handling, Pt3] 1 , 1968, 1323-1324.

45- Raub, E. and Müller, K., Fundamentals of Metal Depositon, Elsevir, 1967, 169-172.

46-Lyman, T., [Ed.], Metals Handbook, [8th edition], 1, American Soc. of Metals, 1964, 1185- 1188.

47- ELFIT Bright Silver Plating Solution [Data], P M D Chemicals Ltd., Broad Lane, Coventry.

48- PMD Transtherm Gold Solution [Data] ,P M D Chemicals Ltd., Coventry.

49- INVAR 36 ,Technical Data , Telcon Metals Ltd., Manor Royal, Sussex.

50- Same as Ref. 45, but 201-245.

51- Same as Ref. 41, but 225- 226.

52-..... Network Analysis at Microwave Frequencies, Application Note 92, Hewlet Packard [U S A].

53-..... Swept Frequency Techniques, Application Note 65, Hewlet Packard, 1965, 20- 22.

54- Ely, P. C.,Jr.,Swept Frequency Techniques, Proc. IEEE, 55, 1967,20-22.

55- Kraus, A, Reflection Coefficient Curves of Compencated Discontiniutes on Coaxial Lines and the Determination of the Optimum Dimensions, Jour. Brit. I R E, February 1960, 137.

56-..... Time Donain Reflectometry, Application Note 62, Hewlet Packard, 1964.

57- Shurmer, H.V., Low levelPrograming for the On-Line Correction of Microwave Measurements, Conf. on Laboratory Automation, I E R E, London, Nov. 1970 [To be presented].

58- Cohn, S.B . Microwave Coupling by Large Apertures , Proc. I R E, 40, 1952, 696- 699.

59- Miedke, R.C., Q for Unloaded Concentric Transmission Lines, Electronics, Sept.1943, 139- 140.

60- Benson, F.A.,[University of Sheffield, U.K.], Private Communication, 1970.

61- Gevers, M.,Measuring the Dielectric Constant and Loss Tangent of Solids at ; 3000 MC/S, Philips Tech. Review, 13, 1951, 61- 70.

62- Wells, J.F.,[Then Mullard Res. Lab. Redhill and now Philips London] Private Communication, 1969.

63- Hirose, H., and Wada, Y.,Dielectric Properties and DC Conductivity of Vacuum Deposited SiO Films, Japanese J our. of Applied Phys., 3, 1964, 179-190.

64- Cullen, A.,L., [University College London],Private Communication, 1969.

65- von Hippel, A.,R., Dielectric Materials and Applications, M I T, 1966, 313

66- Amber Mica Data Sheet, Langley London Ltd., Crawley, Sussex,

67- Ruby Mica Data Sheet, Langley London Ltd.,Crawley, Sussex.

68- Data on Ceramics, Bulletin No 1400, Coors Porcelain Co., U S A.

69- Gevers,M., The Relation between Power Factor and the Temperature Coefficient of the Dielectric Constant of Solid Dielectrics, Philips Research Reports R 20, 1946, 35.

70- Harris, H.V.,[Microwave Associate Ltd.],Private Communication, 1970.

70b- Mehmet, K., and McPhun, M.K., A Sampling Method for the Measurement of the Dielectric Properties of Alumina Substrates, Sch. of Eng. Report, Univ. of Warwick, 1970.

71- Vigourcux,P., Random Errors and Systematic Errors, Collaquium on Analysis of Errors in Measurement Systems, I EE ,April 1970,

72- Coll. on Analysis of Errors in Measurement Systems, I E E Coll. Report No 1970/5, April 1970.

73- Davis, O., Statistical Methods in Research and Prodution, ICI, 1961, 41.

74- Rectorys, K, Survey of Applicable Mathematics, Iliffe, 1969, 1316-1321.

75- Dietrich, C.F., Errors and Their Combinations, Same as ref. 72, 3/1-2.

76- Berry, R.W., et. al., Thin Film Technology, van Nostrant, 1968, 135-142.

77- Holland, L., Vacuum Deposition of Thin Films, Chapman, 1963, 108-140.

78- Chopra, K.L., Thin Film Phenomena, McGraw Hill, 1969, 10-22.

79- Anderson, D., A Summary of Thin Film Deposition Techniques, SP and Solid State Technology, Dec. 1966, 27-29.

80- Walton, B., and Shepherd, e.t., Evaporated Silica Capacitors, I E E Conf. Publications No 12, 1965, 44/1-4.

81- Payne, P. R., Jr., A Controlled Rate Electron BeamEvaporator, Proc.6th Electron Beam Symposium, [Ed. by J R. Moreley], 1965, 314-335.

82- Lewis, B., The Deposition of Alumina ,Silica, and Magnesia Films by Electron Beam Bombardment Evaporation, Microelectronics and Reliability, 3, 1964, 109-120.

83- Yamagishi, K., Vacuum Deposition by means of Electron Beam, First Conf. on Electron and Ion Beam Science and Technology, 1964, [Collected papers published by Wiley, Ed. r. Bakish, 1965], 245-263.

84- Shimoda, R.Y., Comparison of Some Physical properties of Resistance Heat and Electron Gun Evaporation of SiO Film, Vacuum, 18,

1968, 269-272.

85- Scheuerman,R.J., Stresses in Dielectric Films, Conf. on Thin Dielectrics, Electrochemical Soc.,[U S A], 1969, 561- 576.

86- Wehner, K., Sputter Deposition of Dielectric Films, ibid., 117-129.

87- Vossen,J.L.,and O'Neil,J.J., DC Sputtering wit RF induced Bias, RCA Review, December 1968, 566-581.

88- Davidse, P.D.,and Maissiel,L.I.,Dielectric Thin Films Through RF Sputtering Jour. of Applied Pys., 37, 1966, 574-577.

89- Pratt, I.R., Thin Film Dielectric Properties of RF Sputtered Oxides, Solid State Technology, Dec. 1969, 49-57.

90- Probyn, B.A., Sputtering of Insulators in an RF Discharge, Vacuum, 18, 1968, 253-257.

91- Franklin, B.J.,RF Sputtered Quartz Dielectric Capacitors, Signal Res. and Dev. Establishment [Ministry of Technology], Report No 69020, 1969.

92- Jackson, G.N., Review of Published Work on RF Sputtering, Electrical, Research Assn. Report No ERA 70-4, 1970.

93- Vossen, J.J.,and O'Neil, J.J., RF Sputtering , RCA Review, June 1968, 149- 179.

94- Goldsmith,N.,and Kern,W.,The Deposition of Vitrous Silicon Dioxide Films from Silane, RCA Review, March 1967, 153-165.

95- Hass, G.,and Ramsey, J.B., Vacuum Deposition of Dielectric and Semiconducting Films by CO_2 Laser, Applied Optics,8, 1969, 1115-1118.

96- BirVac Manual on Electron B eam Evaporator RG2.

97- Hussain,S.B., Fabrication of CdS p.e. Transducers by Electron Beam Evaporation, J. Sound Vibration, 12, 1970, 177

98- Thomas, J.E., Material Problems in Integrated Circuits, IEEE Intnl. Convention Rec.,Pt. 7, 1967, 95-102.

99- Streoscan Electron Microprobe System, [Cambridge Scientific Instr. Cambridge,].

100- Calby, J.W., Quantitive Microprobe Analysis of Thin Dielectric Films, Thin Dielectric Films, Symposium, Electochem. Soc [USA], 1969, 491- 523.

101- Pliskin, W.A., The Evaluation of Thin Film Insulators, Thin Solid Films,2, 1968, 1-26.

102- Pliskin, W.A., andCastrucci, P.P., Reactivity and Bond Strain of Films obtained by Electron Gun Evaporation of Silicon Dioxide, Electrochemical Technology, 6, 1968, 85-88.

103- Murray, L.A.,and Goldsmith,N., Nondestuctive Determination of

Thickness and Perfection of Silica Films, Jour. of Electrochem. Soc., 113, 1966, 1297- 1300.

104- Shchekochikhin,V.M.,et.al., Investigation of Oxide Films on a Single Crystal by the Infrared Spectroscopy Method, Soviet Phys., Semiconductors, 2, 1968, 542- 545.

105- Hill, N.E., et.al., Dielectric Properties and Molecular Behaviour, van Nostrand, Reinhold, 1969, 429.

106- Espe ,Werner, Materials of High Vacuum Technology, Silicates Vol.2. 1968, 420.

107- Revesz, A.G., New Model for Defects in Noncrystalline Silicon Dioxide, Jour. Non-Crystalline Solids, 4, 1970, 347-356.

108-Jonscher, A.K., Electron Conduction in Dielectric Films, Jour. Electrochem. Soc., 116, 217C.

109- Lending,L., Microwave Engineers Handbook and B.C.,Horizon House, 1966, 84.

110- Wells, J.F.,[Then MRL and now Philips], Private Communication.

111- Ref. 76 but 133-135.

112- Ref. 78 but 321- 322.

113- Weast, R.C., [Ed.], Handbook of Chemistry and Physics, 50th edition, Chemical Rubber Pbl. Co. [USA], 1969, F130-136.

114- Wechsler, A.E.,et.al., Thermal Conductivity and Dielectric Constant of Silicate Materials, N A S A Report CR 61495, 1966, 19.

115- Butlin, R.S., Materials for Microwave Integrated Circuits, Research Report No1 , Sch, of Eng. , Univ. of Warwick, May 1970.

116- Cooke, R.e., Dispersion Characteristics of Microstrip Transmission Lines, European Microwave Conf.,Sept. 8-12, 1969.

117- Presser, A., RF Properties of Microstrip Line, Microwaves, 7, March 1968, 53-55.

118- Stinehelfer,H., Microwave Engineers Handbook and B.G.,Horizon House, 1969, 72.

119- Vendelin, G.D., Limitations on Strip Line Q , Microwave Journal, 13, may 1970, 63-69.

120- Terman, F.E., Radio Engineers Handbook, McGraw Hill,1943, 51.

121- NBS , Radio Instruments and Measurements, U S Circular C74 of National Bureau of Standards, 1937, 246.

122- Michie,D., Lumped Components at X-band, First Annual Report, Sch. of Eng. , Univ. of Warwick, 1970.

123- Lewin, L., Radiation from Discontin uities in Strip Line, Proc. I EE 107C, 1960, 160-170.

APPENDIX 1

Power Loss in the Cavity Surfaces

Consider the cavity shown in Figure 2.4b. The power loss in this cavity will be

$$P_{c1} = \frac{R_s}{2} \int_S \left| H\phi \right|^2 dS$$

Where S is the surface area of the cavity walls.

Separating the cavity wall losses we obtain

$$P_{c1} = \frac{R_s}{2} \left[\int_{S_1} \left| H\phi \right|^2_{r=\frac{D_1}{2}} dS_1 + \int_{S_2} \left| H\phi \right|^2_{r=\frac{D_0}{2}} dS_2 + \int_{S_3} \left| H\phi \right|^2_{z=0} dS_3 \right] \qquad \text{A1.1}$$

Where S_1 is the surface area of the inner conductor

S_2 " " " " " " outer "

S_3 " " " " " " end (shorting) plates.

Substituting the values of $H\phi$ from equation 2.5 in equation A1.1 we obtain

$$P_{c1} = \frac{R_s}{2} \left[\int_0^{2\pi} \int_0^{\lambda} \left(\frac{V_o \cos \frac{wz}{v}}{\eta \frac{D_1}{2}} \right)^2 \frac{D_1}{2} \, d\phi dz + \int_0^{2\pi} \int_0^{\lambda} \left(\frac{V_o \cos \frac{wz}{v}}{\eta \frac{D_o}{2}} \right)^2 \frac{D_o}{2} d\phi dz + \int_0^{2\pi} \int_{\frac{D_1}{2}}^{\frac{D_o}{2}} \left(\frac{V_o}{\eta r} \right)^2 r \, d\phi dr \right] \qquad \text{A1.2}$$

and

$$P_{c1} = \frac{Rs}{\eta^2} \frac{V_o^2}{\eta^2} \left(\frac{1}{D_1} + \frac{1}{Do}\right) \left[z - \frac{\text{Sin } \frac{2wz}{v}}{\frac{2w}{v}} \right]_o^{\lambda} + 2\ln(Do/D_1)$$

$$P_{c1} = Rs \frac{V_o^2}{\eta^2} \left(\frac{1}{Do} + \frac{1}{D_1}\right)\lambda + 2\ln(Do/D_1) \qquad \text{A1.3}$$

(2.12)

APPENDIX 2

Energy Stored the Coaxial Section of Section B (Figure 2.4c)

The energy stored will be the sum of the magnetic and electric energies and is given by

$$W_b = 2\left[\frac{\epsilon_0}{4}\int_V |Er|^2\, dV + \frac{\mu_0}{4}\int_V |H\phi|^2\, dV\right] \qquad A2.1$$

Where V = half the volume of the coaxial section

Substituting the values of Er and Hø from equations 2.4 and 2.5 we obtain

$$W_b = 2\left[\frac{\epsilon_0}{4}\int_0^{2\pi}\int_{\frac{D_1}{2}}^{\frac{D_0}{2}}\int_{\frac{\lambda}{2}}^{\frac{L}{2}}\left(\frac{V_o \sin\frac{\pi z}{v}}{r}\right)^2 r\, dr\, d\phi\, dz + \frac{\mu_0}{4}\int_0^{2\pi}\int_{\frac{D_1}{2}}^{\frac{D_0}{2}}\int_{\frac{\lambda}{2}}^{\frac{L}{2}}\left(\frac{V_o \cos\frac{\pi z}{v}}{\eta\, r}\right)^2 r\, d\phi\, dz\, dr\right] \qquad A2.2$$

Since $\eta = (\mu_0/\epsilon_0)^{\frac{1}{2}}$ and $\left(\sin^2\frac{\pi z}{v} + \cos^2\frac{\pi z}{v}\right) = 1$ then equation A2.2 reduces to

$$W_b = \frac{\epsilon_0}{2}\int_0^{2\pi}\int_{\frac{D_1}{2}}^{\frac{D_0}{2}}\int_{\frac{\lambda}{2}}^{\frac{L}{2}} \frac{V_o^2}{r^2}\, r\, d\phi\, dr\, dz \qquad A2.3$$

Integrating and substituting the boundary values we obtain

$$W_b = \frac{\pi}{2} V_o^2 \ln(D_o/D_1)\,[L - \lambda] \qquad A2.4$$

(2.13)

APPENDIX 3

Energy Stored in the Gap Capacitance

The energy stored in the capacitor is given by

$$W_{ca} = \frac{1}{4} C_{oT1} \left(V_{ab} \right)^2 \qquad A3.1$$

Substituting the value of V_{ab} from equation 2.6 and C_{oT1} from equation 2.9 in equation A3.1 we obtain

$$W_{ca} = \frac{\pi \left[2 \, Vo \, \ln (Do/D_1) \, \sin \frac{wL}{2v} \right]^2}{4 \eta w \, \ln (Do/D_1) \, \tan \frac{wL}{2v}} \qquad A3.2$$

And this simplifies to

$$W_{ca} = \frac{V_o^2 \ln (Do/D_1) \, \sin \frac{wL}{v}}{2 \eta w} \qquad A3.3$$

But $\eta = (\mu_o/\epsilon_o)^2$ and substituting this in equation A3.3 we obtain

$$W_{ca} = \frac{\pi \epsilon_o}{2 \frac{w}{v}} V_o^2 \ln (Do/D_1) \, \sin \frac{wL}{v} \qquad A3.4$$

(2.14)

APPENDIX 4

Power Lost in Section B

Section B (Figure 2.4c) has no real short circuiting planes and therefore the losses will only be in the coaxial surfaces. Then the power lost is given by

$$P_{c2} = \frac{Rs}{2}\left[\int_{S_1} \left|H\phi\right|^2_{r=\frac{D_1}{2}} dS_1 + \int_{S_2} \left|H\phi\right|^2_{r=\frac{D_o}{2}} dS_2\right] \qquad A4.1$$

Where S_1 is the surface area of the inner conductor,
and S_2 " " " " " " " outer " .

Substituting the values of $H\phi$ from equation 2.5 we obtain

$$P_{c2} = Rs\left[\int_0^{2\pi}\int_{\frac{\lambda}{2}}^{\frac{L}{2}}\left(\frac{2Vo\ \mathrm{Cos}\frac{\pi z}{v}}{\eta D_1}\right)^2 \frac{D_1}{2} d\phi\ dz + \int_0^{2\pi}\int_{\frac{\lambda}{2}}^{\frac{L}{2}}\left(\frac{2Vo\ \mathrm{Cos}\frac{\pi z}{v}}{\eta D_o}\right)^2 \frac{Do}{2} d\phi\ dz\right] \qquad A4.2$$

This reduces to

$$P_{c2} = \frac{4\pi Rs\ Vo^2}{\eta^2}\left[\frac{1}{Do} + \frac{1}{D_1}\right]\int_{\frac{\lambda}{2}}^{\frac{L}{2}}\left(\mathrm{Cos}\frac{\pi z}{v}\right)^2 dz$$

And we have

$$P_{c2} = \frac{\pi Rs\ Vo^2}{\eta^2}\left[\frac{1}{Do} + \frac{1}{D_1}\right]\left(L - \lambda + \frac{\mathrm{Sin}\frac{\pi L}{v}}{\pi/v}\right) \qquad A4.3$$

(2. 16)

APPENDIX 5

Application of the Perturbation Method to the Capacitively Loaded Cavity

It is given in the text (page 44) that

$$\frac{\delta f}{f} + j\delta\left(\frac{1}{2Q}\right) = \frac{\epsilon_o(\epsilon - 1)^{Eo}\, E_1\, \frac{D_1^2}{8}\, 2 \times G_o\, \overline{\Pi}}{4 \text{ Energy Stored in the Cavity}} \qquad A5.1$$

The energy stored in the cavity is given by

$$W_T = W_1 + W_2$$

Using equations 2.11 and 2.15 we get

$$W_T = \frac{\pi}{2}\epsilon_o\left[L - \lambda + \frac{\text{Sin}\,\frac{wL}{v}}{w/v}\right] V_o^2 \ln (D_o/D_1) + \frac{\pi}{2}\epsilon_o \ln (D_o/D_1)\, \lambda V_o^2$$

$$= \frac{\pi}{2}\epsilon_o L\, V_o^2 \ln (D_o/D_1) \left[1 + \frac{\text{Sin}\,\frac{wL}{v}}{wL/v}\right] \qquad A5.2$$

Also from equations 2.46 and 2.50 we have

$$E_o = \frac{2V_o}{G_o} \ln (D_o/D_1)\, \text{Sin}\,\frac{w_1 L}{v2} \qquad 2.46$$

A5.3

$$E_1 = \frac{2V_o}{G_o} \ln (D_o/D_1)\, \text{Sin}\,\frac{w_2 L}{2v} \left[\epsilon - \epsilon x + x\right]^{-1} \qquad 2.50$$

Substituting these equations A5.2 and A5.3 in equation A5.1 we obtain

$$\frac{\delta f}{f} + j\delta\left(\frac{1}{2Q}\right) = \frac{2x\ (\epsilon - 1)\ \ln\ (Do/D_1)\ \text{Sin}\ \frac{w_1 L}{2v}\ \text{Sin}\ \frac{w_2 L}{2v}\ \frac{D_1^2}{4Go}}{L\left(1 - \frac{\text{Sin}\ \frac{w_1 L}{v}}{w_1 L/v}\right)\ (\quad - x - x)}$$

A5.4

But (from eqn. 2.10)

$$\frac{D_1^2}{4Go} = \left[\ (1 + m)\ \ln\ (Do/D_1)\frac{w_1}{v}\ \text{Tan}\ \frac{w_1 L}{2v}\ \right]^{-1}$$

And substituting this in eqn. A5.4 it reduces to

$$\frac{\delta f}{f} + j\delta\left(\frac{1}{2Q}\right) = \frac{2x\ (\epsilon - 1)\ \text{Cos}\ \frac{w_1 L}{2v}\ \text{Sin}\ \frac{w_2 L}{2v}}{(\epsilon - \epsilon x + x)\left[\frac{w_1 L}{v} + \text{Sin}\ \frac{w_1 L}{v}\right]\ (1 + m)}$$

A5. 5

Let $P = (1 + m)\left[\frac{w_1 L}{v} + \text{Sin}\ \frac{w_1 L}{v}\right]\left(2\ \text{Cos}\ \frac{w_1 L}{v}\ \text{Sin}\ \frac{w_2 L}{v}\right)^{-1}$

and we obtain

$$\frac{\delta f}{f} + j\delta\left(\frac{1}{2Q}\right) = \frac{x\ (\epsilon - 1)}{(\epsilon - \epsilon x + x)}\ P^{-1}$$

A5.6

(2.54)

Appendix 6

Electroplating Solutions

1. Copper Strike Solution

Silver Cyanide	=	0.75 gm
Copper Cyanide	=	5.75 gm
Potassium Cyanide	=	40 gm
Distilled Water	=	500 ml
Current density	=	15 - 20 mA/cm^2

2. Silver Strike Solution

Elfit plating solution 9 ref. 47)	=	85 ml
Potassium Cyanide	=	20 gm
Distilled Water	=	500 ml
Current density	=	15 - 20 mA/cm^2

APPENDIX 7

7.1 Electric Probe.

The probe assembly is shown in Figure 6.1a, section 6.2.1. The cavity wall, as well as the waveguide wall, was thinned down around the coupling in order to eliminate any transmission line transformation between the cavity and the Waveguide. In the present set up the cavity can be represented as a series tuned circuit across the line.

An interesting result of the test was the effect of the probe material on the measured Q factor, Qo. It was found that a copper probe gave 4% higher Qo, than the brass probe. This was due to lower conductivity of the brass probe than the copper one. A similar effect was observed by another researcher who found that a nickel plated tuning screw gives 0.022dB higher loss than a copper tuning screw when used in a Waveguide system.

7.2 The Floating Disc - Probe.

This was similar to the electric probe except the extension of the probe into the cavity was replaced by a thin disc having a diameter slightly smaller than the coupling hole and centrally situated on the probe end which extended into the waveguide (figure 6.16 section 6.2). The plane of the disc was the same as the surface of the outer diameter of the cavity. This system was supported in the same way as the electric probe as discussed in section 6.2.1.

The coupling arrangement was made of copper and although the measured Qo was the same as the electric probe case, the frequency of resonance was increased by 25MHz. This confirmed the loading of the cavity with the electric probe.

APPENDIX 8

Error Analysis.

The measured VSWR's can be expressed by the following equations:-

$$S_2^1 = S_2 + \gamma_2 S_2 + \alpha_2 S_2 \qquad A8.1$$

$$S_1^1 = S_1 + \gamma_1 S_1 + \alpha_1 S_1 \qquad A8.2$$

Where S_2^1 and S_1^1 are the measured VSWR's with and without the dielectric film with errors. S_2 and S_1 as above but no errors.

γ_2 and γ_1 are the fractional systematic errors in S_2 and S_1 .

α_2 and α_1 are the fractional random errors in S_2 and S_1 :

Dividing equation 1 by eqn. 2 we obtain

$$\frac{S_2^1}{S_1^1} = \frac{[\,1 + \gamma_2 + \alpha_2\,]\,S_2}{[\,1 + \gamma_1 + \alpha_1\,]\,S_1} \qquad A8.3$$

For small errors

$$\frac{S_2^1}{S_1^1} = \frac{S_2}{S_1}[\,1 + \gamma_2 - \gamma_1 + \alpha_2 - \alpha_1\,] \qquad A8.4$$

Systematic errors will have the same sign, because of the small frequency shift and whenthe VSWR's ratio is taken this error will

be reduced to the difference of the two individual errors. In the present case these errors were due to the directivity of the directional coupler, mismatches in the precision reflectometer and the calibration of the system. Therefore γ_2 and γ_1 would have been equal and it is reasonable to assume that $\gamma_2 - \gamma_1 = 0$.

Random errors will have any sign and the errors in S_1 and S_2 will add up giving

$$\frac{S_2^1}{S_1^1} = \frac{S_2}{S_1}\left[1 + \alpha_1 + \alpha_2\right] \qquad \text{A8.5}$$

The repeated measurement on the caviy properties, the return loss measured at resonance gave a variation $\lessdot 0.03$ dB for a return loss of 12.9 dB. This variation was due to random errors in the measured reflection coefficient (return loss $-20 \log \Gamma$ dB)

The relationship between the VSWR, S and the reflection coefficient Γ (Γ taken as magnitude only) is

$$S = \frac{1 + \Gamma}{1 - \Gamma}$$

Differenciating we get

$$\frac{dS}{S} = \frac{2\Gamma}{1 - \Gamma^2}\frac{d\Gamma}{\Gamma}$$

Substituting the values of $\frac{d\Gamma}{\Gamma} = \pm 0.17\%$ and $\Gamma = 0.226$ from the above results we obtain

$$\frac{dS}{S} = \pm 0.081\%$$

But the error in the ratio = sum of these random errors, i.e.

$$\frac{d\left(\frac{S_2}{S_1}\right)}{\frac{S_2}{S_1}} = \frac{dS_1}{S_1} + \frac{dS_2}{S_2}$$

Therefore $$\frac{d\left(\frac{S_2}{S_1}\right)}{\left(\frac{S_2}{S_1}\right)} = \pm 0.162\%$$

Appendix 9

Materials for The Thin Films Deposition

Material		Impurity Level	Suppliers
Metals:			
Aluminium	Grade 1	13 ppm	Johnson, Matthey & Co.Ltd, 73-83, Hatton Garden, LONDON E.C.1
Copper	Grade 1	12 ppm	" "
Chromium	Grade 1	5 ppm	" "
Gold	Grade 1	5 ppm	" "
Silver	Grade 1	10 ppm	J.M & Co. Victoria Road, Birmingham
Nichrome	-	1600	Henry Wiggins & Co. Birmingham.
Dielectrics			
SiO_2 (Spectosil)		0.15 ppm	Thermal Syndicates. LONDON.
Al_2O_3 (Purox)		300 ppm	Morganite Refractones (Sales) Ltd., Neston, Wirral, Cheshire.
SiO		-	-

Appendix 10

Measurement of the Q factor of a resonator using the phase information

Consider a transmission line resonator half wavelength (or multiple of $\frac{\lambda}{2}$) long shunted across a transmission line as shown in figure A10.1a. This can be simplified to obtain an equivalent circuit as shown in figure A.10.1b.

Assuming a matched source and a matched receiver having impedences equal to the characteristic impedance, Z_o of the main transmission line.

Voltage across input impedance Z_{OR} of the receiver is

$$V_R = \frac{E\left(Z^{-1} + Z_o^{-1}\right)^{-1}}{Z_o + \left(Z^{-1} + Z_o^{-1}\right)^{-1}} \qquad \text{A 10. 1}$$

$$= \frac{E}{Z_o Z^{-1} + 1 + 1} \qquad \text{A 10.2}$$

$$Z = r + j\left(wL - \frac{1}{wC}\right)$$

and near resonance $Z = r + j\,wL\,(2\delta)$

$$= r\,(1 + j\,\frac{wL}{r}\,2\delta)$$

$$= r\,(1 + j Q_o\,2\delta)$$

A 10.3

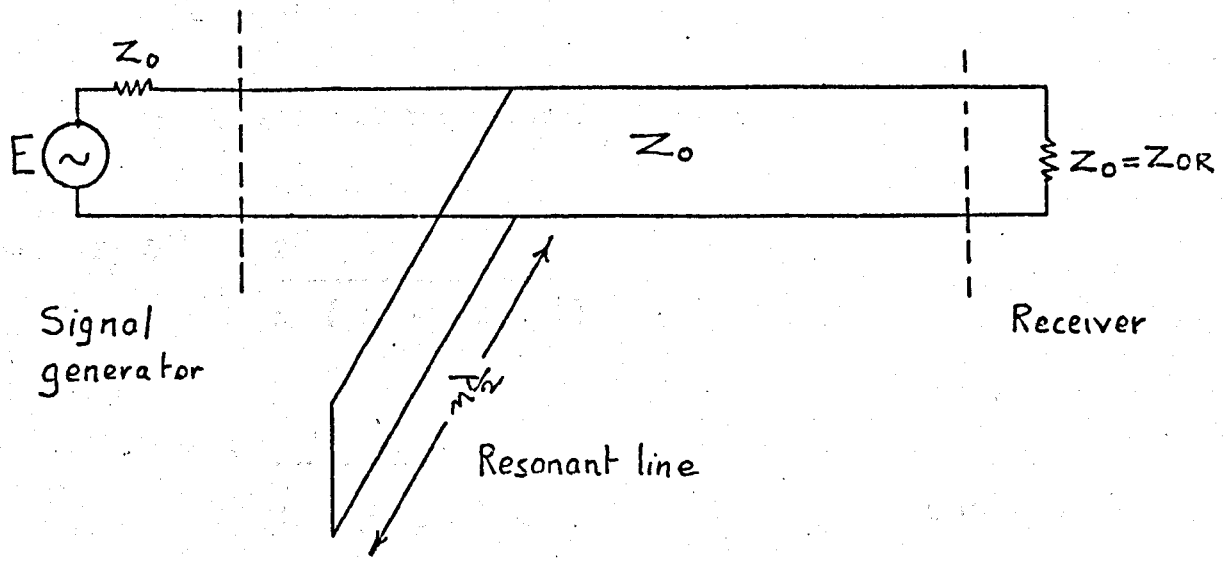

(a) Measurement set up

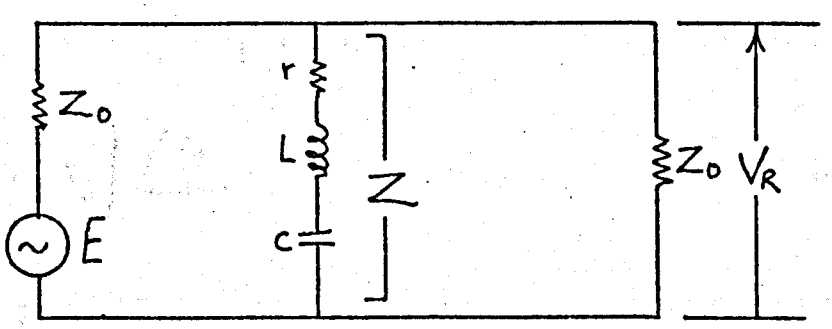

(b) Equivalent circuit representation of (a)

Figure A10.1. Transmission method of measuring Q_o

where $Q_o = \left[\frac{wL}{r} \right]$

$=$ Q factor of resonator

then $Z_o \, Z^{-1} = \frac{Z_o}{r \, (1 + j Q_o \, 2\delta)}$

$$= \frac{\beta}{1 + j Q_o \, 2\delta} \qquad \text{A 10.4}$$

where $\beta = \left[\frac{Z_o}{r} \right]$ A 10.5

substituting this in equation A 10.2 we obtain

$$V_R = E \, \frac{(1 + j Q_o \, 2\delta)}{2 + \beta + j Q_o \, 2\delta} \qquad \text{A 10.6}$$

$$V_R = |V_R| \angle \theta \qquad \text{A 10.6}$$

where $\theta =$ phase of received voltage with respect to source voltage

$$\theta = Tan^{-1} (Q_o \, 2\delta) - Tan^{-1} \left(\frac{Q_o \, 2\delta}{2+\beta} \right) \qquad \text{A 10.7}$$

differentiating θ with respect to δ we get

$$\frac{\partial \theta}{\partial \delta} = \frac{2\,Q_0}{1+(Q_0 2\delta)^2} - \frac{2\,Q_0}{(2+\beta)\left[1+\dfrac{(Q_0 2\delta)^2}{(2+\beta)^2}\right]} \qquad \text{A 10.8}$$

at resonance $\delta = 0$.

therefore $$\left.\frac{\partial \theta}{\partial \delta}\right|_{\delta=0} = 2\,Q_0 - \frac{2\,Q_0}{2+\beta} \qquad \text{A 10.9}$$

In a short circuited ($\lambda/2$) transmission line the resistance r is very small and hence $\frac{Z_0}{r} \gg 1$.

Therefore 2nd term of equation A 10.9 can be neglected, then we obtain

$$Q_0 = \tfrac{1}{2} \left.\frac{\partial \theta}{\partial \delta}\right|_{\delta=0} \qquad \text{A 10.10}$$

But $\delta = \frac{\delta f}{f_0}$

therefore $$Q_0 = \tfrac{1}{2} f_0 \left.\frac{\partial \theta}{\partial f}\right|_{f=f_0} \qquad \text{A10.11}$$

The rate of change of θ with frequency near resonance is so great that any variation due to discontinuities will not affect the measurement. Note that unlike many other methods of Q measurement no knowledge is required in addition of another quantity such as VSWR or resistance at resonance.

Appendix 11

Materials used in Photolithographic Process.

(1) Photo Resist:

Positive Photo Resist: Shipley AZ 111

Developer Shipley AZ 303

Solution: 1 part AZ 303 and 4 parts deionised water

Suppliers: Shipley Chemicals Ltd, Coventry.

(2) Lacomit Masking Paint W. Canning & Co. Ltd., Birmingham.

(3) Photo Resist Filters:

Prefilter AP2501000

Filter UHWP01300

Suppliers: Millipores (UK) Ltd., Wembley

(4) Etchants: This information was obtained from Mr. Hall of AEI - GEC Leicester through Mr. E.G. Coates of University of Warwick.

Material	Etchant
Nichrome	Ferric Sulphate 250 gm
	Nitric Acid (conc.) 375 ml
	Distilled Water 2 litres
Gold	Potassium Iodide 410 gm
	Iodine 100 gm
	Distilled Water 2.5 litres
Copper	Ferric Chloride 400 gms
	Distilled Water 2 litres (or Ammonium Persulphate 500 gms* instead of Ferric Chloride)

Chromium	* Potassium Ferric Cyanide	400 gm
	Sodium Hydroxide	120 gm
	Distilled Water	2.0 litres

* Solutions should be used at 50°C

Discard stock after 7 days.

Plating Solutions

Elfit silver plating solution (see ref. 4.7)

Transtherm gold plating solution (see ref. 4.8)

(obtained from PMD Chemicals, Coventry.)

EXHIBITION:

Technical Press reviews on our exhibit at the 1970 Physics Exhibition, London

(a) Journal of Physics E, June 1970

The Physics Exhibition 1970

Communications

K C Kao
Standard Telecommunication Laboratories Ltd, Harlow, Essex

The development of many devices, instrumentations and systems are aimed directly or indirectly at providing new and improved facilities for communication. At the 1970 Physics Exhibition there were a variety of examples.

~~oscillator module for phased-array radar. The unit incorporated a Gunn diode as the microwave source.~~ Another aspect of microwave integrated circuit was demonstrated by the University of Warwick School of Engineering Science. This was concerned with the measurement of the properties of thin film capacitors made by depositing a thin layer of dielectric followed by a top metallic film on a metallic substrate. The influence of the metallic film on the properties of the dielectric film can be deduced by first measuring the properties of the thin film dielectric using a microwave resonance method in which simple variation of the resonance frequency of a specially designed cavity is measured. The cavity was designed to maximize the influence of the thin film dielectric on its resonance frequency. This was achieved by situating the thin film in a capacitative gap within the cavity.

~~Evanescent waveguides are utilized in the design of a miniaturized high-quality up-converter (Standard Telecommunication Laboratories Ltd). The total volume is ten times~~

(b) Design Electronics , May 1970, p. 46.

Capacitors in microwave integrated circuits

Employment of capacitors in microwave i.c.s at frequencies of the order of 10GHz, although desirable, has been held up due to a lack of suitable measurement techniques and of sufficient knowledge of material properties.

The dielectric constant and loss of a thin film of dielectric is hard to measure without evaporating a metal film electrode on to the dielectric to form a capacitor, but such a film could alter the properties to be measured.

A system shown by researchers from Warwick University's School of Engineering Science illustrates how a computer controlled network analyser model can be used in the measurement of thin dielectric films and components. The basic technique involves the deposition of dielectric film directly into a suitable microwave cavity; the cavity resonant frequency and v.s.w.r. at resonance being measured before and after film deposition. Properties of the film are then calculated from these values.

DESIGN ELECTRONICS

CONFERENCE PUBLICATIONS

A paper entitled " Microwave Measurement of Thin Film Dielectric Properties " was presented by the author (M. K. McPhun as co-author) at the ' Dielectric Materials, Measurements and Applications ' conf. July 20-24, 1970 (Lancaster). It has been published in IEE Conf. Publications No 67/ 70, 42-45. This paper can be found in the following pages.

MICROWAVE MEASUREMENT OF THIN FILM DIELECTRIC PROPERTIES

K. Mehmet and M.K. McPhun

In order to evaluate thin dielectric films for use at microwave frequencies it is essential to be able to measure their electrical properties. However it is very difficult to measure the dielectric constant and loss of a thin film because of its small volume. The only known published work (1) on microwave measurement of thin film dielectrics was at about 2.9GHz. For accurate results this technique required film thicknesses of order 10μm. Other published work (2) describes attempts to measure thin film dielectric properties using the film as the dielectric of a sandwich capacitor. Although these methods are simple, the measured properties cannot be calculated exactly because the series resistance of the electrodes cannot be determined accurately. Also we wish to determine what effect the electrodes have on the properties of the dielectric of a sandwich capacitor.

To overcome the above difficulties we are using the capacitively loaded coaxial cavity illustrated in Figure 1a. The cavity consists of two sections: the centre conductor of the top section is flush with the outer conductor, whilst the centre conductor of the bottom section is shortened by about 20μm. to give the capacitive gap, G_o, between the centre conductors. The mode of resonance used in our measurements is shown in Figure 1b.

In use, the thin film is deposited onto the end of the centre conductor of the top of the cavity. After completing measurements on that film it is then a simple matter to lap off the deposit and reuse the cavity for another measurement.

Theory: The problem has been treated using an equivalent circuit approach and the series tuned circuit configuration was chosen for simplicity. The cavity with no dielectric is represented by Figure 2a where C_o is the gap capacitance and mC_o the capacitance due to the fringing field. Figure 2b shows the cavity equivalent circuit with a dielectric film filling a fraction, x, of the gap. Solving these equivalent circuits, the relative dielectric constant of the film is:

$$\epsilon_r = x \left\{ \left[(m+1) \frac{f1}{f2} \frac{\operatorname{Tan} \frac{2\pi \ell \ f1}{v}}{\operatorname{Tan} \frac{2\pi \ell \ f2}{v}} - m \right]^{-1} + x - 1 \right\}^{-1} \quad \ldots.(1)$$

and the loss tangent of the film is:

$$\operatorname{Tan}\delta = \frac{\epsilon_r}{x} \left[\frac{S2}{S1} - 1 \right] \frac{\left(m \left(\frac{x}{\epsilon_r} + 1 \mp x \right) + 1 \right)^2}{(m+1)} K \quad \ldots.(2)$$

K. Mehmet and M.K. McPhun are with the School of Engineering Science, University of Warwick, Coventry.

Where m is fringing capacitance as a fraction of C_o
x is the fraction of gap occupied by the film
f_2 and f_1 are the resonant frequencies of the cavity with and without the film
2l is the length of the cavity
v is the velocity of light in free space, 3×10^8 m/s.
S_1 and S_2 are the voltage standing wave ratios (VSWR's) at the input to the cavity at resonance without and with the film
K is a constant which depends on the cavity material and dimensions.

Experimental Work: The cavity was made of silver plated Invar because of its low coefficient of expansion. Tarnishing of the silver plating was eliminated by plating with a thin layer (6 nm) of gold. The cavity was designed to resonate at about 9.5 GHz. in X-band and coupled to a waveguide through a dumbbell coupling aperture. Stringent measures were taken to ensure a rigid construction to give repeatable results upon repeated dismantling and assembling of the cavity. The cavity properties were measured using a precision reflectometer, consisting of high directivity waveguide directional couplers and a Hewlett Packard harmonic Frequency Converter and Network Analyser assembly, as the receiving system. Thus the phase as well as the magnitude of the reflection coefficient could be recorded as a function of frequency on an X- Y recorder. The arrangement is shown in Figure 3.

The measurement procedure is as follows. The cavity input reflection coefficient, V.S.W.R., resonant frequency and Q-factor are first measured. Then the top of the cavity is removed and the dielectric film is deposited onto the plane end of the inner conductor. The cavity is again assembled and the new resonant frequency and V.S.W.R. at resonance are measured for the dielectric loaded cavity. Using these measured results and equations (1) and (2), ϵ_r and $\tan\delta$ are determined.

For a typical cavity it was found that the measured unloaded Q-factor was 95% of the calculated value and the resonant frequency within 0.02% of the calculated value. So far we have deposited films of SiO_2 by evaporation using an electron beam evaporating source. The substrate (cavity) was maintained at 200^oC during evaporation. Measurements on these films of SiO_2 of 2μm. thickness gave ϵ_r between 3.9 and 4.2 and $\tan\delta$ of 0.008 to 0.014. It was observed that higher rates of evaporation gave lower values of $\tan\delta$.

Work is in progress to verify the accuracy of equations (1) and (2), and hence the method as a whole, by measurement of known material. This can only be done by mechanically and chemically thinning a section of a bulk dielectric of known properties until it can be inserted in the gap and measured by this method. At the time of writing we are also engaged on measurement of dielectric films of other materials by evaporation and R.F. sputtering. We hope to present the results of these experiments at the conference.

References:

1. Measurement of the Permittivity of Insulating films at Microwave frequencies. H. Sobol and J.J. Hughes, IEEE Trans. June 1967, MTT-15, pp. 377-378

2. Designing lumped elements into Microwave Amplifiers, M. Caulton and W.E. Poole, Electronics, April 14, 1969, pp. 100-110.

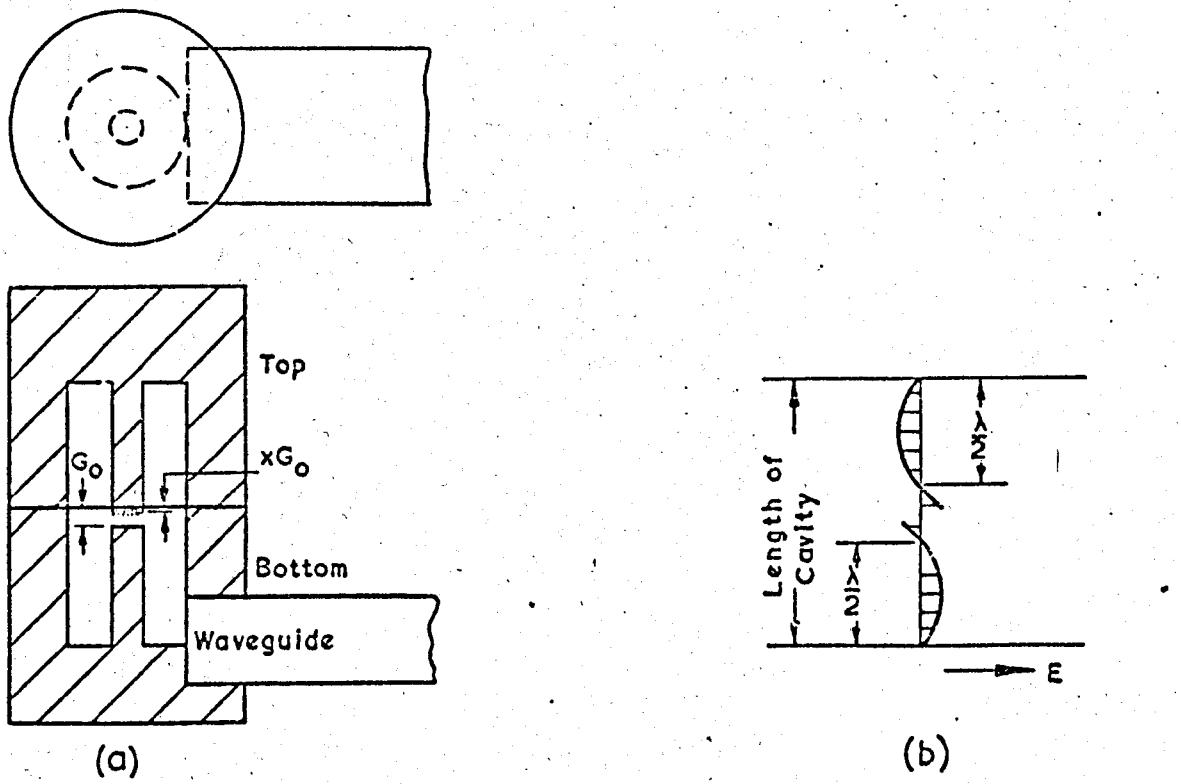

Figure 1a. Axial cross-section of cavity (gap greatly exaggerated)
b. Electric field distribution of cavity.

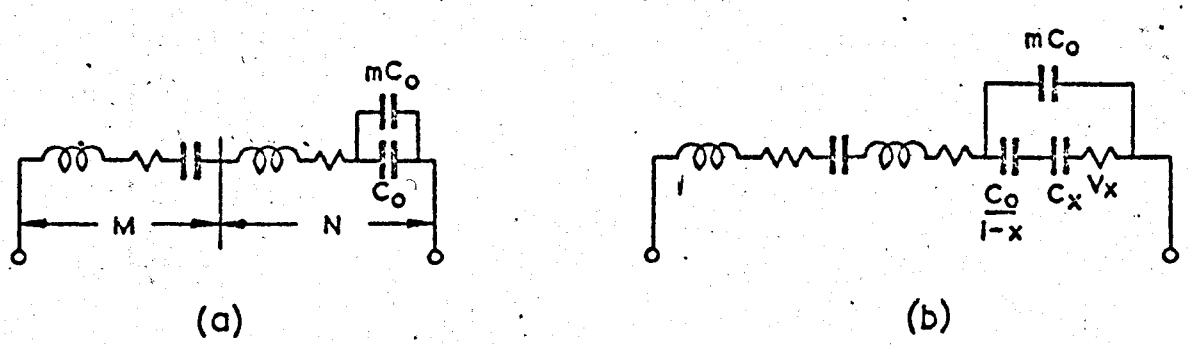

Figure 2. Equivalent Circuits, M represents the extra wavelength and N the length between the half wavelengths of the cavity. (a) Cavity with no dielectric film and, (b) Cavity with film.

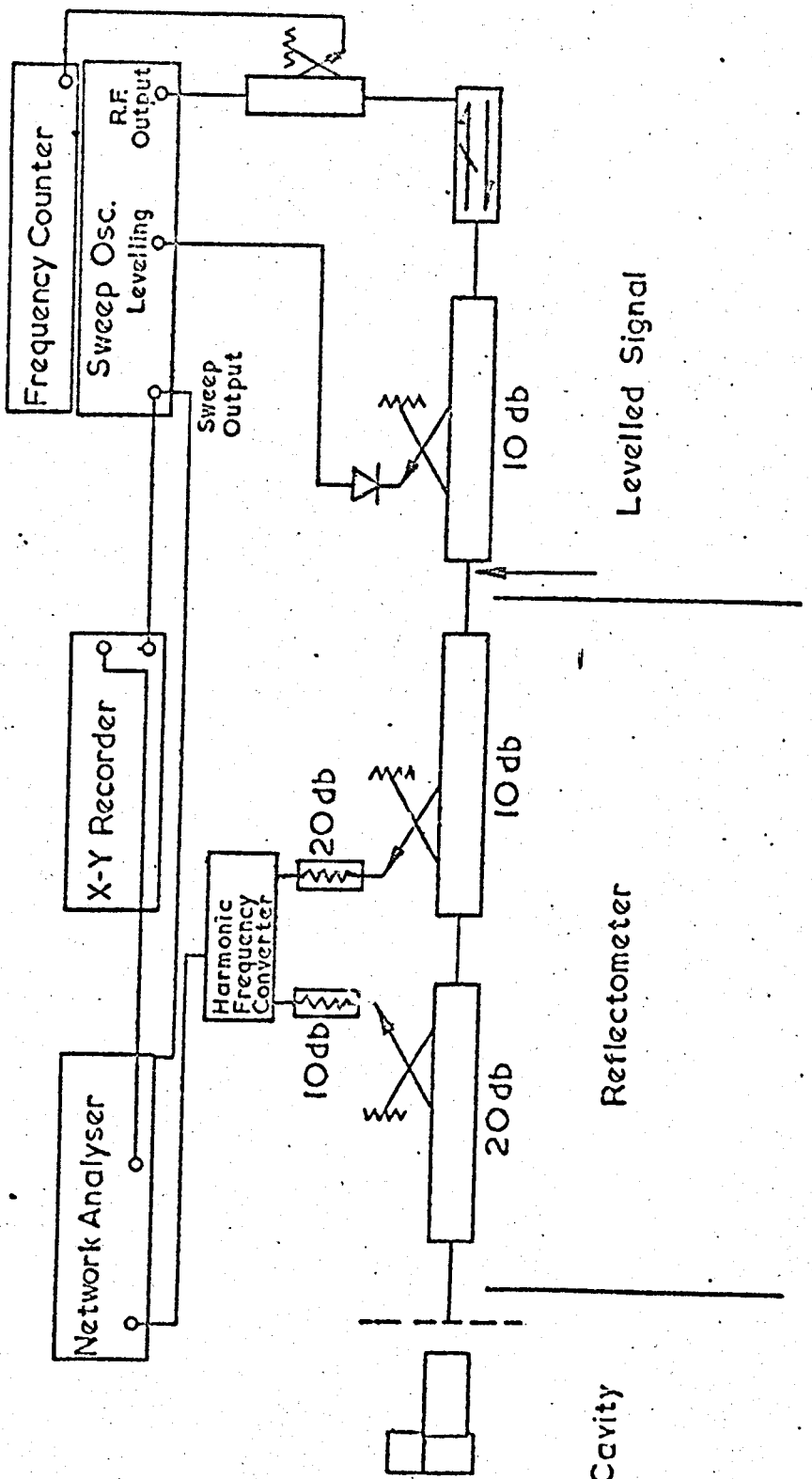

Figure 3. X-Band Reflectometer Unit